ISSN 2398-6611 (Online)

Faculty of Engineering and Technology

Faculty Research Week 2018 Proceedings

14th-18th May

Faculty of Engineering and Technology

James Parsons Building, Byrom Street, Liverpool, L3 3AF

ISSN 2398-6611 (Online)

Table of Contents

ISSN 2398-6611 (Online)

Ruqayah R Al-Dahhan Context-Aware Cloud-Based Access Control for the Internet of Things

Ruqayah R Al-Dahhan, Qi Shi, Gyu Myoung Lee, and Kashif Kifayat
School of Computing and Mathematical Science, Liverpool John Moores University, Byrom Street, Liverpool, L3 3AF, UK
R.R.Aldahhan@2015.ljmu.ac.uk, Q.shi@ljmu.ac.uk, G.M.Lee@ljmu.ac.uk, K.Kifayat@ljmu.ac.uk

Abstract. To massively exploit the strong computing power of cloud service providers and their high bandwidth, it is beneficial to outsource data files to cloud servers that are typically held by different organizations and data owners. However, since most of the outsourced data on untrusted cloud is sensitive, and the control over such data by their owners is lost after uploading to the cloud, various security concerns have arisen. One way to address some of these concerns is to enforce fine-grained access control on the untrusted cloud using some mechanisms of advanced cryptography to forbid illegitimate access to the stored data. Some schemes have been proposed to deliver such access control. However, certain outstanding issues are still not addressed. These challenges are due to the complexity of frequently changing the cryptographic enforcements of the owner access policy in the hosted cloud data files, which poses computational and communicational overheads to data owners. In this paper, we utilize some of the relevant existing systems to propose a novel technique that dynamically changes the access privileges of legitimate users. Our technique assigns processing-intensive tasks to cloud servers without any information leakage to reduce communication and computation costs. That can leverage cloud resources to integrate the Internet of things (IoT) technology and develop various applications which use dynamic context information to improve the process of decision-making. The analytical results and comparisons of our work with related existing systems show that our system is efficient, particularly in terms of policy updating and cipher-text re-encryption. Therefore, our proposed system is suited to many IoT applications that need a practical, secure access control scheme.

Keywords. Access control, revocation, cloud computing.

1. Introduction

One of the key attractive services provided by the cloud is data sharing. In which, data owners are allowed to outsource their data to data storage servers for sharing. However, since those data is outsourced to the untrusted environment which has full control over its stored data, certain security concerns are risen. Therefore; the challenge is how to ensure that the outsourced data is kept under their owners control and is accessed by authorized users.

The technique that has been proposed for resolving this challenge, is access control. However, some requirements still need to be met for this technique to be applicable in a one-to-many communication environment. One of the most major needs is fine grained access control. The second essential thing is the policy that is enforced by this system, ought to be expressive to emulate real-life access control conditions.

Cipher-text policy attribute based encryption (CPABE) is the promising achievement that satisfies these requirements [1]. In which, the data owner can enforce his/her access policy cryptographically.

In any cipher-text policy attribute-based encryption (CPABE) schemes, a set of attributes is assigned to users to be associated with their secret keys. Where, the data owners use these sets of attributes to choose an access structure to define their access policy. Then they encrypt their data under these policies. System users whose attributes satisfy the policy, can decrypt the data and recover the plaintext. In this way, fine grained access control can be achieved.

However, some hurdles in CPABE need to be tackled. One of the major ones is how to revoke the secret key of any user who has no longer be able to access data in the system or reduce his/her access privileges. The process that addresses this dilemma is user/attribute revocation. In which, the potential consequence of invalidating some or all users' access privileges that are assigned at the system initialization phase, is handled. Without embedding the revocation process from the beginning of system establishment, the whole system has to be rebuilt after each event of detecting malicious users or others leaving the system.

For some reasons, addressing the attribute revocation problem is a hard mission[2]. One of the serious reasons is the large basis of users in the cloud environment, who most of them share the same attributes. Resulting in difficulties in revoking attributes from a user without affecting other authorized users or incurring a large burden on the system that due to the need for updating all relevant keys for the non-revoked users and re-encrypting cipher-texts.

Some issues are addressed within the scope of this paper. Firstly, updating the access policy dynamically which resolves the attribute revocation problem. Secondly, delegating the re-encrypting process and updating the cipher-text components to the cloud server without revealing any information of the plaintext achieving privacy preserving revocation. Thus, we can dynamically update the cipher-text which had been created and stored on the cloud storage server according to the new access policy.

The rest of our paper is organised as follows. Section 2 discusses some related studies. Our proposed system will be presented in section 3. Finally, some ideas are concluded in Section 4.

2. Literature review

Although considerable research has been devoted to solving the access control issues, most of the existing studies lack of practicality. In systems that apply the CPABE scheme to satisfy the fine -grained access control requirements, the revocation process is the major hindrance in these systems. For instance, a dynamic user revocation scheme was proposed by Xu et al.[3]. In this scheme, the cloud server is in charge of re-encrypting cipher-text by using its assigned delegation key. However, this scheme does not handle the attribute revocation. So, the user will lose its right of accessing data in the system when it is assigned to the revocation list even if it still has other access attributes.

On the other hand, many recent works have been concerned about the attribute revocation issue. In [4], the authors proposed a system which addresses the problem of revoking users and attributes dynamically. The revocation process is executed by the cloud server which re-encrypts the cipher-text according to the revocation list using the proxy re-encryption techniques and responds the queries of the non-revoked users as well as partially decrypting the cipher-text for them. Moreover, the cloud server has additional shares of the system attributes that are used for attribute revocation. In that way revoking one attribute from some

users' privileges will not affect the access of other legitimate users. However, the system grants the cloud server more control over data access. Moreover, the cipher-text size in this system will increase linearly with the number of the revoked users due to the additional cipher-text header and components.

Adding new attributes to the updated access policy is a critical mission which some of the existing systems do not manage. However, the work in [5] addresses this problem. Where, although the access policy enforced cryptographically, the access policy can be changed dynamically without updating user's secret keys. Dynamic policy update process happens by transforming the old linear secret sharing (LSS) Matrix to an updated one corresponding to their relevant policies. When the two matrices are compared, the attributes that had changed by updating the access policy and the corresponding vectors in the Matrix, will be recognised. The distribution of the re-encrypted cipher-text after updating the policy is similar to the distribution of the old cipher-text. However, many changes frequently occur in a set of cipher-text components and these changes are done by the data owner. That means additional computational burden on the data owner. Moreover, the system re-randomizes the cipher-text before updating it. The re-randomization cost is similar to the cost of the whole encryption cipher-text process which leads to communication and computation overhead.

Therefore, we adopt some of the current tools as a first step towards solving the attribute revocation problem besides tackling the mentioned issues. Where, we present a technique to assign heavy tasks to the cloud service provider. Once the attribute revocation process is needed to be enabled, updating the access policy will be carried out by the data owner, while the cloud server will be responsible of re-encrypting the cipher-text components that the attributes are embedded in. In this case, the cloud server will be in charge of re-encrypting the cipher-text without any information leaking. Finally, in this scheme, security and theoretical performance analysis are carried out showing that our system offloads the computational burden form attribute authority and the data owner.

3. The proposed system

Considering the earlier mentioned requirements, challenges, and the existing serious problems, we formulate a new novel method to address the access control challenges in an untrusted, one-to-many environment and enhance the process of decision-making for access data which stored on the cloud. Providing a system which protects sensitive data and prevents it from being breached or accessed by malicious and illegitimate users, will fulfil most of the IoT applications requirements. This significantly exploits cloud resources as well as integrating two large technologies which are IoT and the cloud.

The strategy of our proposed system is to assign primitive encryption tasks to the cloud server without any knowledge about the data. The process of preventing the cloud server from inferring any information is satisfied by ensuring that the server deals with the encrypted data. Our system contains of four entities (as shown in Figure1) and six algorithms. These algorithms are briefly presented as follows:

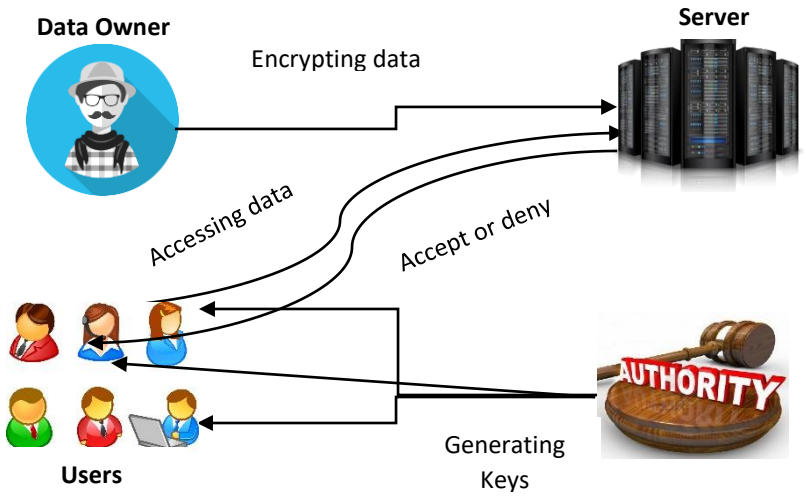

Figure 1: The proposed system framework

- $\boldsymbol{Setup(U)} \rightarrow (\boldsymbol{PK, MSK})$. In which, the attribute authority issues the public key PK and the secret master key MSK. The number of attributes U in the system is taken as the input of this algorithm.
- $\boldsymbol{Encrypt(PK, (W, \rho), M)} \rightarrow \mathbf{CT}$. The data owner encrypts a message M over LSS access structure (W, ρ)using the public key parameters PK. Where, W is a matrix and ρ is the function that maps rows of W to attributes. Part of this algorithm is executed by the cloud server as a second layer over the simple encryption operation which is carried out by the data owner.
- $\boldsymbol{KeyGen(MSK, S)} \rightarrow \mathbf{SK}$. The master secret key and a set of attributes S are used to generate the user secret key which is securely received by the user. This algorithm is run by the attribute authority.
- $\boldsymbol{Decrypt\ (CT, SK)\nabla \rightarrow M.}$ The user utilizes its private key and a cipher-text CT to recover a message, once his attributes satisfy the access structure in the cipher-text.
- $\boldsymbol{Policy\ Update(PK, SKowner, A, \acute{A})} \rightarrow \boldsymbol{ES}$. When the need for policy update occurs, the data owner executes this algorithm. Where the inputs are PK, the private parameters of the data owner SKowner, an old access policy A and a new access policy $\acute{A}$. The policy update algorithm produces a vector of updated shares ES corresponding to $\acute{A}$.
- $\boldsymbol{Re\text{-}Encryption(PK, ES, \acute{A})} \rightarrow \boldsymbol{\acute{C}T.}$ The cloud server runs this algorithm that takes the public parameters PK; the updated shares ES resulted from the $\boldsymbol{PolicyUpdate}$ algorithm, and the new access policy $\acute{A}$ as inputs. Then these inputs are used to create the updated cipher-text $\acute{C}T$. Assigning this mission to the cloud server, eliminates the burden of owners from the expensive re-encryption task, and mitigate the data owner's fear of leaking their data.

Table1: Comparing our system with PU-CP-ABE scheme

Schemes	Time consuming of Encryption (Milliseconds)		
	4 attributes	10 attributes	20 attributes
Our proposed system	210	494	843
PU-CP-ABE scheme [5]	495	1282	2454

4. Conclusion and future work

In this paper, some of the major, current concerns of any access control schemes have been considered for instance, how to achieve data confidentiality, and fine-grained access control in an untrusted, one-to-many environment as well as solving the revocation problem. The proposed system provides a technique to dynamically update the policy and re-encrypt the outsourced cipher-text by incurring low computational cost. The system assigns restricted access privileges to the cloud server to carry out most of the heavy computations without leaking any information about the plaintext. While a low computational cost is posed on the data owner particularly when the frequent revocation event occurs. So far, utilising IoT contextual information to enhance a decision-making process to access to data, serves many applications. Comparing with related systems, the theoretical and the initial experimental findings (as in Table 1) show that our system is more practical and efficient as well as securely resolving the revocation problem on an untrusted server. Finally, for a future work, developing our system to leverage context information to support a process of decision-making to dynamically access to data, is taken into our account.

References

[1] H. Hong and Z. Sun, "High efficient key-insulated attribute based encryption scheme without bilinear pairing operations," *SpringerPlus*, vol. 5, p. 131, 2016.

[2] T. Radhika and S. Vasumathi Kannagi, "Survey on user revocation and fine grained access control of PHR in cloud using HASBE," *International Journal of Computer Science and Mobile Computing*, vol. 3, pp. 452-6, 2014.

[3] Z. Xu and K. M. Martin, "Dynamic user revocation and key refreshing for attribute-based encryption in cloud storage," in *Trust, Security and Privacy in Computing and Communications (TrustCom), 2012 IEEE 11th International Conference on*, 2012, pp. 844-849.

[4] G. Wang and J. Wang, "Research on Ciphertext-Policy Attribute-Based Encryption with Attribute Level User Revocation in Cloud Storage," *Mathematical Problems in Engineering*, vol. 2017, 2017.

[5] W. Yuan, "Dynamic Policy Update for Ciphertext-Policy Attribute-Based Encryption," *IACR Cryptology ePrint Archive*, vol. 2016, p. 457, 2016.

ISSN 2398-6611 (Online)

Phillip Kendrick Multi-Agent Systems for Dynamic Forensic Investigations

Phillip Kendrick, Martin Randles, Abir Hussain
Liverpool John Moores, Department of Computer Science
P.G.Kendrick@2012.ljmu.ac.uk, M.J.Randles@ljmu.ac.uk,
A.Hussain@ljmu.ac.uk

Abstract. Network anomaly detection, focusing on the discovery of post-compromise security events is an important and challenging area of research due to recent advances in cyber threats. Where traditional security technologies such as firewalls and signature-based Intrusion Detection Systems rely on known samples of malicious activity to detect future occurrences, attackers utilising Advanced Persistent Threats (APTs), are increasingly making use of previously unseen zero day exploits to perform targeted and widespread system compromise. Agent-Based Systems (ABS) have arisen as a new and exciting approach to detect and respond to these advanced threats by using more intelligent and automated systems to actively gather and analyse network forensic evidence in real time. This work focuses on the use of ABS to detect indicators of compromise, facilitate the further collection of information based on local views of the network and analyse the security of local network systems. Combined with heuristic-style algorithms to learn the behavioural norms of the local network, agents are used to investigate a wide variety of threats.

Keywords. Multi-Agent Systems, Cyber Security, Network Forensics

1. Introduction

Recent reports [1], [2] have highlighted the need for more reliable detection of attacks occurring within the internal network. The median period between an attack happening and its detection was reported as 205 days for 2015 with only 31% of the breaches internally detected by the target of the attack. With the increasing size of networks and the requirement for organisations to share business-critical information, current cyber security solutions, such as Intrusion Detection Systems (IDS) [3], [4] and manual network forensics [5] have been unable to adapt to modern requirements. The increasing use of mobile and wireless technologies has expanded the boundaries of the traditional network by introducing a dynamic component wherein users and devices may come and go as needed. In addition to this, the pervasive adoption of the Software As A Service paradigm, characteristic of cloud-based software that can be updated or changed with ease, can alter the network's shape by enabling or disabling services and protocols. Furthermore, specific structures such as supply chain networks can increase the digital attack surface if not well protected by scalable security models [6]. Within this context, traditional security technologies have been unable to scale to the necessary levels due to their centralised nature and expensive hardware limiting their application to a single fixed network model [7].

The proposed multi-agent approach uses a collection of agents, which are distinguished from traditional software by their autonomous implementation, to perform a variety of roles in the network security environment. In addition to performing network monitoring and attack detection, currently carried out by IDSs, this research focuses on bestowing agents with the tools to replicate the manual forensic process, currently conducted by trained practitioners, to examining the security environment pragmatically. Bestowing agents with the ability to react to environmental changes, consider the performance of other agents and to work proactively to follow one line of investigation over another, when there is evidence to support it, is the fundamental principle included in the proposed model. This approach to digital evidence collection and cyber security is different from the traditional IDS approaches that typically use either signature, anomaly or misuse detection [8]. The DMASS approach of using automated forensic processes increases the agent's adaptability by enabling it to respond to unforeseen circumstances where the attacker can evade traditional signature or anomaly detection.

2. Related Research

Lorliam et al. [9] propose an unsupervised algorithm to apply Benford's distribution law[1] [10] to flow detection using the observation that normal connections tend to follow the law closely while malicious connections do not. Metrics such as flow size and window size are used to distinguish from the normal and malicious activities. The flow-based approach to attacker detection is noted to be more computationally efficient than lower level approaches that examine the data in more detail (e.g., packet or host-based IDSs) but can miss application layer information that could be of use to the detection process.

Leu et al. [11] propose a profile based behavioural IDS to monitor user system calls and detect anomalous behaviours. The system monitors users from the time they log in to compare the profiles of multiple users to define normal activity. The system reports a recognition accuracy of 98.99% but does not consider the wider security landscape and so can only be used to detect a very limited number of attacks. The IDS, implemented at the host level, assumes a high degree of visibility so that it can monitor both the legitimate and malicious user's system calls and compare the two profiles. The approach does not consider the possibility of more advanced stealthy attackers that may launch attacks from auxiliary devices where the IDS is not installed (e.g., printers and mobile devices). Furthermore, IDSs monitoring system calls are unable to detect a broader range of attacks such as port scans which do not rely on uncommon system calls such as *format*, *del* or *sudo*[2], and instead, use commonly white-listed network commands to perform the attack.

3. Decentralised Multi-Agent Security System (DMASS)

In this section, we present an overview of our MAS for performing network intrusion detection and modelling cyber events. Our approach looks to proactively collect information and search further locations that have, in the past, been found to be a reliable source of information, given the nature of the event detected. Functioning as a set of structurally similar agents that work together to analyse a security event, each agent is specialised towards the collection of data and analysis for one attack vector. Figure 1 shows

[1] Benford's distribution law states that there are measurable differences between naturally occurring and tampered datasets with which can be used to detect fraud and anomalies.

[2] Common commands that are the focus of system call anomaly detection.

a flow diagram of tasks performed by each agent. The system is comprised of multiple agents, each performing these tasks and sharing data to analyse the event.

Figure 1: Decentralised Multi-Agent Security System Flow Diagram

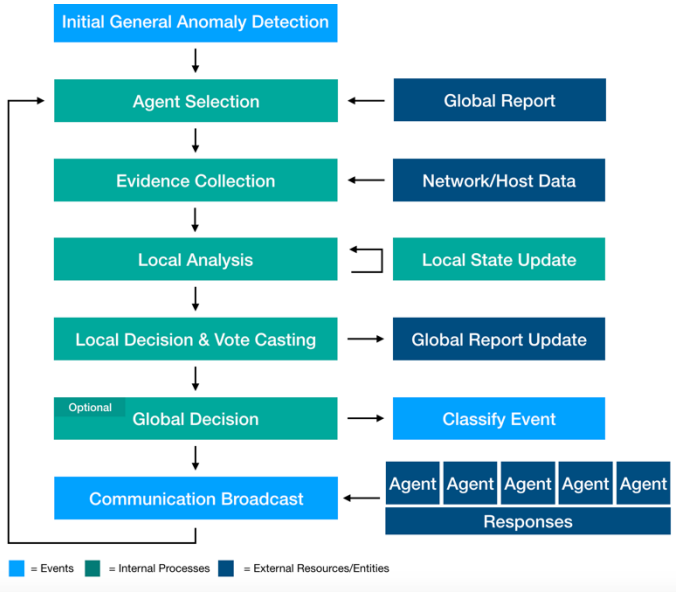

To begin an agent-based investigation into a suspected security event, an initial trigger must occur to begin the process on-demand. While performing continuous security monitoring of an environment is necessary in modern networks, the DMASS approach is instead intended to run only when given cause to do so. The term "extended data collection task" is used to describe the overall process of using the DMASS to gather and analyse security information on-demand and is the primary purpose of the system. However, the individual agents may also be used in a similar way to current IDSs to continually monitor for malicious activity as defined by signatures or anomalous behaviours.

If an agent detects a malicious event, it will become the initiating agents for the extended data collection task, however, if an anomaly is detected by an external system, such as a general network monitoring algorithm, then an agent will be selected that most suitable for analysing the threat. Once an extended data collection task has begun, agent selection is handled by the current agent who selects the agent that is most suitable to contribute to the extended data collection task based on the information that has already been gathered. Other factors, including a fitness function, that rank agents based on their prior participation and performance within the extended data collection task are used to determine which agent should participate next.

Each agent can collect a piece of evidence from the environment, including but not limited to: system logs, security logs, DNS logs, network port information and any data deemed relevant to analysing security events. Agents are limited to one evidence type, with a view to creating groups of specialised agents that are experts in analysing one aspect of a potential security event. Bulk collection and analysis of security data is often done by default; however, this leaves a large network footprint with expensive computational

costs and does not always produce the intended result of a more secure system. With the complexity of modern networks increasing, the likelihood of detecting a false positive is more likely when performing untargeted scans of the environment, the approach taken by this work avoids these potential issues by waiting until relevant information suggesting the presence of an attacker is found.

Central to the concept of an agent based system is the agent's ability to analyse and learn about the environment. Each agent privately and internally maintains information necessary to analyse the evidence gathered in the previous step, this may take the form of signatures, anomaly detection or machine learning techniques. In the case of anomaly detection or machine learning techniques, a local state update may occur following the analysis to update definitions of malicious activity in real time.

The result of the Local Analysis stage is to produce a decision whether the agent believes the evidence gathered is indicative of malicious activity or an innocuous event. Since the whole system is comprised several agents, each with a local analysis of individual aspects relating to the overall security event, the local decisions can be used to judge the performance of the agent compared to all other participating agents, for example, if there is a clear consensus between several agents that an event is malicious but one agent finds it innocuous, the performance rank for the one agent may be downgraded by the others as it fails to come to the group consensus. As previously stated, the local analysis is internal and private to the agent so only the decision (or vote) and any output information is shared. The decisions and output information is encapsulated within the “Global Report”, a data structure containing relevant information about a particular security event that is created by the first agent and transferred between subsequent agents that append information to it.

The global decision stage is an optional process that may be performed at the end of the extended data collection task. The exact time at which this process is performed is dependent on the decision algorithm selected to analyse the event. The global decision marks the end of the agent investigation where a final classification for the event is made, this is done by combining the agent votes using the decision algorithm.

To communicate with other agents, a broadcast system is used to find other agents that can contribute to the extended data collection task. Each agent broadcasts any evidence gathered during the evidence collection stage that it cannot analyse locally and takes requests for participation from other agents.

4. Conclusion

The Decentralised Multi-Agent Security System presented in this paper performs automatic data collection and analysis by using forensic-inspired processes to search for information useful during the analysis of a security event. The system differs from current approaches that are typically centralised or only address a subset of security events providing limited coverage of the network environment. Future work will focus on the development of anomaly-based detection algorithms that make use of the proposed framework to consider attacks from both the local and the global views available to agents. We aim to bring the concepts of situational information and the plausibility of evidence discussed throughout this paper to improve anomaly detection through resulting targeted investigations to find supporting evidence.

References

[1] FireEye, “Threat Report: A view from the front lines,” 2015.

[2] ISACA, “State of Cybersecurity : Implications for 2015,” *CyberSecurity Nexus*, p. 22, 2015.
[3] B. Mukherjee, L. T. Heberlein, and K. N. Levitt, “Network intrusion detection,” *IEEE Netw.*, vol. 8, no. 3, pp. 26–41, 1994.
[4] T. Verwoerd and R. Hunt, “Intrusion detection techniques and approaches,” *Comput. Commun.*, vol. 25, no. 15, pp. 1356–1365, 2002.
[5] M. R. Clint, M. Reith, C. Carr, and G. Gunsch, “An Examination of Digital Forensic Models,” *Int. J. Digit. Evid.*, vol. 1, no. 3, pp. 1–12, 2002.
[6] M. Zolfpour-Arokhlo, A. Selamat, and S. Z. M. Hashim, “Route planning model of multi-Agent system for a supply chain management,” *Expert Syst. Appl.*, vol. 40, no. 5, pp. 1505–1518, 2013.
[7] H.-J. Liao, C.-H. Richard Lin, Y.-C. Lin, and K.-Y. Tung, “Intrusion detection system: A comprehensive review,” *J. Netw. Comput. Appl.*, vol. 36, no. 1, pp. 16–24, 2012.
[8] R. Zuech, T. M. Khoshgoftaar, and R. Wald, “Intrusion detection and Big Heterogeneous Data: a Survey,” *J. Big Data*, vol. 2, no. 1, pp. 1–41, 2015.
[9] A. Lorliam, S. Tirunagari, A. Ho, S. Li, A. Waller, and N. Poh, “Flow Size Difference Can Make a Difference: Detecting Malicious TCP Network Flows Based on Benford’s Law,” in *TBA*, 2016.
[10] D. Digits, N. N. Author, and S. N. Source, “Note on the , Frequency of Use of the Different Natural Digits in,” vol. 4, no. 1, pp. 39–40, 2015.
[11] F.-Y. Leu and K.-W. Hu, “A real-time intrusion detection system using data mining technique,” *Int Conf Cybern. Inf. Technol. Syst. Appl. Conf Comput. Commun. Control Technol. Vol Ii*, pp. 148–153, 2007.

ISSN 2398-6611 (Online)

Paul Ross McWhirter A fully automated pipeline for variability detection and classification for the Small Telescopes Installed at the Liverpool Telescope

Paul Ross McWhirter[12], Dhiya Al-Jumeily[1], Iain Steele[2], Abir Hussain[1] and Marley Vellasco[3]
[1]Applied Computing Research Group, Dept. of Computer Science, LJMU, James Parsons Building, 3 Byrom Street, Liverpool, L3 3AF, UK
[2]Astrophysics Research Institute, LJMU, IC2, Liverpool Science Park, 146 Brownlow Hill, Liverpool, L3 5RF
[3]Pontifícia Universidade Católica do Rio de Janeiro, R. Marquês de São Vicente, 225 - Gávea, Rio de Janeiro - RJ, 22451-900, Brazil
E-mail address: P.R.McWhirter@2014.ljmu.ac.uk

Abstract. From 2009 to 2012 the Small Telescopes at the Liverpool Telescope collected at least 100 observations of 590,492 independent sky sources. An automated pipeline to identify periodic variables and classify them has been developed. Periods are identified using a new genetic algorithm based period estimation method designed to locate optimal candidate periods in the data and discriminate aliased signals. This method uses a Bayesian Generalised Lomb-Scargle code to determine the fitness of candidate periods and a Vuong Closeness test for the correction of aliased signals. 112 features are generated to describe the properties of the identified periodic signals and then classified using a Random Forest model with 250 trees achieving an Area under the Curve (AUC) of 0.808. A second classification model is trained on aliased signals that bypassed the Vuong Closeness test. This model uses 500 trees to achieve an AUC of 0.698. Confident classifications are used to detect additional variable sources using a classifier trained on 38 variability indices using 1000 trees achieving an AUC of 0.683. This produces 98,932 variable sources for future classification and investigation.

Keywords. Astronomical Time-Series, Period Estimation, Variable Stars, Binary Stars, Random Forests, Genetic Algorithms

1. Introduction

The Small Telescopes at the Liverpool Telescope (STILT) is an almost decade old project to install a number of wide field optical instruments to the Liverpool Telescope, named Skycams, to monitor weather conditions and yield useful photometry on bright astronomical sources [1]. The data gathered by the first operating season of the Skycams required development of algorithms and techniques which can automatically exploit the gathered data to catalogue variable sources in the La Palma sky. A previously developed pipeline reduces the Skycam images and produces photometric time-series data named light curves of millions of objects. 590,492 of these objects have 100 or more data points of sufficient quality

to attempt a variability analysis. The large volume and relatively high noise of this data necessitated the use of Machine Learning to successfully extract this information.
The Skycam instruments have no control over the orientation of the Liverpool Telescope and therefore resample areas of the sky almost randomly. This unusually irregular Skycam cadence places increased strain on the algorithms designed for the detection of periodicity in light curves. Traditional period estimation methods suffer many failures due to strongly aliased periods in the Skycam data. We also find that the failure rate is a function of period with longer period signals exhibiting significant error rates. This is a result of poor sampling of long periods by traditional Periodogram optimisation methods as they analyse a strict frequency grid which is linear in frequency space.

We therefore developed an alternative optimisation method based on a novel implementation of a genetic algorithm combined with a generational clustering method. Named GRAPE (Genetic Routine for Astronomical Period Estimation) this method determines the most likely true period based on a Bayesian Generalised Lomb-Scargle (BGLS) fitness function [2]. As the period of a variable light curve is one of the most important measures of the class of a periodic object, it is highly important that this period estimation task be as accurate as possible. GRAPE is used on the Skycam light curves to determine the period associated with the primary periodic variability and to characterise the strength of the signal compared with a constant signal and a spurious sidereal day signal caused by the daily cycle. Combined with a set of features derived from two previous studies and a novel light curve interpolation routine using an algorithm named PolyFit [3], the light curves can be classified. This paper is structured as follows: Section 2 briefly describes the components of the GRAPE method as applied to the automated pipeline. Finally, section 3 overviews the computation of the 112 features used in the classification models and discusses the automated pipeline optimal hyperparameters and cross validation performance in the selection of variable candidate light curves.

2. Genetic Routine for Astronomical Period Estimation

Period estimation tasks are best described as a global optimisation problem across a continuous parameter space. This optimisation must be solvable with a minimal computation of trial periods to identify a global minimum in a cost function. This is a function of the parameter we wish to evaluate, in this case the period of a light curve, and the trial period at the global minimum is the desired result [4]. Evolutionary algorithms are inspired by biological evolution and are capable of exploring a large, possibly high dimension, parameter space efficiently whilst also selecting good candidate results with a high precision. Genetic algorithms are a popular subset of evolutionary algorithms and utilise computational variants of many well-known staples of biological evolution. These include natural selection (survival of the fittest), genetic recombination, inheritance and mutation.

Genetic algorithms operate by employing a set number of individuals (or phenotypes) named the population. These individuals are a set of candidate solutions (in our case candidate periods). The individuals are distributed across the feature space in either a random or in an organised approach, such as from a previously identified underlying distribution. This population is evolved from generation i to generation i+1 until a cut-off point has been reached, either when the best answer reaches a given precision or a predefined number of generations has been computed [4]. The period parameter, must be encoded into a string named a chromosome with each character named a gene. GRAPE utilises base-10 chromosomes where each gene can have an integer value $I \in Z \in \{0\text{-}9\}$ where Z is the set of integers.

Skycam light curves have a baseline of approximately 1000 days which results in a precision of 10^{-10} days for extremely short periods and 10^{-3} days for periods close to the maximum period. A frequency spectrum from 0.05 days to 1000 days and an oversampling factor of 10 would only achieve equivalent worst-case precision on periods under 3 days, and are as low as 2+ day precision above 100 days.

The candidate frequencies must then be evaluated based on their performance on a fitness function which computes how well they fit the data. This sorting is then used to determine which candidate frequencies should be retained to subsequent generations. GRAPE uses the bayesian generalised Lomb-Scargle periodogram (BGLS) as its fitness function [2]. This method is quickly computable due to a lack of any operation more complex than simple summations. BGLS was one of the best performing periodograms when trialled on cross matched SkycamT light curves. The candidate frequencies chromosomes, sorted by the BGLS fitness function, must be used to create the next generation propagating through knowledge gained from the initial population whilst allowing flexibility to explore regions that were not initially scanned. Genetic algorithms use a mechanism analogous to sexual reproduction to generate the subsequent generation. This use of reproduction to propagate a genetic memory through the generations is demonstrated in figure 1 with examples of the three most important steps, fitness-ranking, crossover operations and gene mutations.

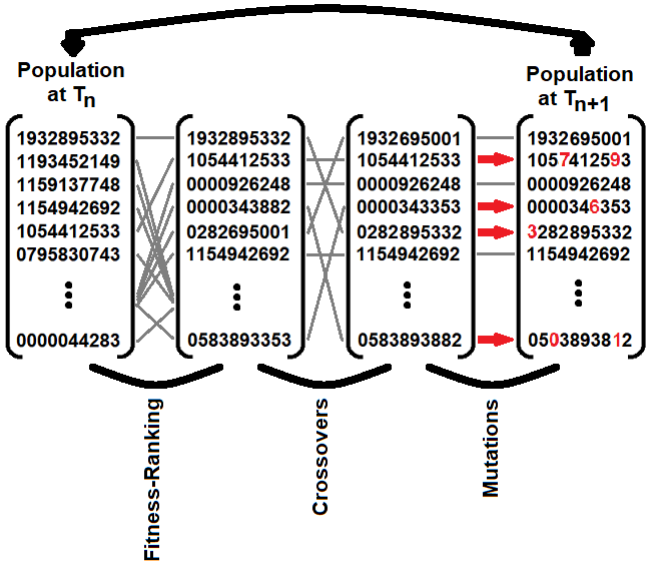

Figure 1: A demonstration of the primary evolutionary methods utilised by GRAPE.

Whilst the genetic algorithm optimises each generation throughout the period parameter space, a k-means clustering algorithm is applied at each generation to deconstruct the candidate periods for a light curve into regions in which the genetic population clusters. These regions are then fine-tuned to return a set of independent period candidates which are then analysed using a Vuong closeness test. The Vuong closeness test is an information theoretic statistic used to discriminate between models. A sinusoidal model is fit using least-squares regression to the light curve as the candidate periods and these models are then compared with the Vuong closeness test. This test has been previously suggested as a potential method to discriminate between aliased and true periods [5]. Therefore each candidate period also has a comprehensive check for aliased periods using this test to determine the most likely true period. These

aliased periods are reflections of the true signal caused by the sampling window function. As the sidereal day (t_{sid} = 0.997 days) is the strongest sampling period, the Vuong closeness test is applied to the 27 periods calculated by equation 1 when f = {1, 2, 3} and j = {-3, -2, -1, -0.5, 0, 0.5, 1, 2, 3}.

$$P_{j,f} = f \frac{t_{sid}}{\frac{t_{sid}}{P_0} + j} \quad (1)$$

The period $P_{j,f}$ which maximises the Vuong Closeness test is selected as the best fit candidate period and used to generate any subsequent features based on the light curve period.

3. Automated Classification Pipeline

Using features produced by Richards et al. [6] and Kim & Bailer-Jones et al. [7], we built up a set of features to train machine learning classification models on 13 variable star types. In addition to this set of features we also developed a semi-supervised set of additional features to describe the shape of light curves phased around the GRAPE candidate period. We investigated the performance of the PolyFit algorithm of Prsa et al., a technique to fit four piecewise polynomials with discontinuous knots capable of connecting across the phase boundary at phases of zero and one [3]. This method was designed to fit eclipsing binary phased light curves however were also described to be fully capable on other variable star types. We found that their original implementation of the algorithm relied on a simple relaxation optimisation where the knots are provided an initial candidate state and relax into the minimum. Unfortunately, the noise present in Skycam light curves prevented this optimisation from converging reliably with the initial knots highly influencing the resulting fit. Using techniques being developed with the GRAPE method, we apply a simple genetic algorithm optimisation routine to this problem with substantial improvement in the reliability of the optimisation at only a slight additional processing cost. The PolyFit model is applied to the candidate period and twice this period for every classified light curve. This interpolation provides features which describe similar statistics to the previously developed methods but which appear significantly more resilient to the Skycam noise and are often preferred by the trained models. In addition, we use Principal Component Analysis (PCA) to investigate a set of 3000 variable light curves and discover that the first ten principal components are sufficient to describe 95% of the variance of the fitted models. This trained PCA model is retained and used to generate novel shape features. Whilst these features are not dominant in their importance to the learned models, they have above average importance and help distinguish some objects in the light curve classification task.

This classification is accomplished using machine learned models which use a set of variable stars classified by the American Associated of Variable Star Observers (AAVSO) cross matched to the Skycam light curves to train two models with 13 variable star classes. The first model is a match model trained using light curves with GRAPE periods which equal or are multiples of the AAVSO catalogue period and the second is for the detection of aliased light curves with the GRAPE periods being either a one or half day alias of the catalogued period. The final classification models generate a training set for a binary variability detection classifier which uses 38 variability indices to select new candidate variables for follow-up classification. The probabilities required for confident classifications are calculated from the cross validation Receiver Operating Characteristic (ROC) through the minimisation of equation 2 named the Index of Union.

$$IU(c) = (|Se(c) + offset - AUC| + |Sp(c) - offset - AUC|) \quad (2)$$

Where c is the cutoff value, IU is the Index of Union, Se is the sensitivity, Sp is the specificity, AUC is the Area under the Curve and offset is a parameter to control the false positive rate.

Using random forest classifiers to train our learned models, we obtained an AUC of 0.808 with 250 trees, 10 features per branch split and 18-sized terminal nodes for our training set of period-matched objects. The alias model obtained an AUC of 0.698 for a set of objects which GRAPE had selected an alias of the catalogue period with 500 trees, 18 features per branch split and 14-sized terminal nodes. The variability detection model, trained using a random forest classifier with 1000 trees, 14 features per branch split and 6-sized terminal nodes, obtains an AUC of 0.683. Applying this model to the 38 variability indices extracted for the 590,492 well-sampled Skycam light curves and an offset of 0.2 yields 98,932 variable candidates for future classification and follow-up. The pipeline is designed to run cyclically and can use confident classifications from the previous cycle to train models with higher performance until the best possible precision for the available data is achieved.

References:

[1] Mawson N R, Steele I A and Smith R J 2013 STILT: System design and performance *Astronomische Nachrichten* 334(7) pp 729–737
[2] Mortier A, Faria J P, Correia C M, Santerne A and Santos N C 2015 BGLS: A bayesian formalism for the generalised lomb-scargle periodogram *Astronomy & Astrophysics* 573
[3] Prsa A, Guinan E F, Devinney E J, Degeorge M, Bradstreet D H, Giammarco J M, Alcock C R, and Engle S G 2008 Artificial intelligence approach to the determination of physical properties of eclipsing binaries. I. the ebai project. *The Astrophysical Journal* 687(1) pp 542–565
[4] Charbonneau P 1995 Genetic Algorithms in Astronomy and Astrophysics *The Astrophysical Journal Supplement Series* 101 p 309
[5] Baluev R V 2012 Distinguishing between a true period and its alias, and other tasks of model discrimination *Monthly Notices of the Royal Astronomical Society* 395(3) pp 1541-1548
[6] Richards J W, Starr D L, Butler N R, Bloom J S, Brewer J M, Crellin-Quick A, Higgins J, Kennedy R and Rischard M 2011 On machine-learned classification of variable stars with sparse and noisy time-series data. *The Astrophysical Journal* 733(1) p 10
[7] Kim D-W and Bailer Jones C A L 2016 A package for the automated classification of periodic variable stars *Astronomy & Astrophysics* 587

ISSN 2398-6611 (Online)

Ghulam Mohi-Ud-Din Efficient short-term electricity load forecasting in Smart Grid using deep learning techniques

Ghulam Mohi-Ud-Din[1], Qi Shi[1], Angelos K. Marnerides[2], Chelsea Dobbins[1] [1]Department of Computer Science, Liverpool John Moores University, UK Email: g.mohiuddin, q.shi, c.m.dobbins@ljmu.ac.uk

[2]School of Computing and Communications, Lancaster University, UK Email: angelos.marneirides@lancaster.ac.uk

Abstract: In the smart grid domain, there are many challenges which are aimed to tackle in this research work related to accurate load forecasting on both distribution centers and customer side. With proper electricity load forecasting, only the required electricity can be produced which helps in saving scarce energy resources. In individual households, customers use many appliances in their daily lives from coffee makers to refrigerators. The electricity load forecasting for individual households can assist customers to plan their electricity usage and take part in demand side management. The customers often find it difficult to manage their bills, so the accurate load forecasting can give them the way to plan their everyday activities to cut down their bills with the help of appliance level load profiles. The existing electricity forecasting models lack in providing high accuracy in load prediction. All these factors create a challenge to develop a generalized short-term electricity load forecasting model for distribution centers and individual households which can provide consistent and energy efficient load forecasting. Index terms— Short term load forecasting, deep learning, neural networks

1. Introduction

Today, there is a lot of enthusiasm to fulfill the global energy needs from alternative energy resources. The fossil fuels such as coal, oil and natural gas have long been used as primary resources for the energy requirements. The alternative energy is an emerging concept, which is the energy produced other than these fossil fuels. In everyday life, we fulfill our needs using electricity. Our whole infrastructure, from households to commercially big industries, depends on electricity. The traditional power systems cannot fulfill the increasing energy requirements and cannot provide higher reliability from many renewable resources. Thus, it is essential to transform traditional power systems, which will be able to integrate energy from all kinds of centralized and distributed sources and further supply energy based on demand.

The smart grid allows utilization of energy resources efficiently with the proper planning of energy generation, integration, transmission, distribution and consumption. With the science and technology advancements, utilities are taking steps transforming their networks towards smart grid by deploying

smart meters as a start where a smart meter is the core element of a smart grid. A smart meter does not only help to utilize electricity efficiently by displaying energy consumption but also uses renewable sources at their full potential and reduces power shortage in developing countries.

There is a major challenge for the power industries to analyze data beyond just extracting information about billing purposes. The reason is that smart meter data growth is exponential and this data traffic contains hidden structures that can provide information about fault detection, theft detection and demand response management [3]. The task of load prediction may utilize a number of heterogeneous features such as date/time, weather, customer socio-economic status, residential appliances and their characteristics, economic and demographic information, customer behaviour as well as contextual information related to social events in a particular area. However, a big challenge lies in selecting the most influential features from the landscape of many available domains that affect the overall demand on power consumption [1].
The existing electricity forecasting models lack in providing high accuracy in load prediction and they are mostly applicable for the specific regions and environmental conditions. Eventually, it is vital to consider all these factors while developing forecasting models. The main contributions of this research work are as follows:

- A dominant feature selection algorithm to increase the performance of forecasting model.
- A hybrid deep learning model to improve the forecasting accuracy and processing time.
- A parallelisation technique to accelerate the analysis of granular electricity consumption.

2. Existing Work

In literature, many researchers have proposed models to forecast electricity load for distribution centres and individual houses and improve accuracy. A number of techniques have been utilized to analyse large scale smart grid data for load predictions based on statistics, machine learning and soft computing. In particular, linear regression and stochastic time series analysis are the main statistical approaches that have been broadly used. The traditional models lack in properly representing complex nonlinear relationships between load and a number of other factors [4]. The artificial intelligence based deep learning methods possess excellent ability to analyse this kind of nonlinear relationship and provide favourable performance regarding load forecasting [2].

3. Methodology

A. Datasets and data preprocessing

There are two electricity consumption datasets which will be used for the experiments in this research. The datasets consist of the electricity consumption recorded from a distribution center and the consumption in individual households.
The datasets contain features which do not properly accentuate the effect of various factors that make electricity consumption proles of users highly non-linear and complex in nature. The factors such

as weather, time, holidays, lagged load and load distribution in different time periods are the most affecting factors to electricity consumption on a day to day basis. The data is analyzed in time and frequency domains to extract features to represent these effects.

4. Experiments and Evaluation

Feed-forward Deep Neural Network (FF-DNN) and Recurrent Deep Neural Network (R-DNN) are used to predict electricity load for the next day and next week. In first step, we use only time domain features and make the prediction for day and week ahead using both FF-DNN and R-DNN models. Due to temperature variations in different seasons, electricity consumption varies considerably and we forecast load in winter, spring, summer and autumn separately. In second step, we use composite features from the time and frequency domains and forecast day and week ahead electricity load using FF-DNN and R-DNN. The fig 1 shows the results of the experiments and provides a performance comparison of tow deep neural networks.

5. Conclusion

The electricity load forecasting is a complex domain, and there are many factors which affect the electricity usage in homes, industries, rural and highly populated urban areas. These factors include social events, weather conditions, consumers electricity consumption routines, renewable and non- renewable energy resources and many others. The highly accurate prediction of electricity load de- mands to include all of the factors affecting the load. The two, large scale state-level and small-scale house-level electricity load datasets have been used in the research work. The deep artificial neural network and recurrent neural network have been applied for day and week ahead load forecasting using the state-level dataset. During the pre-processing of this dataset, a new technique is proposed which converts time domain features into frequency domain features and models a number of important effects related to time, weather, previous day electricity load and data distribution. The experimentation using deep neural networks reveals that the addition of frequency domain analysis of the electricity load dataset improves the forecasting accuracy with very small RMSE, MAPE and MAE errors as compared to only using time domain analysis.

Season	Forecasting Type	MAPE (%)					RMSE (Mw/h)				MAE(Mw/h)			
		Time Domain		Frequency Domain		Other Model	Time Domain		Frequency Domain		Time Domain		Frequency Domain	
		FF-DNN	R-DNN	FF-DNN	R-DNN		FF-DNN	R-DNN	FF-DNN	R-DNN	FF-DNN	R-DNN	FF-DNN	R-DNN
Summer	Day	1.26	1.16	0.060	0.045		209	202	11.86	9.06	103	98	10.67	9.60
	Week	1.03	1.01	0.078	0.056		384	366	16.52	15.33	292	277	13.47	11.97
Winter	Day	1.00	0.97	0.019	0.016	2.47	202	194	3.84	3.55	152	141	2.81	2.63
	Week	1.01	0.98	0.035	0.029	1.21	188	178	6.19	5.73	149	138	4.98	4.54
Spring	Day	0.94	0.82	0.030	0.023	0.36	159	144	4.78	4.35	139	124	4.40	4.21
	Week	0.80	0.76	0.026	0.020	0.54	135	126	4.27	4.02	104	95	3.35	3.10
Autumn	Day	0.91	0.82	0.036	0.026		190	175	6.36	5.86	133	116	5.00	4.42
	Week	0.97	0.83	0.039	0.029		179	162	7.28	6.33	131	118	5.14	4.81
Whole Year	Year	1.42	1.30	0.067	0.057	1.29	306	287	131	119	210	197	6.99	5.96

Fig. 1. FF-DNN and R-DNN performance comparison

References

[1] E. a. Feinberg and D. Genethliou. Load Forecasting. *Applied Mathematics for Restructured Electric Power Systems*, pages 269–285, 2005.

[2] Y.-h. Hsiao. Household electricity demand forecast based on Context Information and User Daily Schedule Analysis From Meter Data. *IEEE Transactions on Industrial Informatics*, 11(1):33–43, 2015.

[3] W. Luan, D. Sharp, and S. Laroy. Data traffic analysis of utility smart metering network. *IEEE Power and Energy Society General Meeting*, pages 1–4, 2013.

[4] M. Zeng, S. Xue, Z. J. Wang, X. L. Zhu, and G. Zhang. Short-term Load Forecasting of Smart Grid Systems by Combination of General Regression Neural Network and Least Squares-Support Vector Machine Algorithm Optimized by Harmony Search Algorithm Method. *Applied Mathematics & Information Sciences*, 7(1):291–298, 2013.

ISSN 2398-6611 (Online)

Upul Jayasinghe Trust Computational Model based on Machine Learning for IoT

Upul Jayasinghe, Qi Shi & Gyu Myoung Lee Computer Science Department, School of Mathematics & Computing Liverpool John Moores University (LJMU), Liverpool, UK {u.u.jayasinghe@2015., q.shi & g.m.lee@}ljmu.ac.uk

Abstract. Despite the rapid development of internet of things (IoT), it remains vulnerable to threats ranging from the risks of data management at the cyber-physical layers to the potential discrimination enabled by biased decision making at the social layer. To address these issues, the concept of trust is introduced as a unique indicator to overcome the perception of uncertainty and risks before making any decisions. However, creating trust is a challenging task due to the volume of diversified influential factors from various systems, applications and users. Hence, most of these research works have been proposed to solve specific issues in a particular application area assuming many conditions like static ecosystem, availability of training data, and human interventions in certain decision-making cases. Therefore, it is essential to have an intelligent trust computation platform which can generate accurate trust values for prospective actors without relying on static training models and external interferences. Thus, we propose an adaptive trust assessment algorithm based on machine learning that autonomically assess and compute all aspects of trust among any entities and make smart decisions considering immediate as well as subsequent threats to the system. The experiment results show the effectiveness of our proposed algorithm over prior approaches.

Keywords. Computational Trust, Feature extraction, Labelling, Classification

1. Introduction

Trust is a crucial fact that affects the appetite of an object to consume a particular service or product offered by another object. Typically, trust can be seen as a metric used to evaluate social actors in consideration of mutual benefits, coordination, and cooperation. Stakeholders continuously update their trust on others in response to the variations of perceptions, generated by direct interactions and based on the opinions of others who are around.

However, the influence of a particular trust attribute (TA) on trust is often determined by a weighting factor, but the assessment of a proper weightage is a complex task due to the fact that trust is a varying quantity which depends on many factors, e.g. expectations of a trustor, time, context, etc. Thus, schemes that are more intelligent are required to find these weighting factors and a threshold that defines a trustworthy boundary. To overcome the weakness about the TA combination and make trust assessment mechanism autonomous, we propose a ML based model to analyse the TAs predict the trustworthiness of prospective transactions based on a trained model. In order to achieve this, we use an unsupervised learning algorithm to identify two different clusters or labels, namely trustworthy and untrustworthy. Then a multi-class classification technique like support vector machine (SVM) is used to train the ML model in order to identify the best threshold level that separates trustworthy interactions from others.

The reminder of the paper is organized as follows. Section 2 provides background and related work on trust. Section 3 briefly explain the feature extraction model based on our previous research. Core of this work that is ML model for trust assessment is discussed in section 4. Simulation results based on the ML model is discussed in section 5 and section 6 concludes our research work outlining future research directions.

2. Background and related work

1.1. Trust in IoT

We use the term "trustor" to represent an object that is expected to initiate an interaction with another object and "trustee" as the second object that provides necessary information towards the trustor upon its request. Formally, we can define trust as a qualitative or quantitative property of a trustee, evaluated by a trustor as a measurable belief, in a subjective or objective manner, for a given task, in a specific context, for a specific time period. The first thing that we want to emphasize in the definition of trust is the nature of the measurement that can take either a quantitative or a qualitative form. Apart from the well-known numerical measurements like similarity, accuracy, etc., qualitative properties like motivation, awareness, and commitment can also be used to judge certain situations in the process of trust based decision making. In addition, it is important to recognize trust as a belief even in the cyber world. That means, trust is a relative phenomenon and 100% belief is neither practical nor achievable in a diverse environment like IoT. Further, trust is a variable in nature and hence cannot be assigned permanently to measure every task and every context of a specific actor or object.

1.2. Knowledge Trust Metric

The knowledge trust metric (TM) covers all aspects of direct trust evaluations, which provide a perception about a trustee before an interaction. This is equivalent to analyzing the resume of a prospective candidate before hiring. To make this possible, it must provide relevant data to the trustor for its assessment. If a certain feature can be represented using a quantitative measurement, then the result is a numerical value in a certain range. As an example, social relationships (e.g. co-location and co-work), credibility factors (e.g. cooperativeness and reward), time dependent features (e.g. frequency and duration of interactions), and spatial features (e.g. mutuality, centrality and community of interest) can be used as direct trust measurements.

1.3. Related Work

On the issue of trust computational methods, authors in [1, 2] explain several trust evaluation schemes based on the concepts of network architecture, policy, reputation, and hybrid methods. Authors in [3], [4] and [5] investigate more innovative models and solutions for privacy, security and data integrity based on statistical and deep learning concepts. Moreover, authors in [6] and [7] propose a regression based model which compares the variation of trustworthiness with respect to trust features in mobile ad-hoc networks (MANET) and WSN. Recently, authors in [8], [9] and [10] present several trust management frameworks based on reinforcement learning and multiclass classification techniques which lay the foundation for the algorithms considered in this work. Even though these research achievements show some prominent results by applying ML techniques, they still lack the potential of being a generic algorithm that can be commonly applicable to any service domains without limiting to specific infrastructures. Moreover, they are missing the information about extracting social features, an intelligent labelling method and a trust prediction technique.

3. Computational Model

Even though an IoT environment produces a large amount of data, it is questionable how much of them can be directly used for the trustworthy evaluation process. Therefore, it is vital to extract trust features by scanning social and system level interaction logs and store them in a data repository (DR) for further analysis. Hence, a numerical model that can extract basic features is discussed here.

We define the assessment of knowledge (K) towards an object j by an object i at time t as $K^x(t)$, where x represents one of the features: Co-work relationship (CWR), Mutuality and Centrality (MC), Cooperativeness-Frequency-Duration (CFD), and Reward. Note that trust assessment is always between two or more objects. Assessment of each individual feature can be found through our previous research in [11] using the data set CRAWDAD [12]. Finally, the traditional approach that combines TAs through a linear equation with weighting factors is shown in (1).

$$K_{ij}(t) = \alpha K_{ij}^{\mathrm{CLR}}(t) + \beta K_{ij}^{\mathrm{CWR}}(t) + \gamma K_{ij}^{\mathrm{CFD}}(t) + \varepsilon K_{ij}^{\mathrm{RS}}(t) + \delta K_{ij}^{\mathrm{MC}}(t) + \eta K_{ij}^{\mathrm{CoI}}(t) \quad (1)$$

4. Machine Leaning Based Model

To overcome the weakness about the linear combination of TA discussed in the previous sections, we propose a ML based model to analyze the TAs extracted before and predict the trustworthiness of prospective transactions based on the trained model as follows.

We use the features defined in section 3, i.e. CWR, CFD, RS, MC and CoI to train our model. They are expressed as a feature matrix $X^{(i)}{}_{(j)}$ where i denotes the i^{th} training sample and j signifies the j^{th} feature among the n features. Moreover, the label of each training sample i is denoted by $\mathbf{y}^{(i)}$. However, training labels are not readily available and a method for the labelling will be discussed in this section. This allow us to identify each training set as ($X^{(i)}{}_{(j)}$, $\mathbf{y}^{(i)}$) for i=1,2,…,m and $\boldsymbol{j}$=1,2,…,n. In the following sub sections, we break down our main algorithm in to two parts and explain it separately in section 4.1, and 4.2 respectively.

1.4. Clustering and Labelling

In this section, we develop an algorithm based on the K-means clustering technique, which is specified in detail in Algorithm I, in order to group interactions based on the aforementioned features and thereby label each interaction as trustworthy or untrustworthy [13]. The K-means algorithm needs to define two initial conditions: number of clusters (k) and initial centroid positions ( ) that each interaction is assigned to. As there is no way to find out these values at the beginning of the algorithm, we randomly assign initial centroid locations for a range of cluster sizes, e.g. from k=1 to k=5. After that, steps 4-9 in Figure 1 are executed until the cluster points " " are not changing any further (i.e. until the convergence). Then, the Elbow method is used to find out the optimum cluster size which gives the lowest value for the K-mean cost function J(c,) where c is the index of a cluster centroid and is the coordinates of cluster centroids with the dimension of k [13].

Note that initial inputs to the algorithm were normalized between [0, 1] in which "0" represents untrustworthiness and "1" the most trustworthiness. Hence, it is logical to label points close "0" as untrustworthy and vice versa after the cauterization step. Therefore, after the step 13 of the algorithm, the clusters close to the origin (i.e. all zero point) of the N dimensional space is marked as "0" or untrustworthy and the cluster away from the origin is identified as a trustworthy region.

1.5. Classification

Having obtained the completed data set ($X^{(i)}_{(j)}$, $\boldsymbol{y}^{(i)}$) via Algorithm I, the next step is to train an algorithm based on a SVM technique which can identify the nonlinear boundaries of trustworthy and untrustworthy interactions. In order to obtain the maximum accuracy of the learning algorithm, the train set is divided into two parts in such a way that the training set occupies 80% of the data and 20% for the cross validation data set which is denoted as ($X^{(i)}_{val}$, $\boldsymbol{y}^{(i)}_{val}$) for i=1,2,…, $\lfloor 0.2*m \rfloor$ and j=1,2,…,n. This is important to avoid overfitting data through the regularization parameter and variance.

```
1.  Input: X        Output: y
2.  Initialize cluster centroids μ1,
    μ2,… ,μk ∈ℜn
3.  for k=1 to 5 do
4.      Repeat until convergence: {
5.          for i=1 to m do
6.              c(i):=arg minj||X(i)- μk||2
7.              μk := Average of points
    assigned to cluster k
8.          end for
9.      }
10.     J(k)(c,μ):=arg mink J(c,μ)
11. end for
12. Optimum k ← Elbow method ← plot
    J(k) vs k
13. for i=1 to m do
14.     if c(i) close to (0,0)
15.         y(i) = 0
16.     elseif
17.         y(i) = 1
18.     end if
```

Figure 1. Algorithm I: Data Clustering and Labelling.

```
1.  Input: X, y, Xval, yval
2.  Output: Weights and Decision
    boundary
3.  //Find best parameters for c and γ
4.  for c, γ=0.01 (multiple of 3) 30 do
5.      model=svmtrain(y,X,RBFK,c, γ)
6.      prediction=svmpredict(yval, Xval
    ,model)
7.      error [c, γ]= predictions ≠ yval
8.  end for
9.  Choose c, γ ← minimum [error]
10. [weights, accuracy, decision
    values]= svmtrain(y,X,RBFK,c, γ)
```

Figure 2. Algorithm II: Classification Model.

In the Algorithm II shown in Figure 2, we use a Radial Basis Function Kernel (RBFK) due to the smaller number of features (n) compared to the training set samples (m) as the authors in [14] have claimed. First, we run the RBFK kernel over multiple instances of regularization parameters and variances in order to find optimum parameters for the learning algorithm as shown in step 4-7 in Algorithm II. As an example both c and are varied as a geometric series (e.g. 0.01, 0.03, 0.09… 30) to save the time and computation resources. Then the parameters, which give the minimum error in the prediction step, are chosen as the optimum factors for the SVM model. Further, it is essential to improve the accuracy of the final ML model and suppress any noise generated by the previous clustering algorithm. Hence, we use regularization techniques to avoid such issues during the training process in Algorithm II.

5. Experiments and Results

1.6. Simulation Setup

After obtaining the trust feature vector X_j for each node pair, they are organized as in (2) to generate the m training samples. The dimension of the training sample matrix is in order of $m \times n$ where m=5776 (node pairs) and n=5. The notation $[.]^T$ is used to denote the transpose of a vector and has the dimension

of m×1. Note that feature normalization is not required here as each feature value is in the range of 0 and 1.

$$[\boldsymbol{X}]_{m\times n} = \begin{matrix}\vdots & \vdots & \vdots & \vdots & \vdots \\ [[CWR]^{\mathrm{T}}[CFD]^{\mathrm{T}}[RS]^{\mathrm{T}}[MC]^{\mathrm{T}}[CoI]^{\mathrm{T}}] \\ \vdots & \vdots & \vdots & \vdots & \vdots\end{matrix} \quad (2)$$

For the multiclass calcification problem, 4620 samples (i.e. 80% of the total samples) are chosen as the training set, and 1156 samples (i.e. around 20% of the total data set) are used as cross validation samples to avoid the data overfitting problem.

1.7. Results

With the successful abstraction of the trust features, the next step is to investigate how to combine each of them to generate a final trust value. To filter out most trustworthiness interactions from untrustworthy interactions, the algorithm explained in Figure 1 is applied and the results obtained are shown in Figure 4. In order to decide the optimum number of clusters, the Elbow method is used as shown in Figure 3. In certain feature combinations, the algorithm is capable to categorize interactions into three groups as trustworthy, neutral, and untrustworthy. Instances where the Elbow method gives K=3 represent such situations. It can be observed that the region above MC=0.6 and CoI=0.6 is the trustworthy region with respect to these two features as in Figure 4.

Having investigated which interactions belongs to the trustworthy region, we have used this information to label the data set. As an example, let's consider the same case in Figure 4. The points around the cluster centroid of the untrustworthy region are labelled as untrustworthy or "0" in the label vector "y", whereas the points outside the untrustworthy centroid are labeled as trustworthy or "1". Then, with the labelled data, we train a model as in Figure 5 that can clearly identify whether incoming interactions are trustworthy based on Algorithm II in Figure 2. Now it is a matter of applying this model to the new data stream to distinguish which interactions fall into the trustworthy region and vice versa without any weight or threshold calculation. This not only reduces the calculation complexity and redundant work but also saves the processing time.

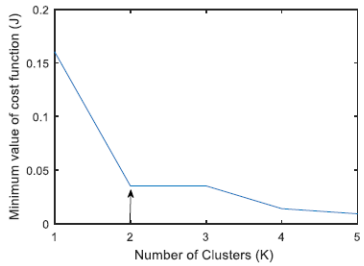

Figure 3. Elbow method: To decide the optimum number of clusters-k.

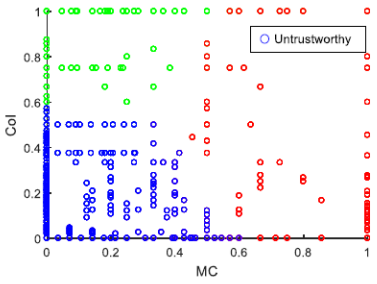

Figure 4. Clustering based on MC and CoI.

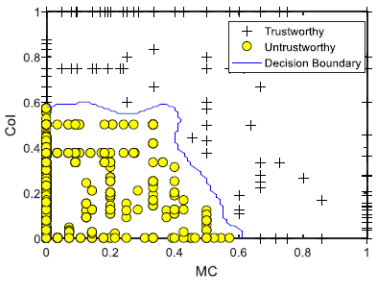

Figure 5. Classification Model based on MC and CoI.

6. Conclusion and Future Work

In this paper, a novel algorithm is proposed as opposed to traditional weighted summations to determine whether an incoming interaction is trustworthy, based on several trust features corresponding to an IoT environment. First, we have presented a generic trust computational model and a feature extraction method that can be applied to any service scenarios in IoT. Then a method for labelling the data depending on their trust-worthiness is realized based on unsupervised learning techniques, which is the vital first step for any system to identify which interactions are trustworthy. Followed by, a trust prediction model, which can correctly identify the trust boundaries of any interactions and learn the best parameters to combine each TA to obtain a final trust value, is proposed based on the well-known SVM model. Our simulation results have shown promising outcomes including the ability and accuracy of the algorithm with respect to identifying trustworthiness interactions.

To establish a distributed platform and address scalability issues, methods like map-reduction and data parallelism is to be considered [15]. Likewise, applications of novel deep learning and reinforcement models are to be investigated as part of our future work.

References

[1] N. B. Truong, U. Jayasinghe, T.-W. Um, and G. M. Lee, "A Survey on Trust Computation in the Internet of Things," *The Journal of Korean Institute of Communications and Information Sciences (J-KICS)*, vol. 33, pp. 10- 27, 2016.

[2] W. Sherchan, S. Nepal, and C. Paris, "A survey of trust in social networks," *ACM Comput. Surv.*, vol. 45, pp. 1- 33, 2013.

[3] F. Fei, S. Li, H. Dai, C. Hu, and W. Dou, "A K-Anonymity Based Schema for Location Privacy Preservation," *IEEE Transactions on Sustainable Computing*, vol. PP, pp. 1-1, 2017.

[4] F. Jiang, Y. Fu, B. B. Gupta, F. Lou, S. Rho, F. Meng, *et al.*, "Deep Learning based Multi-channel intelligent attack detection for Data Security," *IEEE Transactions on Sustainable Computing*, vol. PP, pp. 1-1, 2018.

[5] J. Shen, D. Liu, D. He, X. Huang, and Y. Xiang, "Algebraic Signatures-based Data Integrity Auditing for Efficient Data Dynamics in Cloud Computing," *IEEE Transactions on Sustainable Computing*, 2017.

[6] Y. Wang, Y.-C. Lu, I.-R. Chen, J.-H. Cho, A. Swami, and C.-T. Lu, "LogitTrust: A Logit Regression-based Trust Model for Mobile Ad Hoc Networks," presented at the Proceedings of the 6th ASE International Conference on Privacy, Security, Risk and Trust Cambridge, MA, 2014.

[7] Z. Li, X. Li, V. Narasimhan, A. Nayak, and I. Stojmenovic, "Autoregression Models for Trust Management in Wireless Ad Hoc Networks," presented at the IEEE Global Telecommunications Conference (GLOBECOM), Kathmandu, Nepal, 2011.

[8] F. Boustanifar and Z. Movahedi, "A Trust-Based Offloading for Mobile M2M Communications," presented at the Intl IEEE Conferences on Ubiquitous Intelligence & Computing, Toulouse, France, 2016.

[9] W. Li, W. Meng, L.-F. Kwok, and H. Horace, "Enhancing collaborative intrusion detection networks against insider attacks using supervised intrusion sensitivity-based trust management model," *Journal of Network and Computer Applications*, vol. 77, pp. 135-145, 2017.

[10] A. Bolster and A. Marshall, "Analytical metric weight generation for multi-domain trust in autonomous underwater MANETs," presented at the IEEE Third Underwater Communications and Networking Conference (UComms), Lerici, Italy, 2016.

[11] U. Jayasinghe, H. W. Lee, and G. M. Lee, "A Computational Model to Evaluate Honesty in Social Internet of Things," presented at the 32nd ACM SIGAPP Symposium On Applied Computing, Marrakesh, Morocco., 2017.

[12] P. Anna-Kaisa and D. Christophe. (2012). *CRAWDAD dataset thlab/sigcomm2009 (v. 2012-07-15)*. Available: http://crawdad.org/thlab/sigcomm2009/20120715

[13] X. Amatriain and J. M. Pujol, "Data Mining Methods for Recommender Systems," in *Recommender Systems Handbook*, ed Boston, MA: Springer 2015, pp. 227-262.

[14] C. W. Hsu, C. C. Chang, and C. J. Lin, "A practical guide to support vector classification," Dept. Computer Science, National Taiwan University, Tech. rep.2003.

[15] H.-c. Yang, A. Dasdan, R.-L. Hsiao, and D. S. Parker, "Map-reduce-merge: simplified relational data processing on large clusters," presented at the ACM SIGMOD international conference on Management of data, Beijing, China, 2007.

ISSN 2398-6611 (Online)

Natasa Orphanidou A virtual fencing system for real-time monitoring and controlling animal position and behaviour

N K Orphanidou[1], A Hussain[1], J Sneddon[2], A Shaw[3], P Fergus[1] and C Chalmers[1]
Liverpool John Moores, {[1]Faculty of Engineering and Technology, [2]Natural Sciences and Psychology, [3]Built Environment}, Byrom Street, L3 3AF, Liverpool UK E-mail address: n.k.orphanidou@2015.ljmu.ac.uk

Abstract. A Virtual Fencing system (VF) is a computerised method for creating spatial boundaries of any geometric size and shape without the use of any physical fences or barriers. The purpose of this study is to implement a real time virtual fencing system able to monitor and control the position of sheep using location data and acoustic cues, as well as to predict their behaviour based of accelerometer and gyroscope signals. Additionally, this study seeks to examine the response of the animals on the acoustic cues and the ability of specific sounds to keep the sheep outside or inside a desired area. For the purpose of this research, firstly, an application will be developed for use on smartphone devices to acquire accelerometer, gyroscope, and GPS measurements from the animals' collars attached on 5-7 sheep. The data will be examined and analysed using Machine Learning approach to identify an optimal model for the prediction of animal behaviour. Secondly, sound cues will be investigated through field testing to recognise their effect on sheep and their ability to control and monitor the position of the animals on the pasture. Lastly, the complete system will be tested on a larger flock (20-30 sheep) and it will be evaluated based on its animal behaviour prediction performance, and its capability to keep animals away from the restricted areas using acoustic cues. A real time multifunctional virtual fence system will make available information of where the animals are and what they are doing, where they mostly graze, and what their nutritional habits are during the course of a day. Therefore, decisions about animal health, animal position monitoring, distribution control, and efficient land utilisation can help prevent soil erosion dangers, water pollution and spread of animal diseases.

Keywords. Virtual fence, machine learning, animal behaviour, acoustic stimulus, signal processing, multifunctional systems

1. Introduction

Advancements in the field of computer science and electronics engineering have led to a transformed interest in how to develop systems for more efficient and automated agriculture [1]. A Virtual Fencing system (VF) is a computerised method for creating spatial boundaries of any geometric size and shape without the use of any physical fences or barriers [2]. Virtual Fence (or Fenceless) systems are extensively discussed over the last 30-40 years due to the inflexibility, cost and heavy maintenance demands required upon traditional fences for the containment or exclusion of prey or predator animals from specific areas. Even though, physical fences are 100% stock proof, agricultural fencing was one of the biggest expenses of the 19th century [3][4]. During the years, physical fences were replaced with bared or electric wires which are more flexible and affordable, however, the electric shock can cause harm to the livestock and

wild animals when they try to enter or leave the barriers with the possibility of entrapment. Additionally, wired fences which are currently used provide more flexibility however, the labour needed to maintain and erect them on the pasture is too time consuming. Therefore, VF is considered by the Agricultural community as the next step to replace physical fences. Such a solution will require the barriers to be removed or reduced and visual, auditory, and possibly olfactory cues could replace them as a mean to control the animal's movement and position on the land [5].

2. Background

This section provides some background information of animal behaviour studies investigating the response of the animals to external stimulus. Additionally, previous research studies related to virtual fencing systems and animal activity recognition systems are introduced.

2.1 Animal Behaviour

The livestock's drinking, foraging, habitat selection, and avoiding predator behaviour can be altered based on audio, visual and olfactory cues in combination with positive or negative associations [5]. Therefore, prospects arise for managing and controlling the animal's spatial distribution due to their ability to learn, respond and generalise their response to those cues through training [5]–[7]. In addition, animals can influence each other's behaviour through social learning, and consequently, it might be possible for farmers to train only a few animals instead of the whole flock for a VF system.

2.2 Activity Recognition

Animal activity recognition is an important aspect of farm management. The ability to recognise the behaviour of the animal is an essential part of the system this research aims to develop. The animal's wellbeing can be classified and predicted based on the daily activities of the animals. Evidence from the literature suggest that the animal's daily activity can be used as an indicator of its health. Monitoring the animal's daily activity using sensors can help farmers identify stress and diseases (lameness, fever, pneumonia) on animals, as well as their nutrition intake per day. Such information is time consuming when it is obtained solely through human observation. Additionally, it is noted in the literature that the animal's decreased activity or hyper activity could be an indicator of disease and distress of sheep [9]. There is a large volume of published studies describing the role of identification of animal activity using inertial measurement units (IMUs) and classification techniques. Animal disease, food intake and overall daily activity or inactivity can be predicted and identified when having these data at hand and is considered as a valuable tool in remote monitoring and diagnosis of animal welfare. Positional and animal activity information can be combined and used to qualify patterns of pasture use and animal distribution for targeted animal behaviour. [8] It is noted in the literature that the animal's decreased activity or hyper activity could be an indicator of disease and distress of sheep [9].

2.3 Virtual fence system

Numerous studies investigated the ability of the cattle and sheep to learn a VF system based on cues associated with a negative consequence [10], [11] [12], [13]. For example, in the abovementioned studies a sound warning was emitted to the animal when approaching a restricted area, and if it continued forward, an electric shock was followed. However, for the current research, electric shocks are not considered since they could be harmful for the animals and cause further distress and therefore only audio cues will be used.

A lot of research is conducted for the investigation of the viability of virtual fences. In 1973, Peck [14] patented a system to keep dogs within a specific area. This was the first invention intended to keep animals in a specific area without visible fences. This patent was the base of other patents created over the years to improve the existing system and be used for animal containment without a conventional fence. However, this patent raises issues of inconvenience when the animal is outside the wire and receive the same response once it tries to move back to the allowed area. Many technologies are used during the years for the creation of virtual fences.

Dog training collars, and ear tags mounted on the animals were also used [15] [16] as a virtual fence system which provided electric stimulus and audio in order to prevent animals of approaching a restricted area. Anderson *et al.* [17] tested a VF and concluded that the system was 100% effective in controlling the animal's distribution without any detectable stress which was determined from heart rate measurements. However, since the animal's behaviour cannot be 100% predictable and the virtual fence depends also on the behaviour of the animal to be effective, the authors indicated that the system should not be considered for controlling animals if health or safety issues of the animals or humans would be compromised, however, it could be considered for managing animal distribution. Anderson *et al.* [18], tested again the Directional Virtual Fencing system (DVF) in two cows. Both studies indicated that the system could monitor the direction of the animal. The authors suggested that for more animals, further investigation of the system and animal training is necessary.

Umstatter et al. [10] conducted a study to investigate whether an electric shock could be replaced with aversive sounds. The authors found some very good responses, but these were not consistent enough as they noted that 53% of the cows responded successfully. However, this was only a preliminary study and more research is needed in order to develop a system which alerts the animals without electric shocks as it is banned in Wales and some other European countries [10], and non-electric stimulation is less harmful for the animal. The control of cattle location using broadcast audio from loudspeakers placed around a small paddock instead of any means of electric stimuli was also considered [19]. According to the authors, irritating and acute sounds have a potential to control animal discourage from restricted areas however it is not sufficiently effective to replace conventional fences, more research is needed.

In a recent study, Brunberg *et al.* [20] investigated the ability of ewes with lambs to learn a virtual fencing system. The technology used, namely Nofence, is a GPS virtual fencing system designed to keep sheep within a predefined area. The collars worn by the sheep provide a sound signal when the animal crosses the boundary and a weak electric shock if they continue to walk towards the restricted area. During the experiments, the authors concluded that the Nofence prototype was unable to keep the sheep within the predefined area and thus cannot replace the conventional fences. On the other hand, Campbell et al. [21] noted that the animals can learn the virtual fence system and associate their learning to the auditory cues instead of the spatially restricted area.

According to the literature, training and teaching animals to respond and learn virtual fences based on several means of stimulation is a feasible but a challenging task. Even if this area is studied extensively with cattle, there are still suggestions in the literature that more research is needed especially using sheep.

3. Aims of the research study

The aim of this project is to develop a real time virtual fencing system able to classify and predict the activity of the animals using sensor signals as well as monitoring and controlling their position based on acoustic cues. Additionally, a key component is to investigate the response of the animals on acoustic cues through observation of the animals and their responses using physiological measurements to evaluate the feasibility of a virtual fence system.

An improved virtual fence system is the main drive of this research. Such systems are tested over the past years and are of great socioeconomic and environmental importance. In the recent study, the aim is to investigate hardware opportunities to develop and design an improved device smaller in size, and with increased battery life, which will use only acoustic stimulus for manipulating the animals position. Furthermore, a novel algorithm will be developed for an automatic classification and prediction of animal behaviour in real time. Most of the studies focused on offline data, however, limited studies exist with focus on how to create an efficient technique for real time prediction.

Additionally, another novel characteristic of this research study is the investigation of how the sheep respond to audio through observation, EEG, and HR measurements. EEG and HR signals will be examined in parallel with the frequencies of each sound and through observation of the animals' response. To the best of our knowledge, this is the first time such a method will be used for the examination of the feasibility of virtual fencing systems based solely on acoustics which is also a key component in this research.

4. Methodology

The methodology for the achievement of the research study is divided into five stages

Stage 1: Identifying existing technologies
To gain a better understanding of the research, previous work on virtual fences, animal response to external stimuli and animal activity recognition techniques must be identified. This information will be used for identification of gaps in the literature and opportunities.

Stage 2: Animal Behaviour Monitoring and Data Mining
For the successful investigation of animal response using sound stimulus and for the testing and evaluation of the optimal ML algorithm to be used, data acquisition is the focus of this stage. Smartphone devices will be used to get the data needed using accelerometer and gyroscope sensors. Online training courses will be attended to acquire the desirable knowledge to achieve such a task. Training on android application development and tutorials on Azure Stream Analytics will be undertaken for a two-month period. During this stage, a secondary available dataset consisting of accelerometer and gyroscope signals from sheep behaviour is acquired. Data analysis and machine learning techniques are tested and the more suitable models will be used in the second year of the research for further manipulation of the algorithms for real time data processing and animal behaviour prediction. The methodology consists of data preprocessing, feature engineering and model evaluation and testing. During the summer (June 2018), smartphones will be placed on sheep collars to retrieve behaviour's data. In August 2018, animal observation to identify how they respond to several sound cues will be undertaken and the knowledge gained will be used on the

implementation of the acoustic part of the system for the control and monitor animals position. The acoustic part of the system will be tested further in the second year.

Stage 3: System Design and testing
After gaining an understanding and knowledge regarding the classification model and the sounds that will be best suited to manipulate animal position and correctly detect animal behaviour, the focus will be on the wireless sensor network system software. In this stage, a thorough investigation of sensor availability will be undertaken. During this stage, the selected sensor nodes software will be implemented and further field testing will be undertaken.

Stage 4: Refine Design
Throughout the previous stages, an overall understanding of the system will be obtained and in this stage the focus will be in refining the system by means of model performance and location data accuracy. Furthermore, we will identify if such a system can be used as a virtual fence. In addition to this, changes for improvement of the system will take place.

Stage 5: Solution Development, Final testing, and Evaluation
At this stage, the system will be tested for a final time on the field and it will be evaluated based on its performance by comparing the system's ability to correctly identify the animals' behaviour with human observation. Additionally, the virtual fence system will be tested and evaluated based on its ability to keep animals away from the restricted areas.

5. Implications

An intelligent system will provide information of where the animals are and what they are doing, where they mostly graze, and what their nutritional habits are during the course of a day [25]. Having this vast amount of data at hand, decisions about animal health, animal position monitoring, distribution control, and efficient land utilisation [26] can help prevent soil erosion dangers, water pollution and spread of animal diseases [1]. Therefore the virtual fence will be used to move the animals among the land they graze using acoustic intermittent cues for the manipulation of their location as it is noted in the literature that there is potential to train animals to respond to such stimulus [5],[8]. Thus, the purpose of this research is to investigate and develop a multifunctional fencing system based on acoustics for automatic monitoring and control of free range animals. This research will contribute into various fields such as Machine learning, electronics engineering, and animal behaviour studies.

6. Acknowledgements

The authors would like to acknowledge and thank Liverpool John Moores University, and The Douglas Bomford Trust for the financial and moral support during the project.

References

[1] S. M. Rutter, "13 - Advanced livestock management solutions," in Advances in Sheep Welfare, D. M. Ferguson, C. Lee, and A. Fisher, Eds. Woodhead Publishing, 2017, pp. 245–261.
[2] C. Umstatter, "The evolution of virtual fences: A review," Comput. Electron. Agric., vol. 75, no. 1, pp. 10–22, Jan. 2011.
[3] D. M. Anderson, "Virtual fencing – past, present and future1," Rangel. J., vol. 29, no. 1, pp. 65–78, Jul.

2007.
[4] C. W. Simmons, “Fences, gates and cattle guards,” The Cattleman, vol. 22, no. 32, 1935.
[5] L. D. Howery, A. F. Cibils, and D. M. Anderson, “Potential for using visual, auditory and olfactory cues to manage foraging behaviour and spatial distribution of rangeland livestock,” CAB Rev. Perspect. Agric. Vet. Sci. Nutr. Nat. Resour., vol. 8, Nov. 2013.
[6] J. R. Franklin and G. D. Hutson, “Experiments on attracting sheep to move along a laneway. I. Olfactory stimuli,” Appl. Anim. Ethol., vol. 8, no. 5, pp. 439–446, Jun. 1982.
[7] J. E. Morris, A. D. Fisher, R. E. Doyle, and R. D. Bush, “Determination of sheep learning responses to a directional audio cue,” J. Appl. Anim. Welf. Sci. JAAWS, vol. 13, no. 4, pp. 347–360, 2010.
[8] E. L. Shepard et al., “Identification of animal movement patterns using tri-axial accelerometry,” Endanger. Species Res., vol. 10, pp. 47–60, 2008.
[9] D. A. Gougoulis, I. Kyriazakis, and G. C. Fthenakis, “Diagnostic significance of behaviour changes of sheep: A selected review,” Small Rumin. Res., vol. 92, no. 1, pp. 52–56, Aug. 2010.
[10] C. Umstatter, C. Tailleur, D. Ross, and M. Haskell, “Could virtual fences work without giving cows electric shocks?,” Precis. Livest. Farming 2009 - Pap. Present. 4th Eur. Conf. Precis. Livest. Farming, pp. 161–168, Jan. 2009.
[11] M. Jouven, H. Leroy, A. Ickowicz, and P. Lapeyronie, “Can virtual fences be used to control grazing sheep?,” Rangel. J., vol. 34, no. 1, pp. 111–123, Mar. 2012.
[12] U. C, M.-D. J, and W. A, “Cattle responses to a type of virtual fence,” 2015.
[13] E. D. Ungar, Z. Henkin, M. Gutman, A. Dolev, A. Genizi, and D. Ganskopp, “Inference of Animal Activity From GPS Collar Data on Free-Ranging Cattle,” Rangel. Ecol. Manag., vol. 58, no. 3, pp. 256–266, May 2005.
[14] R. M. Peck, “Method and apparatus for controlling an animal,” 3,753,421, 1973.
[15] T. M. Quigley, H. R. Sanderson, A. R. Tiedemann, and M. L. McInnis, “Livestock control with electrical and audio stimulation.,” Rangel. Arch., vol. 12, no. 3, pp. 152–155, Jun. 1990.
[16] T. M. Quigley, “Method and apparatus for controlling animals with electronic fencing,” 5,408,956, Apr-1995.
[17] D. M. Anderson, Hale, C. S, Libeau, R., and Nolen, B., “Managing stocking density in real time,” in Proceedings of the VIIth International Rangeland Congress, Durban, South Africa, 2003, pp. 840–843.
[18] D. Anderson, B. Nolen, E. Fredrickson, K. Havstad, C. Hale, and P. Nayak, “Representing spatially explicit Directional Virtual Fencing (DVFTM) data,” Jan. 2004.
[19] C. Umstatter, S. Brocklehurst, D. W. Ross, and M. J. Haskell, “Can the location of cattle be managed using broadcast audio cues?,” Appl. Anim. Behav. Sci., vol. 147, no. 1, pp. 34–42, Jul. 2013.
[20] E. I. Brunberg, I. K. Bergslid, K. E. Bøe, and K. M. Sørheim, “The ability of ewes with lambs to learn a virtual fencing system,” animal, vol. 11, no. 11, pp. 2045–2050, Nov. 2017.
[21] D. L. M. Campbell, J. M. Lea, W. J. Farrer, S. J. Haynes, and C. Lee, “Tech-Savvy Beef Cattle? How Heifers Respond to Moving Virtual Fence Lines,” Animals, vol. 7, no. 9, p. 72, Sep. 2017.
[22] J. Yick, B. Mukherjee, and D. Ghosal, “Wireless sensor network survey,” Comput. Netw., vol. 52, no. 12, pp. 2292–2330, Aug. 2008.
[23] M. Marjani et al., “Big IoT Data Analytics: Architecture, Opportunities, and Open Research Challenges,” IEEE Access, vol. 5, pp. 5247–5261, 2017.
[24] C.-Y. Chong and S. P. Kumar, “Sensor networks: evolution, opportunities, and challenges,” Proc. IEEE, vol. 91, no. 8, pp. 1247–1256, Aug. 2003.
[25] D. Anderson, R. Estell, J. Holechek, S. Ivey, and G. Smith, “Virtual herding for flexible livestock management - a review,” Rangel. J., vol. 36, pp. 205–221, 2014.
[26] B. E. Norton, M. Barnes, and R. Teague, “Grazing Management Can Improve Livestock Distribution: Increasing accessible forage and effective grazing capacity,” Rangelands, vol. 35, no. 5, pp. 45–51, Oct. 2013.

ISSN 2398-6611 (Online)

Mohammed Khalaf A Machine Learning Approaches for Clinical Data Analysis with Application

Mohammed Khalaf[1], Abir Jaafar Hussain[1], Dhiya Al-Jumeily[1], Russell Keenan[2]

[1]Faculty of Engineering and Technology, Computing Science Department, Liverpool John Moores University, Byrom Street, Liverpool, L3 3AF, UK.

[2]Liverpool Paediatric Haemophilia Centre, Haematology Treatment Centre, Alder Hey Children's Hospita

M.I.Khalaf@2014.ljmu.ac.uk, {a.hussain, d.aljumeily, F.P.Tso}@ljmu.ac.uk

Russell.keenan@alderhey.nhs.uk

Abstract. Machine learning approach is considered as a field of science aiming specifically to extract knowledge from the data sets. currently, most of healthcare sectors across United Kingdom and indeed internationally are still using manual approach for analysing patient input for sickle cell disease in terms of providing accurate amount of medications. Consequently, this manual procedure depends completely on clinician's experience that can lead to time consuming and stress to patients. Extensive research has indicated that machine learning technique produce important improvements when used for the pre-processing of medical time-series data signals. This technique have also assisted healthcare sectors in obtaining high accuracy in the classification task of medical data sets. We concentrate on enhancing sophisticated machine learning approaches, for the purpose of solving supervised learning problem. It is also we presents a new technique to combine two classifiers between the Levenberg-Marquartdt training algorithm and the k-nearest neighbours algorithm. In this paper, we introduce multi-class label classification problem in order to obtain training and testing methods for each models along with other performance evaluation. In machine learning, the model utilise a training sets in association with building a classifier that provide a reliable classification. This research discusses different aspects of machine learning approaches for the classification of biomedical data. We are mainly focus on the multi-class label classification problem where many number of classes are available in the data sets. The results obtained from a range of models during our experiments have shown that the proposed combination classifiers outperformed among other classifiers.

Keywords. — Sickle Cell Disease; Machine Learning Algorithm; Real-time data; Receiver Operating Characteristic Curve; The Area Under Curve; E- Health

1. Introduction

Sickle Cell Disease(SCD) is considered a long-term disorder which the red blood cells(RBC) change from normal shape as circle to crescent. This in turn results in cells make it difficult to move smoothly

in the vessel, that tends to stick in the vessel wall. In this case, the amount of oxygen flow reduced to nearby tissues, especially for lung. This condition causes chronic pain for SCD patient, and difficulty in breathing and heart receiving insufficient amount of blood, which make situation for patient worse and requires hospitalization. At present, this disease has no proper treatment; therefore, the symptoms can be manager properly by the use of medication, particularly hydroxyurea. It is important for each patient who suffer from this disease is to be diagnosed at early stage and treatment have to begin quickly so that patient able to live in a healthy life.

Machine learning model is considered robust and effective process to analyse medical datasets, which able to gives computer the ability to learn without being explicitly programmed[1].it has been applied to a great number of prediction problem in varying fields such as medical diagnosis, molecular chemistry, information extraction, and social networks and many more. Machine learning is the area of research devoted to and concerned with classification and the concept of learning. Typically, this field is a computation techniques utilising experience to enhance performance, for instance to make correct predictions and classification. The motivation for using machine-learning techniques to handle a potentially unbounded amount of data and process them in terms of achieving the same accuracy and performance. Machine learning consists of utilising classification techniques (classifier) to group a set of symbols into a number of classes depending on their attributes (features). A feature is considered one aspect of a symbol that can help in aggregating it according to each class. One of the significant factors that has strong influence on the success of a learning method is the type of the data that is used to represent the task to be learned.

The remainder of this paper is organized as follows. Section 3 will discuss the methodology of our experiments. The Results will be shown in Section 3, while the conclusion and future work will be shown in Section 4.

2. Methodology

Most studies in the field of machine learning algorithms have been constructed to predict the severe crises of sickle cell disease, rather than using advance prediction to provide accurate amounts of a drug named hydroxyurea/hydroxycarbamide in modifying the disease phenotype [2]. The key feature of learning-based classifiers is their capability to adjust the internal structure depending on input and respective target value (desired output) data. This scenarios is approximated the relations implicit in the delivered training data, therefore elegantly simulating a reasoning task [3]. Currently there is no standardisation of disease modifying therapy management. Using the proposed computerised comprehensive management system, the aim is to produce an optimised and reproducible standard of care in different clinical settings across the UK and indeed internationally.The main backbone of this project is to use recent advances in neural network models, a type of machine learning algorithm, in order to assist the healthcare professionals in offering accurate amounts of medication for each individual patient according to their conditions. In this case, and due to the pattern of the SCD dataset, classification of patient's datasets records at an earlier stage was proposed, according to how much of a dose the patient will need to be taken. This can potentially lower costs, avoiding unnecessary admission to hospitals or special institutions, improve patient welfare and mitigate patient illness before it gets worse over time, particularly with elderly people.

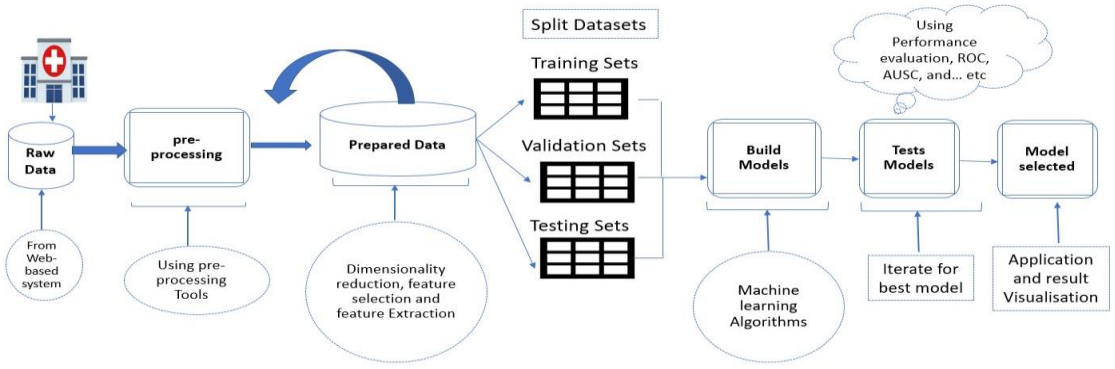

Figure 1. The Methodology Process

The design part will involve building the proposed model and generating the requirements for the prototype. The design and implementation phases will be connected and feed into each other in such a way that when the first step of design has been completed then the implementation section can commence with the improvement of a prototype. The motivation behind doing this method is to evaluate the efficiency and effectiveness of using advanced artificial neural network techniques on SCD datasets, to predict the amount of medication for each patient based on current conditions. In order to carried out our experiments using the SCD dataset, figure 1 illustrated the Proposed Framework Architecture of our research. These phases involved of raw data, pre-processing, structured data, which contains dimensionality (feature extraction and feature extraction), split datasets through building models from training and test sets, selected the candidate model, validation, and the presentation of outcomes. The remainder of the chapter will discuss each of these processes more in-depth within the proposed framework procedure.

3. Results

In this section, we analyse the outcomes from the experiments as listed in tables 1 and 2, showing results for training and testing of the classifiers, respectively. To clarify the results, this study provides further performance visualisations through the use of AUC comparison plots as illustrated in figures 2 and 3

The results gained from the empirical investigation into the use of various types of machine learning models show that the chosen data sets exhibits significant non-linear relationships, presenting a challenge for the test models. Of the combined classifiers under study, the KNNC-LVMNN outperformed the other models as shown in table 2, demonstrating capability both in fitting during the testing phase. The calculated means of AUCs for the KNNC-LVMNN model, obtained for six classes during training yielded an area of 0.99167, in comparison to 0.99167 over the test sample. Classes 1 to 6 were found to show excellent performance and consistent generalisation test sets for this model. KNN were outperformed the combined KNNC-with LVMNN by obtaining 1 (ideal) during the training set. However, KNN performed badly during the test phase compare with the combined model, which obtained 0.80817. It was found that the KNNC-LVMNN model, a standalone neural network and kernel procedure, was able to compete a great result during the testing and training phases in comparison

with other classifiers. We conducted further experiments investigation using SVM model, illustrating that this model obtain 0.89917 during training set, while 0.8885 during testing phase.

Table 1. Classifiers performance with average of six classes (Training)

Model	Sensitivity	Specificity	Precision	F1	J	Accuracy	AUC
ROM	0.493167	0.542	0.178783	0.2531	0.035133	0.543	0.487667
KNNC	1	1	1	1	1	1	1
KNNC-LVMNN	0.99083	0.99683	0.985	0.988	0.98767	0.9965	0.9995
SVM	0.83733	0.8505	0.5575	0.657	0.68767	0.8475	0.89917
LNN	0.845333	0.828167	0.523	0.6395	0.673667	0.8335	0.870333

Table 2. *Classifiers performance with average of six classes (Testing).*

Model	Sensitivity	Specificity	Precision	F1	J	Accuracy	AUC
ROM	0.548	0.547	0.19688	0.2681	0.09483	0.53867	0.52433
KNNC	0.7455	0.76133	0.36383	0.47667	0.50683	0.767	0.80817
KNNC-LVMNN	0.98033	0.986	0.91983	0.94833	0.96767	0.98667	0.99167
SVM	0.86283	0.8385	0.49933	0.6165	0.7015	0.83767	0.8885
LNN	0.830167	0.844167	0.526667	0.637833	0.6745	0.838167	0.848833

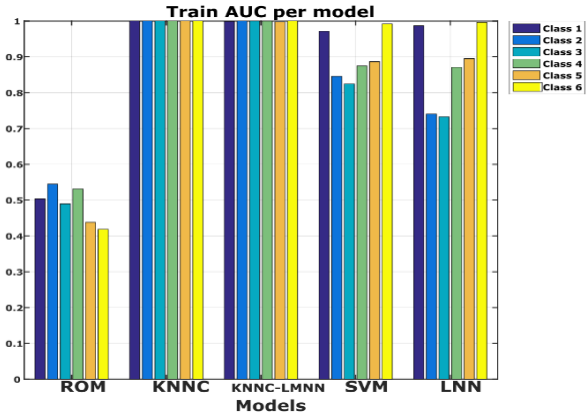

Fig. 2. Train AUC per model

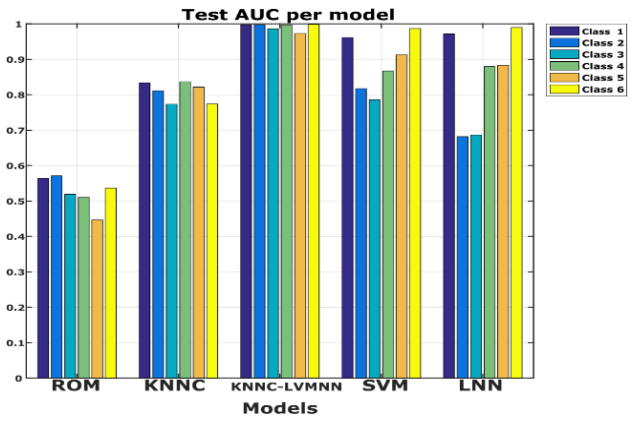

Fig. 3. Test AUC per mode

The plots show in Figures 2 and 3 show the area under the ROC curve (AUC) for each class over each model within our experiment. The discretisation of target values into Class 1: [148 ≤ Y < 427mg], Class 2: [427 ≤ Y < 659mg], Class 3: [659 ≤ Y ≤ 937mg], Class 4: [937 ≤ Y < 1201mg], Class 5: [1201

≤ Y < 1453mg], Class 6: [1453 ≤ Y ≤ 1700mg]. Figure 1 shows the results obtained for the training set and figure 3 the test set, respectively. The AUC value is a scalar summary used to characterise the global capability of a given classifier under study. In our plots, the X axis shows the models and classes, while the Y axis shows the AUC that corresponds to each of the model entries listed over the X axis.

4. Conclusion

This study presents an experimental investigation into the use of different neural network algorithms to classify the level of dosage for SCD. In this paper, various model architectures are used for analysing the medical data sets obtained from SCD patients. The main purpose of this research is to examine the effectiveness of these models in terms of training and testing setting, investigating if such architectures could enhance classification results. It was discovered through experimental investigation, comprising the usage of patient sample data and approaches such as the Levenberg-Marquartdt training algorithm (LVMNN), the k-nearest neighbours algorithm (K-NN), Support vector machines (SVMs), and the baseline models, that the analysis of medical data for the SCD objective is viable and yields precise results. The results obtained from a range of models during our experiments have shown that the combined classifiers LVMNN and K-NN produced significantly better outcomes over the other range of classifiers. The local hospital has supported this research with a more than 1100 sample examples for the purpose of obtaining better services and accuracy. Further research will be recommended to implement to make confirmation on our findings, where a large number of data could be utilised also to advance the performance of the results. This study has indicated only a certain number of machine learning models. In this circumstance, it is recommended however that a machine learning algorithms, for instance, Deep learning techniques and Genetic algorithm could be used to increase the scale and scope of this research

References

[1] A. L. Samuel, "Some studies in machine learning using the game of checkers," IBM Journal of research and development, vol. 3, no. 3, pp. 210-229, 1959.
[2] C. Allayous, S. Clémençon, B. Diagne, R. Emilion, and T. Marianne, "Machine Learning Algorithms for Predicting Severe Crises of Sickle Cell Disease," 2008.
[3] W. Gao, Y. Tian, L. Duan, J. Li, and Y. Li, "Video Scene Analysis: A Machine Learning Perspective," in Video Segmentation and Its Applications: Springer, 2011, pp. 87-116.

ISSN 2398-6611 (Online)

Ahmad Abduallah Synthetic Loading for Symmetrical and Asymmetrical Twelve-Phase Induction Machines

A. A. Abduallah
Department of Electronics and Electrical Engineering,
James Parsons Building, Byrom Street, L3 3AF, Liverpool, UK
A.Abduallah@2016.ljmu.ac.uk

Abstract. High power applications have been progressively utilising multiphase machines, especially machines with multiple three-phase winding sets. The development of the high power twelve-phase machine requires few tests such as the full-load test, where the thermal design of the machines is tested. The most utilised scheme in industry is the back-to-back configuration where another machine is mechanically coupled to the tested machine. This approach has benefit as it can recirculate and hence save on power used during the test. However, the mechanical coupling and resources needed to achieve the test are expensive. Therefore, other alternatives have been introduced to eliminate the high cost of this method. But, the ability to recirculate the power is no longer available with these alternatives. In this paper, a new approach to test the twelve-phase machine thermal design is introduced. Presented method can be used to test the machine's thermal design without the need for mechanical coupling. In addition, recirculation of the power, among the twelve-phase machine winding sets, is obtained. The approach is based on indirect rotor-field oriented control (IRFOC) and vector space decomposition (VSD) approach. The test is implemented by controlling the highest *y*-current component of VSD. By controlling this current, half of the winding sets of the twelve-phase machine will be in motoring mode while the other half will be in generation mode. The proposed approach has been validated through the simulation results.

Keywords. Multiphase machines, Twelve-phase machines, Synthetic loading.

1. Introduction

High power applications, especially in renewable energy, have been progressively exploring and utilising multiphase machines. This is due to their ability to split up the power among n phases ($n > 3$) instead of three in standard three-phase machines (Singh, 2002). Moreover, specific type of multiphase machines, with multiple three-phase winding sets, offers more advantages compared to the other multiphase machines such as increased fault-tolerant capability (from the converter's point of view). Furthermore, these machines are utilising well-established three-phase power electronics technologies (Levi et al, 2007; Levi, 2016).

As the world goes toward the cleaner energy, a lot of research has been conducted on the machine's design for wind turbines. Development of these machines requires various tests such as full-load test or the temperature-rise test. Usually, these tests are conducted using finite element method (FEM) software. This method requires huge computational time, powerful computers and a precise model. However, sometimes performing a practical full-load test is necessary where the customer can see the actual performance of the machine from the test that corresponds to the actual field conditions. Performing the full-load test can

discover and correct any issues before the commissioning of the machine in the plant. Common option for this test is the back-to-back configuration (McSharry et al, 1998). The back-to-back configuration requires the tested machine to be mechanically coupled with another machine of the same (or higher) power rating which acts as a load. However, mechanical coupling is not easy and requires a lot of resources. Therefore, the test is costly because: another machine must be used, the cost of the mechanical coupling is high, the installation and setup are difficult, and the consumed energy by the tested and the coupled machine (the losses) can be significant. For these reasons, an alternative method to perform the full-load test is needed.

Several authors have proposed new approaches to perform the test without the need to couple the tested machine's shaft with another machine. Some of the suggested methods are, two frequency method (Meyer and Lorenzen, 1979), phantom loading (Fong, 1972) and inverter driven method (Sheng and Grantham, 1994; Soltani, Szabados and Hoolboom, 2002). These methods will provide the machine with the same temperature-rise as in the case of the back-to-back configuration where the effective voltage and the stator current are equal to the rated values of the machine (Ho and Fu, 2001). However, for these methods, the power cannot be recirculated hence the losses would be high. The standard method with the back-to-back configuration has the ability to circulate the power e.g. if the dc links of the used converters are connected. In that case the only power withdrawn from the supply is for the losses of the machines and the power electronics converters. However, this way of testing is still very costly for the electrical machines with high power rating (for instance 2 MW wind turbine).

In (Luise et al, 2012) a new approach for testing the machine with the full-load condition, without the need for mechanical coupling with another machine, is introduced. The scheme is capable of circulating the power among the different sectors of the machine. However, the scheme is only applicable to the specific type of machine where the stator winding is split into three-phase sectors which are suitable for parallel operations (Luise et al, 2012). The principle of this test is to connect two sectors of the machine, which are opposite to each other, to the same converter and to control them in motoring or generation mode using sensorless four-quadrant field-oriented control (FOC). The control scheme is set to speed or torque mode depending if the sectors are operating in the motoring or generation mode. During the start-up of the machine, the machine's speed reference is set to the nominal speed while keeping the torque reference at zero. After reaching the rated speed the torque reference for the sectors operating in generation mode is set to the desired negative value. Thus, the speed-controlled sectors work in motoring mode, while the other two sectors are working in generation mode.

2. Synthetic Loading Test for Symmetrical and Asymmetrical Twelve-Phase Machines

The implementation of (Luise et al, 2012) approach to twelve-phase machines is possible using multiple vector control and by considering each winding set as a sector. However, controlling a twelve-phase machine using the multiple vector control scheme is problematic since there is heavy cross coupling between the winding sets, making high performance control difficult. Thus, it is advisable to utilise VSD modelling approach for multiphase machines in general. VSD decouples a multiphase machine into $n/2$ subspaces. Each subspace is completely decoupled from the other subspaces. Moreover, the number of flux/torque producing subspaces is reduced to one (α-β subspace), when VSD modelling approach is used, instead of four when the multi-stator approach is used. The remaining subspaces (x-y subspaces) are loss-

producing planes. Although these subspaces are not required to be controlled in order to control the flux or torque of the machine, they are usually controlled in practice to discard any asymmetries that may be present in the windings of the machine or in the converter. Nevertheless, these *x*-*y* subspaces can be also controlled to achieve post-fault operation of the multiphase machine. VSD transformation for an asymmetrical twelve-phase machine with four isolated neutral points is given as:

$$[\mathrm{VSD}_{12}]=\sqrt{\frac{2}{12}}\begin{bmatrix} \alpha & \cos([\theta_{12A}]) \\ \beta & \sin([\theta_{12A}]) \\ x_1 & \cos(5[\theta_{12A}]) \\ y_1 & \sin(5[\theta_{12A}]) \\ x_2 & \cos(7[\theta_{12A}]) \\ y_2 & \sin(7[\theta_{12A}]) \\ x_3 & \cos(11[\theta_{12A}]) \\ y_3 & \sin(11[\theta_{12A}]) \end{bmatrix} \quad \text{where}[\theta_{12A}]=\pi/12\cdot[0 \;\; 8 \;\; 16 \;\; 1 \;\; 9 \;\; 17 \;\; 2 \;\; 10 \;\; 18 \;\; 3 \;\; 11 \;\; 19] \tag{1}$$

In (Zoric, Jones and Levi, 2018), the authors found the correlations between the VSD and multi-stator (MS) modelling approach for multiphase machines with multiple neutral points. By finding these correlations, or mapping of the winding set *α*-*β* currents into the *x*-*y* currents, the ability to control the individual winding set currents by utilising VSD is possible. The correlations between the MS and VSD approach for the twelve-phase machines can be obtained as follows:

$$[i_{\mathrm{VSD12}}]=\begin{bmatrix} i_\alpha \\ i_\beta \\ i_{x1} \\ i_{y1} \\ i_{x2} \\ i_{y2} \\ i_{x3} \\ i_{y3} \end{bmatrix}=\begin{bmatrix} \frac{1}{2}(i_{\alpha1}+i_{\alpha2}+i_{\alpha3}+i_{\alpha4}) \\ \frac{1}{2}(i_{\beta1}+i_{\beta2}+i_{\beta3}+i_{\beta4}) \\ \frac{1}{2}(i_{\alpha1}-i_{\alpha3}+i_{\beta2}-i_{\beta4}) \\ \frac{1}{2}(i_{\alpha2}-i_{\alpha4}-i_{\beta1}+i_{\beta3}) \\ \frac{1}{2}(i_{\alpha1}-i_{\alpha3}-i_{\beta2}+i_{\beta4}) \\ \frac{1}{2}(i_{\alpha2}-i_{\alpha4}+i_{\beta1}-i_{\beta3}) \\ \frac{1}{2}(i_{\alpha1}-i_{\alpha2}+i_{\alpha3}-i_{\alpha4}) \\ \frac{1}{2}(-i_{\beta1}+i_{\beta2}-i_{\beta3}+i_{\beta4}) \end{bmatrix} \tag{2}$$

One can notice from (2) that the highest subspace *y*-current component is consisting of β_i currents only. Half of the β_i currents are subtracted from the sum of the other half. This is obvious from i_{y3}. Therefore, the synthetic loading test can be applied by using IRFOC and by controlling the *α*-*β* subspace and the last of the *y*-current components. The test can be implemented using the following steps:

1. During the initial acceleration, the machine is set to speed control mode, where *d* and *q* currents are regulated using PI controllers.
2. After the machine reaches the reference speed, the desired synthetic load torque reference T_l^* can be implemented at i_{y3}^* (see Figure 1).
3. Half of the winding sets will be in generation mode (with negative $i_{\beta i}$), while the other half will be in motoring mode (with positive $i_{\beta i}$).

4. The i_{y3}^{*} can be found in the same way for the reference i_q from the torque reference T_e (output of the speed controller).

The synthetic loading test for twelve-phase induction machines schematic is illustrated in Figure 1. The other *x-y* subspaces' currents are set to zero. One can see that instead of using nine PI controllers to implement the regenerative test for twelve-phase machines by using multiple vector control approach, only four PI controllers are required to achieve the same result by utilising the proposed control scheme.

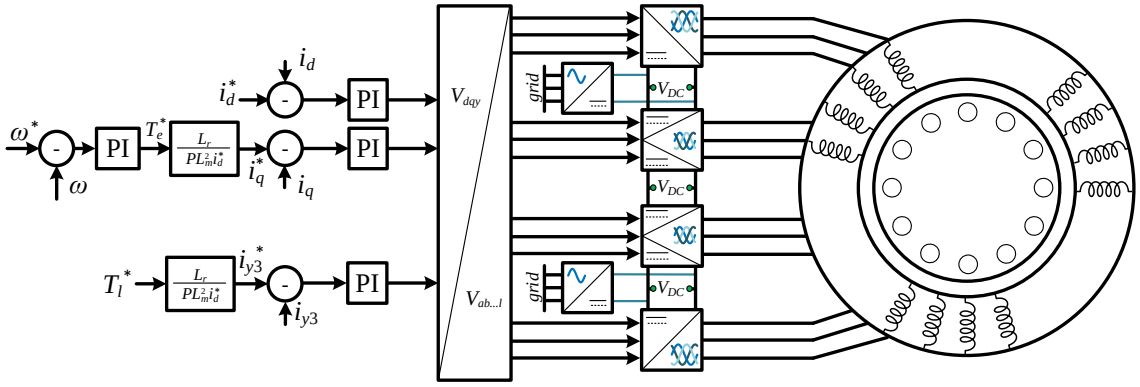

Figure 1: Synthetic loading test control scheme for asymmetrical twelve-phase machine.

3. Simulation Results

The synthetic loading test utilising VSD and IRFOC for twelve-phase machines is validated through Matlab/Simulink. The standard speed-controlled IRFOC scheme is implemented for asymmetrical twelve-phase machine with an extra current controller for i_{y3} as in Figure 1. Initially, the machine's speed reference is set to 950 rpm (99.5 rad/sec). After the machine has accelerated and reached the reference speed, the load torque T_l^* is changed from zero to the desired value, at 1.7 s. The T_l^* is set to be increased every 0.1 s by 4 Nm. The obtained simulation results are illustrated in Figure 2. From the simulation results, after applying the synthetic load torque at 1.7 s, one can notice that the currents in all winding sets are changing according to the change in T_l^*. However, the i_{dq} currents are constants ($i_q = 0$, $i_d = 0.7 \cdot \sqrt{6}$). All the *x-y* loss producing currents are equal to zero excluding i_{y3} where the T_l^* is applied. The winding set powers (Figure 2, third column of the graphs) show the ability of the proposed approach to circulate the power and emulate the rated condition of the machine. The same test is directly applicable to a twelve-phase machine with symmetrical configuration.

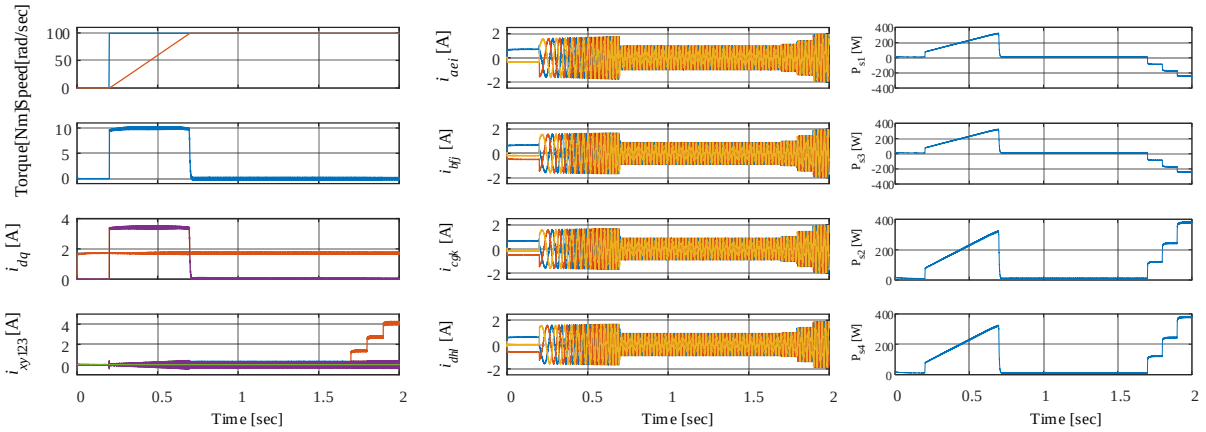

Figure 2: Synthetic loading test simulation results for asymmetrical twelve-phase machine.

4. Conclusion

In this paper, synthetic loading test for symmetrical and asymmetrical twelve-phase machines has been analysed using the new approach. The test is implemented by utilising the IRFOC and VSD modelling approach. The test can be implemented by adding one extra current controller only for the y_3-current component. This current component is found to be consisting of pure β_i current components of the individual winding sets. Moreover, half of the currents appears with a positive and the other half with a negative sign. By implementing the desired torque reference, the temperature-rise test can be achieved. The power is circulated among the winding sets and the necessity for mechanical coupling with another machine is no longer needed. The power drained from the grid will be only to cover the copper, friction and windage losses of the machine, and the power losses of the converters. The developed control scheme has been validated through the simulation results proving that the machine can operate under the nominal speed and currents (causing the temperature-rise) with zero total torque on the shaft.

References

Fong, W. (1972) New temperature test for polyphase induction motors by phantom loading. *Proceedings of the Institution of Electrical Engineers*of Conference.

Ho, S.L. and Fu, W.N. (2001) Analysis of indirect temperature-rise tests of induction machines using time-stepping finite element method. *IEEE Power Engineering Review*, 21 (2), 53-53.

Levi, E. (2016) Advances in converter control and innovative exploitation of additional degrees of freedom for multiphase machines. *IEEE Transactions on Industrial Electronics*, 63 (1), 433-448.

Levi, E., Bojoi, R., Profumo, F., Toliyat, H.A. and Williamson, S. (2007) Multiphase induction motor drives - a technology status review. *IET Electric Power Applications*, 1 (4), 489-516.

Luise, F., Pieri, S., Mezzarobba, M. and Tessarolo, A. (2012) Regenerative testing of a concentrated-winding permanent-magnet synchronous machine for offshore wind generation — Part I: Test concept and analysis. *IEEE Transactions on Industry Applications*, 48 (6), 1779-1790.

McSharry, J.P., Hamer, P.S., Morrison, D., Nessa, J. and Rigsby, J.G. (1998) Design, fabrication, back-to-back test of 14200-hp two-pole cylindrical-rotor synchronous motor for ASD application. *Industry Applications, IEEE Transactions on*, 34 (3), 526-533.

Meyer, A. and Lorenzen, H.W. (1979) Two-Frequency Heat Run - A Method of examination for three-phase induction motors. *Power Apparatus and Systems, IEEE Transactions on*, PAS-98 (6), 2338-2347.

Sheng, M. and Grantham, C. (1994) Synthetic loading of three-phase induction motors by magnetic field magnitude modulation. *IEE Proceedings: Electric Power Applications*, 141 (2), 95-100.

Singh, G. (2002) Multi-phase induction machine drive research—A survey. *Electric Power Systems Research*, 61 (2), 139-147.

Soltani, W., Szabados, B. and Hoolboom, G. (2002) A new synthetic loading for large induction machines with no feedback into the power system. *Energy Conversion, IEEE Transactions on*, 17 (3), 319-324.

Zoric, I., Jones, M. and Levi, E. (2018) Arbitrary power sharing among three-phase winding sets of multiphase machines. *IEEE Transactions on Industrial Electronics*, 65 (2), 1128-1139.

ISSN 2398-6611 (Online)

Steven Duffy A source and drain transient currents technique for trap characterisation in AlGaN/GaN HEMTs

S. J. Duffy[1,a], **B. Benbakhti**[1], **W. Zhang**[1], **K. Kalna**[2], **K. Ahmeda**[2], **M. Boucherta**[3], **N. E. Bourzgui**[3], **H. Maher**[4], **A. Soltani**[4]

[1] Department of Electronics and Electrical Engineering, Liverpool John Moores University, Liverpool, United Kingdom

[2] Nanoelectronic Devices Computational Group, College of Engineering, Swansea University, Swansea, United Kingdom

[3] Institute of Electronics, Microelectronics and Nanotechnology, University of Lille 1, Villeneuve d'Ascq, France.

[4] Laboratoire Nanotechnologies & Nanosystèmes, University of Sherbrooke, Sherbrooke, QC Canada.

[a] S.Duffy@2011.ljmu.ac.uk

Abstract. The source/drain and gate induced charge trapping within an AlGaN/GaN high electron mobility transistor is studied, under normal device operation, by excluding self-heating effects, for the first time. Through direct measurement of current transients of both source and drain terminals, a characterisation technique has been developed to: (i) analyse the transient current degradations from µs to seconds, and (ii) evaluate the drain and gate induced charge trapping mechanisms. Two degradation mechanisms of current are observed: bulk trapping at a short time (<1ms). The bulk charge trapping is found to occur during both ON and OFF states of the device when VDS>0V; where its trapping time constant is independent of bias conditions.

Keywords. AlGaN/GaN HEMTs; Transient Currents; Traps Characterisation; Self-Heating Effects.

1. Introduction

AlGaN/GaN High Electron Mobility Transistors (HEMTs) are predicted to significantly improve efficiency and to dominate applications, e.g. high-power, high-frequency, low-noise, ultra-wide-band communication, ultra-scaled high-temperature, wireless sensors, etc., because of III-Nitrides' wide-bandgaps, high electron saturation velocities and good thermal conductivities [1]. In recent years, these devices have been steadily improving and new record performances have been reported each year [2]. However, their reliability issues persist due to a lack of understanding of physics and mechanisms of charge trapping, self-heating and polarisation [3].

Several studies investigating the current degradation in AlGaN/GaN HEMTs have resulted in differing conclusions [4]–[6]. It is widely agreed upon that transient current degradation involves self-heating and charge trapping, [7]. Some studies of transient drain current suggest that two mechanisms of current degradation of different time constant are caused by both bulk and surface trapping [4], [5]. Other investigations suggest that the two current degradation trends are proportional to self-heating effects that occur at two different times [6]. With the significant impact of the current degradation time constant and magnitude on device reliability and RF performance, it is vital to address its mechanisms and origins.

The aim of this work is to gain insights into the degradation mechanisms of AlGaN/GaN HEMTs, focusing on both source and drain transient current measurements and analyses. We confirm that two current degradation mechanisms occur. At a short time scale (<1ms), the RF performance is restricted by both bulk trapping and self-heating effects. At a longer time scale (>1ms), the dynamic ON resistance degradation is limited mainly by surface trapping accumulation and redistribution. The used device structure and experiment methodology are summarised in Section II, while Section III outlines the results on source and drain current transient measurements, IS and ID, for both degradations. Conclusions are drawn in Section IV.

2. Devices and experimental procedure

2.1 Device Structure and Fabrication

The investigated epi-structure of the AlGaN/GaN Transmission Line Method (TLM) was grown by molecular beam epitaxy on HP-Si (111) substrate, figure 1(a). It consists, from the substrate to the top, of low-temperature AlN(250nm)/GaN(250nm)/AlN(40nm) nucleation layers, a 1.7µm $Al_{0.10}Ga_{0.90}N$ back-barrier to reduce alloy scattering and to improve the carrier confinement of the 2-D Electron Gas (2DEG). A channel is made of a 15nm thick unintentionally doped GaN buffer followed by a 25nm undoped $Al_{0.32}Ga_{0.68}N$ barrier and, finally, a 1nm GaN cap layer. Room temperature Hall measurements yields a sheet resistance of R=398Ω/sq. The CV-technique revealed an electron sheet density of $1.5\times10^{13}cm^{-2}$.

The investigated epi-structure of the AlGaN/GaN HEMT was grown by molecular beam epitaxy (MBE) on HP-Si (111) substrate of a resistivity of 2000Ω.cm, as shown in figure 1(b). MBE was performed using NH_3 for the Nitrogen precursor. The HEMT structure consists, from the substrate to the top, of low-temperature AlN/GaN/AlN (250/250/40nm) nucleation layers, a 1.1µm GaN back-barrier and 1nm AlN exclusion layer to reduce alloy scattering and to improve the carrier confinement of the 2-D Electron Gas (2DEG). A 25nm undoped $Al_{0.28}Ga_{0.72}N$ barrier and, finally, a 1nm undoped GaN cap layer. Room temperature Hall measurements yields a sheet resistance of R=340Ω/sq, an electron sheet density of $1.25\times10^{13}cm^{-2}$, electron mobility of $1480cmV^{-1}s^{-1}$, and dislocation density of $\sim5\times10^{9}cm^{-2}$. The gate metallisation scheme is Ni/Pt/Ti/Mo/Au (5/25/25/30/250nm), where Ti/Al/Ni/Au (10/200/40/100nm) multilayers were used for the source and drain terminals. The contact resistance and specific resistivity are 0.39Ω.mm and $3.8\times10^{-6}\Omega.cm^2$, respectively. The fabrication process flow is similar to that in [8] with additional Si_3N_4 passivation. The I_{DS}-V_{DS} at V_{DS}=20V and I_D-V_G at V_{GS}=0V characteristics of the used AlGaN/GaN HEMT are plotted in figure 1(c).

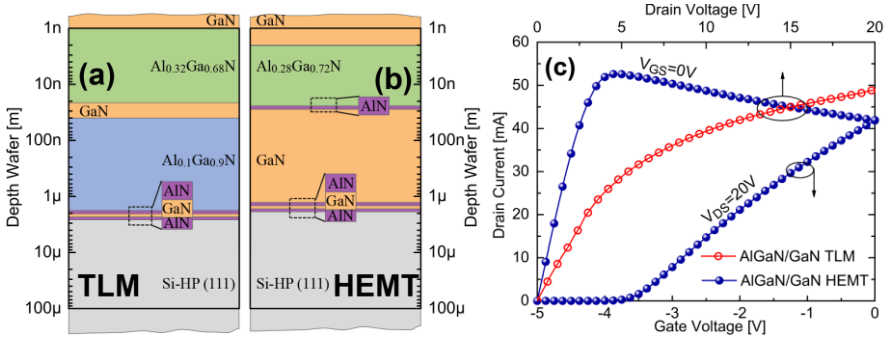

Figure 1: Schematic cross-section of the epi-structures of (a) TLM and (b) HEMT, both grown on Si-

HP(111). (c) I_{DS}-V_{DS} characteristics of used TLM and HEMT (where HEMT is at V_{GS}=0V) and I_{DS}-V_{GS} characteristics at V_{DS}=20V for HEMT. The source-to-drain distance and device width are 5µm and 100µm, respectively, for HEMT and 8µm and 100µm for TLM.

2.2 Experimental methodology

In order to investigate the charge trapping involved in the AlGaN/GaN HEMT structure, we propose two experiments. The pulse waveforms, given in figure 2(a), were used to characterise the bulk trapping mechanism. Here, V_{DS}=0V and V_{GS}=0V were pulsed to V_{DS1} and V_{GS1}, respectively, for a measurement time of $t_{meas,1}$=1s. The pulse waveforms, given in figure 2(b), were used to investigate surface trapping behaviour. Quiescent biasing conditions, V_{DSQ} and V_{GSQ}, were set whereby pre-charging of surface trapping occurred. Measurements were then taken at V_{DS2}=10V and V_{GS2}=0V for a time $t_{meas,2}$=1s. An illustration is provided in figure 2(c) showing both bulk and surface trapping mechanisms.

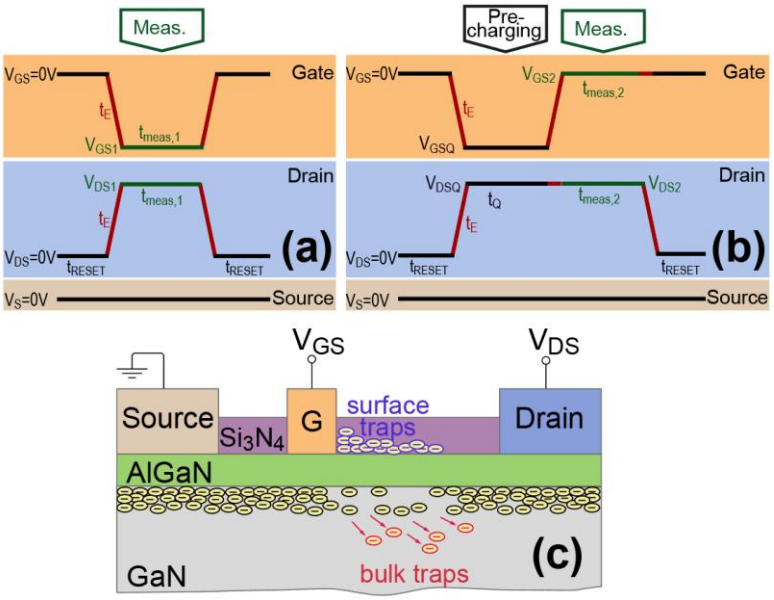

Figure 2: Pulse waveforms used for I_S and I_D transient measurements for: (a) without traps pre-charging and (b) with traps pre-charging, where t_{RESET}=10s and t_E=200ns. (c) The schematic diagram of bulk and surface trapping mechanisms are illustrated for a semi-ON-state at V_{DS}>0V in AlGaN/GaN HEMT.

3. Results and discussion

For the first time, experimental measurements of both source and drain transient currents were analysed to understand charge trapping kinetics under normal device operation. To attain this, the experiment illustrated in figure 2(a) was used. The current transients, I_S and I_D, monitored at V_{DS1}=20V various gate biases, V_{GS1}=0V to -3V, are shown in figure 3. Measurements were also taken for V_{DS1}=10V and V_{DS1}=15V (not shown). Under high V_{DS1}, a large peak in electric field at the drain-side of the gate is induced. As a result, electron trapping in the drain access region of the device increases channel resistance [9]. This is indicated by the difference between I_S and I_D.

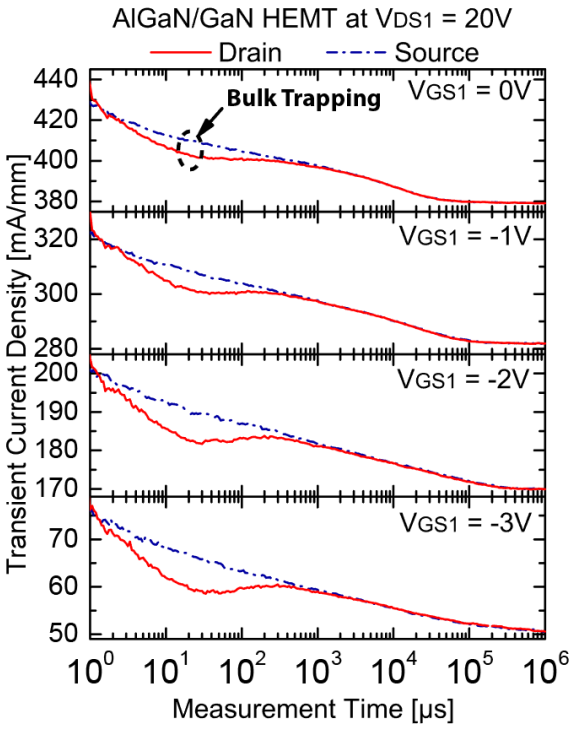

Figure 3: Transient behaviour of the drain, I_D, and source, I_S, currents, versus measurement time on log-scale using the pulse waveforms given in figure 2(a) with V_{DS1}=20V, at V_{GS1}=0V to -3V. Two degradations of current are observed at different time constants, DEG1 and DEG2.

To analyse the effect of the bias conditions on the initial charge trapping phase (DEG1), the difference between I_S and I_D (I_S-I_D) under V_{DS1}=10V, 15V and 20V at different gate biases, V_{GS1}=0V to -3V were measured, figure 4(a). We find that a significant increase in bulk trapped charge density, indicated by the increase of $(I_S\text{-}I_D)_{max}$ from 3.8mA/mm to 7.0mA/mm, is observed when V_{DS1} is increased from 10V to 20V, figure 4(b). However, there is no change in trapped charge density upon increasing the magnitude of V_{GS1}. Also, bulk trapping time constant is shown to be independent of V_{DS} and V_{GS}.

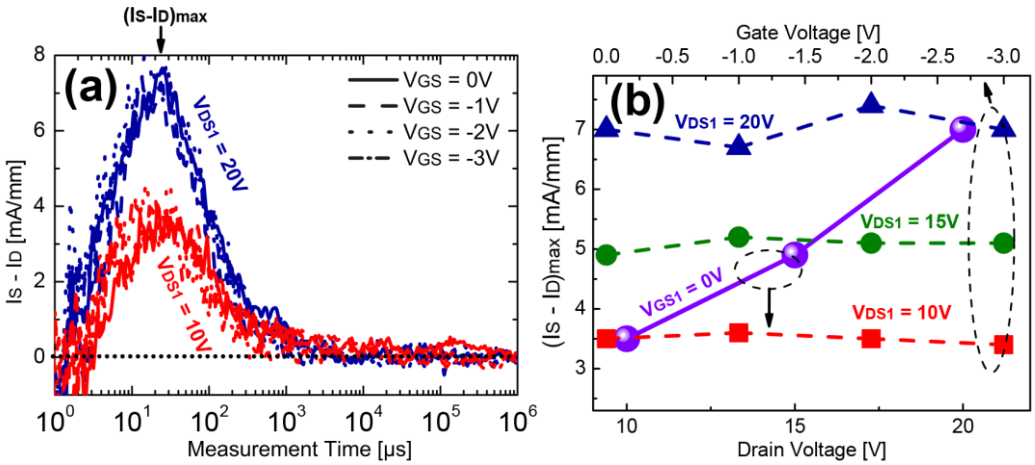

Figure 4: (a) I_S and I_D difference (I_S-I_D) versus the measurement time at V_{DS1}=20V and 10V for different gate voltages (V_{GS1}=0V to -3V); indicating the bulk trapping process (DEG1). (b) The impact of drain voltage, V_{DS1}, and gate voltage, V_{GS1} on $(I_S\text{-}I_D)_{max}$ given at t≈30µs; unlike V_{DS1}, V_{GS1} shows a negligible impact on bulk trapping characteristics.

4. Conclusion

In this paper, a new source and drain transient currents, I_S and I_D, technique for charge trapping characterisation in AlGaN/GaN HEMTs, under normal device operation, has been developed. Using this technique, charge trapping behaviours, with the exclusion of self-heating, have been analysed. The mechanisms of bulk trapping that occurs on a time scale of <1ms has been identified.

Through monitoring the difference between I_S and I_D, bulk trapping time constant is shown to be independent of V_{DS} and V_{GS}. Although, V_{DS} is found to affect the bulk trap density. Large V_{DS} is found to be a cause of bulk charge trapping during both ON and OFF states of the device.

References

[1] J. J. Komiak, *IEEE Microwave Magazine*, vol. 16, no. 3. pp. 97–105, 2015.

[2] Y. Tang, K. Shinohara, D. Regan, A. Corrion, D. Brown, J. Wong, A. Schmitz, H. Fung, S. Kim, and M. Micovic, *IEEE Electron Device Lett.*, vol. 36, no. 6, pp. 549–551, 2015.

[3] K. Ahmeda, B. Ubochi, B. Benbakhti, S. J. Duffy, A. Soltani, W. D. Zhang, and K. Kalna, *IEEE Access*, vol. 5, pp. 20946–20952, 2017.

[4] D. Bisi, M. Meneghini, C. De Santi, A. Chini, M. Dammann, P. Bruckner, M. Mikulla, G. Meneghesso, and E. Zanoni, *Electron Devices, IEEE Trans.*, vol. 60, no. 10, pp. 3166–3175, 2013.

[5] J. Joh and J. A. Del Alamo, *IEEE Trans. Electron Devices*, vol. 58, no. 1, pp. 132–140, 2011.

[6] Y. Zhang, S. Feng, H. Zhu, C. Guo, B. Deng, and G. Zhang, *IEEE Electron Device Letters*, vol. 35, no. 3. pp. 345–347, 2014.

[7] T. A. Chowdhury, *Int. J. Emerg. Technol. Adv. Eng.*, vol. 4, no. 2, pp. 678–685, 2014.

[8] A. Soltani, J. C. Gerbedoen, Y. Cordier, D. Ducatteau, M. Rousseau, M. Chmielowska, M. Ramdani, and J. C. De Jaeger, *IEEE Electron Device Letters*, vol. 34, no. 4. pp. 490–492, 2013.

[9] T. Brazzini, M. A. Casbon, H. Sun, M. J. Uren, J. Lees, P. J. Tasker, H. Jung, H. Blanck, and M. Kuball, *Microelectron. Reliab.*, vol. 55, no. 12, Part A, pp. 2493–2498, Dec. 2015.

ISSN 2398-6611 (Online)

Quang Huy Nguyen Optimized Indoor Positioning for static mode smart devices using BLE

Q.H.Nguyen, P. J., T. T. Nguyen and M. Randles
Faculty of Engineering and Technology, Liverpool John Moores University
Liverpool, UK, L3 3AF
E-mail address: Q.H.Nguyen@20l6.ljmu.ac.uk, {P.Johnson, T.T.Nguyen, M.J.Randles}@ljmu.ac.uk

Abstract. Bluetooth Low Energy (BLE) technology and BLE-based devices such as iBeacons have become popular recently. In this work, an optimized indoor positioning approach using BLE for detecting a smart device's location in an indoor environment is proposed. The first stage of the proposed approach is a calibration stage for initialization. The Received Signal Strength Indicator (RSSI) is collected and pre-processed for a stable outcome, in the second stage. Then the distance is estimated by using the processed RSSI and calibrated factors in the third stage. The final stage is the position estimation using the outputs from the previous steps. The positioning technique, which is an improved Least Square estimation is evaluated against the other well-known techniques such as, Trilateration-Centroid, classic Least Square Estimation in estimating the user's location in the 2D plane. Experimental results show that our proposed approach has promising results by achieving an accuracy of positioning within 0.2 to 0.35m.

Keywords. Localization; Indoor Location; Bluetooth Low Energy; iBeacon, RSSI

1. Introduction

Indoor positioning is the ability to locate people or objects inside a building. The focus and need for this ability has greatly increased recently. Indoor positioning offers four main applications categorized as proximity marketing /advertising, way-finding/ navigation, search/ requesting help, and asset or people tracking. Hence, this topic is a huge attraction for researchers. At present, the well-established positioning systems, such as Global Navigation Satellite System (GNSS) including the famous Global Positioning System (GPS) can only provide good performance in outdoor environment. The signal from satellites is blocked by walls, people and other objects. Moreover, the acceptable error range for an outdoor positioning might be larger than an indoor environment. This means that the available GPS chips on the market cannot adapt to the requirements of indoor positioning. There are several challenges an indoor positioning system need to address: accuracy, complexity, cost, scalability, power consumption, noise and interference [1-2].

In this abstract, a novel optimized approach for indoor positioning from RSSI based estimation using BLE is introduced. In our approach, the environment factor and received power factor are calibrated using linear regression. We have evaluated the effectiveness of the traditional filters such as Kalman filter, Gaussian filter, feedback filter and average filter in combating the instability due to unreliable RSSI feed. Following this, the distance is calculated, and location of the user is estimated using an improved version

of Least Square Estimation. Finally, we have compared the performance of our technique with that of other methods. For this stage of research, we have considered the user's smart device as static with a Line-Of-Sight communication. Our next stage of research will evaluate the technique in real-life environment that includes noise from various sources, and mobility added to the user's device.

The rest of this abstract is organized as follows: section 2 describes our proposed technique; section 3 discusses the experiment and results and section 4 is the conclusion and future work.

2. Proposed Method

2.1 Propagation model and factor calibration

The most commonly used indoor propagation model is the log-normal shadowing. It represents and simplifies the relationship between RSSI, distance and "noise" term as shown in equation (1) below:

$$RSSI = A - 10 \times \eta \times \log_{10}(d/d_0) \quad (1)$$

In this formula, d is the distance between transmitter and receiver; A is the RSSI at a reference distance $d_0 = 1m$; η is the environment factor or "noise" factor.
Under the complexity of different indoor environments such as multipath, human body, interference etc., and devices condition such as battery life, antenna direction, choosing a generic set value of A and η can cause errors in ranging estimation later. Hence, these factors should be calibrated and corrected. Solving (1) gives the value of A, η for a specific area and a device.

2.2 RSSI processing

The RSSI is vulnerable to the environment. It strongly depends on multipath propagation. Various other conditions, such as transceiver direction, battery level, obstacles, device model, etc. will also affect the RSSI value. Hence, smoothing and stabilizing the RSSI signal is critical to achieve a satisfactory result in indoor positioning. Fig. 1 shows the RSSI over time at 1m, 5m and 10m.

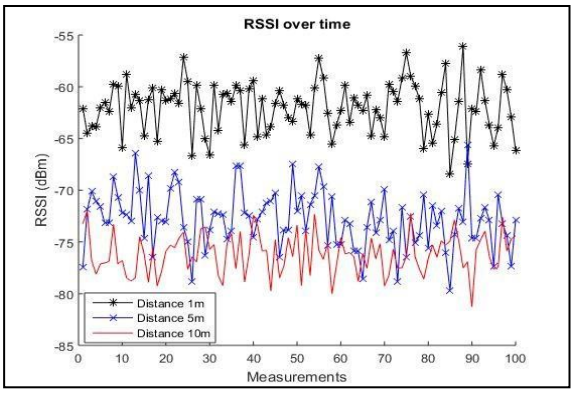

Fig. 1. RSSI over time

Several filters including averaging filter, feedback filter [3], Gaussian filter and Kalman filter [4] were applied for smoothing the RSSI in this work.
On the other hand, to utilise the RSSI processing and minimised error in the later location estimation, the antennas orientation between iBeacons and a BLE receiver were study. We divided the space into eight directions as figure 4. The iBeacons and a mobile device were placed parallel and at same height level. The distance between them are 1m. The results in Fig. 2 shows that, signals are varied as large as 9dBm when iBeacons rotating from West side to East side. This observation recommended that the antennas of beacons should be pointed to user's device within 135 degrees.

Fig. 2. Orientation study

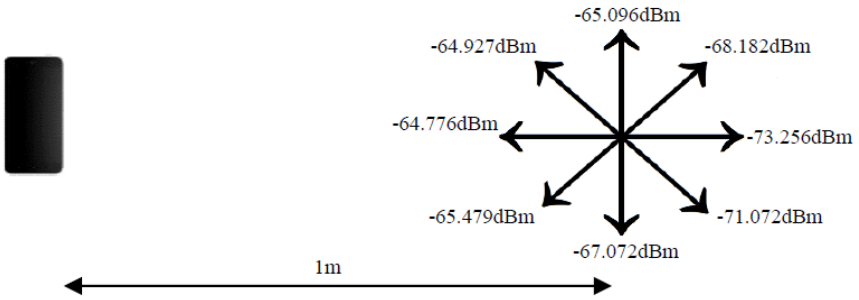

Fig. 2. Orientation study

2.3 Location Estimation

The distance between beacons and a device can be obtained using the log-normal shadowing and calibrated factor as formula 2. Then an improved version of Least Square Estimation (LSE) technique is used to estimate the user's location. In the classic LSE, it always uses the position (0, 0) as the initialization. The main idea of this improvement is cooperating with the priori position which is a trilateration – weighted centroid result and finding the value of change in distance between two immediate states.

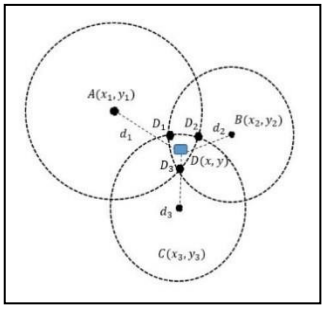

Fig. 3. Trilateration – centroid calculation

Figure 5 shows the trilateration and centroid calculation. The Euclidean distance between the beacon and device, which is represented as a function of x and y, shown below:

$$d_i^k = f(x^k, y^k) = \sqrt{(x^k - x_i)^2 + (y^k - y_i)^2} \quad (4)$$

where d_i^k is the distance from beacon i to device at the time state k (x^k, y^k) is the estimate position and (x_i, y_i) is the beacon i position.

Using Taylor expansion to find the distance in the next time state k+1, for n beacons in 2D dimension and static devices, we can express (4) as a series of matrices representing the coordinates over the Euclidean distance, change in Euclidean distance and change in time states of coordinates (5-7).

$$\mathbf{M} = \begin{bmatrix} \frac{x_1 - x^k}{d_1^k} & \frac{y_1 - y^k}{d_1^k} \\ \vdots & \vdots \\ \frac{x_n - x^k}{d_n^k} & \frac{y_n - y^k}{d_n^k} \end{bmatrix} \quad (5) \qquad \beta = \begin{bmatrix} d_1^{k+1} - d_1^k \\ \vdots \\ d_n^{k+1} - d_n^k \end{bmatrix} \quad (6) \qquad \hat{\mathbf{x}} = \begin{bmatrix} \Delta x^k \\ \Delta y^k \end{bmatrix} \quad (7)$$

This becomes a Least Square problem with solution of finding: $M\hat{x} \approx \beta$. Solving this problem gives us the change in distance between two immediate states.

3. Experimental results

3.1 Calibration and RSSI filtering

The calibrated result gives the environment factor for our testbed as $\eta = 2.6472$. The received signal strength at 1m is A = -54.6476 dBm.

Fig. 4 shows the calibration process and measurements for raw RSSI data and RSSI data after applying feedback filter, Gaussian filter and Kalman filter at 1 meter and 5 meters.

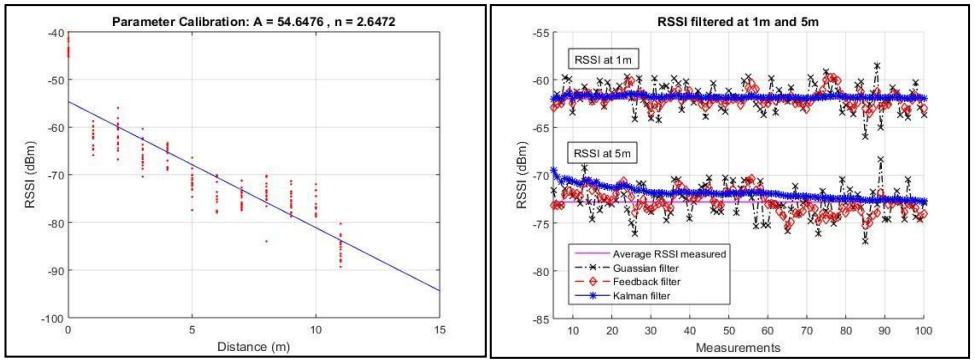

Fig. 4. Calibration and RSSI filtered

The results show that in general all filters help smoothing the RSSI measurement. At 1m, Gaussian filter gives the variance of 1.97 whereas Feedback filter gives the variance of 0.62 and Kalman filter gives the least variance at 0.11. At 5m, Gaussian filter has 2.73 variance whereas Feedback filter and Kalman achieves 1.62 and 1.13 variance respectively. It can be seen that Kalman filter has the best

performance out of the three filters. It smooths the RSSI very close to the mean value.

3.2 Positioning results

Fig. 5 shows the experimental results for the three positioning calculations when applying Kalman filter for RSSI measurements. Table II compares the accuracy among approaches.

As can be seen, our proposed approach has the best performance compared to two other classic approaches in terms of positioning for static device in our specific testbed. The mean error for Trilateration-weighted Centroid is 0.375m. The mean error for classic LSE is 0.333m. The improved LSE performs the best with a mean error of 0.192m. This is the result of correcting factor and smoothing the RSSI value.

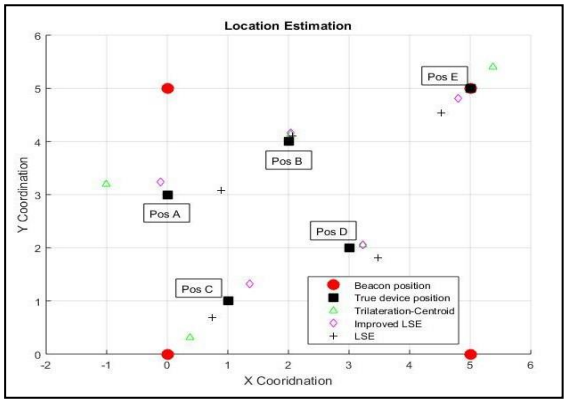

Fig. 5. Indoor positioning results TABLE

I. POSITIONING ACCURACY

Method	Average error	Maximum error
Trilateration-weighted Centroid	0.375 m	1.009 m
LSE	0.333 m	0.89 m
Improved LSE	0.192 m	0.354 m

4. Future work and conclusion

In this work, an optimized indoor localization for static device was proposed. It uses RSSI-based BLE technology. The factor calibration process was explained and several different RSSI filters were tested. Three different approaches namely, Trilateration-weighted Centroid, classic LSE and improved LSE for position estimation were discussed. We have shown that our positioning approach can achieve very high accuracy in terms of positioning for static device and its output is very promising. Experiments results also shows that the improved LSE method outperforms the other techniques with a high accuracy of about 0.2 - 0.35m. As a next step in our research, dynamic devices and tracking application using our approach will be investigated. Also, there will be a remodeling in factor calibration for a more complicated indoor environment.

References

[1] G. Dedes and A. Dempster, "Indoor GPS positioning - challenges and opportunities", VTC-2005-Fall. 2005 IEEE 62nd Vehicular Technology Conference, 2005.

[2] K. Al Nuaimi and H. Kamel, "A survey of indoor positioning systems and algorithms", 2011 International Conference on Innovations in Information Technology, 2011.

[3] J. Anuradha, S. Lokuliyana, D. Chathurangi and D. Vithana, "Indoor Positioning: Novel Approach for Bluetooth Networks using RSSI Smoothing", International Journal of Computer Applications, vol. 137, no. 13, pp. 26-32, 2016.

[4] S. Lee, I. Lim and J. Lee, "Method for Improving Indoor Positioning Accuracy Using Extended Kalman Filter", Mobile Information Systems, vol. 2016, pp. 1-15, 2016.

ISSN 2398-6611 (Online)

Rosie Horner Biomimicry- Can copying the micro-topography pattern of the Cockle Cerastoderma edule give antifouling properties to marine steel?

R Horner [1,3]**, P French** [1,4] **and S Durr** [2,5]
[1] General Engineering Research Institute, Byrom St, Liverpool L3 3AF
[2] School of Natural Sciences and Psychology, Byrom St, Liverpool L3 3AF
[3] R.Horner@2015.ljmu.ac.uk
[4] P.French@ljmu.ac.uk
[5] S.T.Durr@ljmu.ac.uk

Abstract. Biofouling is the unwanted attachment of marine organisms to a surface. It is a costly problem for maritime industries, but it also reduces the survival of fouled marine organisms. However, some marine organisms have evolved defence mechanisms to the problem in the form of micro-scale patterns on their surface. This study uses bio-inspiration of these micro-scale patterns from the common cockle shell to produce patterns on steel using laser processing to reduce biofouling. Steel patterns are submerged in the waterbody at the Albert Dock, Liverpool, and data is collected on settlement of marine organisms on each pattern. The results show that bio-inspired micro-scale patterns are reducing the amount of settlement. Therefore there is potential for bio-inspired micro scale laser patterns to be used as a non-toxic, eco-friendly and universal anti-fouling technology in Martine industries.

Keywords. Fouling, bio-fouling, bio-mimicry, bio-inspiration, micro-textures, antifouling,

1. Introduction

Biofouling is described as the colonisation process of a solid surface submerged in the marine environment (Wahl, 1989). This colonisation of surfaces by marine organisms is a costly problem maritime industries as biofouling can weaken surfaces, increase rust and corrosion and increase drag of ships. It has been estimated that the US navy alone has spent an average of 1 billion US dollars on problems related to biofouling on their ships in the last 15 years (Schultz *et al*, 2011). As money is being lost through biofouling, therefore there is a large market for antifouling (AF) coatings and technologies.

Biofouling has negative effects on maritime industries, however, biofouling also has negative effects on marine organisms. Fouled organisms have a reduction in mobility and reproduction (Buschbaum and Reise, 1999). Reduced mobility will inhibit the fouled organism's ability to forage for food, and escape predators and therefore it will be more likely to die. Reduced reproduction will mean that the fouled organism is less likely to pass on their genes to the next generation. However, there is an instinctive evolutionary pressure to survive and pass on genes to the next generation. This evolutionary pressure to survive has resulted in natural defence mechanisms to develop within species to reduce the effects of biofouling. One of these natural defence mechanisms is micro-topographies on the outermost surface of the skin. Due to convergent evolution, this type of defence mechanism is

seen across a wide range of species including mussels, crabs, sharks and whales (Scardino et al, 2003; Bers & Wahl, 2004; Kirschner and Brennan, 2012; Baum et al, 2002).

This research aims to target the gap in the AF market for a universal, non-toxic, eco-friendly antifouling technology by using laser processing to produce micro-topographies on marine grade steel that mimic the patterns produced on the surface of marine organisms as a natural biofouling defence. We hope that by mimicking the natural defences of marine organisms we can reduce biofouling on steel that is used in maritime industry and provide a safe alternative in the AF market. This project is focused on reducing settlement within the biofilm layer, as this layer is the first to form, and it encourages further settlement of larger macro-foulers. By targeting the biofilm layer, there is less chance of macro-foulers settling as the diatoms and bacteria that is often used as food for larger species will not be present in abundance.

2. Methods

This study focuses on the micro-topography pattern of the common cockle *Cerastoderma edule*. Cockle shell samples were collected from Thurstaston beach, UK, and cleaned in ethanol to remove any debris. The shell was placed under a 3D topography scanner (GFM) and the surface topography was observed (figure 1).

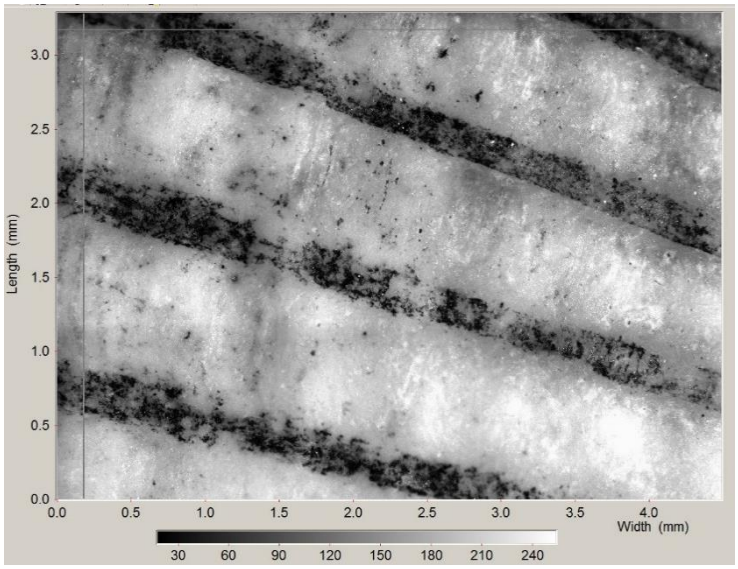

Figure 1 3D scan of Cockle shell C. edule with depth (um) shown by grayscale chart.

The scans revealed that the topography of the shell is straight ridges with valleys between the ridges. With this as inspiration, the laser parameters are programmed and 4 surfaces were produced to mimic the straight lined ridge type pattern of the Cockle shell.

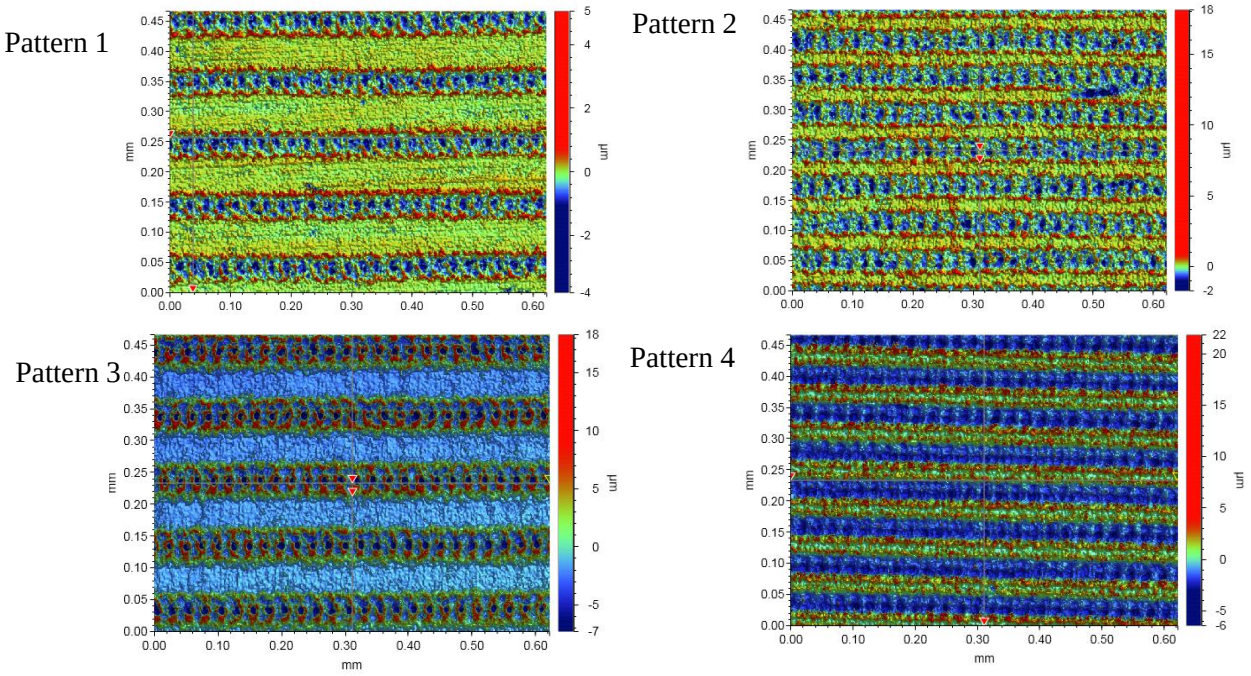

Figure 2 3D scan of Cockle inspired patterns produced using laser processing with height (um) shown by colour chart

The laser processed steel with patterns 1, 2 ,3 and 4 were submerged in the Albert Dock, Liverpool, for a week along with a control panel which was a smooth surface and had no laser processing. There were 5 replicates per pattern.

2.1 Data Collection

Once removed from the dock, panels were preserved in ethanol and photographed under x50 magnification. The number of individuals (a single marine organism) were counted. Statistical analysis of the data collected was carried out in SPSS. A three factor nested ANOVA was used as well as Post hoc Dunnet's test.

3. Results

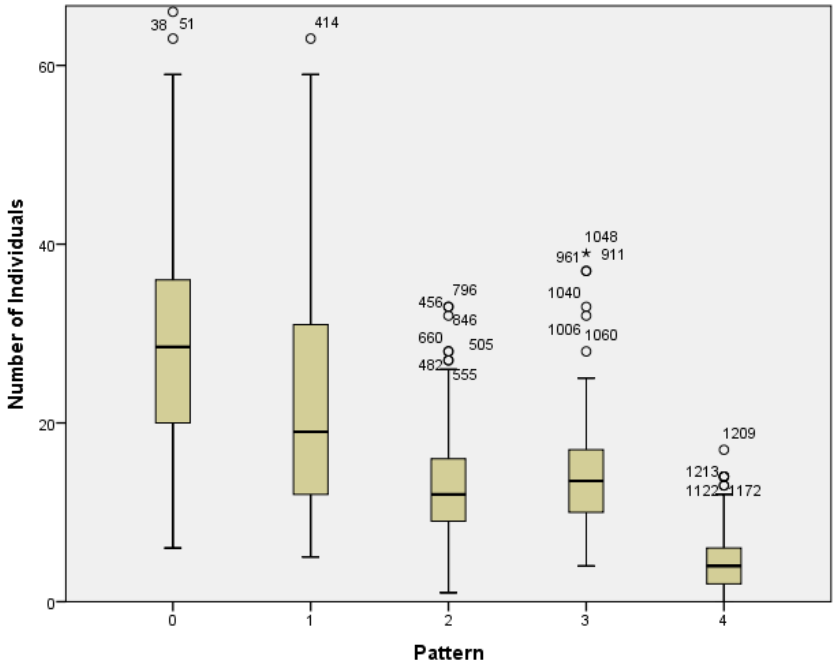

Figure 3 Number of Individuals per Pattern where Pattern 0 is the unprocessed control. All patterns were significantly different ($p<0.01$) expect Pattern 2 and Pattern 3.

All of the patterns showed a significant decrease in the number of marine organisms settled on the surface compared to the control pattern ($p<0.01$). Pattern 4 (figure 3) had the least amount of settlement, therefore was the best AF pattern.

3. Discussion

We have found that laser processing a micro topography pattern onto a steel surface has reduced the settlement of marine organisms. These results are consistent with previous studies on micro-topography patterns such as Sharklet ™ and others on silicones (Schumacher *et al*, 2007), however, these previous studies have been lab based, and tested using only one alga species *Ulva.* Whereas, our results are from a field work study, which is a greater reflection of the real world as our surfaces are submerged in a fully functioning ecosystem, where species interactions and environmental conditions can also effect settlement. This highlights the importance of this study as there are very few field work tests of micro-topographies as an antifouling technology.

It is easier for micro-fouling species such as diatoms and bacteria to settle on smooth surfaces such as the unprocessed control than the micro-topography patterns. The number of attachment point is reduced when the surface is not flat, therefore the individual cannot have full contact with the surface (figure 4), leading to reduced attachment of individuals on micro-topography patterns.

Figure 4 A schematic illustration of theoretical attachment points of a diatom; (a) attachment on a flat surface and (b) attachment where micro-topography is smaller than the diatom adapted from (Adapted from Scardino *et al*, 2006).

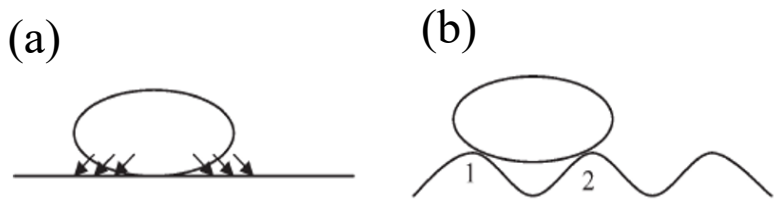

Pattern 4 was the best AF pattern, as it had the least number of individual organisms settled on the surface. Pattern 4 had narrow flats and and deep valleys and it is these characteristics that are similar to the small narrow valleys of the Cockle shell topography that have made it a good antifouling surface. The patterns with larger flats (P1 and P3) had a higher medium settlement than patterns with narrower flats (P2 and P4) because the larger flats allowing a larger flatter space between laser spots for settlement like in Figure 4a to occur.

Table 1 Characteristics of the laser processed patterns.

	Larger flat	Narrow flat
Shallow ridge	Pattern 1	Pattern 2
Deep ridge	Pattern 3	Pattern 4

5. Conclusion

Overall, the concept of using laser processed micro-topographies inspired by natural surfaces to produce an anti-fouling technology looks promising as this study clearly demonstrates laser processing micro-topographies reduces settlement of marine organisms. This study focuses on the patterns produced by *C. edule*, however, for the whole of the PhD project lots of different species will be studied including shore crabs *Carcinus maenas* and mussels *Mytilus edulis.* The hope is that characteristics from these species can be combined in the laser processing stage, to produce an optimum pattern that will be able to be commercialised as an AF technology.

6. References

Baum, C., Meyer, W., Stelzer, R., Fleischer, L.-G., & Siebers, D. (2002). Average nanorough skin surface of the pilot whale (Globicephala melas, Delphinidae): considerations on the self-cleaning abilities based on nanoroughness. Marine Biology, 140(3), 653-657.

Bers, A. V., & Wahl, M. (2004). The influence of natural surface microtopographies on fouling. Biofouling,

20(1), 43-51.
Buschbaum, C. and K. Reise (1999). Effects of barnacle epibionts on the periwinkle Littorina littorea (L.). Helgoland Marine Research 53: 56-61.
Corbett, J. J., and H. W. Koehler (2003), Updated emissions from ocean shipping, J. Geophys. Res., 108, 4650-4661.
Kirschner, C. M., & Brennan, A. B. (2012). Bio-inspired antifouling strategies. Annual review of materials research, 42, 211-229.
Scardino, A., & de Nys, R. (2004). Fouling deterrence on the bivalve shell Mytilus galloprovincialis: a physical phenomenon? Biofouling, 20(4-5), 249-257.
Scardino, A. J., Harvey, E., & De Nys, R. (2006). Testing attachment point theory: diatom attachment on microtextured polyimide biomimics. Biofouling, 22(1), 55-60.
Schultz, M. P., Bendick, J. A., Holm, E. R. & Hertel, W. M. (2011). Economic impact of biofouling on a naval surface ship. Biofouling, 27, 87-98.
Wahl, M. (1989). Marine epibiosis. I. Fouling and antifouling: some basic aspects. Marine Ecology Progress Series, 58, 175-189.

ISSN 2398-6611 (Online)

Harry Pointon Selective high resolution path generation for UAVs with positional assurance validation.

Harry A.G Pointon
Liverpool John Moores, James Parsons Building, Byrom Street, Liverpool, L3 3AF
E-mail address: h.a.pointon@2016.ljmu.ac.uk

Abstract. With the growth in UAV adoption in Search And Rescue (SAR), the need for efficient implementation to minimise the impact of the new technology has been previously investigated. Although pilot guided UAVs have been proven to aid in the processes involved with SAR operations the resource drain of removing crew members from normal operation is often problematic. Autonomous UAVs therefore present the solution, however, the loss of a human's ability to recognise features is a major downside e; therefore the solution is a system capable feature identification such as gas concentration peaks, thermal hotspots or radio frequency signals (RF). To reduce the time cost of mapping a large space, the advantages of covering the space at a "high resolution", low altitude, with fine sweeps must be weighed against the downsides of "low resolution", high altitude and broad sweeps. By utilising a feature recognition system onboard the UAV, a selective approach to the coverage resolution may be adopted, giving context to of the surrounding environment with low "cost" low resolution mapping paths, and high "cost", high resolution passes over areas of interest. One factor which must therefore be investigated is the efficacy of the positional systems of a UAV. Understanding the uncertainty of a positional measurement allows for the specification of coverage density and level to which the SAR operatives may trust the information. From this a faster, more robust implementation of UAVs may be achieved with less impact on the SAR crew members.

Keywords. UAV, Search and Rescue, Localisation

1. Introduction

Many studies have been focused on implementing new technology into proven and conventional Search and Rescue (SAR) operation techniques [1] [2] [3] [4] [5]. The main aspects of focus, being that of communication, command and resource allocation. In other words, how the information gained from the new system is distributed, how this information is filtered, passed and used by those in command of the incident and the impact of employing the proposed technology on workload, time and equipment transport. The technology required to implement large scale outdoor mapping of unknown spaces using unmanned aerial vehicles (UAVs) has in recent years matured to the point at which it is now feasible to for these systems to aid in Search and Rescue operations. A primary advantage of UAVs over traditional airborne reconnaissance is the cost reduction and the speed of deployment [6]. With the increased capability of the platforms, the efficacy of their use must be assessed with respect to their impact on the

SAR team. To what level does the UAV platform impact personnel and resources, and how does this effect balance against their benefit? In SAR operations the initial phase of response is that of investigation, reconnaissance and planning, with periodic returns to this phase to reassess the situation and update information [7]. An issue raised by several studies regarding the use of robotic assistance systems in SAR environments is the level to which the team trust the information supplied by the system. The level of confidence in the assistive technology is related to the use of said technology; if the system is in use by an experienced team familiar with its capabilities and shortcomings they are more likely to more effectively integrate it within their operations, while a team unfamiliar of a system's capabilities are more likely to use the system in a less effective manner [1]. An example of this is the reassessment of information gathered in the initial reconnaissance phase [2]. Unfamiliarity with a system's reliability leads to more frequent returns to update information gathered at best, and at worst a return to traditional techniques to confirm information [1] [3].

One point of application for UAVs is that of aerial mapping of the incident space [2] [3] [1]. As in the event of an earthquake, terrorist incident or lost person in a large area, the available maps may not be up to date due to fire, building collapse, weather or traffic [7] [2]. The area of total coverage path planning for UAVs is much studied, with several effective approaches developed. These approaches are usually dependent upon the characteristics of the space to be covered, whether the area is large or small in scale with regard to the coverage time of a path and whether the area is unknown or is there is prior knowledge. As time is often critical in SAR situations total homogeneous coverage of a space may be inefficient, especially when only a certain area is of interest. Although the context given by a high resolution total area map is useful, the time sensitive nature of incidents means that this method of coverage is also not feasible [6]. The proposed system under development is a method for variable intensity coverage of large outdoor spaces using UAVs aimed at SAR applications. By initially designating a high pass sweep of a space, aimed at the generation of low resolution context, while monitoring for pre-defined "data of interest" fast total coverage of a space may be achieved. In the event of the detection of an example fitting the "interesting data" criteria the altitude and spacing of the sweeps may be altered to increase the resolution of the scan, leading to a more dense mapping of the space.

This approach raises 2 main areas for investigation to allow effective implementation. Firstly, the method of initial coverage generation and its alteration. Secondly the method by which the agent is to be localised. As previously discussed successful integration of a new technology requires the human-robot cooperation be assessed. If the system's accuracy is unknown then integration will suffer. The system's effectiveness is therefore dependent upon the characterisation of its sensing capabilities. If the system's positional estimation is accurate only on an order of magnitude greater than the target size, then the generated high resolution scanned area must account for such uncertainty. From this a certainty of position may be passed to the SAR teams along with an estimate of the space within which the target is located.

2. Total Coverage Path planning

When considering the total coverage of an unknown space, factors such as the aim of the coverage, the sensors employed, prior knowledge of the space and, the movement characteristics dictate the method of path generation [8]. In the case of a UAV, of the multirotor format, the movement may be considered pseudo-holonomic; to say that although there is some form of pose alteration required for translation in

all axis, however this pose alteration is on a scale such that it does not impact its path following capabilities. The case may also be made that due to the disaster relief and emergency response application, there is little or no prior knowledge of the space, so it may be considered empty, therefore requiring total coverage. Obstacles may be considered of no impact as the pathing may take place at an altitude greater than such obstacles may lie. Finally, as the aim of the coverage is to generate an up to date map of the space in question optical sensors are in use. Therefore the coverage may be dictated based upon the characteristics of the camera employed. Based upon these characteristics, a boustrophedon pathing system may be suitable. Boustrophedon pathing being the sweeping of a space perpendicular to it's longest edge, incrementing a set distance and again moving perpendicular until the space is cleared. Issues with this system involve the homogeneous pathing generated, as often an entire space is not of equal interest, so the proposed system would incorporate a variable altitude and coverage density to account for areas of higher "interest".

3. Localisation Technology

As the use case for the defined system is to be outdoors over a large scale unknown environment the possible systems available for localisation may be narrowed down. As the space is unknown, it may be assumed that prior work to prepare the system may not be employed, therefore systems relying upon markers, off-board cameras or beacons in the space are not feasible. As the application is outdoor mapping, and the system a UAV, Global Navigation Satellite Systems (GNSS) may also be considered available. Finally as the UAV system is to be deployed over a large scale space, tracking via RADAR or laser distance measurement systems are also not practical [8] [9]. This is due to the small size of the UAV requiring expensive, complex technology for tracking on that scale, which lies beyond the scope of this paper. Therefore, these constraints leave UAV based positional sensing systems, such as Inertial Measurement Units (IMUs), distance sensing units such as the LidarLite or Ultrasound sensors and GNSS [10]. These systems provide allocation estimate, whose uncertainty is based upon a number of factors. For example, in the case of GNSS systems, solar weather, atmospheric conditions and local structures play a large part in the positional reading's uncertainty [11]. However, it may be assumed in some cases that the uncertainty of a system's positional estimate is gaussian, from this assumption covariance matrices may be constructed. From this covariance matrix or "sensor noise" matrix a state estimation system may be constructed. Using the kinematic equations for the intended system, a theoretical estimate of the agent's position may be generated from the last positional reading. This estimate may then be compared to the input readings form then location sensors and using a "confidence coefficient" an estimate of more certainty may be drawn. This is the foundation for so called "Kalman Filters". Of course the non-linearity of a system must be taken into account when dealing with systems of high to large non-linearity, in these cases an Extended Kalman Filter (EKF), Unscented Kalman Filter (UKF) or, Particle Filter (PF) may be employed [8]. In the case of an EKF non-linearity is taken into account via a Jacobian. A challenge may be drawn from form this formulation of state estimation systems, that the reduction of uncertainty of a localisation system relies upon how well the uncertainty of the sensor is characterised.

3.1 Positional Assurance

UAV systems in the UK are governed by the Civil Aviation Authority (CAA), currently the CAA have issued an set of legislative guidance on the operation of UAVs referred to as the Air Navigation Order 2016 (ANO). Within this are the documents CAP 722 and CAP 393 which deal in more specific details related to the deployment of UAVs and their autonomy. CAP 722 requires a certificate for autonomous systems, this would involve the proposed system of automatic path alteration. A requirement for such a certification is the “integrity of navigational data”, positional assurance of the UAV would fall under this requirement [11]. In this case the requirement for integrity of navigational data may be fulfilled through the characterisation of the positional sensing systems of the UAV.

4. Conclusions

Through the use of state estimation systems more certain estimates of UAV position may be gained, which would allow both more effective implementation in isolation, but also may improve the incorporation of such a system into the existing command and control structure of SAR operations. In terms of legislature, better positional estimates and an understanding of expected uncertainty are aid in the certification process.

Works Cited

[1] J. Casper and R. R. Murphy, "Human–RobotInteractionsDuringtheRobot-Assisted Urban Search and Rescue Response at the World Trade Center," *IEEE TRANSACTIONS ON SYSTEMS, MAN, AND CYBERNETICS*, vol. 33, no. 3, pp. 367-385, 2003.

[2] G. De Cubber, D. Serrano, K. Chintamani, R. Sabino and S. Ourevitch, "The EU-ICARUS project: developing assistive robotic tools for search and rescue operation," in *2013 IEEE International Symposium on Safety, Security, and Rescue Robotics (SSRR)*, Linkoping, 2013.

[3] Q. Hamp, L. Reindl and D. Güthlin, "Decision-making behaviour during urban search and rescue: a case study of Germany," *Disasters* , vol. 38, no. 1, pp. 84-107, 2013.

[4] D. Gilman, P. Meier, A. Klaptocz, L. Dawson, K. Bergotora, J. Karlsrud and S. Ancavil, *Unmanned Aerial Vehicles in Humanitarian Response*, Geneva: United Nations Office for Coordination of Humanitarian Affairs, 2014.

[5] M. Raap, S. Meyer-Nieberg, S. Pickl and M. Zsifkovits, "Aerial vehicle search-path optimisation: A novel method for emergency operations," *Journal of Optimization Theory and Applications* , no. 172, pp. 965-983, 2017.

[6] A. Chaves, P. Cugnasca and J. Neto, "Adaptive Search Control Applied to Search and Rescue Operations Using Unmanned Aerial Vehicles (UAVs)," *IEEE LATIN AMERICA TRANSACTIONS*, vol. 12, no. 7, pp. 1278-1283, 2014.

[7] Government, Department for Communities and Local, *Fire and Rescue Authorities Operational Guidance*, Norwich: TSO (The Stationery Office), 2013.

[8] J. Aulinas, Y. Petillot, J. Salvi and X. Lladó, "The SLAM problem: a survey," in *2008 conference on Artificial Intelligence Research and Development*, Amsterdam, 2008.

[9] R. Munguía, S. Urzua, Y. Bolea and A. Grau, "Vision-Based SLAM System for Unmanned Aerial Vehicles.," *Sensors,* vol. 16, no. 3, pp. 372-394, 2016.

[10] J. Cui, S. Lai, X. Dong and B. Chen, "Autonomous Navigation of UAV in Foliage Environment," *Journal of Intelligent & Robotic Systems,* vol. 80, no. 1, pp. 100-118, 2016.

[11] Civil Aviation Authority CAA, "Unmanned Aircraft System Operations in UK: CAP722," 24 March 2015. [Online]. Available: http://publicapps.caa.co.uk/modalapplication.aspx?appid=11&mode=detail&id=415. [Accessed 20 April 2018].

[12] S. Dogru and L. Marques, "Towards Fully Autonomous Energy Efficient Coverage Path Planning for Autonomous Mobile Robots on 3D Terrain," in *2015 European Conference on Mobile Robots (ECMR)*, Lincoln, 2015.

[13] M. Julia, A. Gil and O. Reinoso, "A comparison of path planning strategies for autonomous exploration and mapping of unknown environments," *Autonomous Robots,* vol. 33, no. 4, pp. 427-444, 2012.

[14] E. Galceran and M. Carreras, "A Survey on Coverage Path Planning for Robotics," *Robotics and Autonomous SYstems,* vol. 61, no. 12, pp. 1258-1276, 2013.

ISSN 2398-6611 (Online)

Alexander Moore Testing Structure from Motion 3-D reconstruction techniques with synthetic data to determine the resulting geometric error

Moore A. J.; Bezombes F. A.; Cullen J.; Shaw A.
General Engineering Research Institute, Liverpool John Moores University, James Parsons Building, Byrom Street, Liverpool, L3 3AF
E-mail address: A.J.Moore1@2010.ljmu.ac.uk

Abstract. This paper aims to demonstrate a comparison between the modelling errors encountered when using a 3-D reconstruction technique, namely Structure from Motion (SfM). An experiment was devised to test the accuracy of the reconstruction and what error, if any, was present in the reconstructed geometry. To eliminate any errors associated with other reconstruction techniques, a completely synthetic, computer generated, dataset was created. This dataset was created in an open-source 3-D modelling programme, Blender, which allowed for full control of camera parameters. A camera motion path was then simulated to emulate the motion that would be used in the real-world. To ensure the error being examined was kept to that of the reconstruction and nothing else, the decision was taken to not use shaded lighting, but have full global illumination of the object. This removes any reconstruction errors associated with shadows. The object, now having a texture overlay, was passed by the camera paths to create the dataset. This dataset was then used in two well-established SfM programmes, Pix4D mapper and Agisoft Photoscan. In the datasets, some variables were changed to examine the behaviour of the software under different conditions, these included whether the scene had a textured or untextured background. A synthetic dataset was chosen purely so that there was a true, absolute geometry that the resulting reconstructed models could be compared back to. Thus it eliminates any comparison errors from having a real-world object which has been digitised using another technique, which would not be a true representation.

Keywords. 3-D modelling, Photogrammetry, Pix4D, Agisoft Photoscan, Structure from motion, Blender, Synthetic data

1. Introduction

Photogrammetric 3-D modelling, namely Structure from Motion (SfM), is a popular technique for the digitisation of real-world objects. The input data for SfM are standard RGB photographs/images, which are analysed to determine points of interest, known as keypoints. These keypoints are examined and matched between images, creating ‘image pairs’ from the images with the best matches. A calibration is then performed to compensate for any lens distortion, subsequent to which a sparse point-cloud representing the geometry can then be created.[1][2]
SfM, in the form of commercial computer programmes, has been widely used in anthropology for the digitisation and analysis of bones and other real-world artefacts. The best-established of these commercial

programmes is Agisoft Photoscan, although there are newcomers which are challenging Photoscan's dominance. This paper will examine Agisoft Photoscan and one of its rivals, Pix4D mapper, to determine the quality of their reconstructions.

2. Method

The basic outline of the testing initially starts with an object, this object is digitised and reconstructed in the SfM programmes. The reconstruction is compared back to the original to determine how accurate the reconstruction is. In order to eliminate any errors which would have manifested when digitising the object with another technique for the comparison with the SfM reconstruction, the decision was taken to keep the workflow entirely within the computer. This meant the creation of artificial, synthetic, geometry which would then be used to create the reconstruction. The reasoning behind this decision was that having a perfect model of the object already in the computer would eliminate any extra errors exhibited when trying to create a digitisation of an existing real-world object.
A 3-D modelling programme, Blender (Blender Foundation), was used to create the model. A cube was chosen as the geometry because of the planar and extreme angular nature of the flat surfaces and sharp corners would test this notoriously difficult aspect of SfM reconstructions. Figure 1 shows several of the stages in creating the dataset.

a

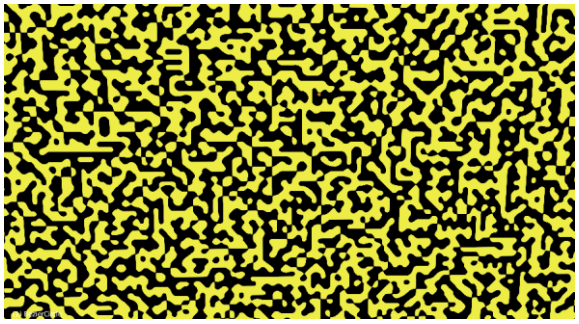

b

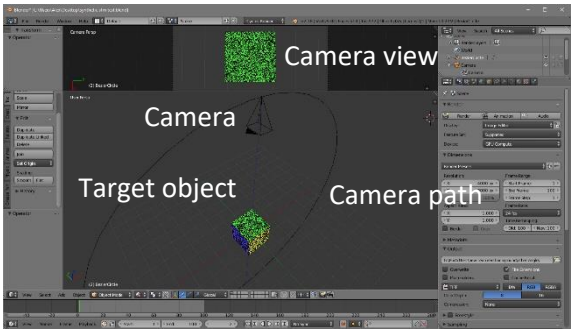

c

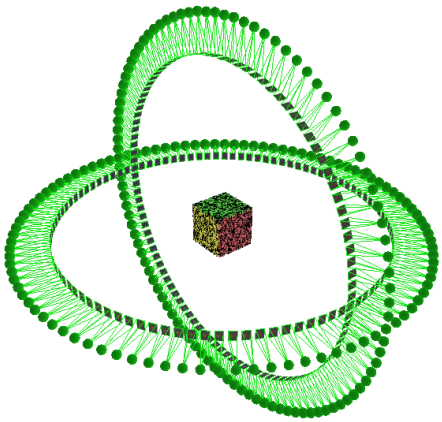

d

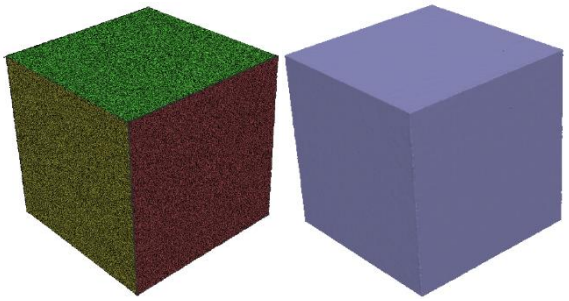

Figure 1 – A figure to show detail of the Musgrave pattern (a), a screenshot of the modelling environment (b), the resulting model with camera paths after SfM reconstruction (c) and the final output models (d) showing the dense point cloud and triangle surface mesh.

SfM works by using texture within an image, if the image contains smooth gradients these gradients cannot be reconstructed properly, but if the image contains a lot of different intensities of colours on a pixel or near-pixel level (something akin to image noise, but static and actually on the object, not created by the camera) then it can be reconstructed. The model of the cube, which is currently blank and so containing none of this 'noise', was required to have texture. This texture was given in the form of a 'Musgrave pattern', a random-noise generating pattern (static once generated). A magnified example of this noise pattern can be seen in Figure 1a. A random pattern was applied to every face of the cube and assigned a different colour depending on the face. This colour difference was solely there to determine if any image misalignments had been suffered during the reconstruction as the software works in monochrome and so was unaffected by the colour. Once the cube had been textured, it could be recorded. A camera path was created, as seen in Figure 1b, with a perfect camera (no lens distortions). This encircled the cube and was set to take 100 images, each of 4000x3000 resolution (1:1 pixel aspect-ratio), during the rotation. For this analysis the perspective is that the object is stationary and the camera is in motion, as that is how it was modelled in Blender. The camera path was rotated 90° from the vertical position to give the horizontal perspective, again recording 100 images. This resulted in a dataset with two views of the object and 200 images. The initial reconstruction and both camera paths exhibiting all 200 images can be seen in Figure 1c. The final dense point-cloud reconstruction and resulting solid-surface mesh can be seen in Figure 1d, with the point-cloud displaying the colour of the reconstruction and the mesh giving a monochrome view of the perceived quality of the flat surfaces and sharp corners of the cube.

Two modelling conditions were required to be tested, one dataset with an untextured background and one dataset with a textured background. This was done to examine both modelling conditions when conducting real-world modelling. An example of this textured and untextured background can be seen in Figure 2. The background was created by using the Musgrave texture, projected onto a 'world sphere' which enveloped the cube and camera. The world sphere was stationary, like the cube, and so was the texture, as can be seen in Figure 2b. This meant the background had parallax when the camera rotated around the cube and could be perceived as 'moving' in relation to the cube on the resulting images.

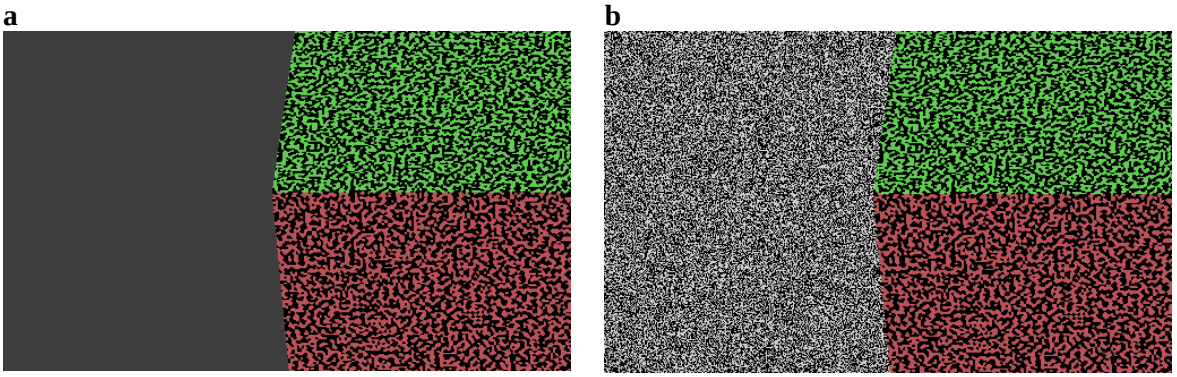

Figure 2 – A Figure to show the two modelling environments, with the untextured background (a) and textured background (b) datasets.

The render was made using a globally illuminated OpenGL output, instead of the traditional light ray-tracing technique. Having the model illuminated globally (for this there was no actual light source, the resulting textures just had their actual original RGB values which simulated global illumination) meant there were no shadows to affect the SfM reconstruction. The camera model used in Blender simulated a pinhole camera, in that there were no distortion artefacts, chromatic aberrations or vignetting to correct in the SfM software. There was also an infinite depth-of-field, in keeping with the pinhole camera model, resulting in a dataset which was fully in-focus. The dataset images were recorded as 8-bit uncompressed TIFF (Tagged Image File Format) images, to remove any potential issues resulting from using a lossy compression format like JPEG.

3. Results

The reconstructions were made with the default settings used on both programmes, this was to ensure a fair comparison as, typically, the user is unlikely to change these settings much, if at all, so the manufacturer recommended settings were used.

All the models being examined are solid-surface triangle-mesh models. Because the computer model contained thirty six vertices only, and the SfM models contained approximately three hundred thousand vertices, they all required being converted into sampled point-clouds for the comparison. This was conducted in CloudCompare, where each model was sampled from a surface mesh to become a point-cloud with a total of 1,000,000 points. This was done because the comparison would have been from the mesh vertex on one model to the mesh vertex on another model, which could have given erroneous readings if the vertices were very distant from one another even though one of them was technically in close proximity to the mesh surface.

The cube model was not subject to a scale, with each side having a length of '1 unit'. SfM is not a scaled reconstruction technique and any scale has to be applied manually during the reconstruction. Any error seen here is scale-independent and so scaling the object was not required.

The analysis provides a result in the form of an absolute distance. This means there is no specific positive or negative displacement recorded, but rather the results are presented as a percentage relative to the overall size of the object. As the results were presented as a percentage difference, it was deemed that 0.05% (0.0005) difference would be the cut-off for a high quality reconstruction as this value provides a reconstruction which is very accurate.

Figure 3 shows the graphical results, along with an image of the cube and any displacements shown with a colour gradient from blue for good a reconstruction quality, through green for a moderate reconstruction quality to red for a poor reconstruction quality.

a

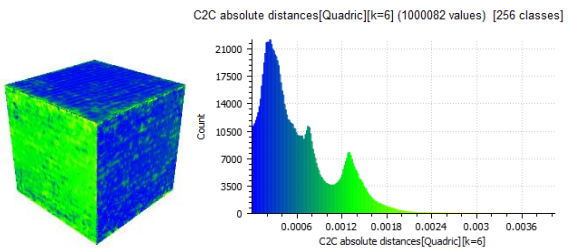

b

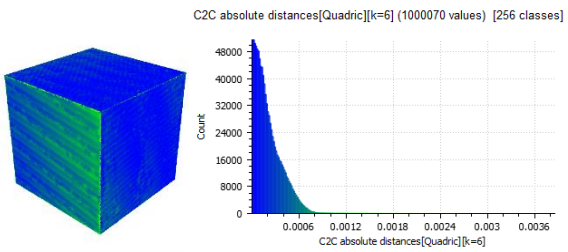

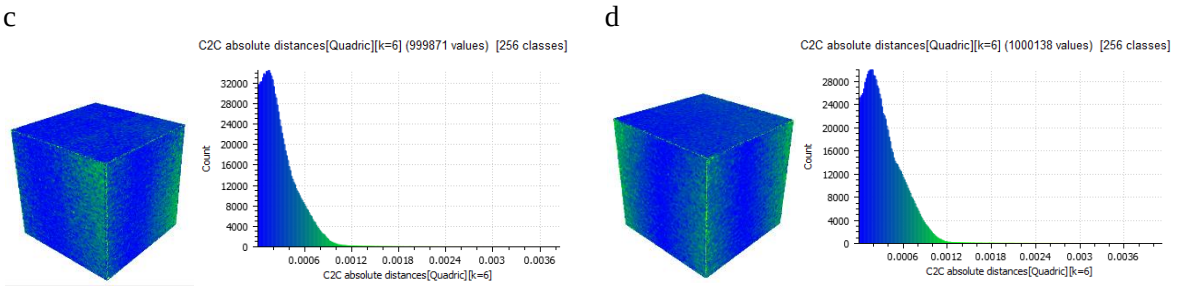

Figure 3 – A figure to show the analysis results, with the Agisoft Photoscan results shown with the textured background (a) and untextured background (b) and Pix4D results shown with the textured background (c) and untextured background (d).

The seemingly large displacement seen in Figure 3a was not expected, this is the Photoscan textured background analysis, exhibiting only 53% of the analysed points within the 0.05% distance quality cut-off. This could have been caused by a camera optimisation error, but the investigation is ongoing. The same can be said for the Pix4D untextured analysis, which was unexpectedly below expectations.
Table 1 shows the numerical figures describing the quality of the reconstruction. The remainder of the analyses, as seen in Figure 3b, c, d, are all similar when it comes to the quality of the reconstruction, as can be seen in Table 1.

Table 1 – A Table to show the quality of the reconstructions.

Model	Percentage of points with a displacement less than 0.05%	Maximum displacement as a percentage of the model size
Agisoft Photoscan Untextured	92	0.3843
Pix4D Mapper Untextured	75	0.4097
Agisoft Photoscan Textured	53	0.4026
Pix4D Mapper Textured	84	0.3836

While every effort has been made to ensure this comparison is fair, it should be treated as a laboratory test, not a real-world test, and so is not an indication of their real-world performance.

4. References

1. Dhond U. R., Aggarwal J. K.; *Structure from stereo-a review* in *IEEE Transactions on Systems, Man and Cybernetics*; Vol. 19, No. 6; Pages 1489-1510; Nov/Dec 1989; Published 1989
2. Marr D., Poggio T.; *A Computational Theory of Human Stereo Vision* in *Proc. of the Royal Society of London*; Series B; Biological Sciences; Vol. 204; No. 1156; Pages 301-328; Published January 1979

ISSN 2398-6611 (Online)

Elizabeth Parrott The emergence of UAV and computer vision techniques within forensic science and policing

E Parrott[1], I De Groote[2], H Panter[3] and F Bezombes[1]
[1]Maritime and Mechanical Engineering, Liverpool John Moores University,
[2]Natural Sciences and Psychology, Liverpool John Moores University,
[3]Liverpool Centre for Advanced Policing, Liverpool John Moores University,
James Parsons Building, 3 Byrom Street, Liverpool, Merseyside, L3 3AF
E-mail address: e.parrott@2012.ljmu.ac.uk

Abstract. As technology progresses new techniques and procedures come into view for the purpose of reducing time, saving money and improving the safety of investigating practitioners. The most influential of these recent techniques has been 3D modelling within forensic science. Computer vision is being implemented across the industry for applications including but not limited to facial scanning, scene reconstruction and burial search. Recently the most profound of these results have come from novel UAV data capture to provide large scale models for crime scene reconstruction. The value of this technology can be seen from crime scene to court room, offering new perspectives in every scenario by extending the reach of the photographer. However to date, there is very little standardized practice for operating these devices specifically for forensic science and police use. From this it is clear to recognise that procedures are yet to be put in place with regard to gathering data of the best evidential value in the most efficient manner. This review therefore outlines the role of computer vision presently within forensics and recognises the future paths and limitations which are likely to arise with regard to implementing UAV technology within forensic science.

Keywords. Forensic science, UAV, computer vision, 3D

1. Introduction

Drone technology has proved popular worldwide because UAVs offer unique viewpoints and enhanced manoeuvrability. There is no doubt the major reason for this popularity in the technology is their use as a sensor platform and specifically their imaging capabilities including photogrammetry, LiDAR and thermal to name the most prominent. Like many industries, the emergency services and private forensic sectors around the globe are beginning to see the value of UAV technology within a law enforcement context because of the unique accessibility and viewpoints that the technology can offer, "Extending the reach of the photographer" (Robinson, 2016). This increased accessibility to complex environments makes UAV's well suited for forensics, policing and crime scene recording with the ability to explore environments potentially hazardous or structurally unsafe for humans to enter such as cliff edges or fire damaged structures. However the usage of UAV technology is something that the police and forensic services within the United Kingdom have not been as quick to uptake in comparison to many other applications such as agriculture (Honkavaara et al., 2013), search and rescue (Tomic *et al*., 2012) and conservation (Koh and Wich, 2012). This precaution is associated to legislation, privacy issues, monetary cost of operation, as

well as the public's perception on the use of UAV's by the police. However, this reluctance of using UAV technology is slowly being overturned by some police forces. Recently it was announced that the London Metropolitan Police would be trialling UAV technology on loan from Sussex and Surrey Police who are pioneering UAV technology in the UK. Examples of the technology trialled by the police so far have all been primarily for outdoor operation and all have required a trained police pilot. The most poignant example of the use of UAV technology within the police force and forensics was during the recent Grenfell Tower fire incident as a commercial DJI Inspire was flown remote control through the highest levels of the building to search and analyse the structure once the fire was extinguished (Figure 1).

The technology of choice for the police and fire service so far appears to be the Aeryon Skyranger (Figure 2) (2017a). This device is marketed as a police and fire investigation tool capable of disaster response, scene reconstruction and scene management and assessment. Nevertheless, equipment cost paired with training costs has resulted in limited popularity of the technology within police and fire departments. On the other hand, forensic science has limited these costs by finding external partners. Currently Cellmark forensics (2017b) one of the major private forensic service providers in the UK has established a partnership with Fly Thru (2017c), a private UAV company advertising the ability to capture data of large outdoor areas without contamination through the use of structure from motion software. Because of this ability, it is no surprise that Fly Thru has such a broad client portfolio including a number of British Police, Fire and Rescue departments and Ministry of Defence. However, the work of this company is limited to outdoors and requires a qualified pilot to fly the UAV and capture the data.

Figure 1 DJI Inspire being used to search the top floors of Grenfell Tower once the fire was extinguished.

Figure 2 Aeryon Skyranger UAV the common choice technology for UK fire and police departments.

2. UAVs in Forensic Science

The range of technology and examination procedures available to forensic practitioners is extensive. Yet despite such an extensive list, recording of a scene is still the timeliest process. This process requires multiple investigators to take photographs, laser scans, measurements, sketches, videos and notes of a crime scene. Completing all of these tasks requires many person-hours of specially trained personnel handling multiple pieces of equipment. In addition to this, contamination is still the most prevalent risk for any crime scene investigator and reducing that risk is the foundation of most forensic and policing

procedures, and the fundamental base for the chain of custody. Edmond Locard's Exchange Principle states, "Every contact leaves a trace" (Locard, 1930a, Locard, 1930c, Locard, 1930b). This principle is more relevant in indoor crime scenes where preservation is more likely as they are generally more sheltered from weather and temperature changes, as well as disturbance (Bond, 2007). When considering all of these factors UAV's within forensic science can offer multiple benefits not only will the lack of contact from a UAV reducing the likelihood of any contamination, as no contact should mean no trace. But also the process of crime scene recording may significantly be reduced with the use of UAVs with varying sensor capabilities and limited human intervention. Although using UAV's within a crime scene offers a great deal of potential for investigators and procedures, it also comes with unique operating challenges and therefore both the technology of the device and equally the constraints of working within a crime scene must be considered. Whilst also meeting the standards to potentially record data of a standard to be admissible in court.

3. 3D Modelling and Forensic Science

Recording of a crime scene is an influential piece of evidence as it can show the relation of objects within a space and reveal evidence associated with a chain of events, this is particularly relevant in the case of fire investigation and road traffic collisions. Commercial software such as Pix4D (2017d) uses structure from motion algorithms to allow for a sequence of photos or video stills to be processed into a 3D model from which measurements can be taken (Figure 3).

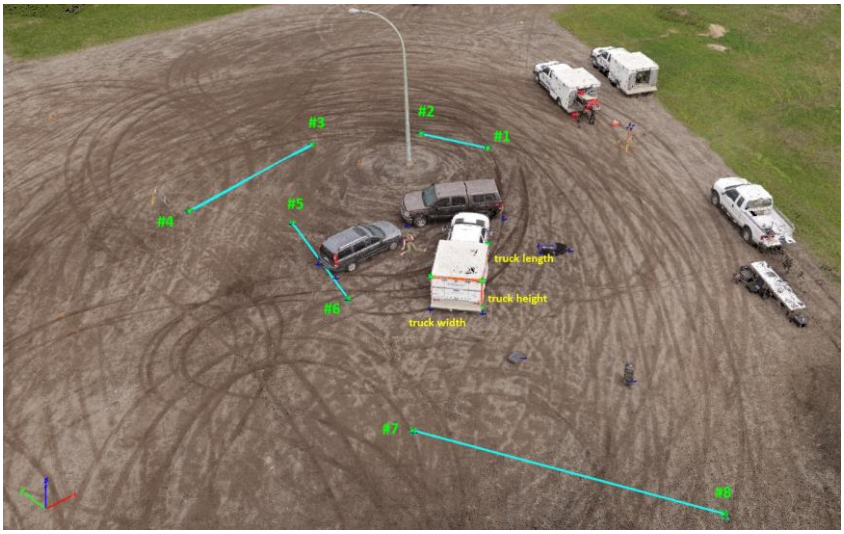

Figure 3 Road Traffic Collision Reconstruction with scale made using Pix4d Software

3D modelling techniques are becoming a valuable forensic tool as they ensure virtual preservation of a crime scene enabling investigators to revisit the scene at any time even once the original scene has been destroyed. This ability is particularly beneficial in scenes which may be subject to a change as they are

either structurally unsafe or exposed to the elements, or in an area with high foot traffic which cannot be closed off for a long period In addition to road traffic collisions, 3D modelling and the ability to live stream sensor data mean that the scenarios that UAV's have potential in is vast for policing and forensics including; disaster management, tactical operations, hazardous materials sites as well as clandestine burial searches. However the use of drone technology within the police to date has been surrounded by controversy. With the public being concerned that the police will misuse the device for spying on members of the public. A solution to these concerns would be to have a standardized operational system in place as is already present for all other pieces of equipment.

In addition to contributing to an investigation 3D modelling techniques may also be invaluable within a courtroom as the position of evidence will be clearly visible in a single model rather than articulating evidence with regard to a number of photos or sketches. A 3D model presented at court would additionally allow a jury to better understand the environment that the crime took place without bias towards the location in comparison to if they were transferred to a physical scene. Also these 3D models have the potential to be very valuable for training purposes among forensic and law enforcement individuals as they can be manipulated into virtual and augmented reality. However the UAV systems outlined so far within this report are all dependent on pilot capability and global positioning systems (GPS) for stability. Therefore something to additionally consider when moving forwards with these devices is that when this technology moves indoors into GPS denied environments the UAV must either been operated by a proficient pilot capable of operating within confined spaces without the aid of GPS stabilization, or the device must be more 'self-aware' with increased intelligence such as collision avoidance capabilities.

4. Conclusion

UAV technology as a law enforcement tool is still within its infancy within policing despite the trials conducted by various departments. Although forensics has come further with adopting these devices the vast scenarios which UAVs could prove useful has not yet been fully exploited. However, we must also take a step back to understand, where these devices are most suited and in what scenarios they will be most beneficial. To date, the police have not fully adopted the technology due to legislation and monetary cost. However, with correct implementation and education of the technology, UAV technology has the potential to offer air surveillance capabilities to many more departments without access to full size aircraft. With regard to forensics there is no doubt that, the technology will be beneficial however; more consideration must be given to standardizing practice and it must be acknowledged that UAV technology may not be suited to all scenarios. In the future another consideration is the likeliness of the technology to become increasing automated becoming less reliant on a human operator and therefore the demand for more intelligent systems.

References

2017a. *Aeryon* [Online]. Available: https://www.aeryon.com/ [Accessed 22nd November 2017].
2017b. *Cellmark Forensics* [Online]. Available: http://www.cellmarkforensics.co.uk/ [Accessed 21st November 2017].
2017c. *Fly Thru* [Online]. Available: http://www.flythru.co.uk/forensic.html [Accessed 22nd November 2017].
2017d. *Pix4D* [Online]. Available: https://pix4d.com/ [Accessed 11th December 2017].
BOND, J. W. 2007. Value of DNA Evidence in Detecting Crime. *Journal of Forensic Sciences,* 52**,** 128-136.
HONKAVAARA, E., SAARI, H., KAIVOSOJA, J., PÖLÖNEN, I., HAKALA, T., LITKEY, P., MÄKYNEN, J. & PESONEN, L. 2013. Processing and Assessment of Spectrometric, Stereoscopic Imagery Collected Using a Lightweight UAV Spectral Camera for Precision Agriculture. *Remote Sensing,* 5**,** 5006.
KOH, L. P. & WICH, S. A. 2012. Dawn of Drone Ecology: Low-Cost Autonomous Aerial Vehicles for Conservation. *Tropical Conservation Science,* 5**,** 121-132.
LOCARD, E. 1930a. The Analysis of Dust Traces. Part I. *The American Journal of Police Science,* 1**,** 276-298.
LOCARD, E. 1930b. The Analysis of Dust Traces. Part III. *The American Journal of Police Science,* 1**,** 496-514.
LOCARD, E., LARSON, D. J. 1930c. The Analysis of Dust Traces. Part II. *The American Journal of Police Science,* 1**,** 401-418.
ROBINSON, E. M. 2016. *Crime Scene Photography*, Academic Press
TOMIC, T., SCHMID, K., LUTZ, P., DOMEL, A., KASSESCKER, M., MAIR, E., GRIXA, I., RUESS, F., SUPPA, M., BURSCHKA, D. 2012. Toward a Fully Autonomous UAV: Research Platform for Indoor and Outdoor Urban Search and Rescue. *in IEEE Robotics & Automation Magazine.*

ISSN 2398-6611 (Online)

Ilaria Frau Screen-printed thick films based on l-cysteine-chitosan ruthenium oxide on planar IDE sensors for EM detection of Cu ions in water

I Frau[1], S Wylie[1], P Byrne[2], J Cullen[3], O Korostynska[1] and A Mason[4]
[1]Built Environment and Sustainable Technologies (BEST) Research Institute, Department of Civil Engineering, Faculty of Engineering and Technology, Liverpool John Moores University, Liverpool, L3 3AF, UK.
[2]Department of Geography, School of Natural Sciences and Psychology, Faculty of Science, Liverpool John Moores University, Liverpool, L3 3AF, UK.
[3]Built Environment and Sustainable Technologies (BEST) Research Institute, Department of Built Environment, Faculty of Engineering and Technology, Liverpool John Moores University, Liverpool, L3 3AF, UK.
[4]Animalia AS, Norwegian Meat and Poultry Centre, PO Box Økern, 0513 Oslo, Norway

E-mail address: i.frau@2016.ljmu.ac.uk

Abstract. Pollutants affect water worldwide and consequently present a risk to both the environment and human health. Metals, including Zn, Pb, Cu, Cd, are a particular cause for concern due to their toxicity and bioaccumulation. Current techniques are not able to monitor water quality continuously, as they are laboratory-based methods requiring sampling and offline monitoring. A potential method that is capable of meeting this demand is the integration of microwave spectroscopy with functional materials to increase the sensitivity and selectivity toward a specific pollutant. This paper presents preliminary results that show that the L-Cysteine-Chitosan-Ruthenium oxide (L-Cy-Ch-Ru) based coatings can differentiate between changes in the Cu concentrations better than the uncoated sensors, especially for concentrations < 1 mg/L, more common range in naturally polluted water. The interaction between Cu ions and 65 µm thick L-Cy-Ch-Ru based coating is reflected in changes in S_{11} and capacitance respectively with R^2=0.99 (at 20 Hz - 20kHz) and R^2= 0.97 (at 1.35 GHz) at 600 seconds. This suggests that functionalised EM sensors can be a viable alternative to detect changes in Cu concentration in water, in-situ and in real-time.

Keywords. Cu pollution, thick film, functionalised EM sensors, microwave spectroscopy, chelating polymers

1. Introduction

1.1. Toxic metal pollution

Mineral extraction has caused global environmental problems, especially due to the dispersion of toxic metals (zinc, lead, cadmium, copper). These cannot be degraded or destroyed by micro-organisms so persist in the environment and can activate, migrate and accumulate in various media under different geochemical and hydrological settings that may directly or indirectly impact plants, animals and humans.

Copper (Cu) pollution of water can cause acute and chronic toxicity at relatively low concentrations, due to its potential for bioaccumulation [1]. Cu concentrations in mine water range from 0.001 µg/L up to 240 mg/L, with surface water being as mayor route for dispersion. Consequently, the UK Technical Advisory Group on the EU Water Framework Directive (UKTAG) established an environmental quality standard (EQS) for Cu in surface water of 28 µg/L [2]. Moreover, EQS for Cu in drinking water have been defined by the World Health Organisation (2 mg/L) and the UN Protection Agency (1.3 mg/L) [3].

1.2 Current development in Cu sensing system

Strategies for continuous monitoring of Cu in water resources are currently limited by logistical constraints, human sampling error and costly off-line laboratory-based methods of analysis. Consequently, it is necessary to develop new sensing systems for continuous detection of Cu (and other toxic metals) in water [3].

1.3. Microwave spectroscopy and f-EM sensors

A potentially novel approach for meeting the current demand for cost-effective real-time water quality monitoring is a microwave sensing method [4]. The principle is based on the interaction of propagating or resonating EM (electromagnetic) waves with a sample under test. The response of the sensor manifests itself as a resonant frequency change, alteration in the signal amplitude or a resonant peak shift. A potential method that is capable of increasing the sensitivity and selectivity toward a specific pollutant is the integration of functional materials [5, 6].

This work describes a novel sensing method using microwave spectroscopy and functionalised electromagnetic (f-EM) sensors with selective chemical materials for continuous detection of Cu ions in water. Planar EM sensors were functionalised with two chelating polymers, namely chitosan and l-cysteine, and a resistive metal oxide, ruthenium (VI) oxide, using screen-printing technology. L-cysteine and chitosan (figure 1a) have reactive amine and hydroxyl groups which serve as the active sites for interaction with Cu ions in aqueous media [7]. A small amount of the metal oxide was primarily used for reaching the right viscosity to be screen-printed. Moreover, this resistive oxide showed an improved performance with higher sensitivity in impedance measurements with Cu ions.

The purpose of this paper is to evaluate the feasibility of using an integrated method using microwave spectroscopy and electrical measurement with f-EM sensors based on L-Cy-Ch-Ru for detecting Cu ions in water with higher specificity than uncoated sensors.

2. Materials and method

2.1. Coating development and characterisation

Eight-pair Au-IDE EM sensors were functionalised by screen-printing a paste mixture based on L-Cy-Ch-Ru (4:4:1) (Sigma-Aldrich 168149, 448869 and 238058). The powders were mixed with an organic binder to obtain a printable paste of the desired viscosity, namely with 7.5wt.% of Butvar B98 (Sigma-Aldrich B0154) in solid form, and a suitable amount of ethylene glycol butyl ether (organic volatile solvent) (Sigma-Aldrich 579556) to form the paste. These two components work as a matrix for developing the paste to be printed with a semi-automatic screen printer (Super Primex) over the planar IDE sensors. Several silver eight-pair IDE patterns were screen-printed *in-situ* at LJMU on microscope slide substrates and covered with paste mixtures using various percentages of the functional materials for an initial characterization using impedance measurements. The thickness of the L-Cy-Ch-Ru based thick film was increased by multiple screen-printing, with suitable curing of the layers in an oven at 150º C for 1 hour between each print. Coating properties were measured through optical (with a UV-Vis Spectrophotometer,

Jenway 7315), structural (with a scanning electron microscope, SEM, model FEI - Quanta 200) and elemental (with a X-Ray Fluorescence Analyser, XRF, model INCA-X-act) measurements.

2.2. Sample preparation

Eight samples of Cu in water at different concentrations (0, 0.1, 0.25, 0.5, 1, 10, 25, 50 mg/L) were prepared by dissolving a defined volume of Cu 1000 ppm ICP standard solution certified (Sigma-Aldrich 68921) in deionised water. For all samples the pH, conductivity and temperature were evaluated using a multi-parameter probe (PCE-PHD 1). All measurements were performed in an air-conditioned environment at a constant temperature of 20°C.

2.3. Microwave and Electrical measurements

In this work, the optical, electrical, and microwave properties of Cu samples were analysed using a UV-Spectrophotometer (200-1000 nm, 3.5 mL sample size) for absorbance measurements; uncoated and f-sensors with L-CyChRu based thick films (65 µm) using an LCR programmable bridge (Hameg 8118, figure 1b) (30 Hz–20 kHz, 400 µL sample size) a Vector Network Analyser (Rohde & Schwarz VNA 24, figure 1c) (10 MHz-8 GHz, 400 µL sample size) and measuring the capacitance and the reflection coefficient (S_{11}) respectively. The LCR meter uses crocodile clips for f-EM sensor and sample interaction characterisation; the EM-sensors were connected with the VNA via a coaxial cable. Cu solutions are placed on the sensor using a specific integrated holder. Each solution was tested (n=5) for 10 minutes with both techniques which permits a continuous measurement to monitor any time variation in the interaction between the coatings and the Cu solutions.

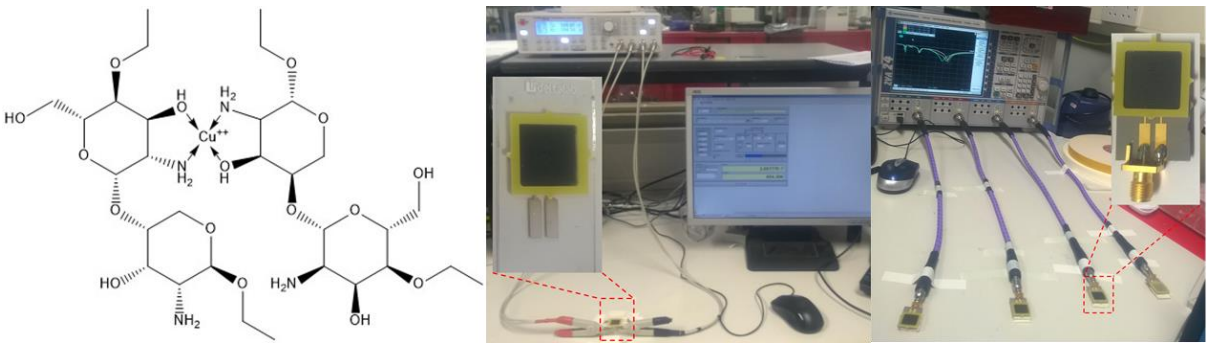

a b c

Figure 1 (a) Sketched model for chelation between chitosan, selective polymer, and Cu ions using Chem3D. Experimental set up (b): LCR programmable bridge connected to an Ag-IDE screen-printed on microscope slide in situ at LJMU connected through crocodile clips; (c) VNA connected with coaxial cables to uncoated and f-EM sensors (Au-8 pair IDEs) with L-Cy-Ch-Ru based thick films.

3. Results and discussion

Exposure of f-EM sensors to Cu-spiked laboratory samples demonstrate the ability to detect changes in Cu concentration with higher sensitivity than uncoated sensors. During the measurements, significant resonant peak shifts were noticed once the different concentrations of Cu samples were placed in contact with the sensor pattern. The response changes due to the effect of the L-Cy-Ch-Ru based thick film has been compared with the uncoated sensors noting significant differences due to the overlay. This

functionalisation enhances the sensor performance significantly, leading to a higher sensitivity of the sensor comparing to bare gold eight-pair IDE electrode, namely in a specific frequency at around 1.35 GHz for Cu detection.

Results with 65 µm L-Cy-Ch-Ru based film illustrate that f-EM sensors were able to detect and distinguish smaller changes of Cu concentration < 1 mg/L at 1.35 GHz better than the uncoated sensors (figures 2a,b) with a higher linear correlation (R^2) (figures 2c,d) and sensitivity, as summarized in table 1. This is important to detect Cu ions in surface and drinking water up to and above the EQS. The dielectric changes are associated with the binding of Cu ions on the coating with a consequent change in complex permittivity, accounted at 1.35 GHz.

Table 1 Linear correlation (R^2), relative standard deviation (RSD) and sensitivity for Cu samples using optical, electrical and microwave methods combined with f-EM sensors.

Measured parameter	R^2	RSD	Sensitivity[1]
Absorbance (at 217 nm)	0.98	1-2 %	0.10
Capacitance using Ag f-EM sensors (at 150 Hz)[2]	0.99	1-3%	7.91 nF
S_{11} using uncoated Au EM sensors (at 1.26 GHz)[2]	0.95	1-3%	0.005 dB
S_{11} using Au f-EM sensors (at 1.35 GHz)[2]	0.98	2-3%	0.018 dB

[1] for every 100 µg/L change in Cu calculated for the range 0-1 mg/L; [2] at 600 sec;

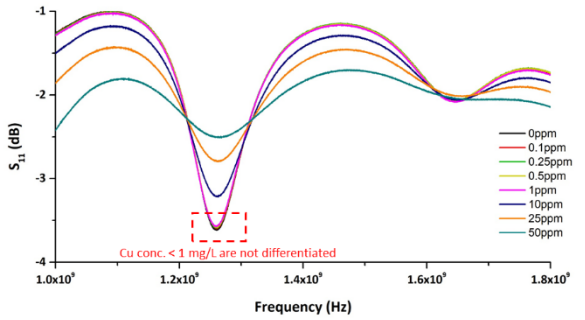

(a)

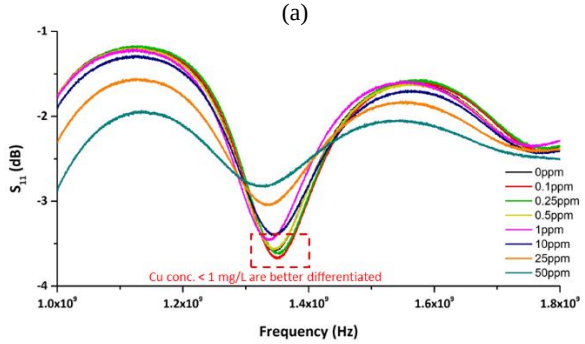

(b)

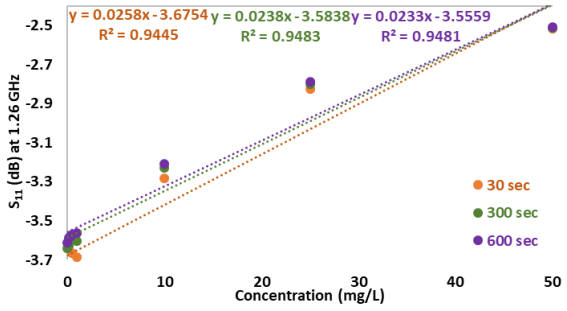

(c)

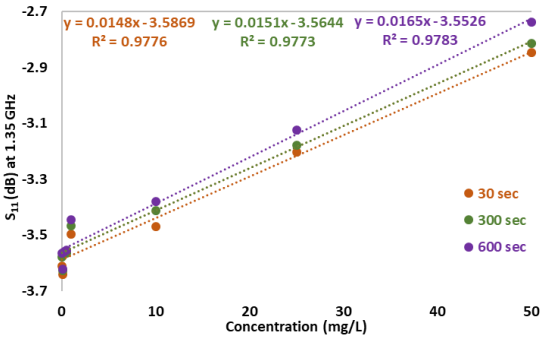

(d)

Figure 2 S_{11} response (1-1.8 GHz) at 10 minutes for diverse Cu concentrations measured with (a) uncoated sensors and (b) f-EM sensors. Their linear correlations at the respective peaks (1.26 GHz and 1.35 GHz) at 30, 300 and 600 seconds of interaction are shown in (c) and (d).

4. Conclusion

This paper communicates the experimental results of using functionalised planar type microwave sensors based on chelating-polymers based thick film for real-time detection of Cu in water. Specifically, eight-pair IDE planar sensors coated with L-Cy-Ch-Ru based coating performed better when detecting lower Cu concentration (0-1 mg/L) than the uncoated sensors.
Further work and field trials are in progress to expand and progress toward the realisation of a sensitive and selective sensor which could offer the ability to monitor and report water quality over large and remote geographical areas for both in-situ and real-time monitoring and will be able to provide an early warning system for pollution events.

Acknowledgements

The authors gratefully acknowledge the support of Liverpool John Moores University, Faculty of Engineering and Technology in conjunction with the Faculty of Science PhD Scholarship Programme which allowed this research to be undertaken.

References

[1] Agency for Toxic Substances and Disease Registry (ATSDR), Toxicological profile for Copper, Atlanta, GA: U.S. Department of Health and Human Services, Public Health Service, 2004. [Online]. Available.
[2] UK Technical Advisory Group on the Water Framework Directive, "UK environmental standards and conditions (phase 1 - SR1-2006)," 2008.
[3] G. Aragay, J. Pons, and A. Merkoci, "Recent trends in macro-, micro-, and nanomaterial-based tools and strategies for heavy-metal detection," *Chemical Reviews,* vol. 111, no. 5, pp. 3433-3458, 2011.
[4] A. Mason *et al.*, "Theoretical basis and application for measuring pork loin drip loss using microwave spectroscopy," *Sensors (14248220),* Article vol. 16, no. 2, pp. 1-13, 2016.
[5] M. H. Zarifi, S. Farsinezhad, M. Abdolrazzaghi, M. Daneshmand, and K. Shankar, "Selective microwave sensors exploiting the interaction of analytes with trap states in TiO2 nanotube arrays," *Nanoscale,* 10.1039/C5NR06567D vol. 8, no. 14, pp. 7466-7473, 2016.
[6] A. Azmi *et al.*, "Performance of Coating Materials on Planar Electromagnetic Sensing Array to Detect Water Contamination," *IEEE Sensors Journal,* vol. 17, no. 16, pp. 5244-5251, 2017.
[7] W. S. W. Ngah and S. Fatinathan, "Adsorption of Cu(II) ions in aqueous solution using chitosan beads, chitosan–GLA beads and chitosan–alginate beads," *Chemical Engineering Journal,* vol. 143, no. 1, pp. 62-72, 2008/09/15/ 2008.

ISSN 2398-6611 (Online)

Tricia Sullivan Long-term optical dimming of KIC 8462852 with Skycam Z

Sullivan, T. and Steele, I.A.
Astrophysics Research Institute, 146 Brownlow Hill, Liverpool L3 5RF
t.sullivan@2015.ljmu.ac.uk

Abstract. We investigate the unexplained long-term secular dimming of KIC 8462852 (Boyajian's Star) at optical wavelengths. This otherwise unexceptional Type F3 star gained notoriety after *Kepler* observed a series of flux dips in a stochastic pattern uncharacteristic of planetary transits. Multiple studies with a variety of instruments have examined subsequent short-term dips to constrain possible causes. However, on longer timescales *Kepler* also produced evidence of slow fading that may or may not be related to short-term behaviour; we study it here. Skycam Z is an instrument mounted on the Liverpool Telescope (LT). It takes optical photometry over 1 square degree for ten seconds of every minute that the telescope dome is open, irrespective of where it points. Since March 2016 the LT's optical polarimeter has observed KIC 8462852 intermittently, enabling Skycam Z to collect photometry at the same time. We developed an automated pipeline to perform aperture photometry on KIC 8462852 and a set of reference objects to measure changes in relative magnitudes. We processed around 2000 images of fields containing KIC 8462852 sampled unevenly between March 2016 and April 2018. We estimate flux loss of $2.4 \pm 0.8\%$ yr^{-1} including dipping events and $1.7\% \pm 0.8\%$ yr^{-1} without dipping. The result exceeds the *Kepler* mission's 2009-2013 findings by a factor of 2-4.
Keywords stars: variables: general– stars: activity – stars: individual: KIC 8462852 – stars: peculiar.

1. Introduction

The Planet Hunters project first observed the unusual behaviour of KIC 8462852 (Boyajian's Star) in *Kepler* light curves. They identified four aperiodic and irregularly shaped flux-dipping events of 3-21% lasting several days each during the interval between 2011 and 2013. Boyajian et al. (2016) reported the findings together with a number of
< 1% dips in the same survey. A follow-up monitoring campaign found four additional 1-4% dips during 2017 whose spectral energy distributions are characteristic of dust (Boyajian et al. 2018, Deeg et al. 2018). In March-April 2018 the star underwent two more dips of ~4-5% (Wherestheflux.com 2018)

A battery of explanations for the dips have been proposed and analyzed, both in the original study and subsequently. A few internal stellar mechanisms have been considered (Foukal 2017, Wright & Sigurdsson 2016), but most models involve obscuration by a variety of external objects such as planetesimals (Boyajian et al. 2016), exocomets on eccentric orbits (Wyatt et al. 2017), a giant ring system (Ballesteros et al. 2017, Kiefer et al. 2017), a transiting brown dwarf with an icy-moon ring system (Bourne, Gary & Plakhov 2017) or a planet in the process of consumption by the star (Metzger, Shen & Stone 2016).

Kepler photometry also revealed evidence of 0.75% yr^{-1} dimming between 2009-2013 uncorrelated to the dips (Montet & Simon 2016), and Simon et al. (2017) find a similar ~0.63% yr^{-1} flux loss between 2015-

2017 using independent photometry, together with some evidence of intermittent brightening. Long-timescale studies of different sets of historic plates yield different measurements of flux loss:

1) 16.4% per century (Schaefer 2016), disputed on statistical grounds (Hippke et al. 2016);
2) 3% per century (Hippke et al. 2017)
3) 12% per century (Castelaz & Barker 2018).

Although less dramatic than the dips, the secular dimming of KIC 8462852 presents an important problem. If dimming is related to the dipping events, then none of the models to date can explain it (with the possible exception of Metzger et al. 2017). If the dimming and dipping are unrelated, then the star is unusual in two orthogonal ways. More data are needed to constrain the magnitude of the long-term dimming and to determine whether or not it is monotonic.

The timescale of this work is ~2 years. The Liverpool Telescope (LT) has been monitoring KIC 8462852 to study its polarization using the RINGO3 instrument (see Steele et al. (2017) for details). Mounted on the LT, the instrument Skycam Z automatically takes optical photometry in exposures of 10 seconds in every minute that the telescope dome is open (Mawson et al. 2013). The Skycam Z archive was accessed to obtain frames that include KIC 8462852 between late March 2016 and mid-April 2018.

2. Data

All data were collected by the LT's Skycam Z as part of its routine optical-wavelength monitoring of KIC-8462852 during the period from 29/03/2016 to 14/04/2018. Skycam Z has a 'zoomed field' Andor ikon-M DU934N-BV camera mounted inside an Orion Optics AG8 telescope with which it parallel points. It has a plate scale of 3 arcsec/pixel over a 1-degree field-of-view and can detect sources down to ~18th magnitude using an unfiltered 'white light' wavelength range that is best calibrated to R-band (Mawson et al. 2013). Sampling is uneven, with some nights having more frames than others.

Every frame was evaluated by eye to remove poor-quality images, including frames in which the telescope was moving when Skycam Z automatically recorded them. Two reference stars R1 and R2 were selected based on their proximity to KIC-8462852, and aperture photometry was performed on a small sample of good-quality images using GAIA software (Currie et al. 2014). The magnitude difference R1-R2 was measured, and the lowest achievable standard error on a small sample by hand was found to be ~0.003 mag. A third reference star R3 was then selected. Details of each star based on APASS (reference) data are shown in Table 1.

Table 1. *Position and brightness of reference stars*

	R1	**R2**	**R3**	**KIC 8462852**
RA (dec. deg.)	301.629848 ± 0.744	301.559552 ± 0.595	301.59858 ± 0.631	301.564455±0.652
Dec (dec. deg.)	44.588739 ± 0.291	44.616203 ± 0.362	44.460626 ± 0.311	44.456863 ±0.345
r'-mag	9.734 ± 0.04*	9.341± 0.04*	11.334 ± 0.045	11.697 ± 0.064

*error estimated from median error on APASS Sloan r' for stars of similar magnitude within 1 square degree

3. Method

Code was developed using the Astropy library (Astropy Collaboration 2013) to locate and perform aperture photometry on the sources automatically. Running the code yielded 2160 frames with a standard error on the magnitude difference R1-R2 of 3.6×10^{-4} mag. Removal of outliers reduced the sample to 1924 with a standard error of 2.3×10^{-4} mag.

To assess the dimming of KIC 8462852, its brightness must be compared to stars whose brightness is constant. The magnitude difference between KIC 8462852 and each reference star was recorded, as well as the magnitude differences between the reference stars. A Spearman correlation test was performed for each of the six pairings with time. Brightness of the reference stars with respect to one another showed a modest but highly significant correlation with time for R1-R2 and R1-R3, but no correlation for R3-R2. This implies that R1 itself may have some variability, but R2 and R3 are validated as constant sources.

Highly significant positive correlations between time and magnitude difference were observed for KIC-8462852 and each of the three reference stars. To explore the correlation, a least-squares linear regression model was fitted to each set of magnitude differences. In order to reduce possible bias introduced by the temporary flux dips, all frames associated with known events *Elsie, Celeste, Skara Brae, Angkor, Caral-Supe,* and *Evangeline* were removed and the analysis repeated. Both sets of results are reported in Section 4.

4. Results

Examination of correlations and linear fits to different regions of the light curve revealed systematics in the 2016 data. These were found to associate with a refocus/recollimation of Skycam Z on 16 August 2016, after which the resolution of images improves. Pending further analysis of the pre-16 August data, we summarize results only after 16 August. All data are plotted in Figure 1, with separate fits before and after 16 August as well as for the 2017-18 season so far. For small values, magnitude change approximately equates to percentage change of flux; e.g., a 0.03 increase in magnitude implies 3% dimming in a year. R1 – R2 shows no significant variability. KIC 8462852 drops by 1.9 – 2.8% yr^{-1}, but when flux change between reference stars is taken into account, we arrive at a more uncertain $2.4 \pm 0.8\%$ yr^{-1} loss.

Results excluding dipping are shown in Figure 2. Note that correlations with time for R3 – R1 and R1 – R2 are not significant. Again, we disregard early data in the overall (red) fit, finding flux loss of 1.2 – 2.0 % for KIC 8462852, which becomes $1.7 \pm 0.8\%$ after allowing for the variability of R2 – R3.

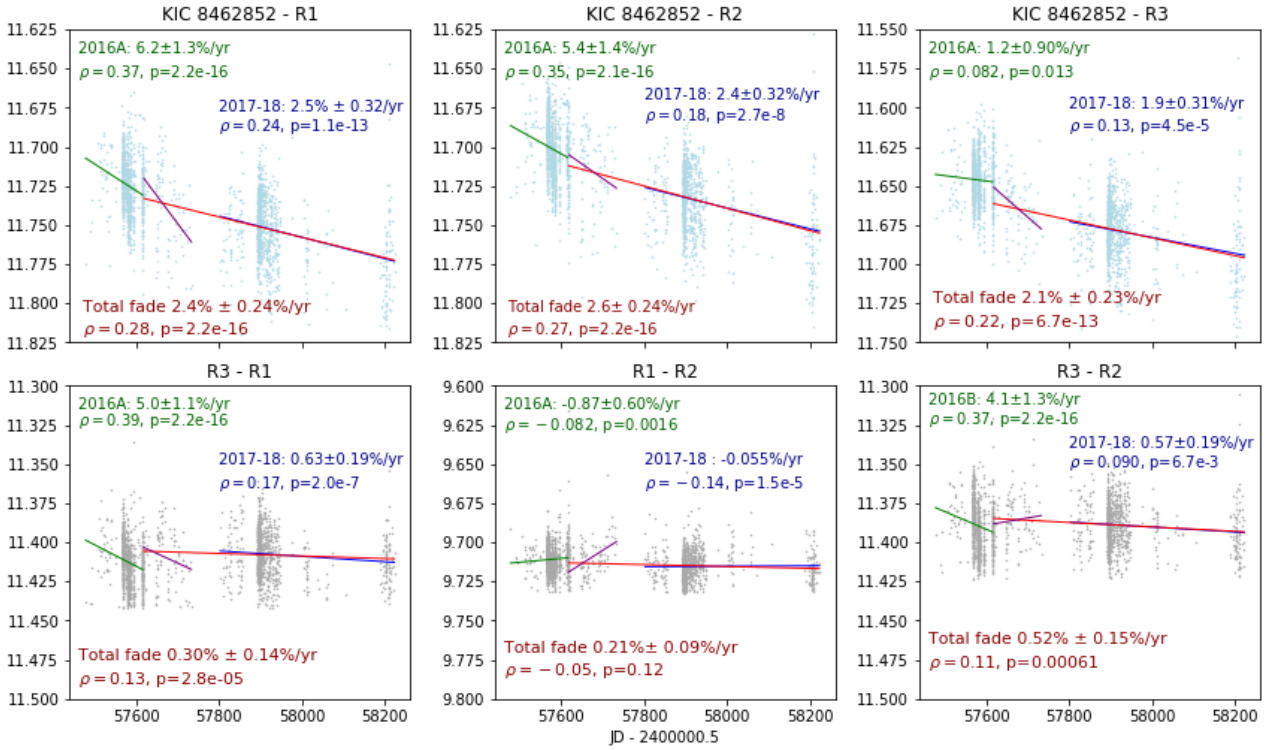

Figure 1 Evolution of magnitude with time of KIC 8462852 with respect to R1, R2, R3 (top row), and evolution of reference stars with respect to one another (bottom). The green, purple and blue lines are linear fits to the 2016 pre-and-post refocus data and 2017-18 data, respectively. The red line is an overall linear fit post-refocusing. Overall annual fade, Spearman's correlation coefficient between magnitude difference and time ρ and its p-value (significance) are inset.

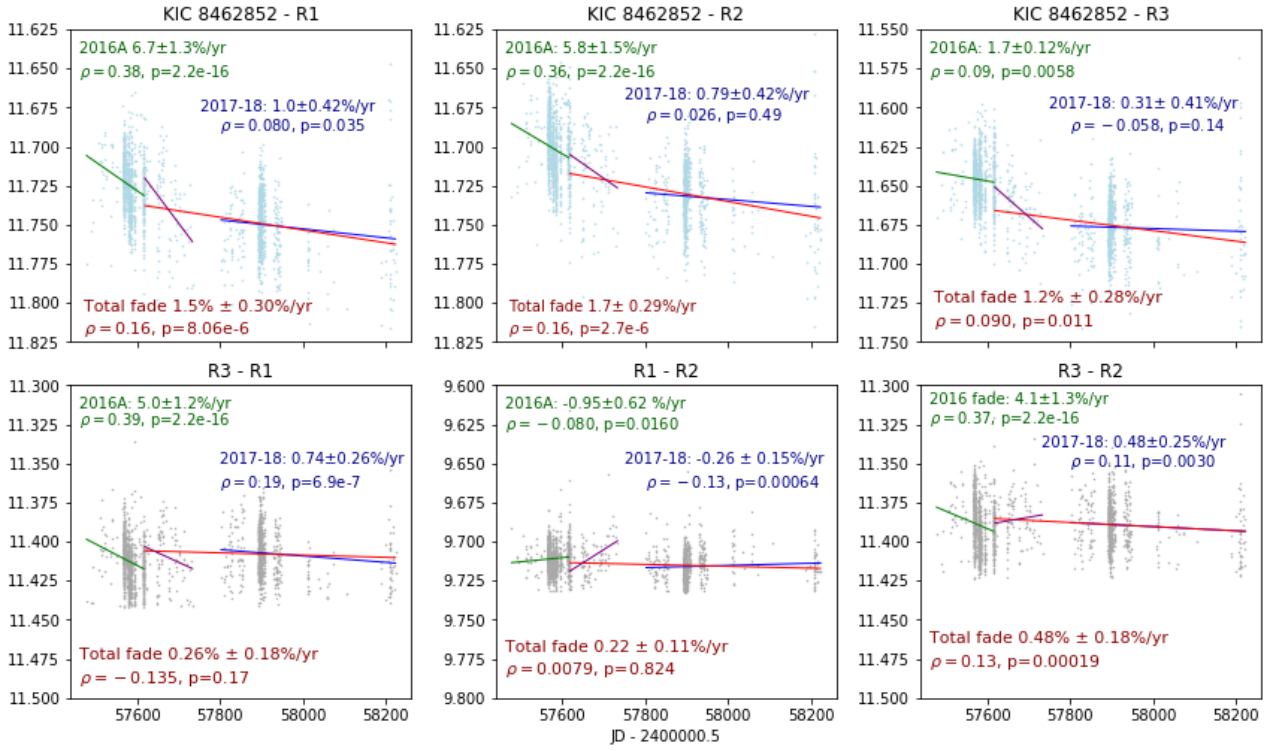

Figure 2 Analogous to Figure 1 but with all dipping frames excluded. Nonlinearity of some kind is suggested in the relationship between the purple and blue line but cannot be confirmed without better understanding of the pre-refocus data (green).

5. Discussion

The ~2% yr^{-1} dimming recorded here exceeds the 0.75% yr^{-1} *Kepler* long-timescale dimming by a factor of ~3. In terms of the historic plates, our dimming is the equivalent of 5-30 years' fade when compared to Schaefer (2016) or Castelaz & Barker (2017), and to up to ~100 years' fade according to Hippke et al (2017). The discrepancy is puzzling. Despite the relatively large scatter in our data, the slopes on the reference stars' magnitude changes can only account for at most 25% of KIC 8462852's dimming. One possible explanation is that long-term dimming is not linear in character and that we have simply measured a steep sub-section of a curved time series that has an overall shallower trend. We note that when dipping events are removed the 2017-18 data alone show no significant downward trend for KIC 8462852 so far, except for a weak, marginally significant dimming against R1 (top left in Figure 2).

Some appearance of curvature is suggested in the plots. This may be related to systematics in the 2016 data, but should be investigated further. With more analysis of these early frames we hope to characterize the systematics better and possibly make corrections. More reference stars are needed as well, including stars of similar magnitude to KIC 8462852, to check whether the slopes recorded here are typical. However, issues with our automated system's detection of dimmer stars and stars with close neighbours must first be surmounted. More observations to increase the total length of time series are also needed.

6. Conclusion

We present measurements of the fading of KIC 8462852 from 17 August 2016 to 15 April 2018 using Skycam Z on the Liverpool Telescope. Estimated flux loss is $2.4 \pm 0.8\%$ yr^{-1} including dipping events and $1.7\% \pm 0.8\%$ yr^{-1} without dipping.

7. Acknowledgements

The Liverpool Telescope is operated on the island of La Palma by Liverpool John Moores University in the Spanish Observatorio del Roque de los Mucha chos of the Instituto de Astrofisica de Canarias with financial support from the UK Science and Technology Facilities Council. TS was supported by the STFC [ST/P006752/1]. The LIV.DAT Centre for Doctoral Training (CDT) is hosted by Liverpool John Moores University/Astrophysics Research Institute and the University of Liverpool. TS thanks Chris Copperwheat, Robert Smith and Paul McWhirter for advice on Skycam Z photometry.

References

American Association of Variable Star Observations 2017, https://www.aavso.org/download-apass-data
Astropy Collaboration 2013. *A&A*, 558, A33
Ballasteros FJ, Arnalte-Mur P, Fernandez-Soto A, Martinez VJ, 2017. *MNRAS* 473:1
Boyajian TS, Alonso R, Ammerman A, Armstrong D, Ramos AA, et al. 2018. *ApJ* 853 L8
Boyajian TS, LCourse DM, Rappaport SA, Fabrycky D, Fischer DA, et al. 2016. *MNRAS* 457(4) 3988-4004
Bourne R, Gary BL, Plakhov A, 2017, *MNRAS* 475
Castelaz M, Barker T 2018. *AAS Meeting #231*, id 349.14
Currie MJ, Berry DS, Jenness T, Gibb AG, Bell GS, Draper PW 2014. *ASP Conference Series* Vol. 485
Deeg HJ, Alonso R, Nespral D, Boyajian T, 2018. *A&A* 610 L12

Foukal P 2017. *Res. Notes AAS* 1(1)
Hippke M, Angerhausen D, Lund MB, Pepper J, Stassun KG, 2016. *ApJ* 825(1):73
Hippke M , Kroll P, Mattai F, Angerhausen D, Tuvikene T, et al. 2017. *ApJ* 837(1):85
Kiefer F, des Etangs AL, Vidal-Madjar A, Hebrard G, Bourrier V, Wilson PA, 2017. *A&A* 608 A132
Mawson NR, Steele IA, Smith RJ, 2013. *Astronomische Nachrichten* 334(7)
Metzger BD, Shen KJ, Stone NC, 2017. *MNRAS* 468, 4399-4407
Montet BT, Simon JD, 2016. *ApJ Letters* 830(2) L39
Shaefer BE, 2016. *ApJ Letters* 822 L34
Simon JD, Shappee BJ, Pojmanski G, Montet BT, Kochanek CS, et al. 2018. *ApJ* 853(1)
Steele IA, Copperwheat CM, Jermak HE, Kennedy GM, Lamb GB, 2017. *MNRAS* 473 L26-L30
Wright JT, Sigurgsson S, 2016. *ApJ Letters* 829 L3
Wyatt MC, van Lieshout R, Kennedy GM, Boyajian TS, 2017. MNRAS 473(4), pp. 5286-5307

ISSN 2398-6611 (Online)

Meghan Hughes Galactic tidal features and their star cluster populations in the context of E-MOSAICS

M E Hughes, J Pfeffer, M Martig and N Bastian
The Astrophysics Research Institute, LJMU, IC2, Liverpool Science Park, 146 Brownlow Hill, Liverpool, L3 5RF
M.Hughes1@2013.ljmu.ac.uk

Abstract. We use a set of 16 E-MOSAICS hydrodynamical zoom simulations of different galaxy halos to identify stellar streams at a redshift of 0. The properties (specifically the age and the metallicity) of the star clusters associated with these streams are compared to the properties of the rest of the star cluster population of the halo. We find very large variations in these properties and explain these variations with the mass and the infall time of the stream progenitor galaxies. More massive galaxies which fell into the main halo more recently will have younger and more metal rich clusters.

Keywords Globular clusters; Stellar streams; Galaxy formation

1. Introduction

In the current galaxy formation paradigm, galaxies grow hierarchically via accretion of diffuse gas and dark matter via filaments and mergers with other galaxies (White & Rees 1978; Schaye et al. 2015).
Mergers with other galaxies can be in the form of a major merger: where two galaxies of similar mass collide, potentially changing the morphological type of the galaxy. Minor mergers, where a galaxy of lower mass is accreted onto a more massive galaxy, happen more frequently and recent minor merger events can leave their trace in the form of galaxy halo substructure.
An abundance of substructure has been observed in our galaxy (Majewski et al. 1996; Newberg et al. 2002; Belokurov et al. 2006) and is most commonly in the form of stellar streams, these are streams of stars which were once their own galaxy, now being shredded and accreted onto our galaxy. Perhaps the most studied stellar stream in our own galaxy is the Sagittarius stream, which originates from the Sagittarius dwarf galaxy (Ibata et al. 1995). The Sagittarius stream is a stream of stars extending both towards and away from the Milky Way centre (Majewski et al. 2003).
All galaxies are known to host globular clusters (GCs), these are dense clusters of stars which have all been born at the same time out of the same material. When a galaxy gets accreted onto another galaxy it brings with it its GC population along with the stars from the dwarf galaxy. The Sagittarius stream is thought to host 5-9 GCs (Bellazzini et al. 2003; Law & Majewski 2010). These star clusters are being integrated into our own GC population in the same way that the stars are being integrated into our stellar population.
GCs which are associated with stellar streams have been formed in a galaxy which has a different star formation history, and hence star cluster formation history, than the galaxy in which they currently reside. Therefore, clusters which are associated with a particular stellar stream will have different ages and metallicities than those clusters which were formed in the main galaxy, and these ages can extend to be much younger than the host galaxy's population (Dotter et al. 2011; Leaman et al. 2013).

Accreted galaxies which cause stellar streams in other galaxies are by definition lower mass than the main galaxy onto which they are falling. Since lower mass galaxies contain lower metallicity stars (Peng & Maiolino 2014) we also expect the GCs associated with stellar streams to have a lower mean metallicity than the rest of the population.

Star clusters have been forming for almost a cosmic time and are far easier to observe in external galaxies than individual stars. This makes a galaxy's star cluster population a powerful tool to use to build up a picture of its formation (Kruijssen et al. 2018). This work aims to use simulations from the E-MOSAICS project to be able to investigate properties of the star clusters which are associated with a stellar stream at redshift 0 i.e. present day. We examine the properties of the star clusters on and off the streams and then relate these properties to the parent galaxy properties.

2. Simulations and Methods

2.1. E-MOSAICS

E-MOSAICS (MOdelling Star cluster population Assembly in Cosmological Simulations within EAGLE) is used to trace GC formation, evolution and disruption in a cosmological simulation. Modelling star cluster systems requires knowledge of the star cluster formation, evolution and disruption processes.

Star cluster evolution depends on the environment and therefore will vary between clusters and galaxies, this requires the ability to model the formation and evolution of galaxies. This is where the EAGLE (Evolution and Assembly of GaLaxies and their Environments) simulations are utilised (Schaye et al. 2015). EAGLE is a set of hydrodynamical simulations of the formation of a cosmologically representative sample of galaxies in a standard cold dark matter universe. The results from EAGLE give a galaxy stellar mass function which reproduces the observed function to less than 0.2 dex over the full resolved mass range, this is a level which had never been produced before in hydrodynamical simulations. For a full description of the models see Schaye et al. (2015).

A sub grid model is used within EAGLE to resolve individual star clusters. Star cluster populations can form each time a star particle is formed. The properties of the cluster population (e.g. age, metallicity and position) are determined by the properties of the star particle is it attached to (Pfeffer et al. 2018).

The mass loss and potential disruption of clusters is also tracked. Mass loss occurs via stellar evolution (which is tracked for each stellar particle by the EAGLE model (Wiersma et al. 2009)) and dynamical evolution in the form of two-body relaxation, tidal shocks and dynamical friction (Kruijssen et al. 2011).

E-MOSAICS predicts well the properties of the star clusters from the properties of interstellar gas in the simulated galaxies. This is confirmed through these properties being relatively similar to observations of young clusters in nearby disc galaxies. The mass functions of clusters formed from the highest pressure and density gas is similar to that observed for the Milky Way. The mass functions of clusters formed from lower pressure gas generally reproduce the high mass end of the Milky Way GC mass function. However, the number density of low mass clusters is over predicted, this is due to the lack of a cold, dense interstellar gas phase in the EAGLE model which would disrupt many of these clusters, this will be addressed in a future generation of models (Pfeffer et al. 2018).

2.2. Methods

The E-MOSAICS simulations are used to find and trace GCs which are associated with stellar streams in the 16 Milky Way like halos. The advantage of simulation based work is the ability to be able to know the positional history of each individual star particle. This allows us to trace the star particle and in this case its associated star clusters in position from formation until redshift 0. This allowed us to view the current

positions of the stars and clusters associated with each individual galaxy accretion event, meaning we could decide whether the stars were in a stream like configuration without the contamination from any other stars or clusters in the main galaxy.
The current positions of the stars from each accretion event was plotted in a stellar density map. Figure 1 shows this process for one of the galaxies which shows a clear stellar stream, where the GCs are shown as coloured points on top of the stellar density map and we show the process of first removing the stars and clusters formed int the main galaxy and then plotting just one of the accretion events.
Furthermore, all of the clusters which were associated with a stream like accretion event were put in the 'on stream' category as this is what an observer would do with kinematic information about the clusters.

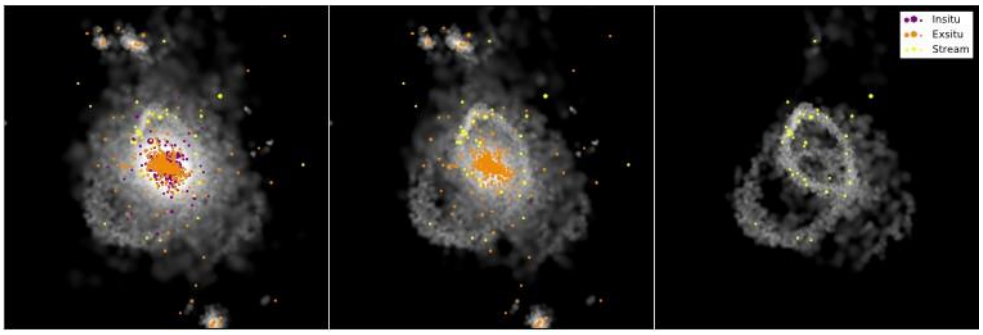

Figure 1. *From left to right the plots show the full galaxy, the accreted component and one clear stream.*

These are in a 300 kpc box.

3. Results

3.1. The relationship between the age and the metallicity of the clusters associated with stellar streams
Figure 2 shows the median age of the clusters on a stream relative to the rest of the population as a function of the median metallicity ([Fe/H]) of the clusters on a stream relative to the rest of the population. Here the large galaxy to galaxy variation in the properties of the clusters is highlighted. The age of the clusters in these streams are neither preferentially older or younger than the rest of the population. However, most of the streams contain clusters which are more metal poor than the rest of the population.

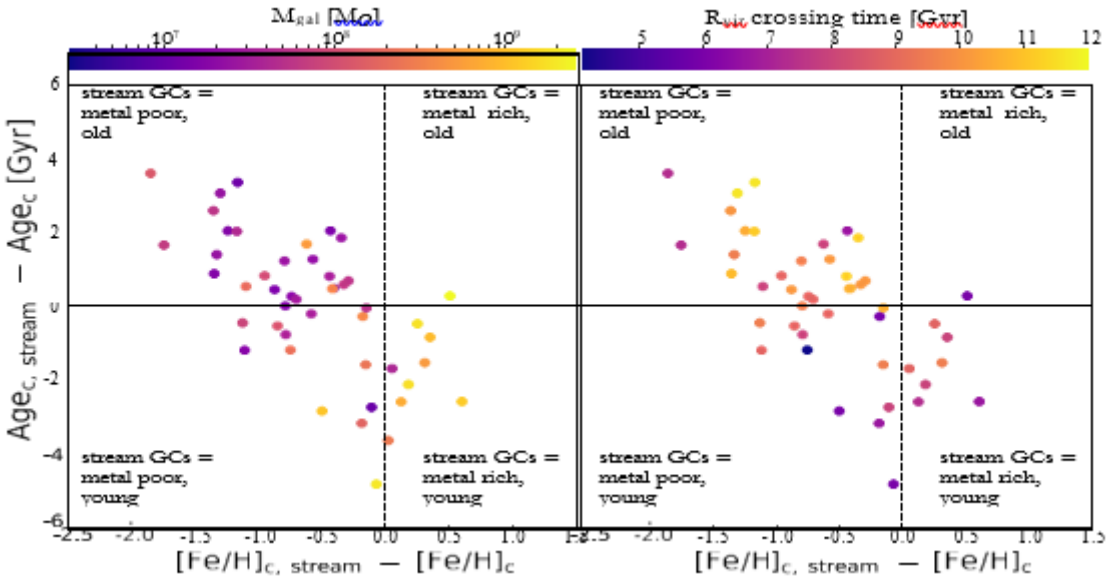

Figure 2. *The difference in the median cluster ages between the stream and non stream clusters plotted as a function of the difference in their median stream metallicities. Each point represents one stream. The non-stream population refers to all the clusters which do not lie on this particular stream; it therefore includes clusters which lie on other streams in this halo. Top panel: the colours represent the host galaxy's stellar mass before infall into the halo. Bottom panel: the colours represent the viral radius crossing time.*

The median age and metallicity of the GCs associated with the streams are anti-correlated and also dependant on the mass (figure 2, left panel) and the time of infall (figure 2, right panel) of their parent galaxy. If a stream hosts GCs which are of older age and lower metallicity than the rest of the population then this stream is likely to have been accreted early on in the formation of this galaxy. This stream is also likely to have been of low mass.

By first order approximation we could say that being more massive and having a younger and more metal rich GC population are simply by-products of a galaxy falling into the halo of the main galaxy more recently. When a galaxy falls into the halo of another galaxy its mass starts to be acquired by the more massive galaxy, meaning the satellite galaxy undergoes gas stripping. With minimal star forming gas the galaxy cannot form any more GCs and so its GC population is frozen. This means that streams caused by galaxies which have entered the halo of the main galaxy more recently can be more massive because the stream progenitor galaxy has been allowed to continue to grow through accretion and star formation in isolation for longer. There is also the second order effect that when more massive satellite galaxies enter the halo of the main galaxy they are able to retain their star forming gas and remain stable for longer than a lower mass galaxy. This means that more massive galaxies can therefore continue to form stars and GCs even after they have entered the halo of the main galaxy. These two effects combined are the reason why we see that streams which entered the halo of the main galaxy more recently and are more massive host younger and more metal rich clusters.

3.2. The relationship between the cluster formation history and the mass and the infall time of the parent galaxy

The cluster age range is a direct probe of cluster formation history, a greater cluster age range means a more extended cluster formation history. Figure 3 shows that more massive satellite galaxies have cluster age ranges which extend to higher values than lower mass satellites. This is confirmation of the explanation given above that a more massive satellite galaxy can have a more extended cluster formation history and contain younger and GCs. However, at a given mass there is still a large scatter in the GC age range. This scatter is related to the variations in the infall time of the satellites, for two satellites of the same mass the one which was accreted long ago has to build up that mass much faster than the one which was accreted more recently. This means that the galaxy which was accreted long ago will have a smaller cluster age range because it had a shorter time in which to form and accrete enough stars to reach this mass.

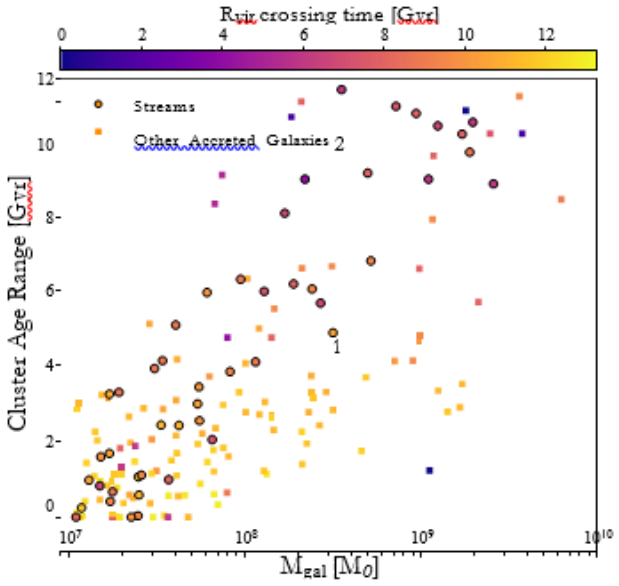

Figure 3*. The age range of the clusters which have been accreted alongside a particular satellite galaxy as a function of the parent satellite galaxy's stellar mass. Each point represents an accreted galaxy, those accretion events which are seen as streams at redshfit 0 are represented by circles and the rest of the accreted galaxies are represented by squares.*

4. Conclusions

We present the star cluster properties of 16 Milky Way like halos of the E-MOSAICS simulations. We specifically investigate the properties of the clusters which are associated with the stellar streams relative to the clusters in the rest of the population and find a significant scatter between the results for each individual stream. This scatter is explained through the mass and the infall time of the stream progenitor galaxy - more massive and recently accreted galaxies include star clusters which are metal rich and younger than the rest of the population.

More recently accreted galaxies can be more massive since they have been allowed to evolve and grow in isolation for longer, however being more massive doesn't necessarily mean that the galaxy was accreted more recently. There are some massive galaxies which were accreted long ago, the time of infall will be reflected in the age range of the clusters associated with this galaxy. A more massive galaxy which crossed the viral radius of the main group long ago had to build up this mass much faster and so will have a much shorter age range than a galaxy of the same mass which was accreted more recently.

In conclusion, we find a much greater scatter between the properties of clusters which are associated with a stellar stream than initially expected. For GCs on stellar streams which would be easily observable in our own galaxy and local group galaxies(> 108 M⊙) we would find that the GCs are on average younger than the rest of the population but there is still a huge scatter on how much younger they would be. The actual values are highly variable from galaxy to galaxy and accretion event to accretion event, with two main factors being the mass of the accreted galaxy and the time this galaxy fell into the halo of the main galaxy.

References

Bellazzini M., Ferraro F. R., Ibata R., 2003, AJ, 125, 188 Belokurov V., et al., 2006, ApJ, 642, L137

Dotter A., Sarajedini A., Anderson J., 2011, ApJ, 738, 74 Ibata R. A., Gilmore G., Irwin M. J., 1995, MNRAS, 277, 781

Kruijssen J. M. D., Pelupessy F. I., Lamers H. J. G. L. M., Portegies Zwart S. F., Icke V., 2011, MNRAS, 414, 1339

Kruijssen J. M. D., Pfeffer J., Crain R. A., Bastian N., 2018, preprint Law D. R., Majewski S. R., 2010b, ApJ, 718, 1128

Leaman R., VandenBerg D. A., Mendel J. T., 2013, MNRAS, 436, 122 Majewski S. R., Munn J. A., Hawley S. L., 1996, ApJ, 459, L73

Majewski S. R., Skrutskie M. F., Weinberg M. D., Ostheimer J. C., 2003, ApJ, 599, 1082 Newberg H. J., et al., 2002, ApJ, 569, 245

Peng Y.-j., Maiolino R., 2014, MNRAS, 438, 262

Pfeffer J., Kruijssen J. M. D., Crain R. A., Bastian N., 2017, 475, 4309 Schaye J., et al., 2014, MNRAS, 446, 521

White S. D. M., Rees M. J., 1978, MNRAS, 183, 341

Wiersma R. P. C., Schaye J., Theuns T., Dalla Vecchia C., Tornatore L., 2009, MNRAS, 399, 574

ISSN 2398-6611 (Online)

Silvia Martocchia Age as one of the major factors in the onset of multiple populations in stellar clusters

S. Martocchia et al.
Astrophysics Research Institute, LJMU
s.martocchia@2016.ljmu.ac.uk

Once thought to be formed by simple stellar populations, where each star shares the same abundance and age within some small tolerance, globular clusters (GCs) have been observed to host multiple populations (MPs) of stars. This evidence has manifested through star-to-star light elements abundance variations (C, N, O, Na), which are not observed in field stars of the same metallicity. These chemical anomalies also show anti-correlations in some elements, such as the Na-O anti-correlation (Carretta et al. 2009) and the C-N anti-correlation (Cannon et al. 1998). Furthermore, evidence for MPs may be assessed through photometry, by looking at splittings and/or spreads in the clusters colour-magnitude diagrams, from the Main Sequence (MS), up to the Red Giant Branch (RGB) and Horizontal Branch (HB), by using suitable colour combinations (e.g., Piotto et al. 2015), sensitive to the elements that vary between the subpopulations.

The origin of MPs is still under debate (e.g., D'Antona et al. 2014, Bastian et al. 2015), and multiple models have been put forward. In the most popular MP formation models, a secondary population (SP) of stars is formed from the ejecta of massive evolved stars from a first population (FP), diluted with some amount of unprocessed material (e.g. Decressin et al. 2007; D'Ercole et al. 2008; de Mink et al. 2009). While the nature of stellar polluters changes in different models, none of these scenarios can reproduce the main observational properties of MPs without making ad hoc assumptions (e.g. Bastian et al. 2015, Bastian & Lardo 2015). Indeed, we still lack a self-consistent explanation of the physical processes at the basis of the MP formation and which property controls whether a GC will host MPs or not.
The presence of multiple populations in GCs appears to be ubiquitous in the most nearby galaxies. Milky Way GCs have been largely studied (Gratton et al. 2012) and almost all old (i.e., >10 Gyr) clusters surveyed so far have been found to host MPs, as well as in the Fornax dwarf galaxy (Larsen et al. 2014), in the Sagittarius dwarf galaxy (Carretta et al. 2014), in the Large Magellanic Cloud (LMC, Mucciarelli et al. 2009) and in the Small Magellanic Cloud (SMC, Niederhofer et al. 2016, Hollyhead et al. 2017). While MPs are commonly detected in massive and old clusters, light elements variations are not found in clusters of comparable age but lower mass (e.g., 104 M⊙, E3, Salinas & Strader 2015). Such evidence led many to support cluster mass as the controlling property on whether a GC will host MPs (Gratton et al. 2012). Nonetheless, the lack of chemical spreads in relatively young (~1-2 Gyr), but still massive (few times 105 M⊙) clusters found by Mucciarelli et al. 2008 suggested that cluster age may play a key role.

We present here the main result from our Hubble Space Telescope (HST) photometric survey. This consists in HST observations of nine star clusters in the LMC/SMC. All sources have similar masses (~105 M⊙) but span a wide range of ages (from 1.5 Gyr up to 11 Gyr). The main goal of our survey is to test whether MPs are exclusively found in ancient GCs, and hence, to shed light on the physical property that controls the onset of MPs. The first main result of my work was the unexpected finding of a strong age dependence in both the onset and the properties of multiple populations in clusters. All clusters in the sample older than 2 Gyr were found to host MPs, while all clusters younger than this limit do not (see

Figure 1). This was a completely unexpected result that has dramatic implications for our understanding of the phenomenon. Additionally, I found that the extent of the MPs (in both chemical spread and in the number of stars that show the strange chemical pattern) both were a strong function of age, with older clusters having more extreme populations. Hence, these results point in a completely new and exciting direction, that the phenomenon is linked to stellar evolution.

Finally, we find that the two populations present in the 2 Gyr old cluster (i.e. NGC 1978) are indistinguishable in terms of age, with a difference of a few Myr or less between them. This support a scenario where no multiple bursts of star formation are invoked for the origin of multiple populations, or that they happened nearly concurrently, i.e. abundance anomalies are not originated by means of multiple generations created over a large time separation.

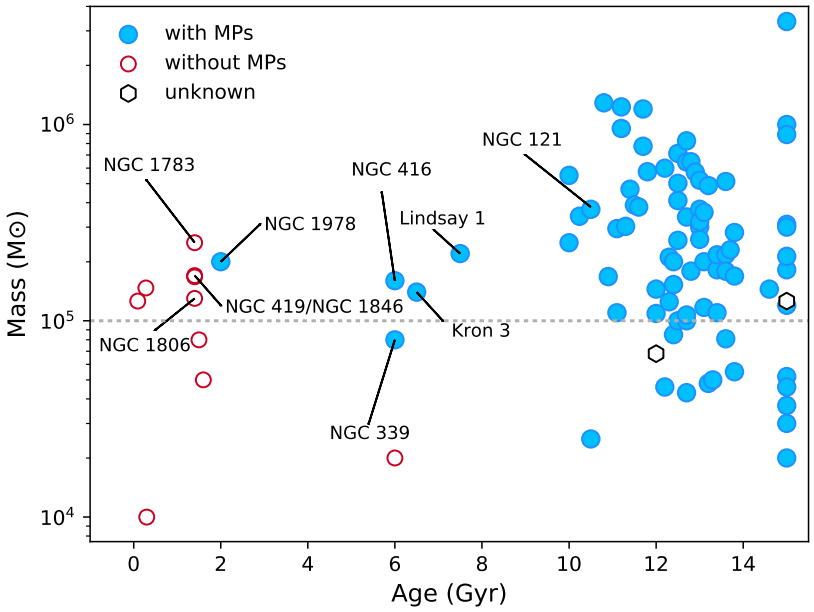

Figure 1. *The relation between age and mass for the clusters in our survey (labelled) as well as clusters taken from the literature. Clusters which are found to host MPs are indicated with blue filled circles while clusters which do not show MPs are marked with red open circles. Clusters where the presence or absence of MPs is still under debate are shown as open hexagons.*

ISSN 2398-6611 (Online)

Robert Poole-Mckenzie Studies of the local dark matter velocity distribution using new cosmological simulations

R Poole-Mckenzie
2.24, Astrophysics Research Institute, 146 Brownlow Hill, Liverpool, L3 5RF r.poolemckenzie@2013.ljmu.ac.uk

Abstract: The detection signal of dark matter (DM) relies significantly on its local velocity distribution. An accurate model of the local DM velocity distribution is essential to obtain reliable constraints on DM particle properties, currently a simple Maxwellian distribution is used. We investigate the local DM velocity distribution using Milky Way mass-like galaxies generated from new, high-resolution, hydrodynamical cosmological simulations. Accounting for the effects of baryon physics, alignment of the galactic disk and the seasonal velocity variation. We define the local region over a radial distance of 8.5 ± 1 kpc and up to ± 1 kpc from the galactic plane. Results show the velocity distribution in the local neighbourhood is not best fitted using a simple Maxwellian distribution. We are investigating the effects of the triaxial shape of the DM halo and of the recently disrupted substructures may have in the local neighbourhood. This work aims to improve the constraints for the direct detection of DM.

Keywords: dark matter, direct detection

1. Introduction

1.1 The cosmological model

Observations of the current large-scale structure distribution of the universe support a well-defined cosmological model, known as □CDM (CDM denoting Cold Dark Matter and □ representing the cosmological constant; a parameter that defines the universes accelerating expansion). □CDM suggests that the universe is comprised of □ 5% baryonic matter (□$_b$); □ 27% dark matter (□$_{dm}$); □ 68% dark energy (□$_□$) [1,2]. □CDM plays a vital role in successfully explaining the formation of large-scale structure, providing significant agreement between observations and theoretical predictions. At the present time, dark matter appears to act as a non-relativistic collisionless fluid [3], matching the growth of large scale structures very well [4]. However, on smaller scales the □CDM model raises several problems, in particular the cuspy-core and missing satellites problems.

1.2 The WIMP paradigm

The idea of dark matter (DM) was first proposed in the early 20th century [5]. Very little is known about DM as a particle, however it must be consistent with several observational constraints [6]. A number of DM particle candidates fall within this wide range of limits, with the most compelling evidence favouring that of the Weakly Interacting Massive Particle (WIMP) [7]. There is no clear definition of a WIMP, however if its existence is proven, it would be a new fundamental particle that interacts via gravity. According to cosmology the WIMP must have been produced thermally in the early universe and have a self-annihilation cross section of $\langle\sigma v\rangle \sim 10^{)*+}$ cm^3 s^{-1} (assuming $\Omega_{\_}{}_{\_}h^* \approx 0.12$) [8].

1.3 Direct detection

The observationally confirmed presence of a DM halo in our galaxy provides an interesting source of investigation for DM particle searches. Several experiments have played an important role in this attempt to directly detect DM in the form of WIMPs via their elastic scattering off of nuclei [9]. Direct DM detection aims to measure the nuclear recoil of a standard model particle as it interacts with a WIMP. The differential scattering rate of a WIMP-nuclei interaction (i.e. the signal expected) can be written as,

$$\frac{dR}{dE}(E,t) = \frac{N_T \rho_\chi}{m_\chi m_A} \int_{v_{min}}^{v_{esc}} v f_E(\vec{v},t) \frac{d\sigma}{dE}(v,E) d^3\vec{v} \qquad (1)$$

where N_T is the number of nuclei per kilogram of the detector, ρ_χ is the local DM density, m_χ and m_A are the DM and nuclei particle mass, $\vec{v}$ is the velocity of the DM particle relative to the Earth, $f_E(\vec{v},t)$ is the velocity distribution of the WIMP relative to the Earth, v_{min} is the minimum velocity a WIMP requires to produce a detection at energy E and v_{esc} is the velocity at which the WIMP is not bound by gravity to the Milky Way.

The signal from the DM interactions relies significantly on the local velocity distribution and the local DM density. An accurate model of the local DM velocity distribution is essential to place improved constraints on the DM particle properties, assuming the standard halo model (SHM) a simple Maxwell-Boltzmann (MB) velocity distribution is used,

$$f(\vec{v}) = \frac{N}{2\pi\sigma_v^2} \exp\left(-\frac{\vec{v}^2}{2\sigma_v^2}\right) \qquad (2)$$

where N is the normalisation constant and σE is the velocity dispersion in one-dimension.

1.4 Simulations

The complex nature of the universe that is observed today can be reasonably well modelled using the latest cosmological simulations. Early N-body simulations focused on the hydrodynamics of formation and cooling of the universe, where agreement between the simulations and observations of galaxies was poor. In recent years with advancement of computing technology, more accurate and higher resolution simulations have been carried out, these include; EAGLE [10], Millennium [11], Illustris [12]. These newer hydrodynamical simulations are advantageous due to their ability to evolve both dark matter and baryonic matter self-consistently. The EAGLE (Evolution and Assembly of GaLaxies and their Environments) project consists of a collection of some of the largest cosmological hydrodynamical simulations ever produced. The simulations use approximately seven billion particles, inside a volume with side length of 100Mpc, to model the formation of galaxies and supermassive black holes in a standard □CDM universe. The simulation originates from a near uniform state before any stars or galaxies have formed. The system is then evolved using the cosmological parameters constrained by Plank satellite data of the cosmic microwave background (CMB).

2. Methodology

We investigate the local DM velocity distribution of 12 Milky Way mass-like halos generated from new, high-resolution, hydrodynamical cosmological simulations called 'EAGLE zooms' (figure 1). These simulations are based on the same structure as the EAGLE project with the addition of improved resolution thanks to the re-simulation of smaller volumes. These simulations can be run with and without baryonic physics, allowing us to directly compare the dark matter only simulations with full baryonic simulations.

Throughout this study we use a coordinate system that is aligned with the inner 20 kpc of the galactic disk. We define the local region as a cylindrical shell, with a radial distance of 8.5 ± 1 kpc and up to ± 1.5 kpc from the galactic plane (where 8.5 kpc is the Suns radial distance from the centre of the Milky Way). The local DM velocity distributions for all halos are fitted with several functions including a

MB distribution. After making several assumptions about DM physical properties, the detection signal for each distribution function is calculated and compared.

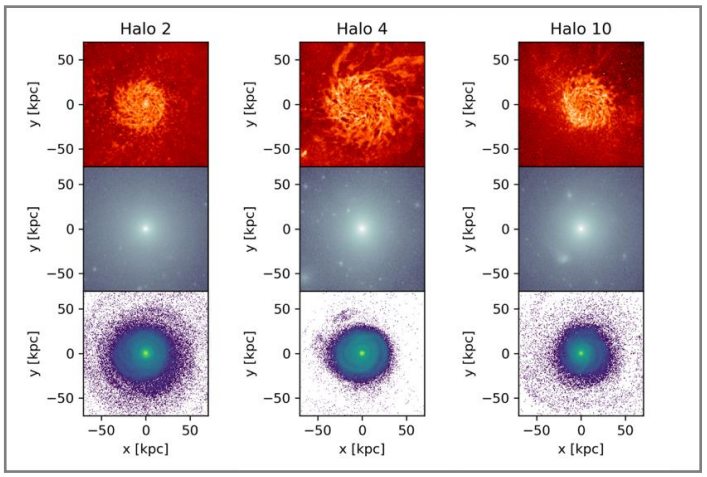

Figure 1 – Shows face-on view (x-y plane) of 3 out of 12 'EAGLE zooms' halos. Top, middle and bottom panels show the gas, dark matter and stellar components, respectively.

3. Results

The local DM velocity distribution for all 12 halos follow a similar distribution, however the exact shape of the distribution does vary from halo to halo (figure 2). Preliminary results show that the local velocity distributions do not follow a simple MB distribution.

We investigated the possibility that the variation in velocity distributions between halos may be associated with the shape of DM halo. The shape parameters (a > b > c) of the DM halos can be calculated using the square root of the eigenvalues from the diagonalisation of the three-dimensional mass distribution tensor,

$$M_{N,X} = \sum_{Z=1}^{N_Z} m_Z x_{N,Z} x_{X,Z}$$

(3) where N_Z is the number of all particles that belong to the halo, $x_{N,Z}$ denotes the element i (with i, j = 1, 2, 3 for a 3D particle distribution) of the position vector of particle p, and m_Z is mass of the p^{th} particle. Initial results show that the triaxiality, sphericity and flatness have no correlation with the local velocity distribution.

4. Future Work

The next step is to determine whether the local DM velocity distribution obtained from the simulations significantly effects the detection signal and what impact this has on the constraints of detecting DM. Additionally, we aim to investigate what factors may be causing the differences seen in the local DM velocity distributions between the halos, one avenue to explore is the merger history of the halos.

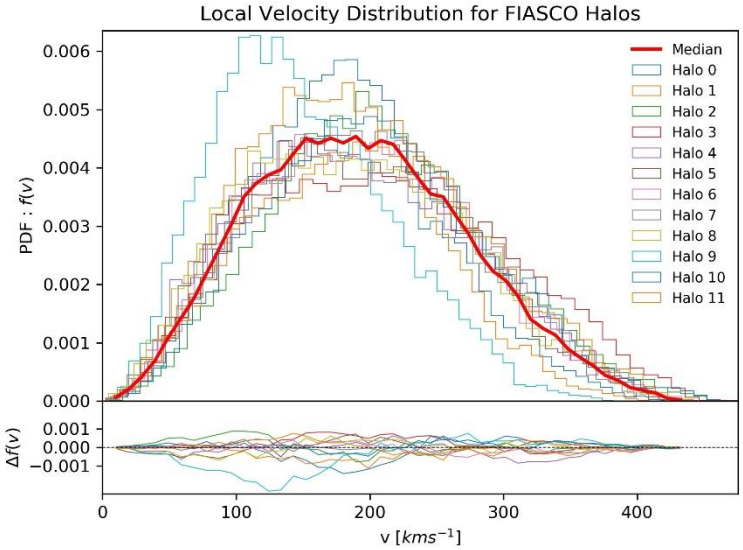

Figure 2 – Top panel: The local velocity distributions for all halos in the 'EAGLE zooms' simulations, where v is the modulus of the velocity vector; the red line shows the median of the halos. Bottom panel: The relative difference of the halos compared to that of the median. The bin size is 10 kms^{-1} in all plots.

5. References

[1] Riess, A. G., et al. (1998). Observational evidence from supernovae for an accelerating universe and a cosmological constant. *The Astronomical Journal*, *116*(3), 1009.
[2] Perlmutter, S., et al. (1999). Measurements of Ω and Λ from 42 high-redshift supernovae. *The Astrophysical Journal*, *517*(2), 565.
[3] Clowe, D., et al. (2006). A direct empirical proof of the existence of dark matter. *The Astrophysical Journal Letters*, *648*(2), L109.
[4] Viel M., Becker G. D., Bolton J. S., Haehnelt M. G., Rauch M., Sargent W. L. W. (2008) Physical Review Letters, 100, 041304.

[5] Zwicky, F. (1933). Die rotverschiebung von extragalaktischen nebeln. *Helvetica Physica Acta*, *6*, 110- 127.
[6] Arcadi, G., et al. (2018). The waning of the WIMP? A review of models, searches, and constraints. *The European Physical Journal C*, *78*(3), 203.
[7] Steigman, G., & Turner, M. S. (1985). Cosmological constraints on the properties of weakly interacting massive particles. *Nuclear Physics B*, *253*, 375-386.
[8] Ade, P. A., et al. (2016). Planck 2015 results-xiii. cosmological parameters. *Astronomy & Astrophysics*, *594*, A13.
[9] Goodman, M. W., & Witten, E. (1985). Detectability of certain dark-matter candidates. *Physical Review D*, *31*(12), 3059.
[10] Schaye, J., et al. (2014). The EAGLE project: simulating the evolution and assembly of galaxies and their environments. *Monthly Notices of the Royal Astronomical Society*, *446*(1), 521-554.
[11] Springel, V., et al. (2005). Simulations of the formation, evolution and clustering of galaxies and quasars. *nature*, *435*(7042), 629-636.
[12] Vogelsberger, M., et al. (2014). Properties of galaxies reproduced by a hydrodynamic simulation. *Nature*, *509*(7499), 177-182.

ISSN 2398-6611 (Online)

Jessica Kitamura Red giant branch stars from the Spitzer-IRAC survey in the Galactic globular cluster ω Centauri

J R Kitamura
Astrophysics Research Institute, Liverpool John Moores University, IC2, Liverpool Science Park, 146 Brownlow Hill, Liverpool, L3 5RF, UK
j.r.kitamura@2015.ljmu.ac.uk

Abstract. It has been known for 50 years that ω Centauri shows an extremely complex stellar chemistry, with large variation in iron ranging from [Fe/H] ~ -2 [Fe/H] ~ -0.6, and light elements (like He, C, N...). Because of its properties it is commonly accepted that ω Cen is the remnant of a dwarf galaxy orbiting the Milky Way and partially disrupted because of tidal interactions. Here we present for the first time a multiband analysis ranging from optical to mid-infrared wavelength of the different subpopulations in the core of ω Cen. This study is based on a proper combination of ground-based and original Spitzer photometric data as well as result from previous spectroscopic surveys.

Keywords. techniques: photometric - infrared: stars - globular clusters: general - stars: Population II - stars: Hertzsprung-Russell and colour-magnitude diagrams

1. Introduction

Stars of all evolutionary stages lose mass and the mass recycled in the interstellar medium will be part of the next generation of stars and planets. The understanding of the mass loss (ML) process that happens in red giant stars of globular cluster (GC) might help us to better estimate the post-main sequence evolutionary stages of the stars and the intra-cluster gas enrichment.
Mass loss in red giant branch (RGB) stars might be one of the reasons for the blue horizontal branch observed in metal-poor GC [1] and explain the period-luminosity relation for RR Lyrae stars, as a considerable amount of mass should be lost not only in the RR Lyrae pulsation phase itself but also during the giant phase [2]. Line profiles asymmetries have been used to prove chromospheric mass motions for individual RGB in GC [3,4]. Both studies detected Hα emission at low luminosities, log $(L/L_{\odot})$ ~ 2.5, and the mass outflow velocities increase with luminosity.
[5] using ISOCAM observations found a mid-infrared excess associated with giants in several GCs and attributed it to dusty circumstellar envelopes. They concluded that the ML occurs mainly at the tip of RGB and is episodic. [6] identified about 100 mid-infrared excess RGB stars in 47 Tuc using Spitzer-IRAC images and derived an empirical mass loss law for Population II stars. Mass loss rates derived from these observations showed that the ML increases with luminosity and it possibly is episodic.
The Galactic GC ω Centauri (also known as NGC 5139) is the most massive (~ 2.9 x $10^6 M_{\odot}$) and luminous GC in the Milky Way, with a complex stellar population sampling probably many different ages, and a large range in iron spanning from [Fe/H] ~ -2.0 to [Fe/H] ~ -0.6 (e.g. [7,8,9]). Due to its properties, it is commonly accepted that this GC is a remnant of a dwarf galaxy orbiting the Milky Way

and was partially disrupted because of tidal interactions (e.g. [10]).

ω Cen was one of the GCs studied by [5], they selected dusty candidates by the (K - 12) colour excess. However, their sample was for a small region of the cluster core, where there is less than 30% of the brightest giants, so they only found the long-period variable (LPV) star 44262 (also known as V42) and could not proceed to the mass loss rate determination. [11] characterized stars observed with Spitzer and selected about 140 mass-losing candidates, most of them AGB stars. They detected stars with the most significant ML to be near the tip of RGB and estimated that the cluster have lost about 2.9-4.2 x $10^{-7} M_{\odot} yr^{-1}$, with more than 60% of this total regarding the three brightest M-type stars. The authors also predicted that if the ML has been constant in the cluster, in the last 3.4 x 10^6 years ω Cen has lost about 1-2 $M_{\odot}$.

In this work we attempt to identify red giant stars with infrared (IR) excess in the Galactic GC ω Centauri. Our observations are based on the Infra-Red Array Camera (IRAC; [12]) on board of the space-based telescope Spitzer. Mid-IR photometry with Spitzer-IRAC assists the detection of the colour excess that comes from the emission of a circumstellar envelope around RGB and AGB stars (e.g. [13,14]) and provides an exclusive opportunity to calibrate stellar populations in colour-magnitude not available from ground-based facilities. The 8μm IRAC band is especially sensitive to the warm dust emission [15]. In chapter 2 is presented details about the observations and the photometry, chapter 3 explains the method used to select the dusty stars and the conclusions can be found in chapter 4.

2. Observations and data reduction

Spitzer-IRAC photometric observations were taken between September 2005 and July 2006. Images were observed in the channels 3.6, 4.5, 5.8 and 8 μm in short- and long-exposure times, covering a 5' x 5' field of view [6,16]. Figure 1 shows the three-colour image of ω Cen.

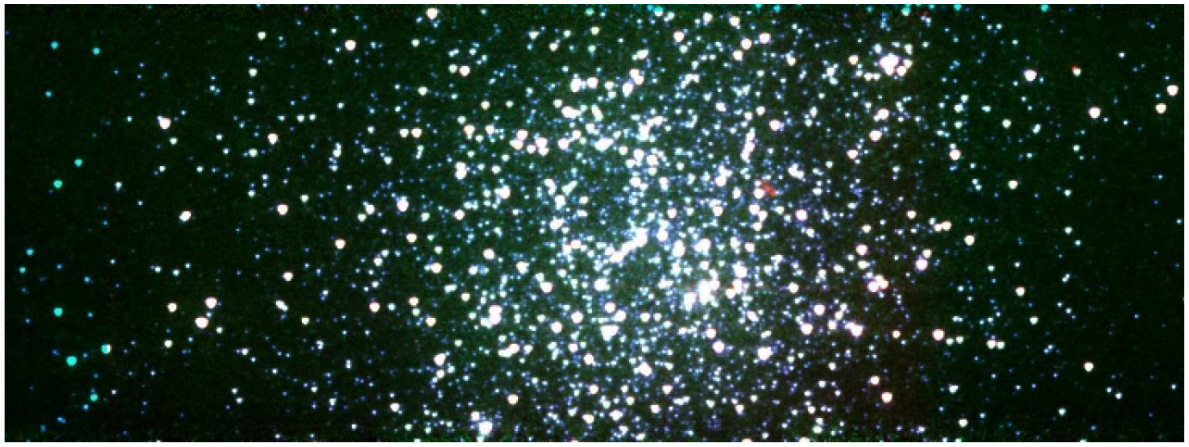

Figure 1: Three-colour image of ω Cen. Red is 8 μm, green is 5.8 μm and blue is 3.6 μm.

Point Spread Function (PSF) fitting was performed for each Spitzer-IRAC channel and exposure times by using ALLSTAR routine of DAOPHOT reduction package [17]. The PSF was set to vary linearly with position in the frame and was constructed from about 40 bright, relatively isolated stars widely

spread throughout the entire image, except for the crowded cluster core that was avoided. To refine the photometric results, all objects with instrumental magnitude error deviating from 1σ were rejected. A few hundredths of magnitude offset in colour were detected between the short- and long-exposure frames. To account for this offset we have taken an average of the magnitude difference within a broad magnitude bin and added it to the magnitude of the short-exposure frames. Then, the short- and long-exposure photometry lists were merged. Stars brighter than the instrumental magnitude 19.5 (where there was no saturation level) in 8μm were selected from the short-exposure while fainter ones were selected from the long-exposure photometry.

The instrumental magnitude of each stars was converted into the Vega magnitude system by using the zero-magnitude flux densities of [18]. Complementary ground-based near-IR photometry has been cross-correlated with the mid-IR Spitzer-IRAC, the SOFI@ESO-NTT [19] catalogue (for the central region ~ 300 pixels radius) and supplemented with the 2MASS catalogue for the external region. The optical catalogues from [20] and [21] have been cross-correlated with the mid- and near-IR photometry list. The final catalogue contains about 4000 stars.

Effective temperatures (T_{eff}) were obtained through the empirical (V - K) colour-temperature relation using the calibrations by [22, 23]. Due to the difference in the photometric systems, we had to transform our K_{2MASS} magnitudes to the Telescopio Carlos Sanches (TCS) photometric system as in [22]. We firstly transformed the K_{2MASS} into the Caltech (CIT) system following the transformation equations provided by [24], and then the K_{CIT} into the K_{TCS} according to [25]. We have assumed [Fe/H] = -1.7 [26], which is the metallicity main peak for ω Cen in its wide metallicity distribution. The distance modulus used to determine the absolute magnitudes is $(m - M)_V = 14.04$ and a reddening of $E(B - V) = 0.11$ [26]. The bolometric magnitude (M_{bol}) was derived from the bolometric corrections presented by [22].

3. Method

Spectral range from 3 to 5 μm is predominantly dominated by photospheric emission in cool and luminous giant stars and it has also contribution of the circumstellar dust emission. In fact, for relatively warm and low luminosity giant, as low mass RGB stars, the fraction of warm and optically thin dust emission from a circumstellar envelope that contributes in the 3-5 μm spectral range is significant. For that, the near- and mid-IR, like (K - 5.8) and (K - 8), colours are more effective in detecting the presence of small amounts of warm dust around low mass RGB [15], whilst the use of only Spitzer-IRAC colours, for instance (3.6 - 8), is mostly sensitive tracing larger amounts of cold dust around cooler and more luminous giants. With all that in mind, the use of the (K - 8) colour as the first method to select stars with a possible dust excess seems to be reasonable.

Firstly, a (K - 8) vs. M_{bol} colour-magnitude diagram (CMD) is constructed as shown in figure 4 (left panel). The mean ridge line was established, and the standard deviation was calculated in different magnitude bins for the stars in the blue side of the line, because those stars are certain to have only photospheric emission. We then flagged the stars in the red side of the line as dusty when they presented a colour excess $\geq +2.5\sigma$ from the mean ridge line. To confirm the selection of the dust excess candidates we used the (K - 5.8) vs. (K - 8) colour-colour diagram (see figure 2 – right panel) as we expect those stars to be redder in other IRAC band.

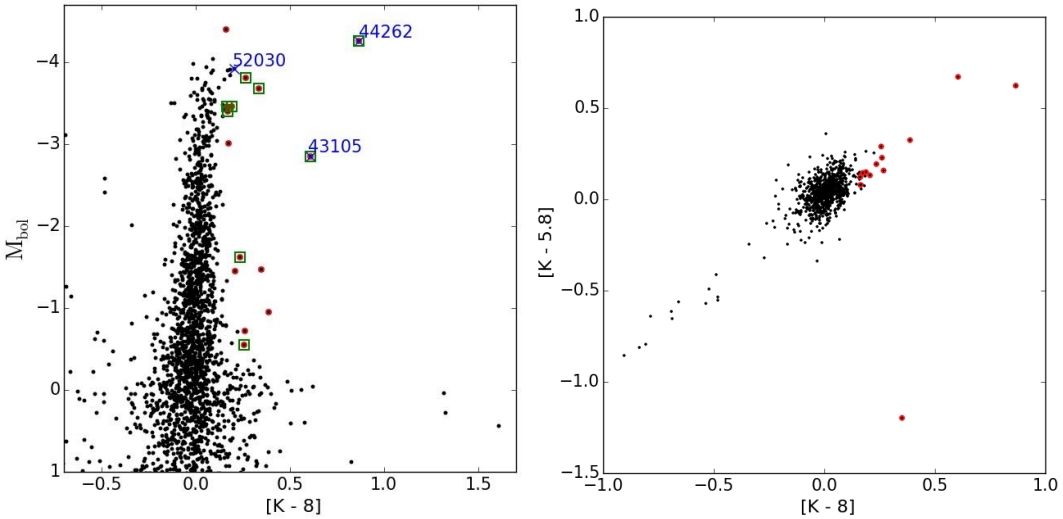

Figure 2: Left - (K - 8) colour vs. M_{bol} CMD for ω Cen. Stars with colour excess are marked with red circles, green squares are ML candidate stars from Boyer et al. (2008) and the blue crosses are known LPV. Right - (K - 5.8) vs. (K - 8) colour-colour diagram. Stars with colour excess are marked with red circles.

Table 1 presents the dusty stars and their IRAC fluxes, the derived effective temperature and luminosity, the metallicity interpolated from theoretical isochrones and whether the star is a RGB, AGB or LPV [27]. Colour excess has been found in 15 stars. A visual inspection in the B, (B - I) CMD made the separation of the RGB from the AGB stars possible. 9 stars in our sample were also identified as ML candidates by [11], all of them are AGB stars and may not present IR-excess. The reddest star has [Fe/H] = -0.7 and it is also the coolest (3452 K). [11] found [Fe/H] = -1.5 for their reddest star. The brightest stars show the metallicity ranging from -1.9 < [Fe/H] < -0.7, [11]'s sample ranges from -2.25 < [Fe/H] < -1.25, intermediate-poor metallicities may suggest that the dust production is not limited to metal-rich stars only. Stars with possible ML in our sample vary 1.2 dex in metallicity.

Table 1: Stars with colour excess

RA	DEC	3μm	4.5μm	5.8μm	8μm	Teff (K)	log (L/L0)	[Fe/ H]	Source type
201.69308	-47.49171	7.100	6.892	6.799	6.554	3452	3.59	-0.7	LPV
201.64748	-47.53004	7.837	7.821	7.752	7.645	4068	3.41	-1.9	LPV
201.77199	-47.48466	6.650	6.841	6.753	6.668	3460	3.65	-1.0	LPV
201.81588	-47.46506	-	7.766	-	7.566	3892	3.36	-1.3	LPV
201.72909	-47.47941	8.070	8.127	8.102	8.060	4033	3.27	-1.6	LPV
201.65332	-47.51379	7.989	8.038	7.992	7.952	3925	3.27	-1.3	LPV
201.49471	-47.60263	-	8.073	-	7.973	3837	3.25	-1.0	LPV
201.71746	-47.43528	8.463	8.536	8.471	8.442	3948	3.09	-1.0	RGB
201.61340	-47.47976	9.522	9.487	9.392	9.457	6034	3.03	-1.9	post-AGB
201.69620	-47.49370	10.142	10.231	10.139	10.099	4381	2.53	-1.3	RGB
201.66968	-47.54969	-	10.452	11.817	10.270	4595	2.48	-1.6	RGB
201.66025	-47.48216	10.416	10.425	10.401	10.322	4415	2.47	-1.0	RGB
201.63629	-47.51306	11.203	11.180	11.098	11.033	5079	2.27	-1.9	AGB
201.64288	-47.51644	11.454	11.462	11.349	11.317	4935	2.17	-1.9	RGB
201.69797	-47.48715	11.402	11.432	11.377	11.409	4807	2.11	-1.6	AGB

4. Conclusions and perspectives

We have catalogued 4000 stars in the GC ω Cen with Spitzer-IRAC mid-IR images, and have detected 15 stars with IR-excess, where only 5 of those are RGB stars. The colour excess may be due to the circumstellar dust around the star after the mass outflow. The ratio of ML-RGB by the total number of RGB is less than that predicted by [6,16] for other local GCs, yet this may still indicate as well that the ML is episodic. For next steps we could consider reproducing the same experiment using observations with a higher resolution photometry, as we improved the number of RGB detected with colour excess over the observations from [5], that have not found RGB losing mass in ω Cen with their ISOCAM observations. We could also acquire spectroscopic data to measure the line profile asymmetry to establish whether those stars show chromospheric mass outflow.

Acknowledgments

J.R.K. acknowledges CNPq - Brazil through the funding 234457/2014-7 for financial support.

References

[1] Rood R T 1973 *ApJ* **184** 815---38

[2] Christy R F 1966 *ApJ* **144** 108

[3] Cacciari C, Bragaglia A, Rossetti E, Fusi Pecci F, Mulas G, Carretta E, Gratton R G, Momany Y and Pasquini L 2004 *A&A* **413** 343---62

[4] Mezsaros S Z, Dupree A K and Szentgyorgyi A 2008 *AJ* **135** 1117---35

[5] Origlia L, Ferraro F R, Fusi Pecci F and Rood R T 2002 *ApJ* **571** 458---68

[6] Origlia L, Rood R T, Fabbri S, Ferraro F R, Fusi Pecci F and Rich R M 2007 *ApJl* **667** L85---88
[7] Norris J E and Da Costa G S 1995 *ApJ* **447** 680
[8] Pancino E, Pasquini L, Hill V, Ferraro F R and Bellazzini M 2002 *ApJl* **568** L101---05
[9] Origlia L, Ferraro F R, Bellazini M and Pancino E 2003 *ApJ* **591** 916---24
[10] Bekki K and Freeman K C 2003 *MNRAS* **346** L11---15
[11] Boyer M L, McDonald I, van Loon J T, Woodward C E, Gehrz R D, Evans A and Dupree A K 2008 *AJ* **135** 1395-1411

[12] Fazio G G *et al.* 2004 *ApJS* **154** 10-17
[13] Frogel J A and Elias J H 1988 *ApJ* **324** 823---39
[14] Origlia L, Ferraro F R and Pecci F F 1996 *MNRAS* **280** 572---78
[15] Origlia L, Rood R T, Fabbri S, Ferraro F R, Pecci F F, Rich R M and Dalessandro E 2010 *ApJ* **718** 522---26
[16] Origlia L, Ferraro F R, Fabbri S, Fusi Pecci F, Dalessandro E, Rich R M and Valenti E 2014 *A&A* **564** A136
[17] Stetson P B 1987 *PASP* **99** 191-222
[18] Reach W T *et al.* 2005 *PASP* **117** 978---90

[19] Sollima A, Ferraro F R, Origlia L, Pancino E and Bellazzini M 2004 *VizieR Online Data Catalog* **342**
[20] Marino *et al.* 2011 *ApJ* **731** 64
[21] Johnson C I and Pilachowski C A 2010 *ApJ* **722** 1373-1410
[22] Alonso A, Arribas Sand Martinez-Roger C 1999 *A&AS* **140** 261---77
[23] Alonso A, Arribas Sand Martinez-Roger C 2001 *A&A* **376**
1039 [24] Carpenter J M 2001 *AJ* **121** 2851---71
[25] Alonso A, Arribas S and Martinez-Roger C 1998 *A&AS* **131** 209---19
[26] Bellazzini M, Ferraro F R, Sollima A, Pancino E and Origlia L 2004 *A&A* **424** 199-211
[27] Lebzelter T & Wood P R 2016 *A&A* **585** A111

ISSN 2398-6611 (Online)

Egidijus Kukstas Environment from cross-correlations: linking effect to the cause in galaxy quenching

Egidijus Kukstas
Astrophysics Research Institute,
Liverpool John Moores University
E-mail address: E.Kukstas@2016.ljmu.ac.uk

Abstract. There is significant evidence that galaxies evolve differently depending on the environment they are in. Galaxies occupying dense parts of the Universe typically tend to be red in colour, elliptical in morphology, and possess suppressed
star formation rates relative to their counterparts in the 'field'.
Despite decades of research, little progress has been made in determining which processes are driving this evolution. We hypothesise that the reason for this is that, until recently, it has not been possible to directly measure the local physical conditions around galaxies. Instead, existing studies have focussed on optical *proxies* for local environment, from galaxy observations alone, and compared these with observed galaxy properties.
However, there has been a revolution in recent years; with large area, precise, and accurate galaxy surveys such as SDSS, DES, and DESI, in addition to CMB (Planck) and X-ray (Chandra, ROSAT) instruments, it is now possible to directly constrain the local hot gas and dark matter properties. The process can be carried out by employing map-based techniques, previously used exclusively in cosmology on CMB and lensing data. Cross-correlating these *direct* measures of hot gas and gravitational components with galaxy properties can effectively constrain the processes of environmental quenching.

Keywords. galaxy evolution, environment, quenching, cross-correlations

1. Introduction

1.1. The hierarchical galaxy formation theory

Under the currently accepted cosmological model, ΛCDM, galaxies form in a bottom-up fashion; beginning with small primordial matter perturbations in the early Universe which then grow under gravitational collapse as the Universe expands and cools. This runaway process of over-densities attracting matter and thus becoming even more massive, attracting even more matter eventually leads to self-similar, elliptical haloes (White & Rees, 1978). Since dark matter dominates the total matter content in the Universe, these haloes contain ~90% dark matter. The other 10%, baryonic gas, follows the gravitational field and settles at the bottom of the potential wells. Since baryonic matter is subject to all hydrodynamic interactions, it heats up and radiates energy – forming stars and galaxies (Mayer, et al., 2008) that we observe.

This is the current picture of the universe as we see it: a three-dimensional web of matter with filaments and sheets linking nodes of over-densities.

1.2. Galaxy evolution

Galaxies evolve by converting hydrogen/helium gas into stars. Hot gas cools, condenses, and is accreted onto a galaxy forming a disc; cold gas collapses into clouds/clumps from which entire populations of stars form. The extent to which this occurs is limited by the amount of gas available and how easily it is allowed to collapse.

Since galaxies trace the underlying density field of the cosmic web, there are many more galaxies in groups/clusters per unit volume than there are in the under-dense regions (voids). This means that the probability and rate of galaxies interacting with one another is significantly higher within groups/clusters. When the two respective populations of galaxies are studied and compared it is found that galaxies which live in dense parts of the Universe tend to have suppressed star formation rates, red colours, and elliptical morphologies (Wetzel, Tinker, and Conroy 2012; Postman and Geller 1984). An example of a galaxy cluster can be seen in figure 1.

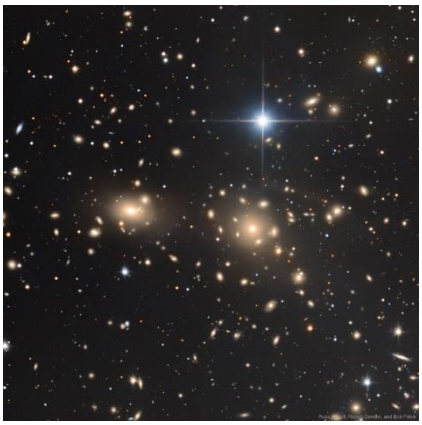

Figure 1: Coma cluster; one of the most massive, nearby clusters observed. Nearly every object in this image is a galaxy, most of which belong to the cluster. The vast majority are yellow/red in colour due to their old stellar populations and elliptical morphologies due to lack of gas. A few blue, star forming galaxies can be seen on the outskirts of the cluster – these are recently accreted galaxies and have not been quenched yet. Image credit: Russ Carroll, Robert Gandler, and Bob Franke; Dan Zowada Memorial Observatory.

1.3. Quenching mechanisms

Anything which acts to interrupt the cooling and collapsing of gas onto galaxies to form stars is said to be quenching star formation. Within groups/clusters, there are three major categories of quenching that can occur: galaxy-galaxy interaction – merging (Mihos 2004) or simply close encounters disturbing the gravitational field around galaxies (Moore and Katz 1998); galaxy-dark matter interactions where a non-isotropic gravitational field (tides) is disturbing the galaxy (Byrd 1990); and galaxy-gas interactions where a galaxy interacts with the hot gas, filling the space between galaxies, experiencing ram pressure stripping (Gunn and Gott Iii 1972) or turbulent viscous effects (Nulsen 1982).

Any one of these effects can be present in a cluster environment, and it is likely that several are acting at once. The question that arises is thus: what are the efficiencies of each and which are the most dominant?

1.4. Current approaches

Conventionally, one would obtain measures of the three cluster components and investigate how strongly they correlate with galaxy properties. By constructing models which describe how these components affect

galaxies one would then be able to describe, in detail, how it happens as well as obtain timescales, rates, and other parameters of interest. Unfortunately, two of the cluster components are extremely difficult to observe, namely, the Intra-Cluster Medium (ICM) and the Dark Matter (DM) halo. The former is very diffuse, X-ray emitting gas – both of which make observations noise-dominated and, therefore, near-impossible to detect for a single halo using current technology. The latter is invisible by its nature and so can only be observed through its gravitational interactions with other objects – either through gravitational lensing or orbital dynamics.

Due to these limitations, environmental research has been limited to optical galaxy observations only, i.e. considering a given galaxy's position in the cluster relative to its neighbours (local density, radial velocity, proximity to the centre, etc.) and inferring properties of the cluster through these secondary proxies. One then relates these environmental properties to a given population of satellite galaxies (their star formation rates, histories, colours, morphologies, etc.) to make statements about the possible processes which might be at play.

The limitations with this approach are quite clear: no direct information about the ICM or the DM halo is used. Instead, weak correlations with significant scatter and complex models are employed to determine the possible quenching process. Each study appears to arrive at a different conclusion and there is no consensus in the community.

2. Cross-correlations

There has been a revolution in observational astronomy in the last ten or so years. Large area surveys of the sky are providing huge amounts of information and, while the quality is not good enough to observe individual haloes, one can use the large area coverage via statistical methods; one such method is cross-correlations.

Cross-correlating of different datasets has been used numerous times in cosmology to constrain the underlying model and its parameters (Hill and Spergel 2014; Giannantonio et al. 2016; Hojjati et al. 2016; Harnois-Déraps et al. 2016), however, this would be the first time where it is applied to the study of galaxy environment. The algorithms are publicly available and can be reused.

Described briefly, cross-correlation involves comparing a map of one set of data to a map of a different set of data as a function of scale. The resulting statistic is called the correlation function in configuration space or a power spectrum in spherical harmonic multipole space. A positive correlation function/power spectrum indicates a correlation between the two quantities being compared.

2.1. Data

The Sloan Digital Sky Survey (SDSS, DR7) (Abazajian et al. 2009) is currently the largest galaxy survey, covering over 8000 square degrees of the northern sky and containing over two million galaxies. For this study a sub-sample was selected satisfying the following selection criteria:

- Successfully derived star formation rates, stellar masses, and redshifts.
- R-band apparent magnitude, $m_r < 17.77$.
- Stellar mass, $M_* > 10^{10} M_\odot$.
- Redshift in the range $0.008 < z < 0.14$.

This is accompanied by observations of the Cosmic Microwave Background (CMB) over the entire sky by the Planck (Planck Collaboration, 2015). These photons are formed early in the Universe and stream towards us, interacting with the cosmic web in the process. The important observable for this study is the

thermal Sunyaev-Zel'dovich (tSZ) effect, which results from CMB photons being inverse-Compton scattered by hot gas along their path. In the process, properties of the hot gas get imprinted in the spectrum of the CMB photons, namely the line-of-sight gas pressure. TSZ, therefore, is a direct measure of gas pressure within clusters.

Another dataset available is the ROSAT All Sky Survey (RASS) (Voges et al. 1999), which is a full-sky scan in the 0.5-2.0 keV energy X-ray band. These are the X-ray photons emitted by hot ICM gas along with other sources. The data is noise dominated and poor in spatial resolution but the all-sky coverage helps compensate for some of these flaws. X-ray photon arrival rate is proportional to the ICM gas density.

3. Results/Conclusions

Maps of tSZ and X-ray photon counts already exist in the desired spherical HEALPix format, it is then necessary to construct equivalent maps of galaxy properties. Each pixel on a HEALPix sphere has a spatial coordinate associated with it and so galaxies can be assigned to pixels according to their RA/DEC coordinates. Two such maps are constructed: one using the selection criteria outlined above, called the total sample, and another using a further constraint selecting galaxies with specific star formation rate below 10^{-11} yr^{-1} ($sSSFR < 10^{-11}$ yr^{-1}), called the quenched sample. A third map can be computed by dividing these two, called the quenched fraction (f_q) map; this takes overall galaxy density out of the consideration and deals with only the fraction of galaxies which are quenched at a given location in the sky. It is expected that f_q will correlate with both tSZ and X-ray signals, the question is: which is stronger?

The observed cross-power spectra show a strong correlation between the total/quenched galaxy samples and tSZ/X-ray signals. The correlation signal for f_q – tSZ/X-ray is significantly weaker but, nevertheless, statistically significant. This marks the first time ever that *direct* correlation measurements like this have been done and is an important discovery that is bound to shape the field of galaxy environment.

One major downside of using angular correlation functions and power spectra is the difficulty of interpreting the results. It is not immediately obvious what the results show by looking at the curves alone. To this effect, cosmological hydrodynamic simulations, where one has fewer limitations on desired parameters, will be employed in order to explain the observed trends. This is the direction the project will take in the future.

References

Abazajian, Kevork N, Jennifer K Adelman-Mccarthy, Marcel A A Ueros, Sahar S Allam, Carlos Allende Prieto, Deokkeun An, Kurt S J Anderson, et al. 2009. "The Seventh Data Release of the Sloan Digital Sky Survey." *The Astrophysical Journal Supplement Series* 182: 543–58. doi:10.1088/0067-0049/182/2/543.

Byrd, Gene. 1990. "Tidal Generation of Active Spirals and S0 Galaxies by Rich Clusters." *The Astrophysical Journal* 350: 89–94.

Giannantonio, T, 3‹ P Fosalba, 4‹ R Cawthon, Y Omori, M Crocce, F Elsner, B Leistedt, et al. 2016. "CMB Lensing Tomography with the DES Science Verification Galaxies." *MNRAS* 456: 3213–44. doi:10.1093/mnras/stv2678.

Gunn, James E, and J Richard Gott Iii. 1972. "On the Infall of Matter into Clusters of Galaxies and Some Effects on Their Evolution*." *The Astrophysical Journal* 176: 1–19.

Harnois-Déraps, Joachim, Tilman Tröster, Nora Elisa Chisari, Catherine Heymans, Ludovic van Waerbeke,

Marika Asgari, Maciej Bilicki, et al. 2016. “KiDS-450: Tomographic Cross-Correlation of Galaxy Shear with Planck Lensing.” *Mon. Not. R. Astron. Soc* 0: 1–14.
Hill, J. Colin, and David N. Spergel. 2014. “Detection of Thermal SZ-CMB Lensing Cross-Correlation in Planck Nominal Mission Data.” *Journal of Cosmology and Astroparticle Physics* 2014 (2). doi:10.1088/1475-7516/2014/02/030.
Hojjati, Alireza, Tilman Tröster, Joachim Harnois-Déraps, Ian G Mccarthy, Ludovic Van Waerbeke, Ami Choi, Thomas Erben, et al. 2016. “Cross-Correlating Planck tSZ with RCSLenS Weak Lensing: Implications for Cosmology and AGN Feedback.” *MNRAS* 0: 1–14.
Mihos, J Christopher. 2004. “The Evolution of Tidal Debris” 217.
Moore, Ben, and Neal Katz. 1998. “Morphological Transformation from Galaxy Harassment.” *THE ASTROPHYSICAL JOURNAL* 495: 139–51.
Nulsen, P. E. J. 1982. “Transport Processes and the Stripping of Cluster Galaxies.” *Monthly Notices of the Royal Astronomical Society* 198 (4). Oxford University Press: 1007–16. doi:10.1093/mnras/198.4.1007.
Planck Collaboration. n.d. “Planck 2013 Results. XXIX. The Planck Catalogue of Sunyaev–Zeldovich Sources.”
Postman, M, and M J Geller. 1984. “The Morphology-Density Relation: The Group Connection.” *The Astrophysical Journal* 281: 95–99.
Voges, W, B Aschenbach, Th Boller, H Bräuninger, U Briel, W Burkert, K Dennerl, et al. 1999. “The ROSAT All-Sky Survey Bright Source Catalogue.”

Wetzel, Andrew R, Jeremy L Tinker, and Charlie Conroy. 2012. “Galaxy Evolution in Groups and Clusters: Star Formation Rates, Red Sequence Fractions and the Persistent Bimodality.” *Monthly Notices of the Royal Astronomical Society* 424 (1): 232–43. doi:10.1111/j.1365-2966.2012.21188.x.

ISSN 2398-6611 (Online)

Sebastian Turner Reproducible k-means clustering in galaxy feature data

Sebastian Turner[1,*], Lee S Kelvin[1], Ivan K Baldry[1], Paulo J Lisboa[2], Steven N Longmore[1], and Chris A Collins[1]

[1]Astrophysics Research Institute, Liverpool John Moores University, 146 Brownlow Hill, Liverpool, United Kingdom, L3 5RF

[2]Department of Applied Mathematics, Liverpool John Moores University, Byrom Street, Liverpool, L3 3AF, UK

*s.turner1@2012.ljmu.ac.uk

Abstract. We test the viability of the k-means unsupervised clustering method as a galaxy classification solution for the unprecedentedly large surveys of the future. We apply the method via a cluster evaluation approach that enables us to identify reproducible clustering structure in spite of stochastic effects. We represent our sample of 7338 galaxies using a preliminary selection of five features: stellar mass, u−r colour, Sérsic index, half-light radius, and specific star formation rate. Reproducible clustering structure is identified in our sample when we search for 2,3,5, and 6 clusters. We show that our clusters are consistent with established notions of a bimodality of galaxies, and reveal an environmental dichotomy of galaxies with intermediate colours.

Keywords. galaxies: general - galaxies: statistics - galaxies: evolution - galaxies: formation - methods: statistical

1. Introduction

Understanding the diversity of galaxies in the Universe is a crucial part of understanding how galaxies form and evolve. For example, the observation of a correlation between the visual morphologies of galaxies and their local environments (Dressler 1980) enables an understanding of the influence of the environment that a galaxy inhabits upon its structure (Toomre & Toomre 1972).

Morphological classifications describe a dichotomy of galaxies, consisting of disk-dominated, clumpy, ”late” type galaxies, and spheroid-dominated, smooth, ”early” type galaxies. Dichotomies of galaxies are also apparent in a variety of other features including stellar mass, colour, size, and star formation activity (Peng et al. 2010; Lange et al. 2015). That they all broadly align with one another suggests the existence of a fundamental bimodality of galaxies in the Universe. In order to uncover the exact nature of this fundamental bimodality, and any potential substructure thereof, all of these features must be considered together.

Meanwhile, approaches to the task of classifying samples of galaxies have had to evolve as sample sizes have increased. It has gone from being handled by experts (10^{2-4} galaxies, e.g. Fukugita et al. 2007) to being crowdsourced (10^{5-6} galaxies, e.g. Lintott et al. 2008). Neither approach, however, will scale to the data volume expected from future surveys ($>10^{9}$ galaxies, e.g. Euclid; Laureijs et al. 2011). Instead, fast and automated methods for galaxy classification will be required. We test an unsupervised clustering method.

Specifically, we test the *k*-means method using a sample of 7338 galaxies from the GAMA survey. We represent our sample using a preliminary five-dimensional feature space. We aim to determine whether analysing a high number of features leads to previously unknown associations between them, whether these associations enable a deeper understanding of the fundamental bimodality of galaxies, and whether these associations engender a clustering structure in the feature data beyond the known bimodality of galaxies. We also aim to describe and explain this clustering structure in the context of current theories galaxy formation and evolution.

The remainder of this paper is structured as follows. In section 2 we describe our *k*-means implementation and our cluster evaluation method. In section 3 we outline our sample, feature selection, and data preparation. In section 4 we present and analyse clustering results, and in section 5 we summarise, conclude, and consider directions for future work.

2. *k*-means and cluster evaluation

The *k*-means method is an unsupervised clustering approach that aims to partition a sample of *N* observations, represented in a *D*-dimensional feature space, into *k* compact, spherical clusters. Each of the clusters (a set of observations *C*) is characterised by its centroid $\bar{c}$; its arithmetic mean in each of the *D* features. The standard *k*-means implementation ("**k-means**"; MacQueen 1967; Lloyd 1982) is a simple, fast algorithm comprising three steps:

(0) Initialise: *k* initial centres are selected (e.g. uniformly at random) from the observations.
(1) Assign: the observations are assigned to their nearest centre; these assignments are clusters.
(2) Update: the centroid of each assignment is calculated; these become the new centres.

Steps 1 and 2 are iterated until there are no further differences between subsequent iterations. The final assignment of the observations may be taken as a classification scheme. The final centroids are cluster archetypes: a k-point characterisation of the sample.

By iteratively recalculating the centroids, **k-means**produces compact, spherical clusters. The compactness of a set of **k-means** clusters, ϕ (equation 1), may be applied as an overall measure of their clustering quality. It is standard practice to select as the optimal solution that with the lowest ϕ.

$$\emptyset = \sum_{j=1}^{k} \sum_{c \in C_j} \|c - \bar{c}_j\|^2$$

k-meansis dependent on the random input initialisation. We mitigate the dependency of **k-means** on the initialisation by applying the random initialisation technique of Arthur & Vassilvitskii (2007), which spreads out the initial centres.

A key consideration with applying *k*-means is the use of a suitable value of k; this is required as an input to the algorithm. Generally, k_{true}, the true number of clusters in a given sample, is not known, and the true clusters in a sample may have a hierarchical structure, such that there are several unknown values of k_{true}. Hence, it is common to trial clustering on a sample at several values of *k* and identify good values for modelling the true clustering structure of the sample post-clustering.

We identify good values of k based on the stability of their clustering solutions (Lisboa et al. 2013). Specifically, we examine the stability of solutions in spite of random initialisations. Those values of k at which solutions are more similar to one another are more stable.

To measure the difference between a pair of clustering solutions at the same k, we use Cramér's *V* index of association (equation 2; Cramér 1946). Here, χ^2 is the chi-squared value for two clustering solutions on the same sample, each consisting of the same number (*k*) of unique labels. *V* is normalised, ranging from 0 for no agreement to 1 for perfect agreement. We assess the stability of an individual clustering solution by calculating its median *V* with respect to other solutions at the same *k*. We assess the stability of a set of clustering solutions at the same *k* by examining their distribution in median *V*.

3. Data

$$V = \sqrt{\frac{\chi^2}{N \cdot (k-1)}}$$

We use data from phase II of the GAMA survey (Liske et al. 2015). There are hundreds of features available in the GAMA database with which to characterise the galaxies in the sample. One may be tempted to find clusters in the sample using all of them at once, in order to "provide the algorithm with as much information as possible". However, as the dimensionality of the feature space containing the sample increases, the observations become more sparse, and **k-means** overfits its clusters to the observations. Representing the sample using a smaller subset of features instead results in clusters that are more readily generalisable to the overall galaxy population. We select features relating to the formation and evolution of galaxies.

The features we select are: stellar mass (M_*), *u-r* colour, Sérsic index (*n*), half-light radius ($R_{1/2}$), and specific star formation rate (*SSFR*). We transform all features to logarithmic units (apart from *u-r* colour, which is already logarithmic) to remove heavy skews from their distributions. These features are also all commonly represented in logarithmic units in the astrophysical literature. We truncate our sample in each of the features to remove outliers, which strongly influence the centroids that **k-means** calculates. Finally, we normalise the data using *Z*-scores (equation 3) in each feature to overcome any bias of k-means toward any of the features based on intrinsic numerical range. This standardised data set now represents our final sample.

$$Z_f = \frac{f - \bar{f}}{\sigma_f}$$

We conduct a Spearman rank-order correlation analysis of our final sample. We note that $u-r$ colour is involved in the two strongest correlations of features (with M_* and *SSFR*) for our sample, suggesting redundancy. We opt to retain it, however, to strengthen the bimodal structure of the data. This will encourage **k-means**to search for more clusters within the two peaks of the bimodality at higher values of *k*. Other correlations that exist among our selection of features are weaker and do not suggest any further significant redundancies. Our three most correlated features (*M**, *u-r*, and *SSFR*) are expected to dominate much of the clustering, as they extend the shape of our sample in feature space. Finally, we also retrieve environmental data for our sample. We adopt the surface density Σ_5, defined using the projected comoving distance from a galaxy to its fifth nearest neighbour, as a measure of local environmental density (Brough et al. 2013). This feature is only available for 4195 of the 7338 galaxies in our sample, and is mostly available for galaxies in higher density environments.

4. Results

In figure 1 we map the stabilities of solutions found by **k-means** in our galaxy sample at different values of *k*. The distributions of 200 median *V* at each *k* are represented using histograms plotted along each of the black baselines. The heights of the histograms are normalised. Additionally, we show the means of these distributions as vertical red lines. We note a gap across all distributions, appearing to separate two distinct regimes of stable and unstable solutions. We demarcate these regimes using the vertical dashed black line at median V = 0.9. We find uniformly stable clustering at k = 2, 3, 5, and 6. From each of these values of k, we select those with the lowest ϕ as our best solutions.

In figure 2 we show the clusters from each of these solutions as coloured contours, plotted over a scatter plot of our sample in the *u-r* colour vs. *M** plane. This plane is well established as exhibiting a bimodality of galaxies, which we demarcate using the dashed black line. We find that agreement of our clusters with this bimodality of galaxies improves with the number of clusters. At higher k, the additional centroids enable k-means to explore subtler structures of our sample in feature space and hence better probe the bimodality of galaxies while also finding distinct groups of galaxies. This distinct groups are recognisable as green valley galaxies and dwarf galaxies, which have been described previously (Salim et al. 2007, Schawinski et al. 2009).

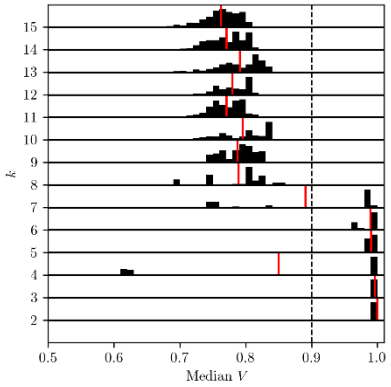

Figure 1: Galaxy stability

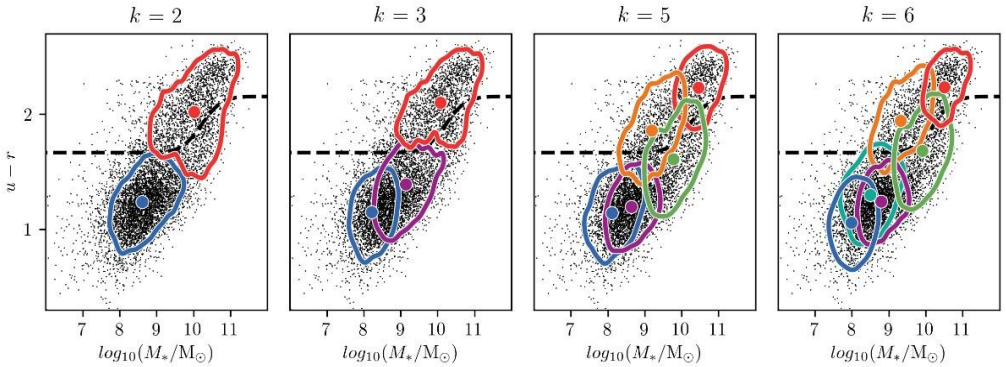

Figure 2: Clusters visualised in the colour-mass plane

Our clusters are also consistent with expected trends of our features with environment. Clusters containing galaxies that are low mass, blue, disky (low *n*), and star forming also contain galaxies in lower density environments. Of particular interest are clusters with intermediate *u-r* colours (plotted in orange and green in figure 2) in $k = 5$ and $k = 6$. Despite being adjacent in the colour-mass plane (and in other feature planes as well), they exhibit markedly different average environments. This suggests that there are two ways for galaxies to evolve through the green valley (the intermediate colour region of the colour-mass plane), consistent with the model of Schawinski et al. (2014).

5. Summary

We report the results of a test of the *k*-means unsupervised clustering method as a galaxy classification solution for the next generation of surveys. It is tested on a sample of 7338 galaxies from the GAMA survey. We find stable clustering structure in our sample when searching for 2, 3, 5, and 6 clusters. Agreement of our clusters with established notions of a bimodality of galaxies improves as we use more clusters to model the data, due to the improved ability of **k-means**to model subtler structure in our sample. **k-means** is also able to identify recognisable subclasses of galaxies, such as green valley galaxies and dwarf galaxies. Furthermore, we find an environmental dichotomy of galaxies with intermediate colours, which is consistent with recent suggestions of two environmentally dependent modes of evolution for green valley galaxies.

6. References

Arthur D., Vassilvitskii S., 2007, *in Proceedings of the Eighteenth Annual ACM-SIAM Symposium on Discrete Algorithms*. pp 1027–1035
Bamford S. P., et al., 2009, *MNRAS*, 393, 1324
Brough S., et al., 2013, *MNRAS*, 435, 2903
Cramér H., 1946, *Mathematical Methods of Statistics. Princeton Mathematical Series*, Princeton University Press
Dressler A., 1980, *ApJ*, 236, 351
Fukugita M., et al., 2007, *ApJ*, 134, 579
Lange R., et al., 2015, *MNRAS*, 447, 2603
Laureijs R., et al., 2011, preprint, (arXiv:1110.3193)
Lintott C. J., et al., 2008, *MNRAS*, 389, 1179
Lisboa P. J., Etchells T. A., Jarman I. H., Chambers S. J., 2013, *BMC Bioinformatics*, 14, S8 Liske J., et al., 2015, *MNRAS*, 452, 2087
Lloyd S., 1982, *IEEE Transactions on Information Theory*, 28, 129
MacQueen J., 1967, *in Proceedings of the Fifth Berkeley Symposium on Mathematical Statistics and Probability*, Volume 1: Statistics. pp 281–297
Peng Y.-j., et al., 2010, *ApJ*, 721, 193
Salim S., et al., 2007, *ApJS*, 173, 267
Schawinski K., et al., 2009, *MNRAS*, 396, 818
Schawinski K., et al., 2014, *MNRAS*, 440, 889
Toomre A., Toomre J., 1972, *ApJ*, 178, 623

ISSN 2398-6611 (Online)

Kate Furnell The Growth of BCGs and ICL in X-ray Selected Clusters

Kate Furnell (sup. Chris Collins)

1. Introduction

A complete understanding of the growth of Universal large-scale structure (LSS) is one of the primary goals of modern cosmology. Such structures which make up the so-called 'cosmic web' - 'nodes' (gravitationally-bound groups and clusters of galaxies), 'filaments' (lower-density connective 'strings' of galaxies) and 'voids' (vast under-densities of galaxies) - have been observed extensively in nature (figure 2); initially by Fritz Zwicky, with widespread cataloguing later by individuals such as George O. Abell in the early-to-mid 20th century (e.g. Zwicky 1937; Abell 1958), and to a more extensive scale by recent spectroscopic surveys of galaxies (e.g. 2dFGRS, Colless et al., 2001 and later 6dFGRS, e.g. Jones et al., 2004). Our comprehension of how matter - baryonic (protons, neutrons, electrons) and dark - collapses to form these structures, and the rate at which this happens, is partially governed by our understanding of cosmology (presently, assumed to be cold dark-matter dominated with a cosmological constant, aka ΛCDM e.g. Riess et al., 1998).

There are numerous observational methods employed to estimate the cosmology of the Universe, which are often combined to tighten constraints on the parameters used to describe said cosmology. These include (but are not limited to): tracking the counts of galaxy clusters and groups over cosmic time in X-rays/SZ (e.g. REFLEX, Bohringer et al., 2001; Planck Collaboration, 2015), analysing the power spectrum of the cosmic microwave background (CMB, e.g. Planck Collaboration, 2015), measuring baryon acoustic oscillations (BAOs, e.g. Percival et al., 2010) and source-lens reconstruction models from observed gravitational lenses (e.g. Collett et al., 2014). This work specifically focusses on galaxy clusters, exploiting such surveys as SPIDERS-Clusters (e.g. Clerc et al., 2016) and the XMM Cluster Survey (XCS, Romer et al., 2001). The benefit of these surveys is that the sample clusters are detected in X-rays (primarily from their Intracluster Medium, or ICM, a hot, gaseous component of clusters); a comparatively less biased means of selection to photometric methods (e.g. Bohringer et al., 2001).

Effective comparisons between observed cluster properties and outputs from hydrodynamical simulations remain critical when attempting to accurately model LSS. In recent years, cosmological hydrodynamical simulations have been reasonably successful in reproducing the structures observed in nature (e.g. Millennium, Springer et al., 2005; see figure 1, BAHAMAS, McCarthy et al., 2016).

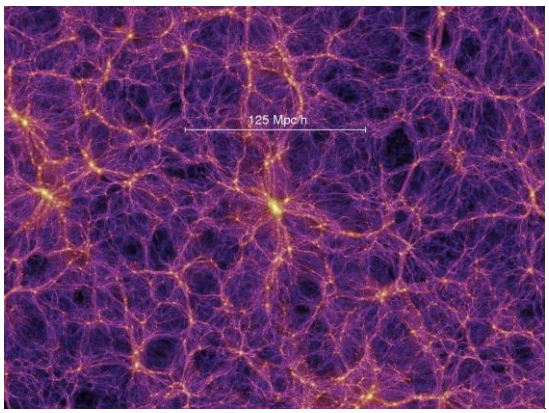

Figure 1: Dark matter output from the Millennium Simulation at 'present' epoch (courtesy: MPA).

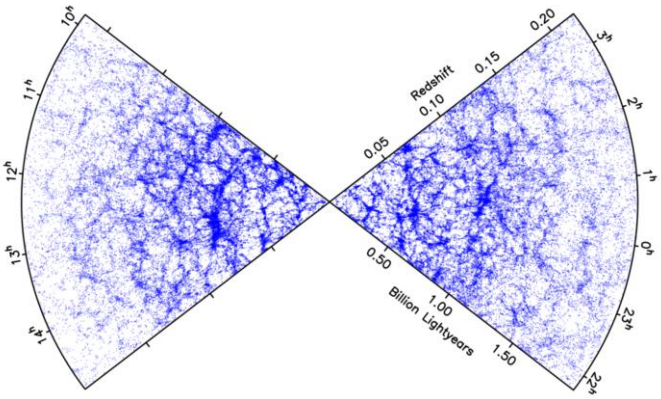

Figure 2: 2dF Galaxy Redshift Survey. Each blue point is a galaxy (courtesy: Colless et al.,

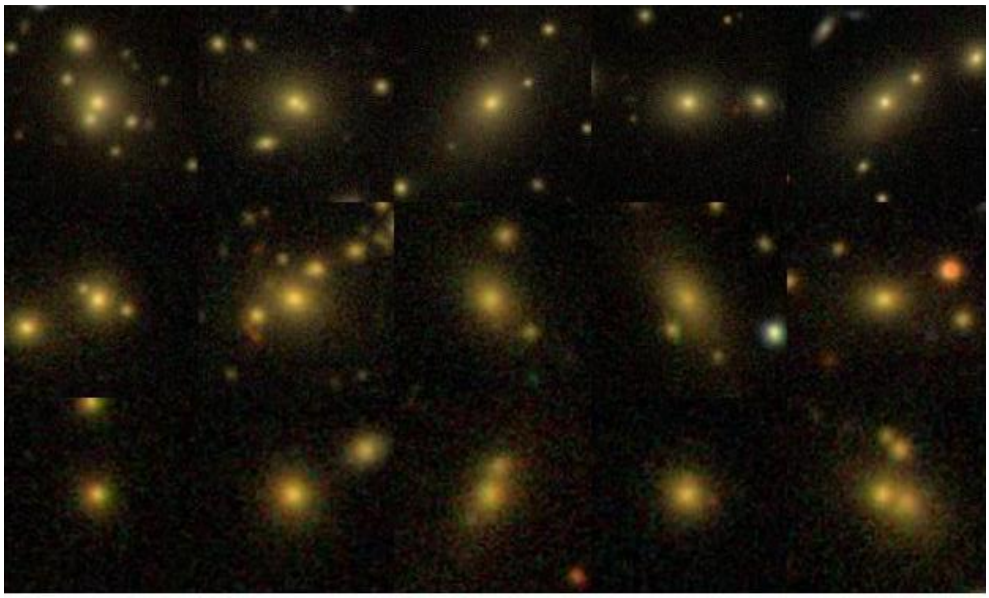

Figure 3: Selection of BCGs in SDSS data (false-colour gri). Each of the three rows represents the bottom 25%, median and top 25% respectively in terms of distance. As is visible, a number of BCGs have characteristically extended stellar haloes.

However, for example, at individual cluster scales, there are numerous key inconsistencies; this has motivated higher-resolution 'zoom' simulations with more complex 'subgrid' physics to better understand these differences (e.g. C-EAGLE, Barnes et al., 2017), as well as studies applying semi-analytic models (SAMs) to simulated dark matter haloes (e.g. De Lucia & Blaizot, 2007).

These discrepancies are especially striking in the case of Brightest Cluster Galaxies (BCGs, see figure 3); massive, often non-star forming, galaxies which primarily reside at the X-ray peak of galaxy clusters, a proxy used for the bottom of the gravitational potential well (e.g. Lin & Mohr, 2004). For example, there are unresolved tensions with most cosmological simulations regarding 'profile cuspiness' (e.g. Navarro, Frenk & White, 1996), with observed BCGs having a 'core' present in their dark-matter density profiles (e.g. Newman et al., 2013b) which cannot readily exist in the ΛCDM paradigm for non-self-interacting dark matter (e.g. Harvey et al., 2017). Vitally, there are also tensions present between the observed stellar mass growth rate of BCGs (e.g. Collins et al., 2009; Burke et al., 2012), and that in simulations (e.g. De Lucia & Blaizot, 2007; Laporte et al., 2013; Ragone-Figueroa et al., submitted), with simulations generally predicting significantly more rapid rates of growth (2-4 times) than those observed in nature.

One of the proposed 'solutions' to this 'missing mass' phenomenon in BCGs is analysis of the co-evolution of cluster BCGs with the Intracluster Light (ICL, e.g. Zwicky et al., 1952b; Gunn & Gott, 1972; Donzelli et al., 2011, and numerous others). The ICL is a low-surface brightness (<1% sky, e.g. Bernardi et al., 2017), diffuse stellar component in clusters which is composed of stars not gravitationally bound to galaxies within the cluster. The origin of the ICL is debated extensively in the literature; whether it originates primarily from BCG-passive satellite mergers (e.g. Burke & Collins, 2013; Gonzalez et al., 2005), tidal stripping from infalling, younger satellites (e.g. DeMaio et al., 2017; Morishita et al., 2017), in-situ star formation due to ICM collapse in the case of gas-rich clusters (Puchwein et al., 2010), or, a combination of these.

Here, we attempt to understand the evolution of BCGs and ICL via a two-pronged approach. Firstly, we analyse the morphologies of a large sample of BCGs up to intermediate epochs (N = 329, < t_{Hubble} -3.5 Gyr, where t_{Hubble} ~ 13.7 Gyr, aka. age of the Universe) with the environmental properties of the host cluster in which they reside, to gain greater insight into the properties of BCGs at recent epochs (Furnell et al., 2018). Secondly, we will introduce our current work, which involves analysing a smaller, more distant cluster sample (N = 23, < t_{Hubble} - 6 Gyr) with exemplary photometric imaging depth, within which we attempt to measure the ICL (Furnell et al., in prep). We wish to establish in our work if there are clear links between the evolution of the BCG and ICL, and how the morphology and composition of one may be influenced by the other.

2. BCGs in SPIDERS

To understand the structural link between BCGs and environment at close epochs, in Furnell et al., (2018) we created a sample of 329 BCGs from the X-ray selected SPIDERS clusters survey (Clerc et al., 2016). The sample was visually inspected to ensure the robustness of the BCG identifications, though this is less ambiguous for high-mass clusters like those in SPIDERS. We then outlined three cluster properties of interest: X-ray luminosity (a proxy for the hot gas content), richness (related to the number of cluster members), and cluster halo mass (derived from velocity dispersion of cluster member galaxies).

We proceeded to model the light profiles of our BCGs with a single-Sérsic (Sérsic, 1963) using the SIGMA pipeline (Kelvin et al., 2012), which was previously used successfully in the GAMA survey to measure the profile parameters of over 10^5 galaxies. We tested the ability of our pipeline to recover

parameters from SDSS data using ~20,000 model profiles; finding a bias in recovered profile slope with respect to model surface brightness. We therefore limited our final science sample to 198 BCGs, which were less likely to suffer from this effect. We then derived stellar masses for our BCGs based on the updated scaling relation from Taylor et al. (2011).

From a statistical analysis of our sample, we outline several key results linking BCG stellar mass to morphology. Firstly, that we find that the scale sizes of the BCGs in our sample are highly correlated with their stellar masses, in common with numerous other studies. Secondly, we found our BCGs are to be significantly more massive and extended than the population of galaxies in the SDSS with similar structure (figure 5). Thirdly, we detect a weak correlation between BCG mass and profile slope, inferring that more massive BCGs may tend towards having slightly more centrally-concentrated light profiles.

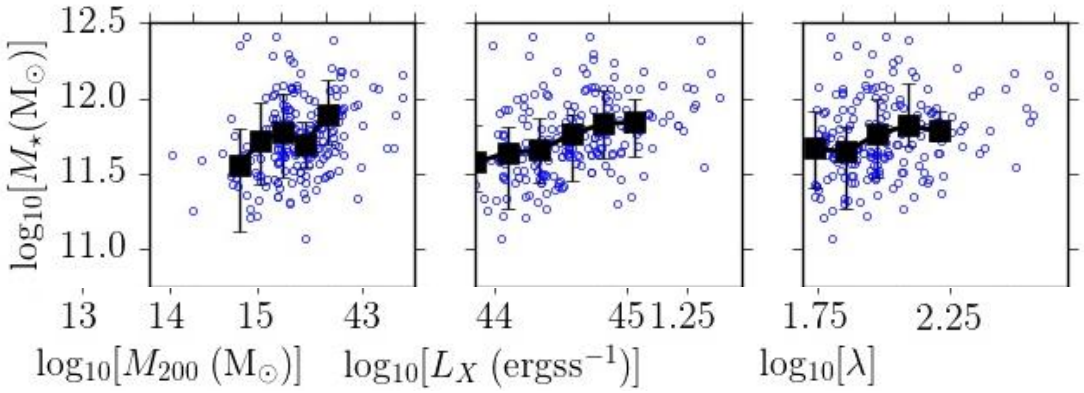

Figure 4: Correlations between environmental parameters and BCG mass. We find no significant correlations with either profile size or slope with environment independently of BCG mass.

Comparing BCG morphology with environment, we find, in general, that significant correlations exist between the masses of our BCGs and all three of the cluster properties explored in this study (richness, cluster mass and X-ray luminosity). However, fixing for selection bias with distance, we do not find any significant correlation with richness - indicating that it is likely to be less useful measure of environment in this context. We also find no evidence that environment, at the redshift of our clusters, has any influence over the size-stellar mass relation of our BCGs, nor is there evidence for any correlation between the profile slopes of our BCGs and the cluster environment.

From this work, we conclude that BCGs, in rich, X-ray selected clusters such as those in SPIDERS, appear to have no significant environmental dependence on their structures, independently of their mass, up to z ~ 0.3. If the primary driver behind growth of BCGs is indeed through multiple satellite mergers (e.g. Ostriker & Tremaine 1975), it is therefore likely that within the halo mass range of the clusters explored in this work, their mass assembly has predominantly occurred at earlier times (>3.5 Gyr).

3. Intracluster Light in XCS Clusters with Hyper Suprime-Cam

Our current work involves analysis of deep imaging data using the Hyper Suprime-Cam instrument on the 8m Subaru telescope (e.g. Aihara et al., 2017), within which we have a sample of 23 clusters selected in X-rays from the serendipitous XCS survey. The clusters were selected which had spectroscopically confirmed BCGs; they also have both size and mass estimates from X-rays (XMM-Newton). They also have membership estimates, performed using the same algorithm as in the SPIDERS survey, which we are currently in the process of using to estimate contamination levels.

Due to the ICL being a faint component, it is necessary to perform careful masking and post-processing routines; this is done in lieu of the pipeline, which is untenably computationally expensive to run. Upon performing corrections on the images for background flux over-subtraction using 'divot correction' (figure 5, Kelvin et al., in prep); we are currently at the stage of procuring photometry, where we are following a similar method to the isophotal thresholding technique used in Burke et al., (2012). We anticipate that this challenging work will lead to a paper in the upcoming year (Furnell et al., in prep).

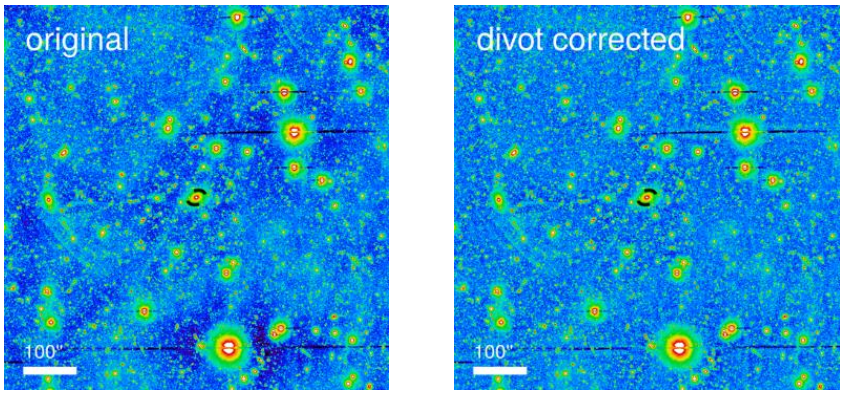

Figure 5: Original HSC image (left) compared with the 'divot corrected' image (right). The flux over-subtraction (dark blue) has been modelled using realistic profiles and summed back on. The BCG for this cluster is at the centre of the image.

References

Abell, G.O., 1958, *The Astrophysical Journal Supplement Series*, *3*, p.211

Aihara, H., Arimoto, N., Armstrong, R., Arnouts, S., Bahcall, N.A., Bickerton, S., Bosch, J., Bundy, K., Capak, P.L., Chan, J.H. and Chiba, M., *Publications of the Astronomical Society of Japan*

Barnes, D.J., Kay, S.T., Bahé, Y.M., Dalla Vecchia, C., McCarthy, I.G., Schaye, J., Bower, R.G., Jenkins, A., Thomas, P.A., Schaller, M. and Crain, R.A., 2017, *Monthly Notices of the Royal Astronomical Society*, *471*(1), p. 1088

Bernardi, M., Fischer, J.L., Sheth, R.K., Meert, A., Huertas-Company, M., Shankar, F. and Vikram, V., 2017, *Monthly Notices of the Royal Astronomical Society*, *468*(3), p. 2569

Böhringer, H., Schuecker, P., Guzzo, L., Collins, C.A., Voges, W., Schindler, S., Neumann, D.M., Cruddace, R.G., De Grandi, S., Chincarini, G. and Edge, A.C., 2001, *Astronomy & Astrophysics*, *369*(3), p. 826

Burke, C., Collins, C.A., Stott, J.P. and Hilton, M., 2012, *Monthly Notices of the Royal Astronomical Society*, *425*(3), p. 2058

Burke, C. and Collins, C.A., 2013, *Monthly Notices of the Royal Astronomical Society*, *434*(4), pp.2856-2865.

Clerc, N., Merloni, A., Zhang, Y.Y., Finoguenov, A., Dwelly, T., Nandra, K., Collins, C., Dawson, K., Kneib, J.P., Rozo, E. and Rykoff, E., 2016, *Monthly Notices of the Royal Astronomical Society*, *463*(4), p. 4490

Colless, M., Dalton, G., Maddox, S., Sutherland, W., Norberg, P., Cole, S., Bland-Hawthorn, J., Bridges, T., Cannon, R., Collins, C. and Couch, W., 2001, *Monthly Notices of the Royal Astronomical Society*, *328*(4), p. 1039

Collins, C.A., Stott, J.P., Hilton, M., Kay, S.T., Stanford, S.A., Davidson, M., Hosmer, M., Hoyle, B., Liddle, A., Lloyd-Davies, E. and Mann, R.G., 2009, *Nature*, *458*(7238), p. 603

Collett, T.E. and Auger, M.W., 2014, *Monthly Notices of the Royal Astronomical Society*, *443*(2), p. 969

De Lucia, G. and Blaizot, J., 2007, *Monthly Notices of the Royal Astronomical Society*, *375*(1), p. 2

DeMaio, T., Gonzalez, A.H., Zabludoff, A., Zaritsky, D., Connor, T., Donahue, M. and Mulchaey, J.S., 2017, *Monthly Notices of the Royal Astronomical Society*, *474*(3), p. 3009

Donzelli, C.J., Muriel, H. and Madrid, J.P., 2011, *The Astrophysical Journal Supplement Series*, *195*(2), p.15.

Furnell, K.E., Collins, C.A., Kelvin, L.S., Clerc, N., Baldry, I.K., Finoguenov, A., Erfanianfar, G., Comparat, J. and Schneider, D.P., 2018, *arXiv preprint: arXiv:1804.02868*

Gonzalez, A.H., Zabludoff, A.I. and Zaritsky, D., 2005, *The Astrophysical Journal*, *618*(1), p.195

Gunn, J.E. and Gott III, J.R., 1972, *The Astrophysical Journal*, *176*, p.1

Harvey, D., Courbin, F., Kneib, J.P. and McCarthy, I.G., 2017, *Monthly Notices of the Royal Astronomical Society*, *472*(2), p. 1972

Jones, D.H., Saunders, W., Colless, M., Read, M.A., Parker, Q.A., Watson, F.G., Campbell, L.A., Burkey, D., Mauch, T., Moore, L. and Hartley, M., 2004, *Monthly Notices of the Royal Astronomical Society*, *355*(3), p. 747

Kelvin, L.S., Driver, S.P., Robotham, A.S., Hill, D.T., Alpaslan, M., Baldry, I.K., Bamford, S.P., Bland-Hawthorn, J., Brough, S., Graham, A.W. and Häussler, B., 2012, *Monthly Notices of the Royal Astronomical Society*, *421*(2), p. 1007

Laporte, C.F., White, S.D., Naab, T. and Gao, L., 2013, *Monthly Notices of the Royal Astronomical Society*, *435*(2), p. 901

Lin, Y.T., Mohr, J.J. and Stanford, S.A., 2004, *The Astrophysical Journal*, *610*(2), p. 745

McCarthy, I.G., Schaye, J., Bird, S. and Le Brun, A.M.C., 2016, *Monthly Notices of the Royal Astronomical Society*, p.2792

Morishita, T., Abramson, L.E., Treu, T., Schmidt, K.B., Vulcani, B. and Wang, X., 2017, *The Astrophysical Journal*, *846*(2), p. 139

Navarro, J.F., Frenk, C.S. and White, S.D., 1997, *The Astrophysical Journal*, *490*(2), p. 493

Ostriker, J.P. and Tremaine, S.D., 1975, *The Astrophysical Journal*, *202*, p. 113

Percival, W.J., Reid, B.A., Eisenstein, D.J., Bahcall, N.A., Budavari, T., Frieman, J.A., Fukugita, M., Gunn, J.E., Ivezić, Ž., Knapp, G.R. and Kron, R.G., 2010, *Monthly Notices of the Royal Astronomical Society*, *401*(4), p. 2148

Planck Collaboration, 2015, *Astronomy & Astrophysics*, *581*, p. 14

Puchwein, E., Springel, V., Sijacki, D. and Dolag, K., 2010, *Monthly Notices of the Royal Astronomical Society*, *406*(2), p. 936

Riess, A.G., Filippenko, A.V., Challis, P., Clocchiatti, A., Diercks, A., Garnavich, P.M., Gilliland, R.L., Hogan, C.J., Jha, S., Kirshner, R.P. and Leibundgut, B.R.U.N.O., 1998, *The Astronomical Journal*, *116*(3), p.1009

Romer, A.K., Viana, P.T., Liddle, A.R. and Mann, R.G., 2001, *The Astrophysical Journal*, *547*(2), p. 594

Sérsic, J.L., 1963, *Boletin de la Asociacion Argentina de Astronomia La Plata Argentina*, *6*, p. 417

Springel, V., White, S.D., Jenkins, A., Frenk, C.S., Yoshida, N., Gao, L., Navarro, J., Thacker, R., Croton, D., Helly, J. and Peacock, J.A., 2005, N*ature*, *435*(7042), p. 629

Taylor, E.N., Hopkins, A.M., Baldry, I.K., Brown, M.J., Driver, S.P., Kelvin, L.S., Hill, D.T., Robotham, A.S., Bland-Hawthorn, J., Jones, D.H. and Sharp, R.G., 2011, *Monthly Notices of the Royal Astronomical Society*, *418*(3), p. 1587

Zwicky, F., 1952, *Publications of the Astronomical Society of the Pacific*, *64*(380), p. 242

Zwicky, F., 1937, *The Astrophysical Journal*, *86*, p.217

ISSN 2398-6611 (Online)

Lawrence Short Using Massive Stellar Clusters to Study the Cepheid Period-Age Relation

Lawrence Short, David Bersier and Nate Bastian
Astrophysics Research Institute, Liverpool John Moores University,
Liverpool Science Park ic2, 146 Brownlow Hill, Liverpool L3 5RF, UK
E-mail address: L.A.Short@2015.ljmu.ac.uk

Abstract. For more than a century classical Cepheid variable stars have been important in their use as standard candles for Astrophysicists. The famous period-luminosity relation has long been used for distance determination, but less well known is the Cepheid period-age relation. This is due to massive stars evolving more rapidly than low mass stars so they reach the instability strip at a younger age. The relatively low density of more massive stars also means that they will experience longer pulsation periods. Stellar clusters provide the ideal laboratory for calibrating the period-age relation as the distance, composition and age for each star is the same. Once the period-age relation in calibrated it allows us to attribute an age to any Cepheid in the field. We will present an empirical Cepheid period-age relation derived from data we have obtained of young and massive clusters in the Large Magellanic Cloud. The range of observed pulsation periods for Cepheids in the older clusters within our dataset spans less than half a day. However for the younger clusters the period range spans several days. The higher mass (younger) Cepheids cross the instability strip multiple times during their blue loop phase, leading to a spread of periods within the young clusters. However, the observed period spread is not compatible with the models. We will discuss these results in the context of young cluster evolution as well as future work that may shed light on this discrepancy.

Keywords. stars: variables: Cepheids – galaxies: individual: Large Magellanic Cloud: stellar clusters.

1. Introduction

1.1 Classical Cepheids

Classical Cepheid variable stars (Cepheids) are radially pulsating stars that exist in a narrow temperature band, known as the instability strip (IS), during a star's evolution whose brightness or luminosity varies on a regular period. Cepheid variable stars typically have one mode of pulsation which can be either fundamental or first overtone but they can pulsate in higher order overtone modes as well. Cepheids have been important distance indicators for stellar populations within nearby galaxies ever since Henrietta Leavitt discovered the Period-Luminosity relation or Leavitt Law in 1912 [1]. This extends further as the Leavitt Law makes Cepheids advantageous in luminosity calibration of Type Ia supernovae which are then used for distance on a cosmological scale[2].

1.2. Stellar Clusters

Stellar clusters are effective tools the study of stellar evolution as all of the stars are just about the same

age and at the same distance. Stellar clusters can be studied with the aid of a Colour-Magnitude Diagram (CMD), where the luminosity or absolute magnitude of a star is plotted against its effective temperature or colour. Stars at different evolutionary stages occupy different regions of the CMD. An isochrone is a theoretical model representing a population of stars of different masses but of the same age and chemical composition just like in a stellar cluster. By fitting isochrones of different ages to the CMD of a cluster one can determine the cluster's age by the best fitting isochrone. Cepheids exhibit a Period-Age (PA) relation as theory shows that more massive stars evolve to the Cepheid region (instability strip) of the CMD earlier in their life. Stellar clusters are the easiest way to measure ages of stars hence the ages of Cepheids in clusters can be determined. Therefore Cepheids in young clusters will have longer periods than Cepheids in old clusters [3].

2. Data

1.1. Clusters in the LMC

We are using 6 clusters in the Large Magellanic Cloud (LMC) whose most up-to-date ages obtained from isochrone fitting can be found in table 1.

Table 1. *The most recent age estimations for each of the stellar clusters in our dataset.*

Cluster	Age (Myr)
NGC 1818	30 [4]
NGC 1850	93 [5]
NGC 1866	177 [5]
NGC 2031	140 [6]
NGC 2136	123 [5]
NGC 2157	98 [5]

1.2. Observations

We have data covering ~45 epochs per cluster with both V and I filters. The observations were taken at the Faulkes Telescope South at the Siding Spring node of the Las Cumbres Observatory in New South Wales, Australia. The data was taken with two different cameras; the first camera covers November 2013 until February 2014 and the second covers October 2015 until February 2016. This means that these two sets of data need cross-calibrating.

3. Method

1.3. Image Subtraction

We use an image subtraction method to create flux difference light curves of any variable object in an image which can then be converted into magnitude light curves. The images need to be aligned to one another before a template can be produced by averaging together the highest quality images. The template is then subtracted from every image at each epoch. The image subtraction software used is called HOTPANTS [7] which is based on the ISIS image subtraction package [8,9]. The subtracted

images contain light and dark spots which indicate any objects that have changed in brightness, see figure 1. The residual flux for each of these objects is measured in order to produce the differential flux light curves.

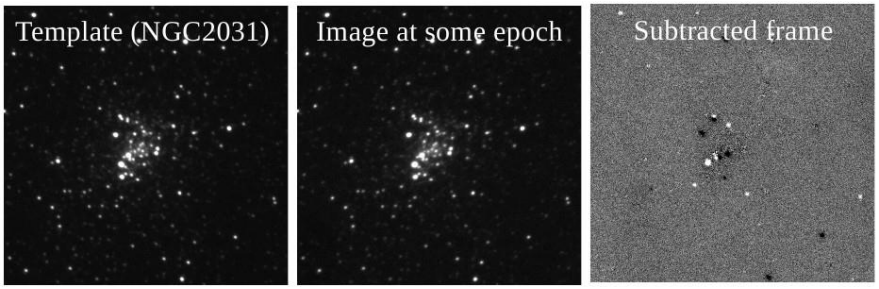

Figure 1. *The left-hand panel shows the template image produced for cluster NGC 2031. The central panel shows an image of NGC 2031 from some epoch taken at random. The right-hand panel shows the subtracted image where the light and dark spots indicate the stars that have gotten brighter or fainter respectively.*

1.4. Calibration

We calculate the magnitude offsets between the template and each image using aperture photometry on the non-varying or standard stars in the field. The residual flux of each variable object at every epoch is converted to the magnitude scale and the offsets applied.

1.4.1. Cross-Calibration

There are two sets of data using different cameras, as discussed in section 2.2, which need to be cross-calibrated so that the light curves can be merged together. We perform aperture photometry using the Image Reduction and Analysis Facility (IRAF) on both of the data sets. We can then calculate the transformation equations needed to match the magnitude scale of the older data set to the newer observations. The equation takes into account a magnitude term and a colour term (the difference in magnitude between V and I).

4. Results

1.5. Period Search

Once all of the light curves are calibrated we can perform a period search on them using the phase dispersion minimisation (PDM) technique as described by Stellingwerf, 1978 [10]. We then then have periods for all of the Cepheids present in each cluster. For the range of fundamental mode Cepheid periods observed in our clusters see table 2.

Table 2. *The range of periods in the observed fundamental mode Cepheids for each cluster.*

Cluster	Period Range (days)
NGC 1818	40.0
NGC 1850	8.6 – 18.7
NGC 1866	2.8 – 3.3
NGC 2031	2.8 – 3.4
NGC 2136	4.4 – 9.1
NGC 2157	7.7

1.6. Light Curves

Our Light curves can then be folded by their periods in order to show how the brightness of each star changes with time. For examples of folded Cepheid light curves see figure 2.

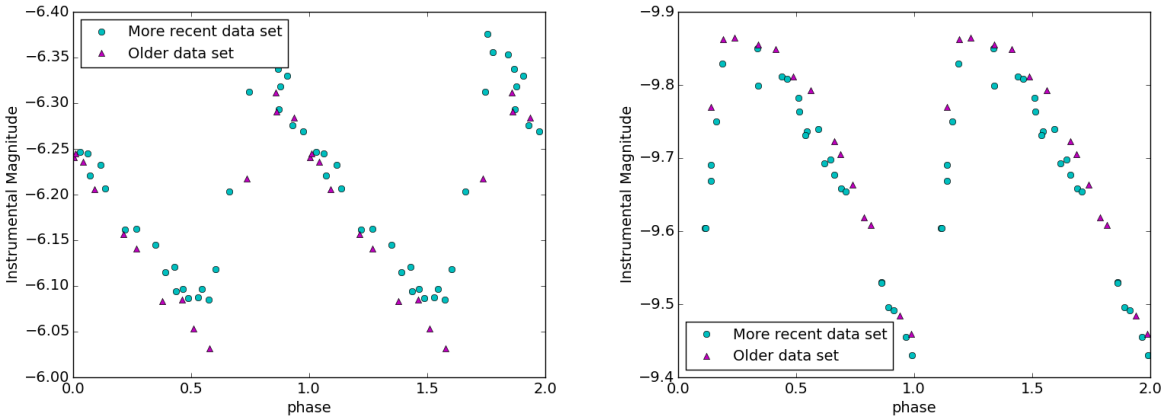

Figure 2. *The left-hand panel shows the folded light curve of a Cepheid with a period of 3 days in cluster NGC 2031. The cyan circles show data points from the more recent data set whereas the magenta triangles represent the older observations. As we can see the cross-calibration described in section 3.2.1 has brought the two data sets onto the same magnitude scale. The right-hand panel shows the same but for a Cepheid with a period of 40 days in cluster NGC 1818.*

1.7. Period-Age Relation

The logarithm of the ages of each cluster is plotted against the logarithm of the mean period of their inhabiting Cepheids yielding a linear relation. We then compare our empirical fit with previous empirical and modelled PA relations (see figure 3). Note that we have excluded NGC 2031 from our fit due to the lack of an up-to-date age estimation.

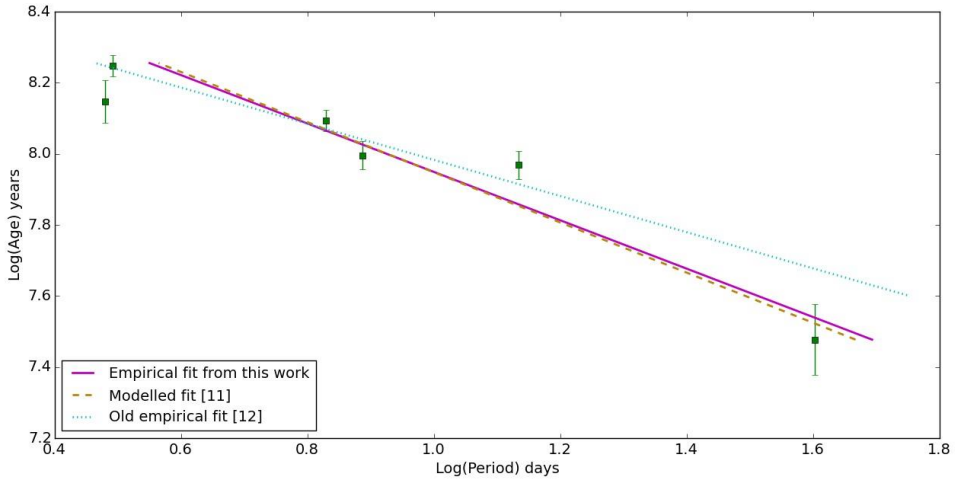

Figure 3. Period-Age relation for Cepheids in LMC clusters. The green squares show the age of a cluster against the mean period of its Cepheid population. The solid magenta line shows the empirical fit from this work. The dashed yellow line shows the modelled fit from Anderson et al. 2016 [11]. The dotted cyan line shows the empirical fit from Efremov 2003 [12].

5. Discussion

1.8. Giving an age to Cepheids

We present here our empirical PA relation derived from fundamental mode classical Cepheids present within stellar clusters in the LMC. The Cepheids were found using image subtraction methods and their periods were determined using the PDM technique applied to Light curves produced from our subtracted images. The cluster ages are determined by isochrone fitting and are taken from the literature (see table1). We produce a linear fit with the younger end showing longer periods and the older end showing shorter periods as expected. The fit to our data is in good agreement with recent models [11] but differs somewhat from the previous empirical fit [12]. Using this PA relation we can determine the age of any Cepheid in the LMC based purely on its pulsation period.

1.9. Period range

The periods of Cepheids in NGC 1850 ranges from 8.6 to 18.7 days, this 10 day spread is larger than we would expect from models. As massive stars evolve they go through phases known as the blue loop where they rapidly get hotter and cooler again causing them to pass through the IS several times. The period range of expected periods for the different crossings of the IS is less then what we observe. Further investigation needs to be done to determine whether both Cepheids are cluster members or not.

6. References

[1] Leavitt H S and Pickering C 1912 *HarCi* **173** 1
[2] Sandage A, et al. 1992 *ApJ* **401** L7
[3] Bono G, et al. 2005 *ApJ* **621** 966
[4] Li C, et al. 2013 *MNRAS* **436** 1497
[5] Niederhofer F, et al. 2015 *A&A* **575** 62

[6] Mould J, et al. 1993 *ApJ* **408** 108
[7] Becker A 2015 *Astrophysics Source Code Library* ascl:**1504**.004
[8] Alard C and Lupton R 1998 *ApJ* **503** 325
[9] Alard C 2000 *A&AS* **144** 363
[10] Stellingwerf R F 1978 *ApJ* **224** 953
[11] Anderson R I, et al. 2016 *A&A* **591** A8
[12] Efremov Yu N 2003 *ARep* **47** 1000

ISSN 2398-6611 (Online)

Kevin Tsang Seeing the Cepheids in the Triangulum Galaxy in a new light

Kevin Tsang[1], Lawrence Short[1], David Bersier[1] and Victoria Scowcroft[2]
[1]Astrophysics Research Institute, Liverpool John Moores University, IC2, Liverpool Science Park, 146 Brownlow Hill, Liverpool, L3 5RF, United Kingdom.
[2]Department of Physics, 3 West, University of Bath, Claverton Down, Bath, BA2 7AY, United Kingdom
E-mail address: K.Tsang@2011.ljmu.ac.uk

Abstract. Around 2000 Cepheids were detected in the nearby spiral Triangulum Galaxy. Cepheids are variable stars that exhibit regular pulsations in brightness with each oscillation lasting days to weeks. The length of the pulsations of a Cepheid is strongly tied to its average intrinsic brightness; the longer the pulsation period, the brighter on average the Cepheid is will be. This is known as the period-luminosity relation or Leavitt Law. Images were taken of the galaxy using three visible-wavelength filters: Sloan *g*, *r* and *i*. By combining the Cepheid brightnesses through these filters with their oscillation periods, new Leavitt Laws were created for those filters. These new observationally derived Leavitt Laws were compared against a set of semi-empirically derived Laws and show good agreement. Using the new Leavitt Laws, a distance of 2.59 million light years to the Cepheids (and therefore the Triangulum Galaxy) was estimated.

Keywords. Cepheids, Leavitt Law, period-luminosity relation, Sloan, M33, distance, photometry

1. Introduction

1.1. Background

One of the key fundamental parameters of any astrophysical object is their distance from us. For each cosmic distance scale (interplanetary, interstellar and intergalactic), there exist various well-established methods with which to estimate distances. At the interstellar and intergalactic scales, Cepheid variable stars provide one such method. Cepheids are bright stars that exhibit regular pulsations in brightness with each oscillation lasting days to weeks (see 1). The average brightness[3] of a given Cepheid is correlated with its oscillation period: the brighter the Cepheid, the longer the period. This phenomenon is referred to as the period-luminosity relation or Leavitt Law after its discoverer Henrietta Swan Leavitt who first remarked on the correlation [1].

[3] In astrophysical contexts, the brightness of an object is referred to as its "magnitude". The magnitude system is logarithmic and the more negative the magnitude value, the brighter the object.

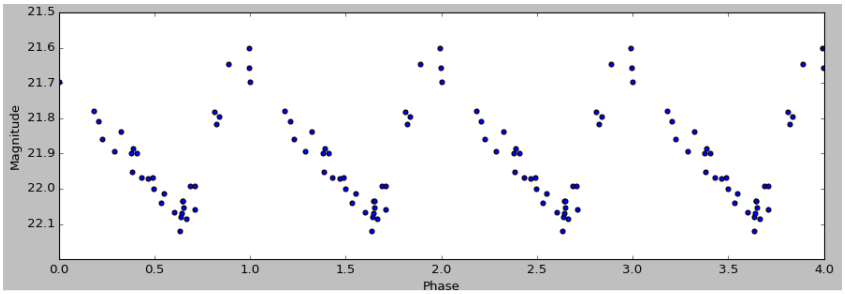

Figure 1: Light curve of a Cepheid over five oscillation periods

Leavitt Laws are usually expressed in the following form:

Equation (1)

$$M = a \log_{10} P + b$$

— where M is the magnitude of the Cepheid, P is the pulsation period in days, and a and b are constants.

By measuring the oscillation period of a given Cepheid, the absolute magnitude of that Cepheid can be determined using equation 1. Comparing the calculated absolute magnitude of the Cepheid with its measured apparent magnitude will yield a distance estimate to the star.

The observed magnitude of a Cepheid depends on the filter that was used to make the observations. As a result, each filter will have its own Leavitt Law which is characterised by the values for a and b.

1.2. Data

Images of the Triangulum Galaxy (also referred to as M33) were taken between 2003 and 2005 as part of a variability survey [2]. The images were captured using the MegaCam instrument at the Canada-France-Hawaii Telescope (CFHT) with Sloan-band filters *g'*, *r'* and *i'* (see 2). Around 36000 variable objects were detected in M33, around 2000 of which were classified as Cepheids and were catalogued.

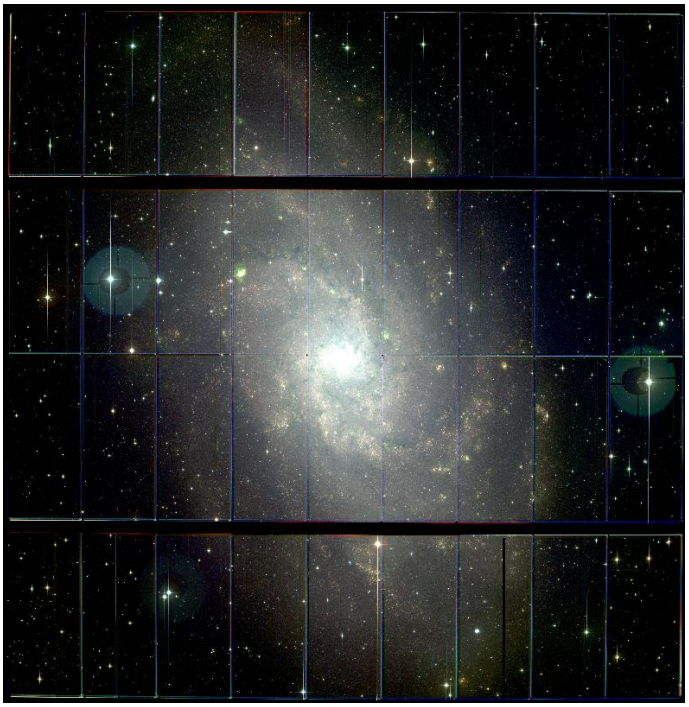

Figure 2: Stacked M33 image of CFHT g', r', and i' data

Further images were taken of M33 using the Wide Field Camera (WFC) at the Isaac Newton Telescope (INT) again using the Sloan filters *g'*, *r'*, and *i'*. Concurrent observations were made of the Stripe 82 region to provide a set of standard stars with which to calibrate the M33 data. The INT images were stacked together to improve the signal.

1.2. Aims

The aims of this project are to measure and calibrate the magnitudes of the Cepheids in M33 in the Sloan filters to create a set of observationally derived Sloan-band Leavitt Laws. Those Leavitt Laws will then be used to estimate a distance to M33.

2. Methods

2.1. Photometry

Astronomical photometry is the measurement of the brightness of objects in the sky. In the current era where charge-coupled devices (CCDs) are used to capture images of the sky, there are two main methods of stellar photometry: aperture photometry and point spread function (PSF) fitting photometry. Aperture photometry essentially measures the stellar flux within an aperture (usually circular) around a star on the CCD image with the background sky subtracted. PSF fitting photometry is more involved. Images of stars on a CCD are roughly disk-shaped. The shape of the stellar image is not a representation of the physical

shape of the star[4] but rather the result of optical distortions that arise from atmospheric effects, tracking irregularities of the telescope, non-uniform focus, and other blurring effects. The shape of the stellar profile on the CCD image is referred to as the point spread function and can vary across the image. PSF photometry attempts to model the stellar PSF and its variations and to fit that model to each detected star. The amount of scaling between the PSF model and the actual stellar PSF yields the magnitude of the star.

A major disadvantage inherent to aperture photometry is its inability to deal with high levels of stellar crowding where stars are close together. An aperture centred on one star may capture light from nearby stars, resulting in overestimates of measured brightness. With PSF photometry, it is possible to simultaneously model multiple stars in close proximity to account for crowding and overlapping profiles.

The images that are used in this project exhibit high levels of crowding (see 3). PSF photometry is therefore the more suitable method of magnitude measurement. The photometry software packages used are SExtractor [3] and PSFEx [4].

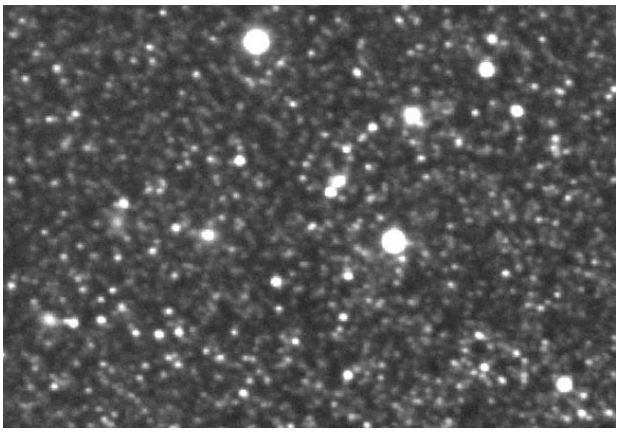

Figure 3: Dense stellar field of M33

2.2. Cepheid Identification

Over 500,000 stars in the INT M33 images were detected and whose *g*, *r* and *i* magnitudes were measured and calibrated to the standard system. This extensive catalogue of stars was then cross-referenced with the Cepheid catalogue produced from Hartman et al.'s variability survey and matched on the basis of sky positions. From our INT M33 catalogue of a half-million stars, 1735 stars were identified as Cepheids; those 1735 Cepheids now have both period data and calibrated Sloan-band *g*, *r* and *i* magnitudes.

[4] Stars are sufficiently far away that they are, to an approximation, "point sources"—sources of light with no apparent angular size.

3. Results

3.1. Leavitt Laws

With periods and magnitudes now available, new Leavitt Laws can now be constructed. Determining the values for the slopes and intercepts of the Leavitt Laws (a and b in equation 1) is achieved through linear regression with the BCES algorithm [5]. Plots of the Cepheid data and the derived Leavitt Laws are shown in 4.

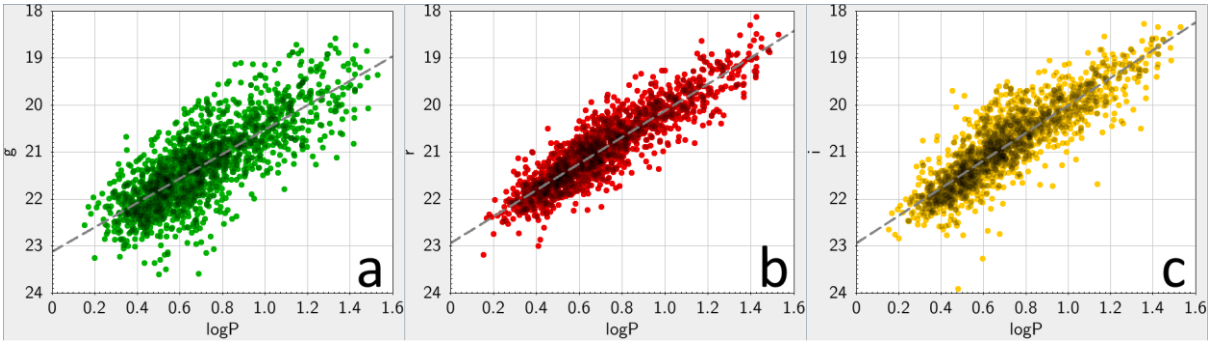

Figure 4: Sloan-band Leavitt Laws in the a) g filter, b) r filter, and c) i filter

The Sloan-band Leavitt Laws are presented in numerical form in Table 1. Also shown in table 1 are the semi-empirical Leavitt Laws constructed by Ngeow and Kanbur; they had transformed *B*, *V* and *I* Cepheid magnitude data into *g*, *r* and *i* magnitudes and fitted Leavitt Laws to them [6].

Table 1: Observationally derived Leavitt Laws from this work and semi-empirically derived Laws from Ngeow & Kanbur

Filter	This work	Ngeow and Kanbur
g	$-2.595\log_{10}P + 23.12$	$-2.518\log_{10}P + 17.17$
r	$-2.822\log_{10}P + 22.94$	$-2.819\log_{10}P + 17.03$
i	$-2.932\log_{10}P + 22.94$	$-2.928\log_{10}P + 17.06$

The slopes from this work and Ngeow & Kanbur shown in Table 1 show excellent agreement. The large differences in intercepts are not unexpected. The Leavitt Laws constructed by Ngeow & Kanbur were derived using Cepheids in the Large Magellanic Cloud, a satellite galaxy of the Milky Way that is much closer to us than M33. It is this difference in intercepts that will allow distance estimates to be made.

3.2 Distance Estimate

Using the semi-empirical Leavitt Laws of the Large Magellanic Cloud and a known distance to the Cloud of 49.97 kiloparsecs, a distance estimate to M33 can be extrapolated. A value of 794 kiloparsecs (2.59 million light years) is the result.

4. Conclusions

The Sloan-band magnitudes of 1735 Cepheids in the Triangulum Galaxy were measured using PSF photometry and were combined with existing period data to create a set of Sloan-band Leavitt Laws. Comparisons with semi-empirically derived Laws show good consistency in the slope values while the differences in intercepts were used to establish a distance of 2.59 million light years to the Galaxy.

References

[1] H S Leavitt, "1777 variables in the Magellanic Clouds," *Annals of Harvard College Observatory,* vol. 60, p. 87, 1908.

[2] J D Hartman, D Bersier, K Z Stanek, J-P Beaulieu, J Kaluzny, J-B Marquette, P B Stetson and A Schwarzenberg-Czerny, "Deep Canada-France-Hawaii Telescope photometric survey of the entire M33 galaxy - I. Catalogue of 36000 variable point sources," *Monthly Notices of the Royal Astronomical Society,* vol. 371, no. 3, p. 1405, 2006.

[3] E Bertin and S Arnouts, "SExtractor: Software for source extraction," *Astronomy and Astrophysics Supplement,* vol. 117, p. 393, 1996.

[4] E Bertin, "Automated Morphometry with SExtractor and PSFEx," in *Astronomical Data Analysis Software and Systems*, Boston, Massachusetts, USA, 2011.

[5] M G Akritas and M A Bershady, "Linear Regression for Astronomical Data with Measurement Errors and Intrinsic Scatter," *Astrophysical Journal,* vol. 470, p. 706, 1996.

[6] C-C Ngeow and S M Kanbur, "Semiempirical Cepheid Period-Luminosity Relations in Sloan Magnitudes," *The Astrophysical Journal,* vol. 667, no. 1, p. 35, 2007.

ISSN 2398-6611 (Online)

Thomas Sedgwick The galaxy stellar mass function and low surface brightness galaxies via core-collapse supernovae

Thomas M. Sedgwick, Ivan K. Baldry and Philip A. James
Astrophysics Research Institute, Liverpool John Moores University, IC2, Liverpool Science Park, 146 Brownlow Hill, L3 5RF
E-mail address: T.M.Sedgwick@2013.ljmu.ac.uk

Abstract. Using exploded stars, or supernovae, as pointers to their host galaxies, we find ~150 previously unidentified low surface brightness galaxies (LSBGs) located in IAC Stripe 82 Legacy coadded imaging. Core-collapse supernovae (CCSNe) host galaxy statistics are used as a tracer of the z<0.3 star-formation-rate density (SFRD) as a function of host galaxy mass, from which the star-forming galaxy stellar mass function (GSMF), unbiased by galaxy surface brightness, is derived. Due to sample completeness, we find galaxy number density to continue to increase as a power law down to the low mass limit of $\sim 10^{6.4}\,M_{\odot}$. We test the effect of selecting only galaxies of existing catalogues using CCSNe and find an increase to the low-mass galaxy population ($\log(M_{*}/M_{\odot}) \lesssim 10^{8}$) compared with that found from alternative GSMF derivations, as well as a lack of turn-down in number density in the low mass limit, for both the SDSS-IV catalogue and IAC Stripe 82 Legacy Coadd catalogue, indicating the prevalence of dwarf galaxies and helping to bridge the gap between the observed galaxy number counts and those expected from □-CDM cosmological simulations.

Keywords: galaxies: luminosity function, mass function — galaxies: star formation — galaxies: distances and redshifts — supernovae: general — methods: statistical

1. Introduction

1.1. The Galaxy Stellar Mass Function & Λ-CDM Cosmology

The Galaxy Stellar Mass Function (GSMF) is the measure of the number of galaxies per cubic megaparsec, as a function of galaxy stellar mass. Its form can reveal information crucial to our understanding of galaxy evolution, of which mass is known to be a primary driver. The precise form of the GSMF can be used to constrain cosmological models.

The □-CDM model is widely considered the 'standard model' of modern cosmology due to its ability to predict several key observables. These include the angular size of initial density fluctuations in the primordial universe as seen in the cosmic microwave background [2], as well as large-scale structure, with model results matching the observed complex filaments and cosmic web [4]. The predicted relative abundances of elements in the universe are also found to be consistent with observations, as is the acceleration of the universe from distant galaxies and type Ia supernovae (SNe), explained through the invocation of dark energy [9].

However, Λ-CDM has not yet been able to match the observed form of the galaxy stellar mass

function (GSMF), with the numbers of observed dwarf galaxies being significantly less than those predicted from simulations invoking a Λ-CDM cosmology. This discrepancy may not be a fault of Λ-CDM, however. There is considerable difficulty in calculating the form of the galaxy stellar mass function, which arises due to biases intrinsic to almost all galaxy surveys. As most dwarf systems ($\sim 10^8$ $M_\odot$) generally have intrinsically lower surface brightnesses than their higher mass counterparts, the lower mass end of the GSMF may be frequently underrepresented. Developing techniques to increase completeness of the low mass end of the GSMF must be the focus should one wish to use it to assess the nature of the cosmology, and indeed, of galaxy evolution.

Here we develop and implement one such technique, using the Stripe 82 Supernova Survey [11], the largest supernova survey to date, to create a sample of galaxies located via core-collapse supernovae positions. As CCSNe peak at luminosities of up to 10^8–$10^9 L_\odot$, they can be used as location markers for their host galaxy. Several of these hosts may be previously unidentified LSBGs.

2. Data

This work makes use of data from the following 3 surveys:

1. Stripe 82 Supernova Catalogue of Sako et al. 2014 [11], forming the basis of the supernova sample.
2. SDSS-IV Galaxy Catalogue [1] (referred to simply as SDSS), forming the basis of the galaxy sample used to locate CCSN hosts.
3. IAC Stripe 82 Legacy Galaxy Catalogue [7] (referred to simply as Stripe 82 or S82): coadded imaging for each of the *ugriz* photometric bands, from SDSS over the run of SDSS-main and the supernova survey epoch. ~100 images are median stacked to produce deeper imaging crucial for LSBG detection. These data form the galaxy sample utilised in the cases where a SN host galaxy is not found by SDSS. In such cases, the Stripe 82 galaxy catalogue is used, and if the host is again uncatalogued, the raw *.fits* images are used to locate LSBGs using bespoke source extraction.

3. Methodology

3.1 Star and AGN Removal

We remove non-supernovae from the supernova survey sample, building on the classification attempts of Sako et al. 2014 [11] (Hereafter S14) to remove these objects. 10258 transient sources were found by S14. We first remove variable stars (3532) (objects detected over multiple observing seasons); and AGN (334) (identified spectroscopically via their broad hydrogen lines), leaving both spectroscopically confirmed supernovae and photometric supernova candidates.

We remove those photometric SN candidates found within 1" of an SDSS star (843). The remaining 5549 objects are very likely to be supernovae.

3.2 *Sample Completeness*

One advantage of using point sources as pointers to galaxies is that we can easily verify the completeness of the sample. As long as no objects are missed by the detecting apparatus, SN counts should rise with magnitude with an n=2 power law, due to the increased area of universe sampled with increased magnitude depth. We hence remove supernovae candidates fainter than $r_{peak,sn} = 21.8$, where this power law breaks down. Stripe 82 images of the SN regions were inspected to ensure the point

source was visible. It was found that the SN peak-magnitude cut removed any remaining spurious objects. We are left with 2778 SNe in the sample.

If a host galaxy is found for each of these supernovae we can say that the resultant galaxy stellar mass function is complete, and not biased towards higher surface brightness galaxies. We hence turn our attention to identifying each host galaxy.

6.1 SN-Galaxy matching

SN positions were cross matched with those of SDSS-IV galaxies [1]. Care is taken to ensure the galaxy is the genuine host: Ellipticity corrected, galaxy radius-normalized separation is used along with SN magnitude and galaxy radius uncertainty to list the 3 most likely host candidates, before manual inspection of coadded *gri* images of the SN region. 85% of SNe are matched to an SDSS galaxy. Of the remainder, 55% are matched to a Stripe 82 coadd galaxy, leaving ~150 uncatalogued LSBGs. Figure 1 shows example Stripe 82 coadded *gri* imaging used for inspection. The top panels show SNe successfully matched, and the bottom panels show examples of our 'new' LSBGs identified via SN position.

6.2 Bespoke Source Extraction

To obtain photometry for our LSBGs, necessary for estimations of galaxy redshifts and stellar mass, we derive *ugriz* fixed-aperture (*r*-band defined) photometry via sExtractor. Bespoke source extraction setups are used in such a way as to reproduce both the SDSS and Stripe 82 magnitude distributions, whilst obtaining photometry for our newly discovered LSBGs. Photometry is found for all galaxy candidates, verifying the lack of remaining spurious detections in the SN sample.

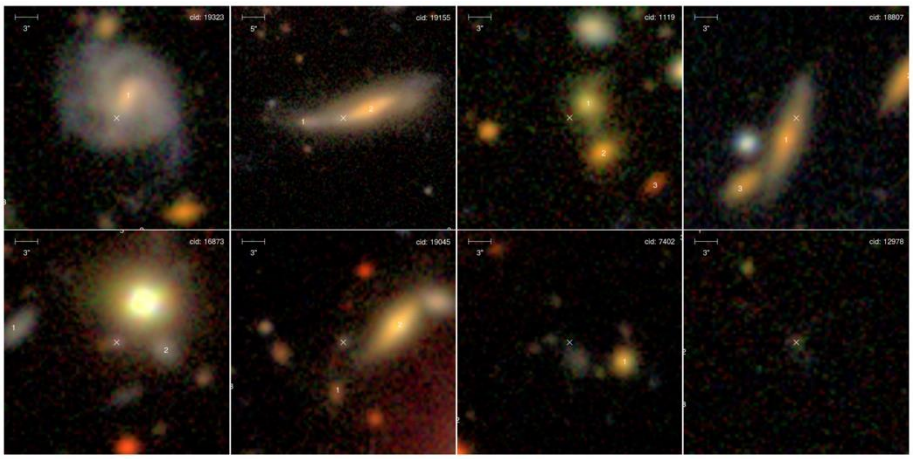

Figure 1. *Example IAC Stripe 82 Legacy gri imaging. Top panels show SNe successfully matched to their host galaxy, with the 3 most probable host candidates (1, 2 & 3), and supernova position (x) labelled. Bottom panels show new LSBGs not found in the SDSS or Stripe 82 catalogues, found from SN matching*

6.3 Photometric redshifts using zMeDIC

To derive galaxy stellar masses utilised by the SFRD and GSMF, we use the prescription of Gilbank et al. 2011 (hereafter, G11) [8], for which absolute *z*-band magnitude is required (along with (*g*-*i*) colour) to infer stellar mass. In turn, to calculate absolute magnitude we require galaxy redshifts. Ideally, we would have spectra for each of our 2778 SN-host galaxies or the supernova itself, from which redshift could be inferred via well-established redshift template techniques [5]. However, 45% of the sample do not possess spectroscopy.

We hence develop and utilise an artificial neural network technique, referred to as zMeDIC, to estimate redshifts for these galaxies. The code is trained on 90% of the spectroscopic redshift sample and validated using the remaining 10%, to find the strongest correlations of *ugriz* colours, supernova peak magnitude and galaxy surface brightness, with redshift. A hard maximum to the redshift of each galaxy is used to improve results; a maximum arises due to the finite range of supernova luminosities [10]. The code is designed specifically to perform well for a small galaxy sample such as ours, with
$\sigma_{z\,,rms}$=0.052. We choose not to train zMeDIC on a larger sample, such as the entire Stripe 82 galaxy sample, to avoid unnecessary biases in redshift assignment, which would in turn bias the resultant galaxy stellar mass estimates.

4. Results & Discussion

4.1. Star formation rate density

The star formation rate density (SFRD) describes the number of solar masses put into new stars $yr^{-1}Mpc^{-3}$. As the lifespans of stars which end their lives as CCSNe are small relative to the timescales on which galaxies evolve, the number of CCSNe as a function of their host galaxy mass should follow the same distribution as the SFRD. We perform a 1000 iteration Monte Carlo (MC) technique which folds the uncertainty on our photometric redshifts into the final CCSN number densities as a function of mass, as well as smaller yet significant uncertainties from spectroscopic redshifts, magnitudes and the G11 mass conversion. For each iteration we perform a $z<0.3$ cut, to correctly volume limit the sample. We height-scale the MC-mean CCSN number densities to the SFRD of G11, over the range of masses for which the SFRD of G11 is deemed to be complete.

Figure 2 compares the SFRD derived with and without our newly classified galaxies. We compare to the SFRD obtained by G11 (using the spectral fitting method of Brinchmann et al. (2004) [6] applied to the full Stripe 82 galaxy catalogue). We height-normalise (between $9<\log(M_*/M_\odot)<11$) our CCSN host galaxy counts Mpc^{-3} to the G11 SFRD. The clear result is that with or without the addition of our LSBGs to the Stripe 82 catalogue, the form of the SFRD is in agreement for high masses but deviates significantly for $\log(M_*/M_\odot)\lesssim 9$. Comparing the results of G11 with the SFRD formed from SDSS galaxies only, using our CCSN selection method, we find a factor ~2.5 increase to the SFRD at $\log(M_*/M_\odot)\sim 8$. This factor becomes ~5 when including our newly catalogued LSBGs. The SDSS and SDSS+S82+LSBG samples evaluate the SFRD down to $\log(M_*/M_\odot)=7.0$ and $\log(M_*/M_\odot)=6.4$; 1 and
1.6 dex deeper than assessed by G11, respectively. The lower limit is restricted only by the observing period of the supernova survey. At our lowest galaxy stellar masses, one has to deal with the fact that

the mean timescale between supernovae explosions across the region starts to exceed the survey observation period.

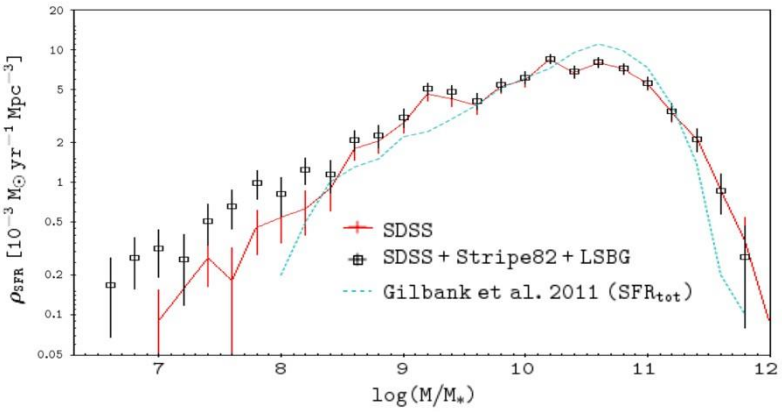

Figure 2. *The z<0.3 SFRD, derived using core- collapse supernova statistics. Shown in red, SFRD using core-collapse supernovae host galaxies within the SDSS-IV catalogue only. In black, the same but with additional host galaxies added, from the IAC Stripe 82 catalogue or from bespoke source extraction of this work. In cyan, for comparison, SFRD of Gilbank et al. 2011 derived using the Brinchmann et al. 2004 spectral fitting procedure.*

4.2 The star-forming galaxy stellar mass function

The star-forming GSMF can be derived from the SFRD via assumptions about specific SFR as a function of galaxy stellar mass. i.e. if we assume constant SFR per solar mass, as a function of galaxy stellar mass, then $\phi_M dM \propto \rho_{SFR}/(M_*/M_\odot)$. We height normalise between $9<\log(M_*/M_\odot)<11$ once again, to the star-forming galaxy number densities of Baldry et al. 2012 [3], to obtain an estimate for galaxy number density Mpc^{-3}dex^{-1}, shown in Figure 3.

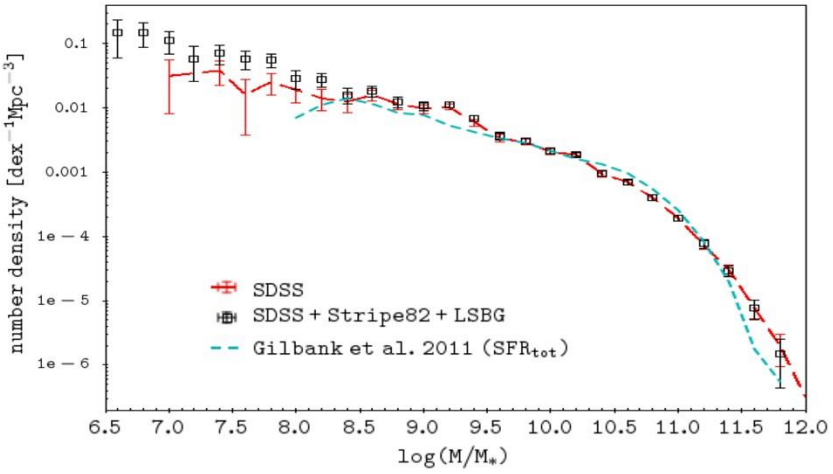

Figure 3. *The z<0.3 GSMF, derived using core- collapse supernova statistics and assuming constant specific star formation rate as a function of host galaxy mass. Each colour series corresponds to the data sets described in Figure 2.*

To compare the effect of the choice of galaxy catalogue, we show the results from the SDSS sample, and this work's sample (SDSS+Stripe 82+LSBG). We also compare with the GSMF derived from G11's SFRD, which shows a downturn in counts for $\log(M_*/M_\odot) \lesssim 8.5$ when applying the same assumptions. Conversely, we observe a clear lack of downturn in galaxy counts in the low mass limit for both of our samples. The inclusion of additional LSBG galaxies in the sample results in galaxy counts continuing to rise as a power law, down to the stellar mass limits of the sample ($\log(M_*/M_\odot) = 6.4$). A galaxy selection using CCSNe appears to successfully remove Malmquist bias, and the completeness of the sample can be confirmed simply via a cut on supernova apparent magnitude, whilst obtaining results consistent with alternative GSMF derivation-methods for the mass ranges for which they are deemed reliable. We have demonstrated a method which significantly reduces tension between observations and the simulated predictions of galaxy number densities derived via a Λ-CDM description of the universe.

5. References

[1] Abolfathi, B. et al., 2017, ArXiv, e-print, arXiv:1707.09322 [2]
Ade, P. A. R. et al., 2013, A&A, 571, 1
[3] Baldry, I. K. et al., 2011, MNRAS, 421, 621
[4] Benson, A. J., 2010, Physics Reports, 495, 33
[5] Bolton, A. S. et al., 2012, AJ, 144, 144
[6] Brinchmann, J. et al., 2004, 351, 1151
[7] Fliri A. A. & Trujillo B. B., 2016, ApJ, 305, 23
[8] Gilbank, D. G. et al., 2011, MNRAS, 412, 2111
[9] Perlmutter, S. et al., 1999, ApJ, 517, 565
[10] Richardson, D. et al., 2014, AJ, 147, 5
[11] Sako, M. et al., 2014, ArXiv, e-print, arXiv:1401.3317v1

ISSN 2398-6611 (Online)

Nicole Gerber Development of a procedure reference model for the alignment of non-medical support service applications in hospitals ensuring the correct delivery and display of relevant key performance indicators

Nicole Gerber
Liverpool John Moores University, Department of the Built Environment
Byrom Street, Liverpool, L3 3AF, United Kingdom
N.Gerber@2014.ljmu.ac.uk

Abstract. The healthcare industry and particularly hospitals undergo a structural change. Driven by the need to reduce costs while raising quality, systematic and empirically based data and solutions are requested by the hospital industry. Currently, applications of non-medical support services in hospitals are mostly very fragmented due to the fact that firstly no holistic view or integration efforts were undertaken between the different disciplines in the past and secondly, due to the fact that so far rather little investments were made in this context. Where reference models are available, they focus on specific views and/or deal mostly with medical rather than non-medical areas. The research aim is therefore to develop a procedure reference model providing the necessary information about how to systematically align applications in the non-medical support processes in hospitals in order to ensure the correct delivery and display of relevant key performance indicators. As the output will be a model and thus an artefact, the overall research design is based on Design Science Research principles, combining empirical data gathering and analysis with modelling methods. After the theorizing phase during which an in depth understanding of the context was reached, the model was developed in the modelling phase. Currently, during the evaluation phase, the model is being validated in the field.

Keywords. Healthcare, Hospitals, non-medical support services, Facility Management, reference modelling, Design Science Research, Method pluralism,

1. Introduction

1.1 Research context of the thesis

The healthcare industry and particularly hospitals are currently undergoing a structural change due to social, technological, political and economical impacts like an aging population, rapid medical and medical-technical progress, growing complexity in the medical treatment, skills shortage, the need for increased quality assurance, more patient orientation and new financing processes (Braun von Reinersdorff, 2007; Busse and Geissler, 2017; Fischer, 2017; Wasem, 2017).

Driven by the need to reduce costs while raising quality in order to cope with the increasing competition, systematic and empirically based data and solutions are requested by the hospital industry, particularly in Switzerland (Angerer et al., 2017; Berger et al., 2015; Cosandey, Roten and Rutz, 2018). Currently, applications of non-medical support services in hospitals are mostly very fragmented because firstly, no holistic view or integration efforts were undertaken between the different disciplines in the past and

secondly, due to the fact that so far rather little investments have been made in this context; where reference models are available, they focus on specific views and/or deal mostly with medical rather than non-medical areas (Gerber and Perschel, 2016; Gerber et al., 2017).

The research question of this thesis is therefore: “What is the procedure and its relevant aspects for integrating non-medical-support service applications in hospitals so that relevant key performance indicators for a systematic controlling and optimization can be generated and delivered as effectively and efficiently as possible?” As a consequence, the research aim is to develop a procedure reference model providing the necessary information about a standardized procedure and its relevant aspects for aligning non-medical-support service applications in hospitals so that relevant key performance indicators for a systematic controlling and optimization can be generated and delivered.

By dealing with this question and aim, the following contribution to innovation can be provided:
- developing the area of non-medical support services and application management in hospitals in a holistic way by applying systematic research
- applying an innovative method-pluralistic research design combining empirical mixed methods with Design Science Research principles in general and in the environment of healthcare in particular

1.2 Main advances since the last report

At the stage of the last report, literature research, a quantitative survey collection and analysis had been conducted and an iteration of qualitative expert interviews was realised. Meanwhile, the qualitative interviews have been analysed, based on which, a meta-model, a procedure reference model and six inherent component models were constructed and documented including two input documents. The evaluation iteration was prepared and the above mentioned models are currently being evaluated by the means of expert interviews.

1.3 Relevant interim results

Figure 1 gives an impression on the current draft of the above mentioned meta-model and figure 2 on the procedure reference model, both currently being evaluated

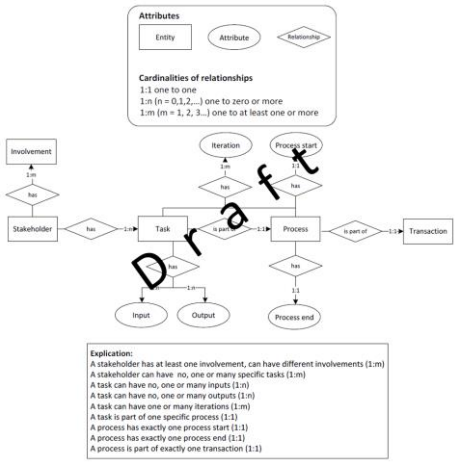

Figure 1: Draft version of entity-relationship meta-model in modified Chen notation

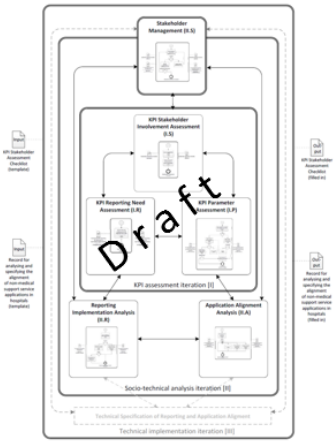

Figure 2: Draft version of procedure reference model in BPMN 2.0 notation

In terms of the thesis document, the introduction (chapter 1), the conceptual background (chapter 2), the methodology (chapter 3) and the research conducted (chapter 4) has been worked on.

2. Conceptual background

In order to cover the research domain, the following state of the art of relevant topics are presented in the conceptual background chapter:
- Healthcare and hospitals in general and within the Swiss context in particular
- Management Research and non-medical support-services in hospitals
- Information Technology, Information Systems Research, Application Systems, all in general and in healthcare particular
- Key Performance Indicators and reporting, both in general, in healthcare and for non-medical support services in particular
- Stakeholder Management in general, in healthcare and within Information Systems in hospitals in particular
- Models in general and reference models in particular

The context of the topics covered in the conceptual background is illustrated in figure 3

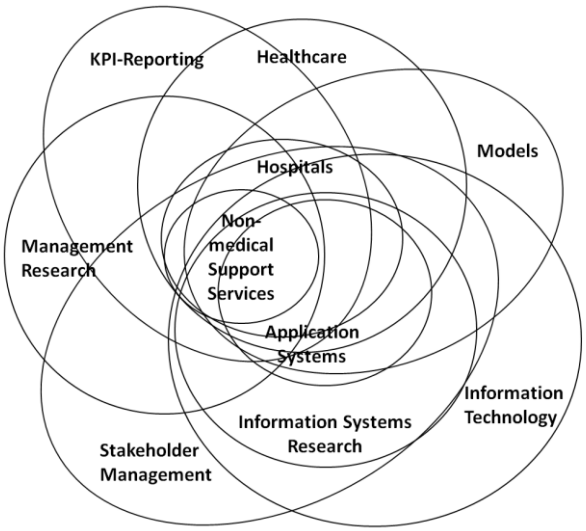

Figure 3: Illustration of conceptual background of the thesis

3. Research methodology

In the thesis, a method-pluralistic research approach has been chosen based on an underpinning philosophical grounding of pragmatism and an epistemological pluralism. Namely, the methods of empiricism (Mixed Methods) and Design Science Research (reference modelling) are combined throughout the research project being structured in the phases of "Theorizing", "Modelling", "Evaluation", "Reflection" and "Dissemination" according to Gerber et al. (A case for more Design Science Research in Management Research, in publication).

4. Research conducted

In the "Theorizing" phase, empirical Mixed Methods with an explanatory sequential design (investigation with quantitative methods and explanation with qualitative methods) with a predominance of the qualitative approach according to Creswell (2014) was conducted. In both iterations, the sample was composed of managers in the context of applications and/or software architecture in Swiss hospitals. In the "Building" phase, the procedure reference model was constructed including six component models on the basis of the BPMN 2.0 notation (BPM Offensive Berlin, 2011) and the entity-relationship meta-model on the basis of the modified Chen notation (Academic encyclopedias, no date; Chen, 1976). Ethical considerations were and will continuously be considered.

5. Current status and next steps

In the current "Evaluation" phase, in a first iteration, the design-objectives of the constructed models are evaluated by means of semi-structured expert interviews in a first iteration, again with the sample profile of the "Theorizing" phase. A second empirical evaluation iteration will follow; the exact method will be decided after the analysis of the first iteration. In addition, the thesis document will be completed.

Acknowledgements

I would like to thank everybody, who supports me with my thesis - particularly Dr. Matthew Tucker -and I wish Dr. Nazali Mohd Noor all the best for his recovery.

References

Academic encyclopedias (no date) Modifizierte Chen Notation, [Online], Available: http://deacademic.com/dic.nsf/dewiki/968169.

Angerer, A., Schmidt, R., Moll, C., Strunk, L. and Brügger, U. (2017) *Digital Health - Die Zukunft des Schweizer Gesundheitswesens*, Winterthur: ZHAW Winterthurer Institut für Gesundheitsökonomie.

Berger, J., Bienlein, B., Schürch, D. and Wegmüller, B. (2015) *Spitäler*, in Oggier, W. (ed.) *Gesundheitswesen Schweiz 2015 - 2017 - Eine aktuelle Übersicht*, Bern: hogrefe.

BPM Offensive Berlin (2011) *BPMN 2.0 - Business Process Model and Notation*, [Online], Available: http://bpmb.de/poster.

Braun von Reinersdorff, A. (2007) *Strategische Krankenhausführung - Vom Lean Management zum Balanced Hospital Management*, 2nd edition, Bern: Verlag Hans Huber.

Busse, R. and Geissler, A. (2017) Ziele des Gesundheitssystems, Strategien der Gesundheitspolitik und Herausforderungen für Krankenhäuser. Eine kurze Einführung, in Debatin, J. F., Ekkernkamp, A.; Schulte, B.; Tecklenburg, A. (eds) *Krankenhausmanagement – Strategien, Konzepte, Methoden*. Berlin: Medizinisch Wissenschaftliche Verlagsgesellschaft.

Chen, P.P.-S. (1976) The Entity-Relationship Model--Toward a Unified View of Data, *ACM Transactions on Database Systems*, vol. 1.

Cosandey, J., Roten, N. and Rutz, S. (2018) *Gesunde Spitalpolitik - Mehr Transparenz, mehr Patientensouveränität, weniger "Kantönligeist"*. Zürich: Avenir Suisse.

Creswell, J.W. (2014) *Research Design. International Student Edition. Qualitative, Quantitative, and Mixed Methodes Approaches*, Los Angeles: Sage.

Fischer, A. (2017) Serviceorientierung: Der Patient im Fokus, in Debatin, J. F., Ekkernkamp, A.; Schulte, B.; Tecklenburg, A. (eds) *Krankenhausmanagement – Strategien, Konzepte, Methoden*. Berlin: Medizinische Wissenschaftliche Verlagsgesellschaft.

Gerber, N. and Perschel, W. (2016) 'Aus neuen Erkenntnissen folgen neue Herausforderungen', *clinicum*, vol. 3, pp. 98-99.

Gerber, N., Perschel, W., Tschümperlin, C., Wattenhofer, D. and Hofer, S. (2017) *ApplikaS – Application catalogue for Non-medical Support Services in Hospitals – based on German original*. Wädenswil: ZHAW Institute of Facility Management.

Gerber, N., Tucker, M. and Susanne, H. (in publication) *A case for more Design Science Research in Management Research*.

Wasem, J. (2017) Wichtige Umfeldbedingungen, in Debatin, J. F., Ekkernkamp, A.; Schulte, B.; Tecklenburg, A. (eds) *Krankenhausmanagement – Strategien, Konzepte, Methoden*. Berlin: Medizinisch Wissenschaftliche Verlagsgesellschaft.

ISSN 2398-6611 (Online)

Layth Kraidi Analysing the Critical Risk Factors in Oil and Gas Pipeline Projects by Using Fuzzy Logic Theory

L Kraidi [1, 2], R Shah [1], W Matipa, [1] and F Borthwick [1]
1 Department of the Built Environment, Faculty of Engineering and Technology, Liverpool John Moores University, Byrom Street Campus, Liverpool. L3 3AF
2 PhD Student, Henry Cotton Building, 15-21 Webster Street, Liverpool, L3 2ET, UK. Email: L.A.Kraidi@2016.ljmu.ac.uk

Abstract. Oil and Gas Pipeline (OGP) projects are a safe mood to transport the oil products. However, a massive range of risk factors (RFs) increases the risk of OGPs' failure. Third-Party Disruptions (TPD) like terrorism and sabotages attacks is one of the most dominated causes of the pipelines' failure globally. The domain of risk management in these projects has a lack of verified historical data about OGPs' accidents to analyse the RFS, particularly about TPD RFs. Correspondingly, the operations of OGPs projects often require an unconventional risk management approach, especially in insecure areas. This paper aims to overcome the uncertainty in analysing the RFs based on a more holistic Risk Management Framework (RMF), which was designed to work in three phases as follows. Phase I carries out extensive and worldwide investigations to bridge the gap of identifying the critical RFs in OGP projects. Phase II designs a questionnaire survey based on the findings of phase I to collect the stakeholders' perceptions about probability and severity of the RFs on OGPs projects. Phase III designs a risk simulation model by using fuzzy inference system in MATLAB to deal with the uncertainty in analysing the RFs that results from the lack of data and experts' judgments. The results of simulating the RFs reviled that terrorism and sabotage, corruption, low public legal and moral awareness about OGPs projects, insecure areas and thieves are the most critical RFs in OGPs in Iraq.

Keywords. Oil and gas pipelines, Risk management framework, risk analysis, stakeholders' judgement, and fuzzy inference system.

1. Introduction

Oil and Gas Pipelines (OGPs) must be planned, designed, installed, operated and maintained regarding the safety requirements to transport the petroleum products safely. However, several Risks Factors (RFs) threaten the safety of these projects during the planning, construction, and operational stages, such as Third-Party Disruption (TPD) and corrosion, design and construction defects, natural hazards, operational errors and many more [1]. TPD reveals to any external factors that damage the pipelines, which is the major cause of OGPs failure globally [2].

The process of managing the RFs requires identifying the RFs that threaten the pipelines based on a real database about the pipelines' failures reasons [3]. A real database defines as the records of the pipelines' design; the maps of pipelines' routes; pipeline fault and accidents data; previous inspections and surveillance records; operational pressure and pressure test records; pipeline maintenance records; and modification records [4]. Such a database is not available in the troubled and developing countries [4]. Moreover, most of the risk analysis models are not comprehensive because they are considering one or two RFs at a time [5]. Hence, there is a vital need to help the stakeholders to focus on the most vulnerable segments of pipelines' safety by employing a more practical risk management approach based on a Risk

Management Framework (RMF). The RMF will adopt a qualitative data analysis, a statistical methodology-based, and fuzzy logic theory to identify and analyse the RFs that associated with OGPs in a more holistic approach to enhance the safety of OGPs projects, particularly in the troubled countries.

2. Research approach

Deterministic and simulation are the main two ways that are using to calculate the probability of failure. The deterministic approach utilises the related data to assess the probability conditions. And the simulation approaches utilises correlation analysis with the age and the conditions of the pipes to assess the probability of failure based on the historical records [6]. Both of these two approaches were used in this study. Mubin & Mubin, [7] developed a risk management model to provide recommendations for risk management for gas pipeline projects in the construction stage in Pakistan. In this model, a data bank was created to register the RFs, which were simulated by using Monte Carlo risk simulation. Schwarz et al., [8] developed a risk management procedure to evaluate the RFs to support decision-making processes in projects. The model started by defining the scope of the projects, the criteria of the risk management, and identifying the RFs. Then the Artificial Neural Network (ANN) and many experts' judgments were used to analyse the RFs. El-Abbasy et al., [9] have done a study to assess the performance of water distribution networks in Qatar and Canada by using a fuzzy analytical network. In this paper, these models were adapted to develop a more holistic and effective RMF by bridging the highlighted gaps in these models as presented in figure 1.

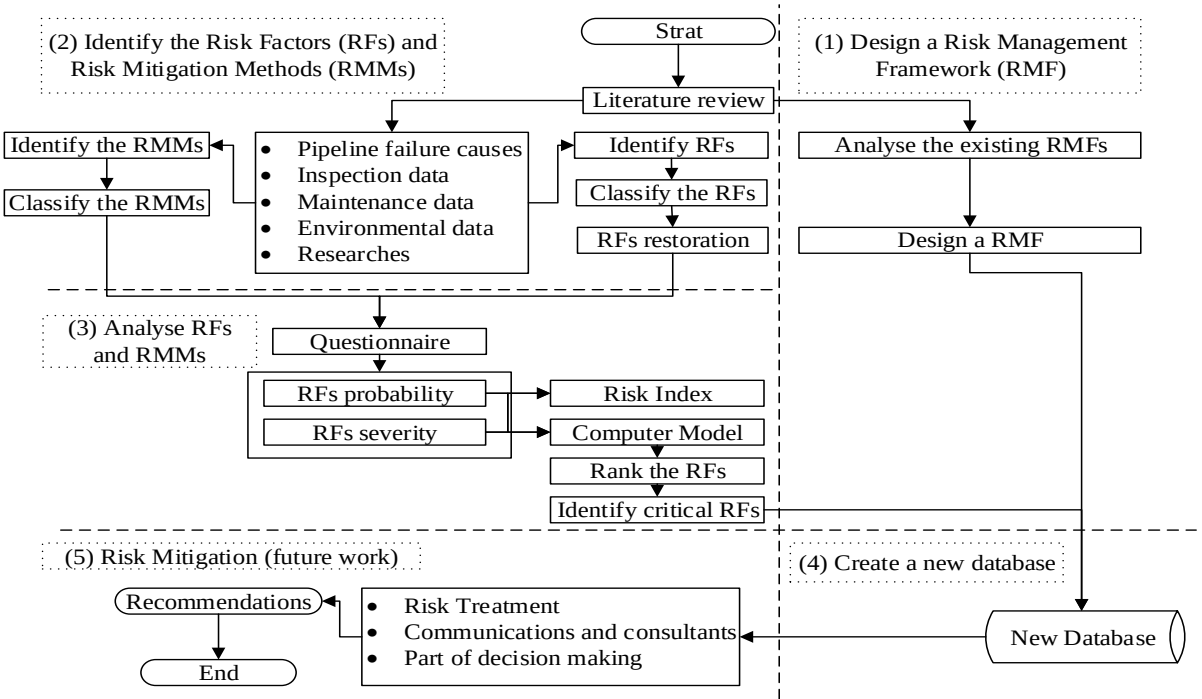

Figure 1: Risk Management Framework (RM F) [4]

Figure 2: (a) The arithmetic of fuzzy inference system (FIS) [12], (b) FIS with two inputs (RP and RS) and one output RI [10] and (c) fuzzy membership functions.

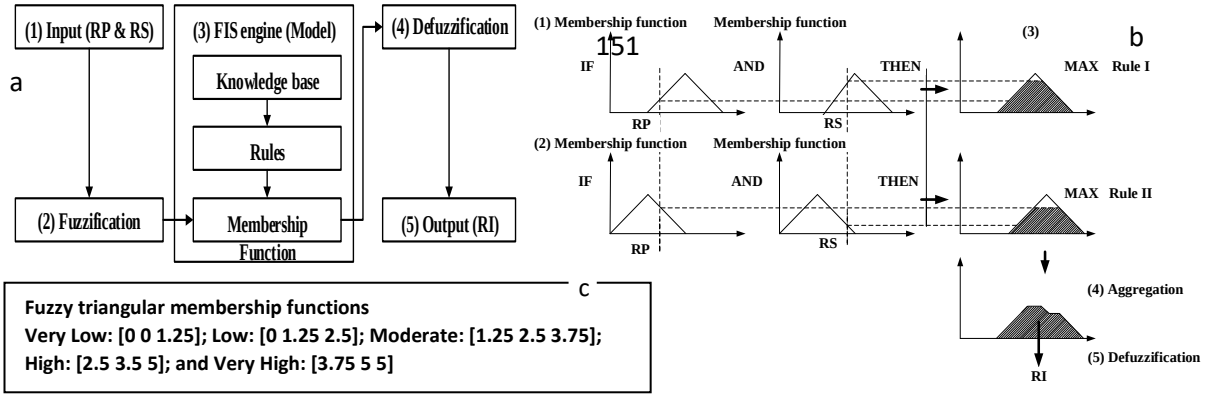

Flowing the procedure of the RMF, extensive investigations were carried out to identify the RFs in OGP projects in different circumstances worldwide, especially in the insecure areas to overcome the problem of data scarcity about the RFs. Thirty RFs were identified and listed in this paper as shown in table 1. Based on the findings of these investigations, a questionnaire survey was designed to analyse the probability and severity of RFs in OGP projects in Iraq. The probability of the RFs was evaluated on a scale [rare, unlikely, possible, likely and almost certain]. The severity of the RFs was evaluated on a similar scale [negligible, minor, moderate, major and catastrophic]. In such situation, the fuzzy logic theory is a useful tool that could be used to deal with the cases of risk analysis for many sciences when there are no precise values and sharp boundaries [11]. As shown in table 1, the process of FIS has the following. Fuzzification, which is about providing the crisp inputs for the FIS by generating sets of membership's functions for the inputs [Risk Probability (RP) and Risk Severity (RS)]. The Knowledgebase, which is about defining the rules "If-Then rules" that controlling the behaviour of the FIS. Then, propose membership functions by using Mamdani algorithm. Finally, defuzzification, the centroid method of defuzzification was used to obtain the final outputs [crisp Risk Index (RI)].

3. Results

The results of analysing the RFs are presented in table 1.

Table 1: The findings of the investigations about the RFs and the results of the RFs analysis.

RFs [4]	RP	RS	RI	Ranking	Risk Range (see figure 2-c)
Terrorism & sabotage	3.995	4.490	3.99	1	High
Corruption	3.980	4.323	3.87	2	High
Low public legal & moral awareness	3.712	4.106	3.80	3	High
Insecure areas	3.717	4.192	3.76	4	High
Thieves	3.692	4.081	3.75	5	High
Corrosion & lack protection against it	3.687	3.990	3.72	6	High
Lack of proper training	3.646	3.859	3.71	7	High
Improper safety regulations	3.687	3.960	3.70	8	High
Exposed pipelines	3.667	3.949	3.70	9	High
Improper inspection & maintenance	3.657	3.899	3.69	10	High
Conflicts over land ownership	3.495	3.646	3.68	11	High
Shortage of the IT services & modern equipment	3.667	3.924	3.68	12	High
Weak ability to identify & monitor the threats	3.631	3.848	3.67	13	High
Design, construction & material defects	3.333	3.611	3.64	14	High
Lack of risk registration	3.566	3.662	3.60	15	High
The pipeline is easy to access	3.631	3.773	3.57	16	High
Limited warning signs	3.626	3.732	3.56	17	High
Little researches on this topic	3.621	3.697	3.55	18	High
Lawlessness	3.606	3.682	3.54	19	High
Stakeholders are not paying proper attention	3.530	3.652	3.51	20	High
Public's poverty & education level	3.449	3.611	3.49	21	High
Inadequate risk management	3.227	3.505	3.48	22	High
Leakage of sensitive information	2.980	3.399	3.38	23	High
Threats to staff	3.323	3.571	3.35	24	High
Operational errors	3.101	3.409	3.30	25	High
Geological risks	2.747	3.182	3.17	26	High
Natural disasters & weather conditions	2.652	3.066	3.10	27	High
Hacker attacks on the operating or control system	3.066	3.066	3.03	28	High
Vehicles accidents	2.465	2.970	2.80	29	Moderate
Animals accidents	1.894	2.020	1.95	30	Low

4. Summary

The developed RMF provides a comprehensive and systematic approach of OGPs risk management, specifically for the organisations that just began to mitigate OGPs RFs more effectively. Using the fuzzy logic in the process of the risk assessment remedies the problems of the traditional approaches to risk management. The results of questionnaire survey were used to provide real input for a computer based-model was developed to simulate the RFs and RMMs by using FIS toolbox in MATLAB.

Iraq needs to overcome many formidable challenges and RFs that are obstructing the OGPs system and the development of new projects. While various problems and risks were found as pipeline failure causes, TPD recognizes as one of the most prevailing causes of OGPs failure in Iraq. Raking the RFs by using FIS shows the range of the risk is from low to high. In this paper, a new database has been greeted to store real information about RF identification and risk analysis; this paper's findings and recommendations to be used for future researchers.

The future is to evaluate some Risk Mitigation Methods (RMMs) by using qualitative and quantitative methods. Estimate the consequences of OGPs failures. And, analyse the RMMs in term of time and cost-effective on the projects.

5. References

1. Wan C, & Mita A (2010). Recognition of potential danger to buried pipelines based on sounds. *Structural Control and Health Monitoring*, **17(3), 317–337**. https://doi.org/10.1002/stc.302.
2. Hopkins P, Fletcher R, and Palmer-Jones R. (1999). A method for the monitoring and management of Pipeline risk - A Simple Pipeline Risk Audit (SPRA). *In 3rd Annual Conferences on Advances in Pipeline Technologies & Rehabilitation* (**Vol. 44, pp. 0–24**).
3. Balfe N, Leva M C, McAleer B, and Rocke M. (2014). Safety risk registers: Challenges and guidance. *Chemical Engineering Transactions*, **36, 571–576**. https://doi.org/10.3303/CET1436096.
4. Kraidi L, Shah R, Matipa W and Borthwick F. Analysing the Critical Risk Factors of Oil and Gas Pipeline Projects in Iraq. *The 3rd BUiD Doctoral Research Conference 13th of May 2017*. PP 133- 148.
5. El-Abbasy M S, Senouci A, Zayed T, Parvizsedghy L and Mirahadi F. (2016). Unpiggable Oil and Gas Pipeline Condition Forecasting Models. *Journal of Performance of Constructed Facilities*, **30(1), 4014202**. https://doi.org/10.1061/(ASCE)CF.1943-5509.0000716.
6. Elsawah H, Bakry I, and Moselhi O. (2016). Decision Support Model for Integrated Risk Assessment and Prioritization of Intervention Plans of Municipal Infrastructure. *Journal of Pipeline Systems Engineering and Practice*, **7(4), 4016010**. https://doi.org/10.1061/(ASCE)PS.1949-1204.0000245.
7. Mubin S, and Mubin G. (2008). Risk analysis for construction and operation of gas pipeline projects in Pakistan. *Pak. J. Engg. & Appl. Sci*. **Vol, 50(4), 55–60**.
8. Schwarz J, Sandoval-Wong J A and Sánchez P. (2015). Implementation of artificial intelligence into risk management decision-making processes in construction projects (pp. 361–362).
9. El-Abbasy M S, El-Chanati H, Mosleh F, Senouci A, Zayed, T, and Al-Derham H. (2016). Integrated performance assessment model for water distribution networks. *Structure and Infrastructure Engineering*, 1–20. https://doi.org/10.1080/15732479.2016.1144620.
10. Zadeh L A. (1965). Fuzzy sets. Information and Control, **8, 338–353**.
11. Jamshidi A, Yazdani-Chamzini A, Yakhchali S H and Khaleghi S. (2013). Developing a new fuzzy inference system for pipeline risk assessment. *Journal of Loss Prevention in the Process Industries*, **26(1), 197–208**. https://doi.org/10.1016/j.jlp.2012.10.010.

Acknowledgement

The financial support from the Ministry of Higher Education and Scientific Research, Iraq and AL-Muthanna University is highly appreciated.

ISSN 2398-6611 (Online)

Keyur Joshi Determining the dielectric property of milk products for online quality monitoring using microwave spectroscopy

K H Joshi[1], P Kot, A Shaw, and S Wylie
Built Environment and Sustainable Technologies (BEST) Research Institute,
Department of Built Environment,
Liverpool John Moores University,
Liverpool,
L3 3AF
[1]K.H.Joshi@2014.ljmu.ac.uk, P.Kot@ljmu.ac.uk, A.Shaw@ljmu.ac.uk ,
S.Wylie@ljmu.ac.uk

Abstract. In this article, a novel approach is introduced for quality testing of milk products by determining their dielectric property with the help of microwave spectroscopy. The tests were carried out on three predominant categories of milk products in the commercial market; namely skimmed milk, semi-skimmed milk and whole milk, purchased from high-street supermarket. Electromagnetic (EM) wave spectroscopy was used to record the dielectric property of the milk samples, in terms of dielectric permittivity. This database was then analysed to determine the overall quality of given milk products in terms of type of milk i.e. milk contents, and bacteria adulteration i.e. aging. The proposed methodology attempts to resolve the limitations of milk quality testing schemes being employed currently in practice to give a milk quality monitoring system, which is non-destructive, real-time, less expensive, and less tedious compared to other existing standards. The proposed technique enables quality monitoring without the need of making or adding reagents to original milk samples, making it a time and resource saving technology as compared to conventional methods. The results achieved through this method are promising and clearly distinguishes the milk types based on their fat content which in turn helps with milk adulteration with added water. With further optimisation in the prototype design of the used EM wave sensor system, it can be applied in practice for online monitoring of milk products and quality control.

Keywords. adulteration, dielectric property, electromagnetic wave sensors, microwave spectroscopy, milk quality monitoring, spoilage detection, real-time.

1. Introduction

Microwave spectroscopy is broadly defined as “the study of interaction between matter and radio waves of wavelengths (λ) between a few metres to few tenths of a millimetre” [1]. It was broadly introduced first by Drude with experiments related to dielectric properties of matter using radio waves. The use of microwave spectroscopy has become prominent since world war-II with radar and other technical developments in microwave generation of techniques. Subsequently this technique has been used for a wide variety and broad range of applications in recent advancements, e.g. drug detection in blood [2], drip

loss in meat products [3], water contaminants analysis [4], determining moisture content of building fabrics [5] etc.

For the development of a novel technique, which can assess overall quality of milk products, using microwave spectroscopy, it could aid to have the required understanding of dielectric properties of milk. It was found in the literatures reviewed that the dielectric constants for raw milk (with 100 % concentration of milk) and diluted milk (with 70 % milk concentration to deionized water), both, decrease with increasing frequency. This phenomenon was identified to occur more so at the lower frequency range of 10–4500 MHz but this decrement in values for dielectric constant for raw milk was more rapid than in the case of diluted milk, at room temperature of 22 °C This work attempts to determine the dielectric property of milk products [6]. For raw milk, these values of decrement were 97.7, 68.1, and 65.9, whereas for 70%, diluted, milk solution the same were 93.3, 70.9 and 69.1, at 10 MHz, 915 MHz, and 2450 MHz of frequencies, respectively. Another potential indicator for predicting milk concentration, and freshness, is its dielectric loss factor. The researchers further observed that because the adulteration of milk with water dilutes the overall milk concentration, ionically, the loss factor tends to decrease with the increased amount of water content, i.e. decreasing milk concentration.

Researchers in another similar work concluded that, for cow's milk, its protein content as well as the temperature of milk affect both the values of dielectric constant and the loss factor. The frequency of electric field, also, influences these two values. Within the range of 10–4500 MHz, the dielectric constant decreased with increasing frequency [7]. The value of dielectric loss factor increased with increasing temperature below frequency values of around 600 MHz and decreased above 1000 MHz of frequency values. A poor correlation was observed between the amount of protein content and dielectric constant in the region of 100–600 MHz frequency values. Based on these dielectric constant values, it meant that this frequency range was insufficient for being used to develop milk protein detector.

2. Measurement of dielectric property of milk

Materials can be classified according to their complex-valued dielectric permittivity (ε), upon comparison of its real (ε′) and imaginary (ε″) components. To understand the dielectric property characteristics of milk the milk types, i.e., with respect to their fat components, the dielectric property of milk was determined and analysed for all 3 milk types, in this work as explained in this section. Table 1 shows how the ratio of these two values is used to determine the dielectric property of the material under test.

Table 1. *General Classification of Materials based on Permittivity*.

$\varepsilon_r''/\varepsilon_r'$	**Current Conduction**	**Field Propagation**
0	-	Perfect dielectric lossless medium
$\ll 1$	Low-conductivity material; Poor conductor	Low-loss medium; Good dielectric
≈ 1	Lossy conducting material	Lossy propagation medium
$\gg 1$	High-conductivity material; Good conductor	High-loss medium poor dielectric

∞	Perfect conductor	-

2.1. Sample preparation

Three commercially purchased milk products of each category – skim milk, semi-skim milk and whole milk were tested to determine their dielectric parameters. The milk products were purchased from a high street supermarket for the longest available expiry dates and were made into 4 samples each of the size 250 ml. The dielectric data was measured for everyday morning at approximately same time for Monday (Day-1), Tuesday (Day-2), Wednesday (Day-3), Thursday (Day-4), Friday (Day-5) and then the following Monday (Day-8), when the milk samples were spoiled.

Following table 2 notes down the compositional elements of each milk type that was considered for the test measurements using coaxial probe analysis of dielectric property in terms of dielectric permittivity.

Table 2. *Milk compositional values for each milk type under test.*

Typical Values (per 100 ml)	**Milk Categories**		
	Skimmed milk	**Semi-skimmed milk**	**Whole milk**
Energy (kJ)	147 (35 kcal)	209 (50 kcal)	268 (64 kcal)
Fat (g)	0.1	1.8	3.6
Saturates (g)	<0.1	1.1	2.3
Protein (g)	3.4	3.6	3.2
Carbohydrates (g)	5.0	4.8	4.7
Sugars (g)	5.0	4.8	4.7
Salt (g)	0.1	0.1	0.1
Calcium (mg)	124.0	124.0	120.0

2.2. Instrumentation and experimental setup

The dielectric permittivity was measured for each milk type between the frequency values 2 GHz to 8 GHz. The choice of frequencies was based on the design constraint to cover key frequency values from the Industrial, Scientific and Medical (ISM) band for future integration of the corresponding industry oriented sensor design. The measurement conditions are shown in table 3. Figure 1 gives tests lab setup.

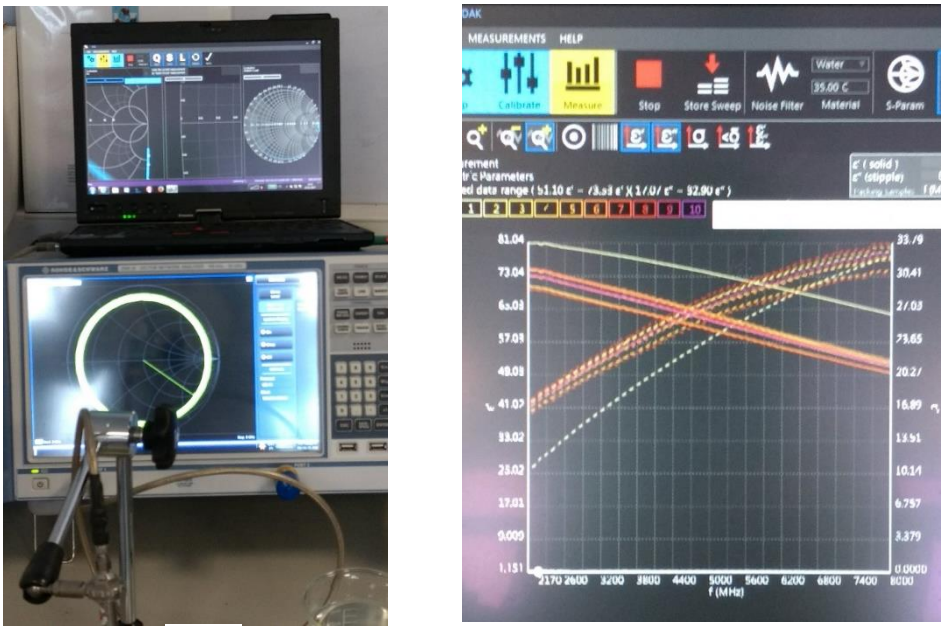

(a) (b)

Figure 1. *(a) Dielectric Property Measurement DAK Kit, (b) Dielectric Permittivity values vs. Frequency graphs for Skim, Semi-skim and Whole Milk Samples.*

Table 3. *Milk compositional values for each milk type under test.*

Specifications	**Values**
No. of Milk Types	3 Milk Types (Skim, Semi-skim, Whole) x 4 samples
Repetitions	4 times each (for 6 days)
Sample Size	≈ 250 ml (for coaxial probe)
Test Period / Lab Temperature	1 week (Day No.: 1, 2, 3, 4, 5, and 8) / 13 °C ± 2 °C
Coaxial Probe /Frequency sweep	SPEAG DAK 3.5 / 2 GHz – 8 GHz
Channel Specifications	TOSM calibration / 0 dBm Base Power
VNA / Step Size	R&S® ZNB 20 100 kHz – 20 GHz / 5 MHz

3. Results and discussion

The dielectric permittivity values are plotted against the frequency range 2GHz-8GHz as recorded from dielectric property test measurements for all three milk types as illustrated in figure 2. It is evident that this analysis was able to make distinctive classification for the three types of milk samples.

Also, the results achieved here show a gradual decay in the dielectric permittivity with increasing frequency values, which compliments the results achieved by other researchers and briefly discussed in introduction section of this article.

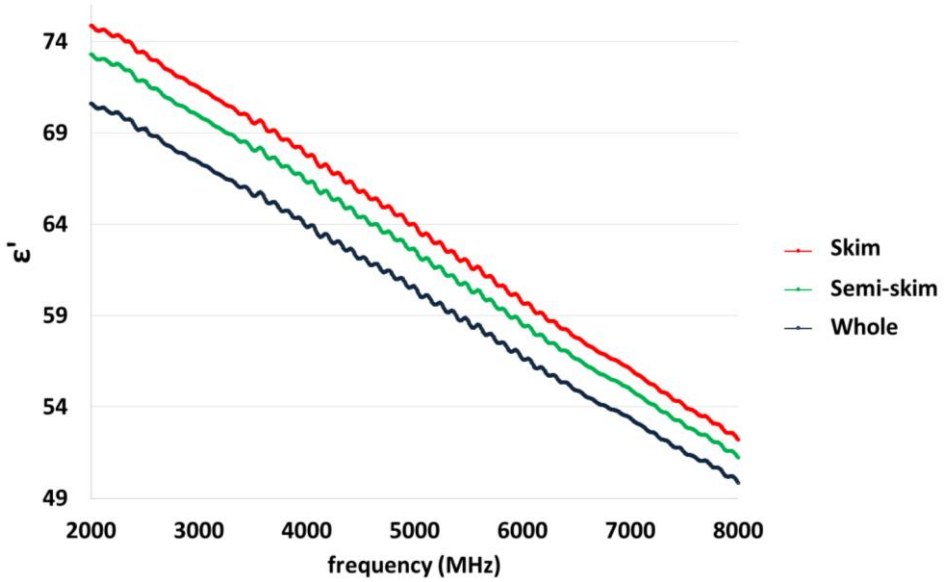

Figure 2. *Dielectric Permittivity Vs. Frequency Values for three milk types*

4. Conclusion

It was concluded that the results achieved are clearly able to classify the milk types based on their fat contents. Therefore grading of unknown milk samples was possible based on this dielectric property analysis of commercially available milk types. This real-time method is particularly useful in markets where fragmented milk production takes place in unorganised sectors and therefore where there is more vulnerability of milk adulteration such as added water in milk to gain commercial profits.

References

[1] Townes C. The present status of microwave spectroscopy. *Ann N Y Acad Sci.* 1952;55:745–50.
[2] Joshi KH, Al-Manasra M, Mason A, Korostynska O, Powell AK, Ortoneda-Pedrola M, et al. Detection of Heparin Level in Blood Using Electromagnetic Wave Spectroscopy. In: 2016 *9th Int. Conf. on Developments in eSystems Engineering (DeSE)*. IEEE; 2016. p. 329–34.

[3] Mason A, Abdullah B, Muradov M, Korostynska O, Al-Shamma'a A, Bjarnadottir S, et al. Theoretical Basis and Application for Measuring Pork Loin Drip Loss Using Microwave Spectroscopy. *Sensors*. 2016;16(2):182.
[4] Korostynska O, Mason A, Al-Shamma'a AI. Flexible microwave sensors for real-time analysis of water contaminants. *J Electromagn Waves Appl.* 2013;27(16):2075–89.
[5] Kot P, Shaw A, O Jones K, Cullen J, Mason A, Al-Shamma'a AI. The feasibility of using electromagnetic waves in determining the moisture content of building fabrics and the cause of the water ingress. In: *Proc. of the 8th Int. Conf. on Sensing Technology*. Liverpool; 2014. p. 604–8.
[6] Guo W, Zhu X, Liu H, Yue R, Wang S. Effects of milk concentration and freshness on microwave dielectric properties. *J Food Eng.* 2010;99(3):344–50.
[7] Zhu X, Guo W, Jia Y, Kang F. Dielectric Properties of Raw Milk as Functions of Protein Content and Temperature. *Food Bioprocess Technol* (2015) 2015;670–80.

ISSN 2398-6611 (Online)

Md Jobayer Bhuyan Improving Land Administration through Total Quality Management (TQM) Approach in Bangladesh

Abstract. Land is the ultimate resource, human life cannot sustain on earth without it. For the production of wage goods such as grains, sugarcane and cloth land is the chief element; in fact, every commodity human uses can be ultimately traced back to land. So human interest in land is universal and it is one of the human rights. However where there is an interest there is a dispute. Consequently land dispute arise from land interest. As interest in land is universal, land dispute is also universal. In Bangladesh, particularly multiplicity of documents and the diversity of ways by which land information is recorded give rise to disputes amongst owners and other interest groups, as such this hampers sustainable development of the country. The Government of Bangladesh has taken numerous measures over the decades to reform and streamlines land administration; so that land sector would be managed efficiently and effectively. However, studies have shown that still there are loopholes and governance deficits in different areas of land administration and service provisions. Elimination of these loopholes and governance deficits require integrated approach with effective land laws along with well structured land administration, dynamic land management in an environment of good governance and amicable mechanism of dispute settlement. Total Quality Management (TQM) is an integrated approach which considers the whole system including all the processes and workforce. The concept of TQM has been very successful in many different industries, particularly in private sector. Therefore, understanding the effect of TQM in different industries and considering the paramount significance of land administration, this research aims to investigate the quality of existing land administration system in Bangladesh in order to develop a quality framework within the broad concept of TQM.

Keywords: land administration, management, LAS, quality, TQM

1.1 Research Problem

To improve the quality of administration, effectiveness and flexibility of whole organization an integrated approach is required (Ali, 2013); TQM is an integrated approach, which considers the whole system including all the processes and workforce (Oakland, 1993, Kanji, 2012). In private sector, the concept of TQM has been very popular for improving business performance, researchers have also recommended improving quality of administration in public sector across Europe by quality inspection, quality control, and system oriented quality control assurance through TQM (Löffler, 2013; Hsiao and Lin, 2008). In relation to applying TQM concept to land administration, a published work is found to have been conducted in context of Pakistan (Ali *et al*., 2013). For developing TQM guidelines to improve this public sector, they have taken into account institutional and technical aspects but not taken into consideration essential legal aspect. According to UN (2015), these guidelines are incompatible in different countries, due to distinct nature of society, culture, economic condition, local traditions and existing infrastructure of the countries of the world. Therefore, there is a need to design a methodology for analysing quality of land administration within a country as a standalone exercise with all possible quality indicators (UN, 2015).

2.0 Aim and Objectives of the Research

Using Bangladesh as a case study, the research aims to investigate the quality of existing land administration system in order to develop a quality framework within the broad concept of TQM.

The aim of the research will be achieved by meeting the following objectives:

1. To conduct a critical literature review of existing management processes and pitfalls of land administration in Bangladesh.
2. To examine the legal, institutional and technical contributing elements for assessing the quality of existing LAS.
3. To define and examine the quality indicators considering the legal, institutional and technical aspects of LAS in order to evaluate the quality.
4. To develop a framework within the broad concept of TQM in order to eliminate underlying issues and to improve efficiency and effectiveness of LAS.

3.0 Research Methodology

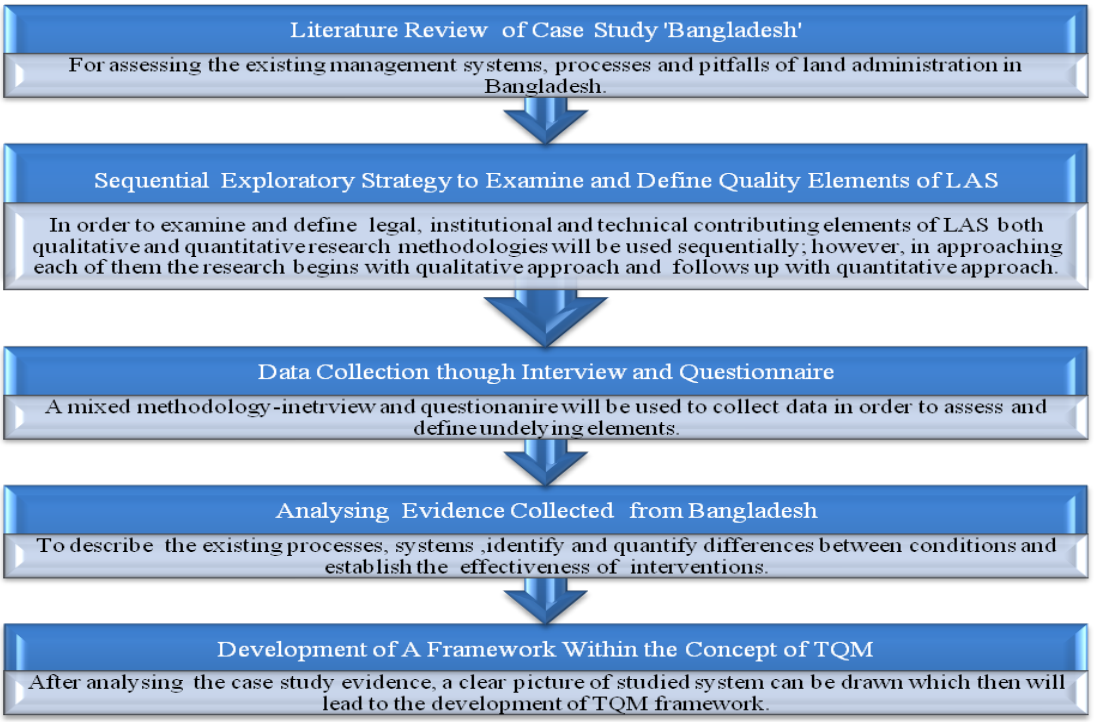

3.1 Data Type, Population and Sampling

The primary data will be collected at 2 stages from Bangladesh. In Bangladesh, LAS is overseen by a commissioner in every division and all the activities of land administration in every division is carried out under same jurisdiction. Hence, a division, Chittagong (Southern Bangladesh) will be selected for the

purposes of data collection. From the sampled division, data will be collected from officials of the Directorate of Land Records and Survey, Land Reform Board and Land Appeals Board as well as district officers, *Upazilla* officers (Sub-district Officers), *Tehsilders* (Local Revenue Collectors), owners of land, law professionals, real estate agents and bank officials who will all be purposively selected. An ethical approval was gained from Liverpool John Moores University in September 2017 for stage-1 of the research, reference: 17/BUE/007

Data Analysis

Qualitative Data

Data management and analysis of interview (stage-1) performed using NVivo 10 qualitative data analysis software. Thematic analysis then can be undertaken as described by Braun and Clark (2006). The results from the analysis will be used to design questionnaire.

Stakeholders	No of Participant	Transcription of Interviews from recordings/notes(words)
Government Officials	1 ×District Officer 2×Sub-district officer 2×*Tehsilder*	1812 1089,2149 1209, 1296
Law Professional	1×Rahman Chamber 2×Chowdhury Chamber	535 639, 970
Land Owners	7×Land Owners	820, 727,954,532,757,705,624

To gain insights of the underlying problem of land administration system of Bangladesh a semi-structured interview questions was distributed among three different types of stakeholders: government officials, land owners and law professionals. A total of 15: 5 government officials, 7 land owners and 3 law professionals have responded and given consent to take part in the study. From all the interviews, transcripts were imported into Nvivo-10 forming the project resources

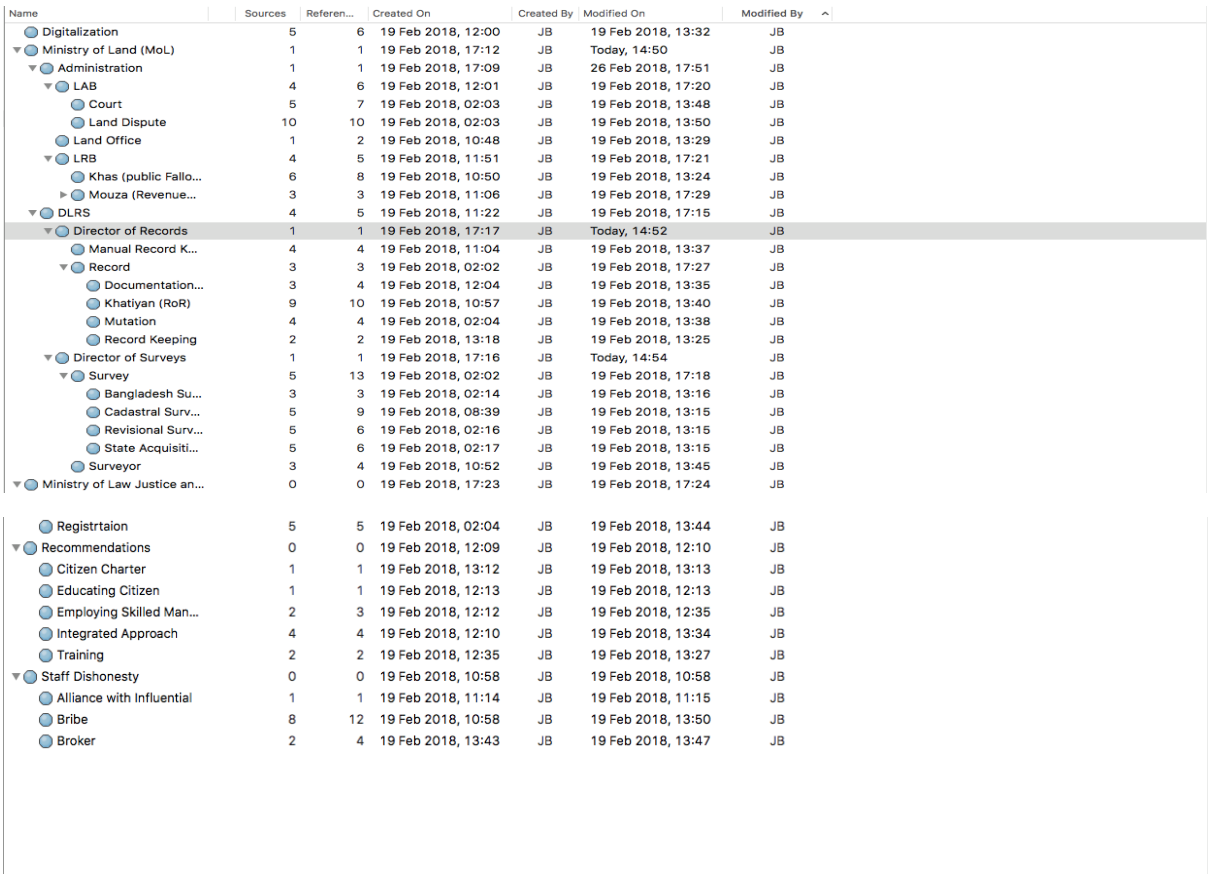

Name	Sources	Referen...	Created On	Created By	Modified On	Modified By
Digitalization	5	6	19 Feb 2018, 12:00	JB	19 Feb 2018, 13:32	JB
Ministry of Land (MoL)	1	1	19 Feb 2018, 17:12	JB	Today, 14:50	JB
Administration	1	1	19 Feb 2018, 17:09	JB	26 Feb 2018, 17:51	JB
LAB	4	6	19 Feb 2018, 12:01	JB	19 Feb 2018, 17:20	JB
Court	5	7	19 Feb 2018, 02:03	JB	19 Feb 2018, 13:48	JB
Land Dispute	10	10	19 Feb 2018, 02:03	JB	19 Feb 2018, 13:50	JB
Land Office	1	2	19 Feb 2018, 10:48	JB	19 Feb 2018, 13:29	JB
LRB	4	5	19 Feb 2018, 11:51	JB	19 Feb 2018, 17:21	JB
Khas (public Fallo...	6	8	19 Feb 2018, 10:50	JB	19 Feb 2018, 13:24	JB
Mouza (Revenue...	3	3	19 Feb 2018, 11:06	JB	19 Feb 2018, 17:29	JB
DLRS	4	5	19 Feb 2018, 11:22	JB	19 Feb 2018, 17:15	JB
Director of Records	1	1	19 Feb 2018, 17:17	JB	Today, 14:52	JB
Manual Record K...	4	4	19 Feb 2018, 11:04	JB	19 Feb 2018, 13:37	JB
Record	3	3	19 Feb 2018, 02:02	JB	19 Feb 2018, 17:27	JB
Documentation...	3	4	19 Feb 2018, 12:04	JB	19 Feb 2018, 13:35	JB
Khatiyan (RoR)	9	10	19 Feb 2018, 10:57	JB	19 Feb 2018, 13:40	JB
Mutation	4	4	19 Feb 2018, 02:04	JB	19 Feb 2018, 13:38	JB
Record Keeping	2	2	19 Feb 2018, 13:18	JB	19 Feb 2018, 13:25	JB
Director of Surveys	1	1	19 Feb 2018, 17:16	JB	Today, 14:54	JB
Survey	5	13	19 Feb 2018, 02:02	JB	19 Feb 2018, 17:18	JB
Bangladesh Su...	3	3	19 Feb 2018, 02:14	JB	19 Feb 2018, 13:16	JB
Cadastral Surv...	5	9	19 Feb 2018, 08:39	JB	19 Feb 2018, 13:15	JB
Revisional Surv...	5	6	19 Feb 2018, 02:16	JB	19 Feb 2018, 13:15	JB
State Acquisiti...	5	6	19 Feb 2018, 02:17	JB	19 Feb 2018, 13:15	JB
Surveyor	3	4	19 Feb 2018, 10:52	JB	19 Feb 2018, 13:45	JB
Ministry of Law Justice an...	0	0	19 Feb 2018, 17:23	JB	19 Feb 2018, 17:24	JB
Registrtaion	5	5	19 Feb 2018, 02:04	JB	19 Feb 2018, 13:44	JB
Recommendations	0	0	19 Feb 2018, 12:09	JB	19 Feb 2018, 12:10	JB
Citizen Charter	1	1	19 Feb 2018, 13:12	JB	19 Feb 2018, 13:13	JB
Educating Citizen	1	1	19 Feb 2018, 12:13	JB	19 Feb 2018, 12:13	JB
Employing Skilled Man...	2	3	19 Feb 2018, 12:12	JB	19 Feb 2018, 12:35	JB
Integrated Approach	4	4	19 Feb 2018, 12:10	JB	19 Feb 2018, 13:34	JB
Training	2	2	19 Feb 2018, 12:35	JB	19 Feb 2018, 13:27	JB
Staff Dishonesty	0	0	19 Feb 2018, 10:58	JB	19 Feb 2018, 10:58	JB
Alliance with Influential	1	1	19 Feb 2018, 11:14	JB	19 Feb 2018, 11:15	JB
Bribe	8	12	19 Feb 2018, 10:58	JB	19 Feb 2018, 13:50	JB
Broker	2	4	19 Feb 2018, 13:43	JB	19 Feb 2018, 13:47	JB

Figure 4.2*: Thematic Map of the Analysis*

4.0 Future Work

Questionnaire -Based on the primary analysis of the issues, questionnaires will then be developed and distributed among stakeholders to collect quantitative data to gain deep insight of what are the most important quality indicators of LAS. This quantitative data will provide information about the world in the form of numbers. The understanding of the quality indicators will be achieved though structured questionnaires, which will be distributed among 120 stakeholders- members of Land Reform Board (LRB), members of Appeals Board (LAB), district officers, *upazilla* officers and *Tehsilders*, owners of land, law professionals, real estate agents and officials of bank.

Sample- will be purposive. N=140 comprising of 50× government officials, 20× law professionals, 50× land owners ,10× real estate agents and 10× bank officials. The sample sub-groups have been deliberately chosen because their views are relevant to the issue concerned.

Analysis: Data collected through questionnaires will be analysed through SPSS software. Analysis of data collected through both qualitative and quantitative approach will be integrated during interpretation phase which would provide the status of quality indicators in the study area. This detailed assessment would

further lead to the formulation of the necessary guidelines in the broad concept of TQM for improving the quality of land administration in Bangladesh.

References

Ali, Z. Tuladhar, A. M.; Zevenbergen, J. A. Bhatti, M. A. (2013) Developing a Framework to Apply Total Quality Management Concepts to Land Administration in Pakistan, *American Journal of Rural Development*. **2** (4), 74-80.
CARE (2003) *Land Policy and Administration in Bangladesh: A Literature Review* [Online] Available at: http://www.carebangladesh.org/publication/Publication_7013284.pdf [Accessed 13/04/2016]
Creswell, J. (2014) *Research Design: Qualitative, Quantitative and Mixed Method Approaches*, 4th ed. London: SAGE
Löffler, E. (2013) *Defining Quality in Public Administration*, Quality in Public Administration Basic Concepts and Comparative Perspective, Latvia, NISPAcee Conference
Mia, S. R. (1996) *Rules on Mutation*, Dhaka: Naya Dunia Publication
Mohiuddin, T. (2008) Land Administration in Bangladesh: Mismanagement through Misfeasance, *Jahangirnagar University Planning Review (JUPR)*, 6
Nahrin, K. and Rahman, M. S. (2009) Land Information System (LIS) for Land Administration and Management in Bangladesh. *Journal of Bangladesh Institute of Planners*. **2**, 116-125.
UN (2015) *The Application of Geospatial Information – Land Administration and Management*, [Online] Available at: http://ggim.un.org/docs/meetings/GGIM5/land%20admin%20and%20mngnt%20background%20paper%203.2%20final.pdf [Accessed on 20 July 2016]
UNPAN (2016) *Digitalizing Land Registration in Bangladesh* [online] Available at: http://www.unpan.org/PublicAdministrationNews/tabid/115/mctl/ArticleView/ModuleID/1467/articleId/23326/Default.aspx [Accessed 28 April 2016]
Worldometers (2016) *Population in Bangladesh* [online] Available at: http://www.worldometers.info/world-population/bangladesh-population/ [Accessed 25 April 2016]
Zevenbergen, J., Vries, W. D. Bennett, R. M. (2016) *Advances in Responsible Land Administration*, New York: CRC Press

ISSN 2398-6611 (Online)

Goran Omer Development of an electromagnetic sensor as an NDT method to assess the integrity of marine structures

G S Omer, M Riley, P Kot, W Atherton, A Shaw, S Wylie, M Magomed, J D Cullen
Built Environment and Sustainable Technologies research Centre (BEST), Liverpool John Moores University, Byrom Street, Liverpool, L3 3AF, UK
g.s.omer@2015.ljmu.ac.uk,M.L.Riley@ljmu.ac.uk, P.Kot@ljmu.ac.uk, W.Atherton@ljmu.ac.uk, A.Shaw@ljmu.ac.uk, S.R.Wylie@ljmu.ac.uk, M.Muradov@ljmu.ac.uk, J.D.Cullen@ljmu.ac.uk.

Abstract:

Deterioration of concrete due to corrosion of reinforcement is the most serious durability problem faced by the construction industry. The aim of this research is to investigate the use of an electromagnetic (EM) wave sensor for detection of chloride level in concrete structures. Chloride ion penetrates into concrete, which results in deterioration (cracking and spalling due to the corrosion of reinforcement). This process is a major concern for engineers and owners of bridges and marine structures. The novel non-destructive electromagnetic (EM) wave sensor will be investigated to monitor concrete structure in real time to provide the necessary information for identifying the level of chloride ions in concrete. Data analysis will provide the information about the condition and level of chloride within concrete structure. This research involves the design and construction of an electromagnetic (EM) wave sensor that operates at the frequency range between 2 GHz and 13GHz, at a power of 0dBm. Finally, the graphical interface package LabVIEW was used to control the frequency sweep for the sensor and to capture the data from the sensor. Based on the findings of this project, the electromagnetic (EM) wave sensor is capable to be utilised as an alternative non-destructive method for identifying level of chloride into the concrete blocks.

Keywords: Horn antenna; Electromagnetic waves; Microwaves; Sensor; Concrete slab; Chloride

Introduction and background:

Reinforcement corrosion caused by the presence of chloride ions in the neighbourhood of the re-bars has been identified as one of the major causes of deterioration of concrete structures. The chlorides could find their way to concrete either as part of constituent materials when sea sand is used, or, by gradual permeation and diffusion as in the case of marine structures, or, cases where de-icing salts used to melt away snow on highways. Thus, determination of chloride content in a concrete structure is an important

part of periodic non-destructive testing carried out for structures identified to be vulnerable to chloride induced reinforcement corrosion [1]. In many concrete structures, chloride content caused reinforcement corrosion in the neighbourhood of the reinforcing bars is not almost contained from the beginning. A common cause of reinforcement corrosion is the gradual permeation and diffusion of chloride ions from the surface of concrete. Chloride attack is a particular problem for marine structures and highways concrete, where de-icing salts are used to melt away snow. The process of deterioration of the corrosion continues based on the availability of moisture, oxygen and carbon dioxide and the presence of chloride ions in the concrete [2].

Carbonation occurs when carbon dioxide from the air enters the concrete and reacts with hydroxides, such as calcium hydroxide, to form carbonates. In the reaction with calcium hydroxide, calcium carbonate is produced: $Ca(OH)2 + CO2 \rightarrow CaCO3 + H2O$ [3].Then this response decreases the concrete pH to as low as 8.5, at the level that the passive film on the steel is not steady. In good-quality concrete carbonation, the process is usually slow; it has been estimated that carbonation will proceed at a rate of up to 0.04 inches per year. Concrete structures in marine environments such as bridge substructure elements come directly under the exposure category[4]. Three areas of concrete structures in marine environments can be distinguished regarding corrosion: the submerged zone (always below seawater), the splash and tidal zone (Intermittently wet and dry) and the atmospheric zone (well above mean high tide and infrequently wetted)[5].

Microwaves have been identified as being sensitive to moisture content. For non-destructive testing, many applications for moisture determination use the microwave method. In the microwave technique, valuable information about the permittivity of the sample is known [4]. As water has high a microwave frequency compared to dry materials, it is easily measured using the technique. Other apparatus able to measure moisture content can be destructive for building fabrics such as bricks, concrete, blocks, plaster, etc., as they require additional drilling into the wall to take a sample of the content. Furthermore, these types of methods provide inexact results. The Compton provides enhanced results scattering of gamma ray's method [6].

Moreover, it is even more essential for inspection methods to spread electromagnetic (EM) waves through the structure and determine building fabric failures, such as concrete flat roof membrane failure, marine structures. Research has been undertaken in developing a novel method that would use EM waves to resolve the problems mentioned above. Different ranges of EM waves were used for testing as well as horn antennae, which will be used to identify the best parameters to provide accurate measurements [7].

Methodology and Results:

Understanding the essential principles of the mechanism of chloride ion attack and the problem associated with chloride present in the concrete structures. The theory was studied to provide an understanding of corrosion process, and some electrochemical corrosion rate measurement techniques. Also understanding, the impact of chloride content, moisture and temperature on the dielectric constant of the concrete structures. The developing of novelty of using Microwave spectroscopy to determine the

chloride of the concrete structure in real time and in non-destructive manner. The horn antenna will assist to identify the location of the reinforcement in the concrete structures. Horn antenna has been design to be able to carry out many measurements without being worried with its displacement. In addition, the sensor designed operates in frequency ranges between (2 to 18 GHz) and the measurements were provided by s-parameters namely S_{11} or S_{21}.The following Fig.1 and Fig. 2 shows the full experiment setup during the sample test.

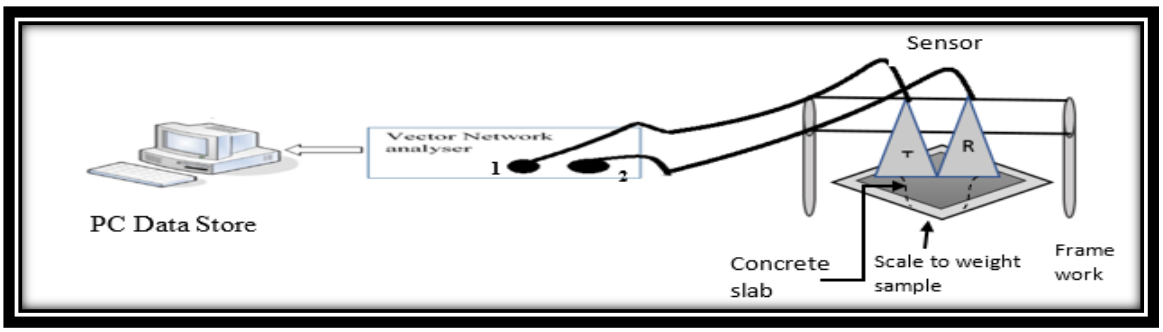

Fig. 1: A Block diagram of experimental setup

Fig. 2: S_{21} Measurements of drying off process slab for 72 hours (salt water)

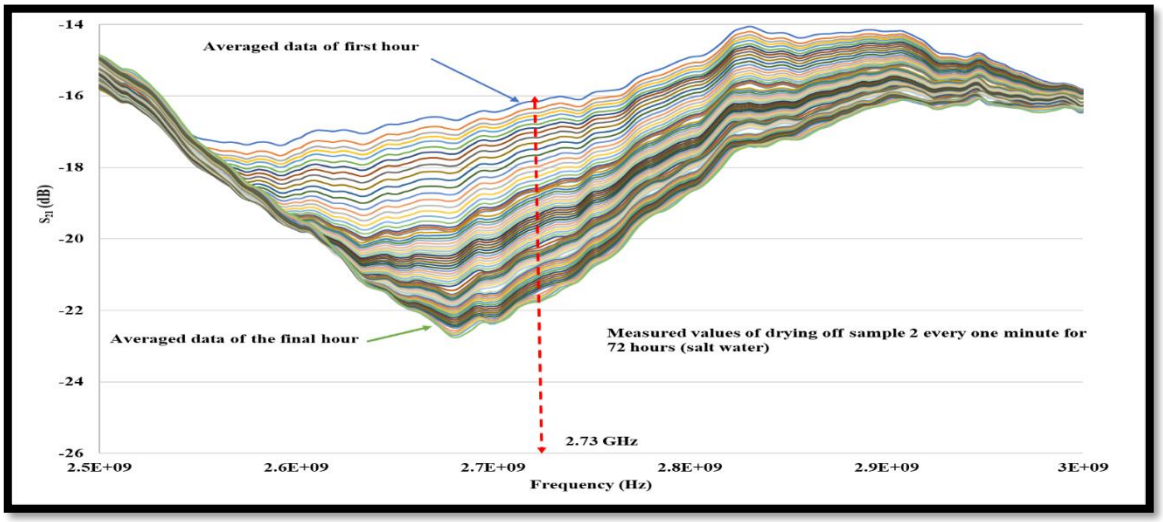

Fig. 3: Salt water drying off on the paving slabs experiment results

Fig. 3 shows the S_{21} measurements of the concrete cube taken everyone minutes during 72 hours. It can be seen that there are a noticeable change in EM signature. The changes are supposed to be caused by the decreasing amount of salt water in the concrete cubes.

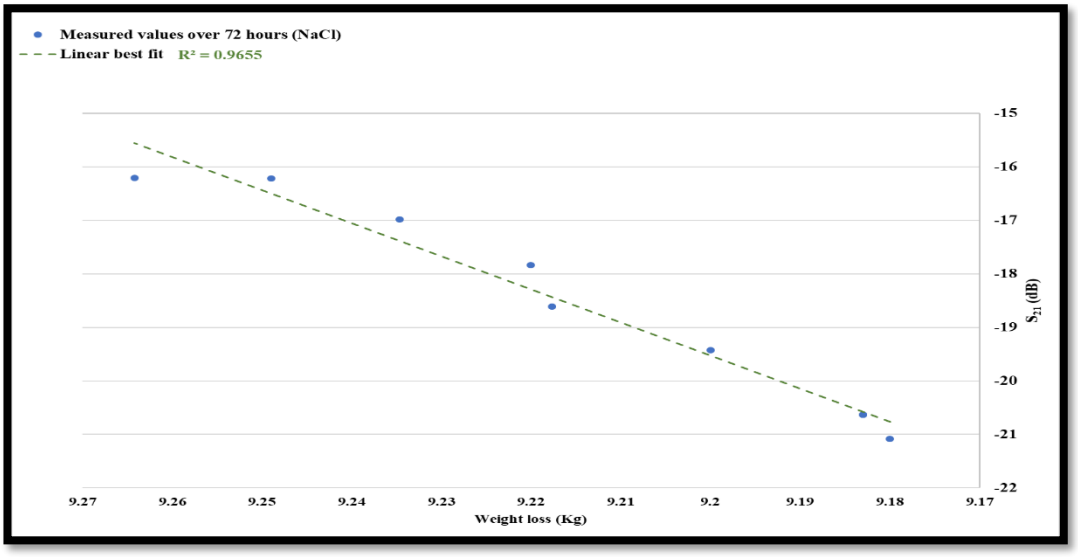

Fig 4: Linear best fit (R^2=0.97)

Fig 4 shows the linear best fit at 2.73GHz over 72 hours weight loss. R^2=0.97 which is the reasonable accurate results for correlations between S_{21} parameter and chloride and moisture loss in concrete slab.

Conclusions and Future work: Preliminary experiments provide capable results that the electromagnetic waves at frequency ranges between (2 to 13.0GHz) can be used to investigate chloride content in marine concrete structures in real time measurement's and in non-destructive manner. Future work will test concrete structures, by exiting method and comparing it with the innovative technology method and do some more experiment test at different temperature conditions.

References:

[1] Spitzlei, M., *Choosing a Method for Measuring youir Materials Moisture content*, in *Article*. 2002. p. 1-9.

[2] Zhou, Y., et al., *Carbonation-Induced and Chloride-Induced Corrosion in Reinforced Concrete Structures.* Journal of Materials in Civil Engineering, 2015. **27**(9): p. 04014245.

[3] Bioubakhsh, S., *The penetration of chloride in concrete subject to wetting and drying*, in *Faculty of the Built Environment*. 2011, Univerity College London: UCL (University College London). p. 355.

[4] Verma, S.K., S.S. Bhadauria, and S. Akhtar, *Review of Nondestructive Testing Methods for Condition Monitoring of Concrete Structures.* Journal of Construction Engineering, 2013. **2013**: p. 1-11.

[5] Humphreys, M., et al., *Strategies for Minimising the Whole of Life Cycle Cost of Reinforced Concrete Brodge Exposed to Aggressive Environments.* Report, 2008: p. 1-12.

[6] Bucuresu, D., *NON- destructive measurment of Moisture in Building Materials by Compton Scattering og Gamma Rays.* 2011. **63**(1): p. 61-75.

[7] Bavusi, M., et al., *Electromagnetic Sensing Techniques for Non-Destructive Diagnosis of Civil Engineering Structures.* 2012.

ISSN 2398-6611 (Online)

Franziska Honegger Towards an optimal FM Communication in Swiss Hospitals - the Development of a Communication Framework

Author: Franziska C. Honegger
Faculty of Engineering and Technology
E-mail address: F.C.Honegger@2014.ljmu.ac.uk

Abstract The research deals with facility management in hospitals. Within that, communication is an important management task for an organisation to function. There are frameworks suggesting how to facilitate effective management communication. But they are very general and not particularly fitted to the needs of FM in hospital. But every hospitals FM communicates internally and externally through different channels. As there is no particular framework guiding this process there is a possible lack of effectiveness and efficiency to be tackled by evidence based research. In short: There is no yet any evidence based research focusing on FM communication in Swiss hospitals. Based that following research question is looked at: What are optimum communication procedures in terms of roles, channels and content in order to facilitate effective and efficient support services in Swiss hospitals? Hence the research aims to develop a framework guiding an optimal communication in Swiss hospitals' FM departments. The framework incorporates evidence-based information on the appropriate use of different communication channels, states responsibilities of different roles and points out relevant content to be processed in order to facilitate an effective and efficient FM. The framework is applicable to FM departments in Swiss hospitals. Currently, after three year of part time research, the theoretical framework is shaped and the first part of the field work (qualitative data collection) took place.

Keywords. Facility management, Healthcare, Hospitals, Communication

1. Introduction

1.1 Research Context - What is FM in hospitals?

Healthcare systems, and within that hospitals, around the world are struggling with their finances. To face a tightening financial environment also Swiss hospitals need to improve their process effectiveness and efficiency. This drive for improvement not only affects hospitals' core functions of treatment and care, but also their non-medical support processes. These can be put under the umbrella of facility management (FM) (Gerber and Klauser, 2015). FM is defined as the "integration of processes within an organisation to maintain and develop the agreed services which support and improve the effectiveness of its primary activities" (CEN, 2006 p.5). The role and relevance of FM is critical as 25-40% (Abel and Lennerts, 2006, Jensen, 2008) of hospitals total costs are incurred by the various support processes.

1.2 Research Problem

Communication is an important management task for an organisation to function. There are frameworks suggesting how to facilitate effective management communication. But they are very general and not particularly fitted to the needs of FM in hospital.

But every hospitals FM communicates internally and externally through different channels. As there is no particular framework guiding this process there is a possible lack of effectiveness and efficiency to be

tackled by evidence based research. In short: There is no yet any evidence based research focusing on FM communication in Swiss hospitals.

1.3 Research Question

Based on the apparent research problem, the following research question was proposed:

What are optimum communication procedures in terms of roles, channels and content in order to facilitate effective and efficient support services in Swiss hospitals?

1.4 Research Aim & Objectives

To answer the research question, the following aim is devised:

To develop a framework guiding an optimal communication in Swiss hospitals' FM departments.

The framework incorporates evidence based information on the appropriate use of different communication channels, states responsibilities of different roles and points out relevant content to be processed in order to facilitate an effective and efficient FM. The framework is applicable to FM departments in Swiss hospitals.

The following objectives were set to operationally investigate the above aim:

A. Establish concepts to inform subsequent aims, particularely the applied research tools. Concepts are derived from the fields of healthcare and organisational theory. Focusing on FM procedures in healthcare and communication concepts within organisational theory.

B. Establish existing communication activities in hospitals FM departements. To state current communication procedures in terms of channels used, responsibilities and content. **Guiding sub-question: How does communication in hospitals FM departments look like**?

C. Develop the initial framework for optimal FM communication based on key results from objectives A and B.

D. Validate initial framework in order to ensure applicability in practice.

E. Produce evidence based communication framework supporting an optimal communication in Swiss hospitals' FM departments.

1.5 Contribution to Knowledge

This PhD research provides evidence of originality as it goes beyond the predominant generic guidelines of corporate communication by firstly combining management theory, focusing on corporate communications, with the particularities of FM in Swiss hospitals and secondly by providing tangible guidance for FM practitioners on how to apply the findings for the benefit of hospitals FM departments.

2. Methodology

A mixed methods research design

This research takes place within the field of business and management research. Because it focuses on topics relevant to business and management disciplines including economics, human resource management organisational behaviour, management strategy and operation management (Myers, 2009). This field also requires the research results to have some practical value of benefit to the business (Easterby-Smith et al., 2012), which is the strong intention of this research's objective E. As guiding

conceptual framework to develop a meticulous methodology the “research onion” of Saunders et al. (2016) was adopted. Figure 1 shows the applied methodological choices.

3. Results

Currently, after three years of part time research, the theoretical framework is shaped and the first part of the fieldwork took place. Hence partial results of objectives A and B can be presented in the short opportunity of this extended abstract.

Excerpt Objective A - Theoretical framework: The underpinning theoretical framework is extensively discussed in the thesis theoretical background. Adopting the analogy of a funnel, main threads about healthcare, and hospitals as vital parts of it, organisational theory dealing with the elements of an organisation, the particulars of FM, specifically FM in hospitals and organisational communication are neatly presented leading up to this research’s core: FM in hospitals, the role of communication. This content builds the backbone to develop the applied data collection and analysis instruments leading to objective B. And of course the theoretical framework further serves to discuss results.

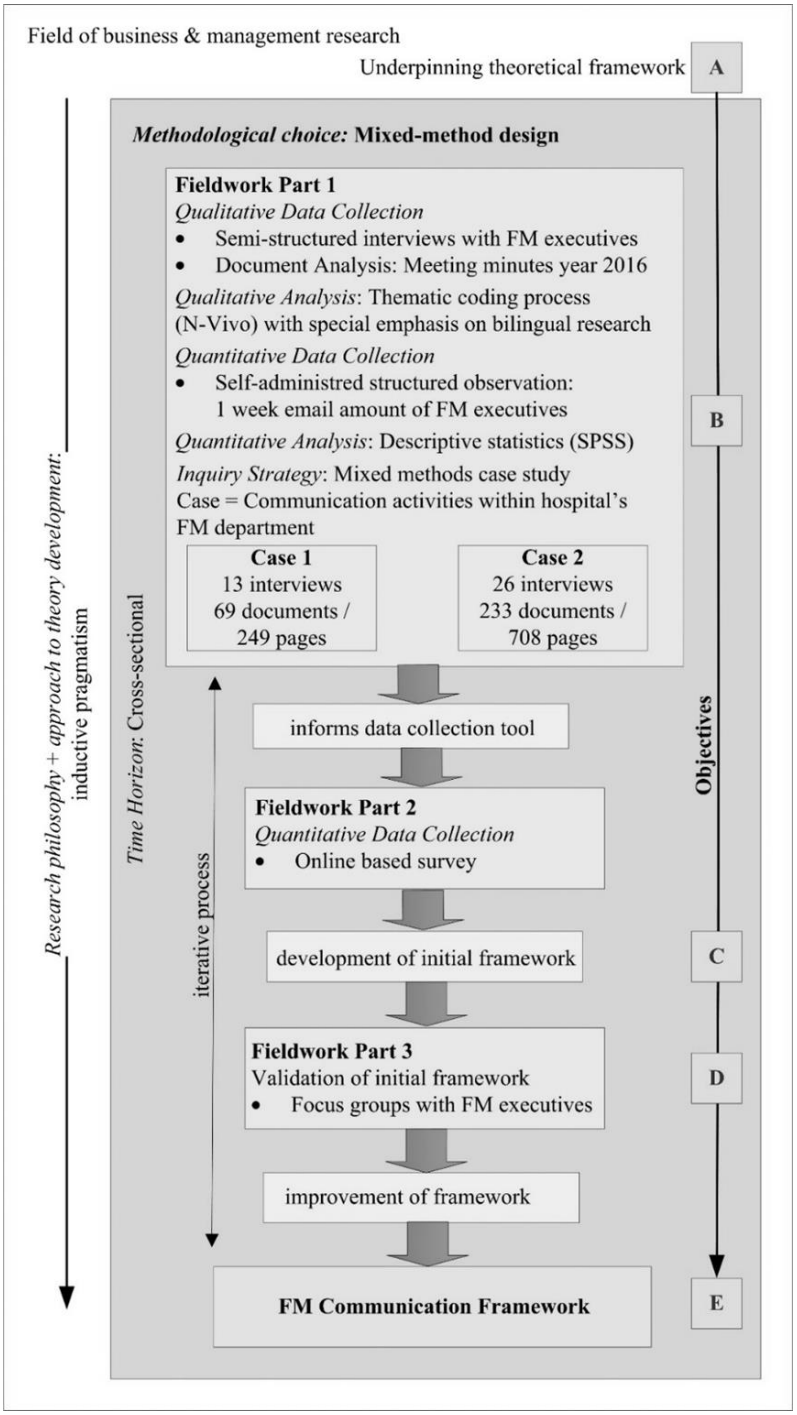

Figure 1: Overview applied methodology

Excerpt Objective - Email Communication: The commanding (Cole and Kelly, 2011) or also called directing (Miles, 2012) part of management tasks involves activities including leading, motivating and communicating with staff as individuals, groups or the organisation as a whole (Miles, 2012). The manager has five communication channels at his command: Mail (documented), telephone (purely verbal), unscheduled meeting (informal face-to-face), scheduled meeting (formal face-to-face), and tour (observational) (Mintzberg, 1971), for today email (documented) and meetings via electronic means (such as Skype) need to be added. Despite the strong adoption of interpersonal communication methods, such as instant messaging, social networking and chat, Email use continues to grow in the business world (The Radicati Group Inc., 2018). Chui et al. (2012) found that an average employee spends 13 hours a week reading and responding to email, being the most time-consuming work activity. These authors key takeaway is that Email overload is a global epidemic. According to a study (The SaneBox Gang, 2016), the average inbox contains only 38% important, relevant emails. This means 62% of the emails in the average inbox are not important and can be processed in bulk. This is alarming as Email interruptions are a drain on productivity. As Jackson et al. (2003) found that it takes an average of 64 seconds to recover from an email interruption (regardless of the email's importance) and return to work at the same work rate as before the interruption, hence is critical to batch-process unimportant emails.

The question for this research was – how many emails does a FM executive in a Swiss hospital process? The answer gave 25 executives by collected this data through a self-administered observation for a cross-sectional period of 7 days. Figure 2 displays an excerpt of the results.

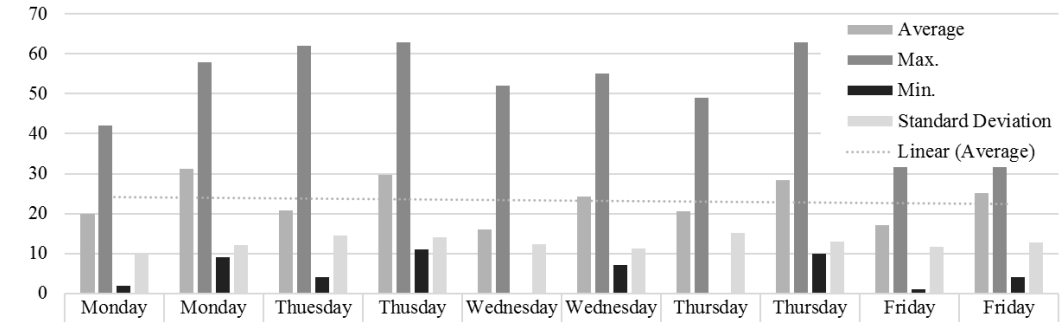

	Monday _To	Monday _From	Thuesday _To	Thusday _From	Wednesday _To	Wednesday _From	Thursday _To	Thursday _From	Friday _To	Friday _From
Average	20	31	21	30	16	24	20	28	17	25
Max.	42	58	62	63	52	55	49	63	44	54
Min.	2	9	4	11	0	7	0	10	1	4
Standard Deviation	10	12	14	14	12	11	15	13	12	13

Figure 2: Weekday email statistics of 25 FM executives in a hospital

Besides giving valuable insights by quantifying the omnipresent "email overload", these results assist in the development of the quantitative data collection instrument of the upcoming survey. They provide evidence based response categories for items such as: "How many emails are you receiving from internal senders (on average per day)?

4. Outlook

Finish this PhD thesis by continuing to investigate the research aim.

5. References

ABEL, J. & LENNERTS, K. 2006. Cost allocation for FM services in hospitals. *The Australian Hospital Engineer*, Volume 29.

CEN 2006. Facility Management – Part 4: Taxonomy, Classification and Structures in FM. Brussels: European Committee for Standardization.

CHUI, M., MANYIKA, J., J., B., DOBBS, R., ROXBURGH, C., SARRAZIN, H., SANDS, G. & WESTERGREN, M. 2012. The social economy: Unlocking value and productivity through social technologies. McKinsey Global Institute.

COLE, G. A. & KELLY, P. 2011. *Management theory and practice*, Andover : Cengage Learning, 2011.

EASTERBY-SMITH, M., THORPE, R. & JACKSON, P. 2012. *Management research*, London, SAGE.

GERBER, N. & KLAUSER, V. 2015. *Service Catalogue for Non-medical Support Services in Hospitals (LekaS) SN EN 15221-4: adapted, expanded and commented branchspecifically*. Wädenswil: Zurich University of Applied Sciences Institute of Facility Management.

JACKSON, T., DAWSON, R. & WILSON, D. 2003. The Cost of Email Interruption. Lincoln: Computer Science Department, Loughborough University.

JENSEN, P. A. 2008. *Facilities management for students and practitioners*, Lyngby, Centre for Facilities Management - Realdania Research - DTU Management Engineering, Technical University of Denmark.

MILES, J. A. 2012. *Management and Organization Theory*, Jossey Bass Ltd.

MINTZBERG, H. 1971. Managerial Work: Analysis from Observation. *Management Science*, 18**,** B97-B110.

MYERS, M. D. 2009. *Qualitative research in business & management*, Los Angeles ; London : SAGE, c2009.

SAUNDERS, M., LEWIS, P. & THORNHILL, A. 2016. *Research methods for business students*, Harlow, Essex, Pearson Education Limited.

THE RADICATI GROUP INC. 2018. Email Statistics Report, 2017-2021. Palo Alto: The Radicati Group Inc.

THE SANEBOX GANG. 2016. Email Overload: Research and Statistics Available from: https://blog.sanebox.com/2016/02/18/email-overload-research-statistics-sanebox/ [Accessed 21.1 2018

ISSN 2398-6611 (Online)

Jacob Greene Non-Invasive Monitoring of Glycogen in Real-Time Using an Electromagnetic Sensor

J Greene[1], B Abdullah[1], J Cullen[1], O Korostynska[1], J Louis[2], A Mason[3].

[1] Faculty of Engineering and Technology, BEST Research Institute, Liverpool John Moores University, Liverpool L3 3AF, UK.
[2] Faculty of Science, School of Sports and Exercise Science, Liverpool John Moores University, Liverpool L3 3AF, UK.
[3] Animalia, Norwegian Meat, and Poultry Research Centre, Oslo, Norway.
E-mail address: J.Greene2013@ljmu.ac.uk

Abstract. This work presents a novel non-invasive electromagnetic sensor operating at microwave frequencies for real-time monitoring of glycogen in-vitro, developed for forthcoming human trails. Muscle glycogen availability, through diet, is a fundamental component of an athlete's lifestyle and is a critical factor in elite performance. However, the existence of convenient non-invasive real-time measurement technique remains elusive. Glycogen from oyster mixed into a water solution was used to manipulate concentrations observed in healthy human subjects ranging from 0 - 400mmol/L. The electromagnetic sensor used frequencies between 10MHz and 4GHz, allowing an ideal range to locate any possible frequencies that match glycogens electromagnetic footprint. Data produced from the scattering parameter S_{11} identified a strong linear correlation between glycogen (mmol/L) and S_{11} (dBm), $r = 0.9$, $p = \leq 0.002$, with a $R^2 = 0.87$ at 2.110171503 GHz. This paper provides the first significant data that an electromagnetic sensor can successfully monitor change in glycogen concentration. This provides an encouraging basis for future work to create a practical non-invasive method for in-vivo detection and quantification of glycogen in human skeletal muscle. The progression of this research will be to analyse the sensor during different glycogen depletion exercise trails in human subjects.

Keywords. ***glycogen; non-invasive; electromagnetic sensors; microwave spectroscopy***

1. Introduction

1.1. Technology in Sport

In recent years, there has been an emergence of wearable technology allowing athletes, coaches, and physicians to monitor performance indicators and rudimentary biomarkers. Data previously unavailable, enables sports scientists, practitioners, and coaches a better insight into the physiological demands of their athletes, allowing for more specific training protocols, thus minimizing injury and improving performance [1, 2]. Monitoring complex biomarkers provide a difficult challenge, often requiring more invasive producers in a clinical setting. Skeletal muscle glycogen is a key indicator of athletic performance and a predictor of fatigue, despite the continued advances in technology, there remains an encompassing device that is non-invasive, continuous and accurate. The aim of this study was to analyze a novel real-time electromagnetic sensor, detecting glycogen concentration in a water solution, thus providing the necessary preliminary data needed to advance to human trails.

1.2. Glycogen and athletic performance

Professional athletes and coaches are in a constant effort to maximize performance and aid recovery through improving training protocols to ensuring optimal nutritional strategies. Carbohydrates (CHO) are an important source of fuel and energy for intense and continued bouts of exercise. Glycogen is a polysaccharide containing hundreds of glucose molecules, equating to the storage form of carbohydrates within animals. In humans, only the liver (~100g) and skeletal muscle (~400g) cells can store significant quantities of glycogen. Glycogen is one of the main energy sources for adenosine triphosphate (ATP) production, enabling muscle contraction during a wide variety of exercises, from short high-intensity exercises to longer endurance type exercises. Normal levels of muscle glycogen stores for a well-trained athlete can usually fuel sporting activity for up to 60–90 min. However, exercise intensity (energy expenditure) contributes significantly to the contribution of CHO metabolism for ATP production. Increasing CHO consumption in the days before a major endurance competition is known as "CHO loading", this super-compensates muscle and liver glycogen stores and has been common practice since the 1960s [3]. In recent years, there has been emerging acceptance that CHO availability is highly individualized and needs to be adjusted to meet the energy demands of the athlete [4]. Many scientists and coaches now are beginning to see the benefits of day-by-day and meal-by-meal manipulation of CHO availability and stepping away from the high CHO diet at all times approach. Furthermore, there is more understanding of the role CHO availability as a regulator of training adaptations and how different nutritional strategies influence performance. However, for practitioners without access to laboratories and equipment that can monitor glycogen levels non-invasively and regularly, reliance on meticulous calculating of dietary intake and energy expenditure will have to be sufficient.

1.3. The elusive gold standard - Muscle biopsies

Since the 1960s, invasive muscle biopsies have remained the gold standard method for the analysis of skeletal muscle glycogen in humans [5]. Although biopsy equipment has improved throughout the years, this procedure does have its limitations. Administration by a trained practitioner within a controlled sterile laboratory environment is needed, meaning glycogen can only be assessed before and after exercise, protocols. Athlete willingness to undergo muscle biopsies before competition and throughout the season is often hindered due to its invasive nature and the aftercare treatment required. It usually takes between 5-7 days for soreness and swelling to fully dissipate and can potentially leave small scars. Athlete monitoring in real-world settings is limited and this technique would not be used as a tool to regularly ensure optimal glycogen stores have been reached. Muscle biopsies remain the chosen method for glycogen analysis despite its drawbacks, until an alternative device is available which reaches a high standard of accuracy, allowing portable, real-time, and non-invasive assessments.

1.4. Electromagnetic Sensors as a Solution

A research team from Liverpool John Moores University have developed a novel sensing system based on electromagnetic (EM) wave technology, this technique is a rapidly developing multipurpose system that can be applied across a range of materials and industries. Previous research has highlighted that EM sensors provide a viable alternative to current industrial and medical devices due to its non-invasive and real-time nature. Recently, EM sensors have been successful in monitoring parameters in human subjects during exercise, such as monitoring blood lactate during exercise [6]. The principle of microwave spectroscopy is based on the singular interaction between the electromagnetic nodes at precise frequencies with the specific properties of the sample under examination, such as conductivity (the ability to conduct an electric current) and permittivity (the measure of how an electric field is affected by a dielectric medium) [6]. When the sensor is placed in the vicinity or direct contact with a sample, the change in the

reflected (S_{11}) and transmitted (S_{21}) microwave signals can be correlated with the composition and concentration of the material (figure 1).

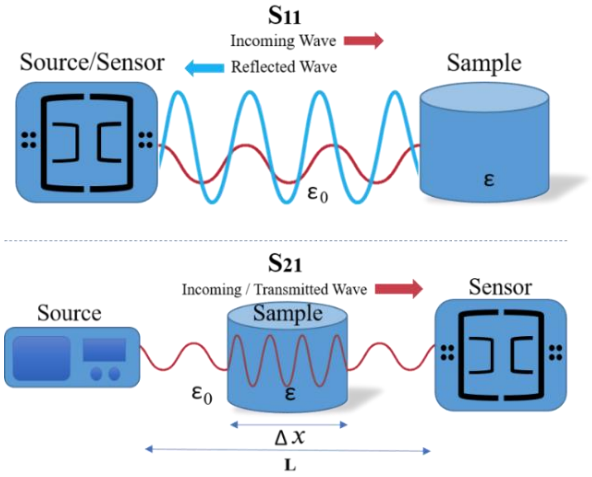

Figure 1: Schematic showing the change in the reflected (S_{11}) and transmitted (S_{21}) microwave signal, interacting with a sample determining the composition and concentration.

2. Methodology

2.1. Experimental setup:

Table 1. Measurement Specifications / Storage Conditions.

No. of Measurements	7 Samples x 5 Repetitions = 35
EM Sensor	2 Ports (S_{11}-S_{21})
Volume of Samples	200ml
Temperature	20 °C
Frequency Sweep	10MHz – 4GHz
Channel Base Power	0 dBm

2.1. Glycogen from oyster

The glycogen used in this experiment was glycogen (Sigma, G8751) from oyster (Type II). The glycogen was dissolved in water by stirring continuously for 2 hours. Glycogen concentration was as follows: 400mmol/L, 200mmol/L, 100mmol/L, 50mmol/L, 25mmol/L, 12.5mmol/L, and 0mmol/L. The glycogen concentration range was carefully selected to mimic glycogen quantities (mmol/kg w.w) in average healthy humans under varying nutritional conditions [7].

2.3. Electromagnetic sensor

The setup was supported by a Rhode and Schwarz ZVA24 Vector Network Analyzer (VNA). The electromagnetic resonance sensor used for this work has two ports allowing for the measurement of both the reflected S_{11} and transmitted S_{21}. A custom-made plastic casing was engineered to ensure no movement and allowed for precisely 200µl of glycogen to be inserted.

2.4. Statistical Analysis

Enterprise IBM SPSS 22 Statistical analysing package was used to determine the significance of the data. Pearson's correlation was used to report the S-parameters of glycogen and correlation was significant at the 0.01 level. Microsoft Excel 2013 was used for the visual interpretation of the data.

3. Results and Discussion

3.1. S_{11} Parameter.

When observing the S_{11} data, the analysis identified that there was a strong linear correlation ($R^2 = 0.87$, $p \leq 0.002$) observed between S_{11} (dB) and glycogen (mmol/L) at 2.11 GHz, shown in figure 2. However, there is notable variation shown in the data collected, this can be attributed to the measurement method being perhaps sub-optimal for collecting highly repeatable data. Nevertheless, since the in-vitro measurement of glycogen concentration was to determine whether the sensor could monitor and detect changes, the results are considered sufficient as the impetus for further in-vivo study.

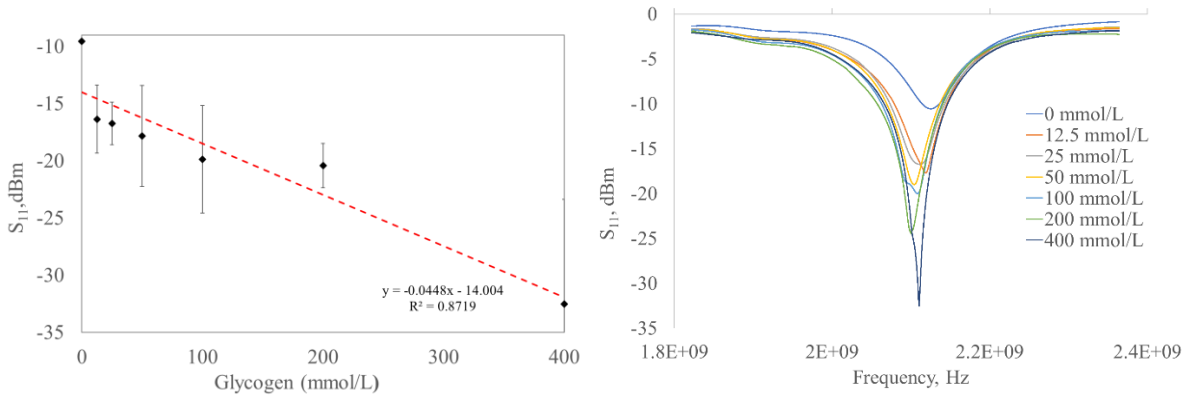

Figure 2: The linear relationship between S_{11} variations (mean ± SD) and glycogen concentrations at a 2.11 GHz (right). S_{11} signal distribution of microwave sensor between 1.8 -2.4 GHz frequency ranges under different concentrations of glycogen (mmol/L) (left).

3.2. S_{21} Parameter

In S_{21} data, variation exists at approx. 1.7 and 2.1-2.6 GHz, but correlation is poor ($R^2 < 0.5$). This outcome is not too disappointing however for two reasons: Firstly, the poor repeatability is likely attributable to the measurement method used in this experiment and secondly, 2-port measurements are viewed as less interesting than 1-port for practical reasons of cost and system complexity in the eventual effort to make the system wearable in some form.

4. Conclusion

A major benefit of a non-invasive real-time deceive is the potential monitoring of live patient information, current techniques, as noted earlier do not give enough resolution to understand whether a patient's glycogen levels are rising or falling. Consequently, providing intervention strategies can be challenging, often involving calculations of energy expenditure and dietary intake. Thus, being able to track the direction of glycogen during exercise is perhaps as important as knowing its absolute value. This study has shown that S_{11} EM wave sensors, operating at 2.11GHz, are able to detect changes in glycogen concentration. Thus, with further research, has the potential of becoming a novel approach as an alternative non-invasive method to monitor changes in glycogen levels in-vivo. This technique shows a promising future and currently leads the way in the hunt for a practical non-invasive method for the continuous monitoring of glycogen. This would solve many of the issues faced by scientists and coaches using invasive equipment, restricted to laboratory environments. However, work in this paper limited to in-vitro measurements, additional in-vivo studies will be required to enable the technique to have practical application.

5. References

[1] J. D. Bartlett, F. O'Connor, N. Pitchford, L. Torres-Ronda, and S. J. Robertson, "Relationships between internal and external training load in team-sport athletes: evidence for an individualized approach," *International journal of sports physiology and performance,* vol. 12, no. 2, pp. 230-234, 2017.

[2] B. M. Jackson, T. Polglaze, B. Dawson, T. King, and P. Peeling, "Comparing Global Positioning System (GPS) and Global Navigation Satellite System (GNSS) Measures of Team Sport Movements," *International journal of sports physiology and performance,* pp. 1-22, 2018.

[3] J. Bergström, L. Hermansen, E. Hultman, and B. Saltin, "Diet, muscle glycogen and physical performance," *Acta Physiologica Scandinavica,* vol. 71, no. 2-3, pp. 140-150, 1967.

[4] S. G. Impey *et al.*, "Fuel for the work required: A theoretical framework for carbohydrate periodization and the glycogen threshold hypothesis," *Sports Medicine,* pp. 1-18, 2018.

[5] J. Bergström, "Percutaneous needle biopsy of skeletal muscle in physiological and clinical research," *Scandinavian journal of clinical and laboratory investigation,* vol. 35, no. 7, pp. 609-616, 1975.

[6] A. Mason *et al.*, "Non-Invasive In-situ Measurement of Blood Lactate using Microwave Sensors," *IEEE Transactions on Biomedical Engineering,* 2017.

[7] J. A. Hawley, E. J. Schabort, T. D. Noakes, and S. C. Dennis, "Carbohydrate-loading and exercise performance," *Sports medicine,* vol. 24, no. 2, pp. 73-81, 1997.

ISSN 2398-6611 (Online)

Rebecca Randles The development of a methodology to measure undergraduate science student learning gain

Rebecca J Randles[1], Alison J Cotgrave[1] and David McIlroy[2]
School of Built Environment[1] and School of Natural Sciences and Psychology[2]
Liverpool John Moores University, Byrom Street Campus, Liverpool, L3 3AF
E-mail address: R.Randles@2013.ljmu.ac.uk, A.J.Cotgrave@ljmu.ac.uk and D.McIlroy@ljmu.ac.uk

Abstract. Learning gain has quickly become a topic of interest to many higher education institutions who recognise the need for better measures of Learning Gain within an English context. HEFCE have invested £4 million from 2015 to support work that began as pilot projects and lead to the national mixed methodology learning gain project. What HEFCE have failed to consider is looking at learning gain at a subject level rather than an application of one measure for all students. This research has developed a methodology to measure undergraduate science student learning gain after originally conducting interviews with STEM subjects and deciding to focus more specifically. A questionnaire was created which looked at student independent learning, engagement, critical thinking and communication. This questionnaire was validated and tested for reliability by students and members of staff. So far in this project, to test the measure, one set of data has been collected from Level 4 and 5 undergraduate science students. It is hoped that following these students across their time at the university will show a projection of the students learning gain and will be able to identify even minute changes to the chosen aspects. Ultimately, this measure could potentially be used in line with the teaching excellence framework to universities with a similar format as the one in which the measure was created.

Keywords. Learning gain, higher education, skills, university, learning outcomes

1. Background

Currently in higher education, the teaching excellence framework (TEF) has been a topic of discussion and scrutiny (BIS 2015; Parker, Cleaver, and El-Hakim 2016; Raban and Cairns 2015). Recently, learning gain has been added as one of the metrics, this is interconnected with student learning outcomes with a small difference (HEFCE 2016). Learning gain is defined as the 'distance travelled' by a student in their skills, competencies or personal development whereas learning outcomes is defined as the 'output' from the students degree (McGrath et al. 2015). The Higher Education Funding council for England conducted pilot projects into learning gain using a wide range of measures and methodologies (HEFCE 2017). Some of these measures included standardised tests that are already being utilised in the United States (US) (HEFCE 2017).

In the US, learning gain metrics are much more established. Randles and Cotgrave (2017) conducted a literature review on the current measures in the US and concluded that it is difficult to determine which measures would work within an English higher education context. This may be due to the differences in

US and English education; whilst the US degree system allows students to study more than one subject, the English system focuses on one specific discipline (Bishop 2016). This may mean that the skills which are gained are much more specialised to a specific discipline. This was also supported by the HEFCE pilot projects which found differences across subject disciplines (Howson 2017). Therefore, it would be beneficial to narrow down the focus of learning gain to specific subjects.

Self-reported measures are a common method of collecting student data such as the National Student Survey (NSS) and involves asking students to report on their own skills (Bowman 2010). There has been some scrutiny with these types of measures as Bowman (2010) and Porter (2013) have discussed that the problem occurs when students may report that a certain construct has improved when it has not, or may report no improvement when they have. However, Douglass, Thomson, and Zhao (2012) conducted a study which compared student grade point average (GPA) with their self-reported learning gain. It was found that higher GPA was connected to higher levels of self-reported learning gain, suggesting students are accurately able to report their performance over time. Therefore, as self-reports are more efficient and cost-effective they would be a beneficial use for learning gain.

This research focused on science-based subjects, this is due to original pilot interviews with STEM subjects which found that there were differences even across STEM subjects in the way in which they discussed critical thinking and opportunities for personal development during their degree. It was expected that students would improve from time one to time two and that Level 5 students would be higher than Level 4 students.

2. Methodology

2.1. Participants

In the first phase of the questionnaire, 90 were level 4 and 67 were level 5 of 157 participants. In the second phase of the questionnaire, 54 were level 4 and 45 were level 5 of 99 participants. Table one shows the distribution of genders as well as mean and standard deviation of ages.

	Level 4 Male	**Level 4 Female**	**Level 4 Age Mean**	**Level 4 Age SD**	**Level 5 Male**	**Level 5 Female**	**Level 5 Age Mean**	**Level 5 Age SD**
Phase one	27.8%	71.1%	19.4	1.94	26.9%	73.1%	21.54	3.80
Phase two	18.5%	81.5%	21.57	4.73	26.9%	77.8%	20.98	3.56

Table one: Participant age and genders separated by Level.

The majority of participants came from Psychology (16.6% of participants phase one, 14.1% of participants phase two). However, there was a total of 20 different science-based subjects which participated in the questionnaire.

2.2. Procedure

Following from interviews with STEM students, the scope for students narrowed to science-based subjects due to the differences in the way in which the students discussed their critical thinking and aspects of their degree. As a result of these interviews; critical thinking, working with others and communication were chosen as constructs. Student engagement and independent learning were also decided to be measured as it was identified that this could be a possible variable that can affect the results of the constructs which is not a direct fault of the universities. A self-survey questionnaire was then created, it was piloted by students and was found to have high reliability (α= 0.83). It was also discussed with members of staff for validity on the constructs, generally the comments were positive but there were some which involved the changing of wording of some questions, the questionnaire was amended accordingly. The questionnaire was then distributed to science-based students via email, at this stage only level 4 and level 5 students were contacted as in the following year level 5 and 6 will be contacted to follow across the entire degree. The questionnaire contained a PIS as well as a consent page which participants had to agree to before moving onto the next page. Participants were tested at more than one point in time as changes in the constructs over time is what is of interest. This first phase was sent in November and the second phase in March. Originally, the phases were supposed to be September and January however, due to unexpected obstacles this became delayed. All data is anonymised and no data was looked at on an individual basis. The answers to each construct was averaged as the result for each level at each of the phases e.g. for critical thinking the total of all of the questions which asked about constructs of critical thinking were averaged. The results were exported and analysed using SPSS.

3. Results

3.1. Engagement

	Lv 4 Mean	***Lv 4 SD***	***Lv 5 Mean***	***Lv 5 SD***
Phase one	61.20	9.07	62.31	9.27
Phase two	60.79	9.27	62.93	12.18

Table two: Mean and Standard Deviations for phase one and two on the construct of student engagement.

Table two shows that there has been a slight decrease in level 4 student engagement from phase one (M= 61.20, SD = 9.07) and phase two (M = 60.79, SD = 9.27). This suggests that as the year has progressed the students have become less engaged with their course, this could be for a number of reasons such as increased difficulty. However, this difference was not significant ($p>.05$). This may be due to the difference being so minute. The drop for level 4 is unexpected, however qualitative data that is due to be collected should hopefully explain this outcome. With Level 5 student engagement, however, it appears there is a slight increase in student engagement from phase one (M=62.31, SD = 9.27) to phase two (M=62.93, SD = 12.18). This suggests that students may have become more engaged with their course as time has gone on. However, again, this difference is not significant ($p>.05$) which once again may be due to the small difference. There may be a more significant difference at a larger time difference. In addition, Level 5 student engagement was found to be higher than that of level 4.

3.2. Critical Thinking

	Lv 4 Mean	***Lv 4 SD***	***Lv 5 Mean***	***Lv 5 SD***
Phase one	56.81	8.19	58.34	5.62
Phase two	57.87	6.10	58.60	6.89

Table three: Mean and Standard Deviations for phase one and two on the construct of student critical thinking.

Table three shows a slight increase in level 4 student critical thinking from phase one (M=56.81, SD = 8.19) to phase two (M = 57.87, SD = 6.10). This suggests that students critical thinking is increasing with the time that they are spending on their course. Again, this difference is not significant (p>.05). In addition to this, there has also been a minute increase for level 5 students from phase one (M=58.34, SD = 5.62) to phase two (M=58.60, SD=6.89). This difference was also not significant (p>.05). Furthermore, level 5 students have found to have higher levels of critical thinking than level 4, which is expected.

3.3. Working with Others/Communication

	Lv 4 Mean	***Lv 4 SD***	***Lv 5 Mean***	***Lv 5 SD***
Phase one	54.99	8.19	58.29	7.96
Phase two	55.61	9.17	59.15	8.94

Table four: Mean and Standard Deviations for phase one and two on the construct of Working with others and communication.

Table four shows an increase in level 4 student communication from phase one (M=54.99, SD = 8.19) to phase two (M=55.61, SD=9.17). This was also the same for level 5 from phase one (M=58.29, SD =7.96) to phase two (M=59.15, SD = 8.94).This increase suggests that participants are improving on their communication skills and engaging more with others as the year goes on. The differences between phase one and two for level 5 students was not significant (p>.05). Which was also the same for level 4. In addition, there was also a large increase from level 4 to level 5 in communication.

3.4. Conclusions/Discussion

The results of this study indicate that although there has been slight changes on these constructs, the changes may not be big enough to be significant. This shows that further phases are needed in order to see if there are significant changes. In addition to this, qualitative data is needed, particularly to explain the drop in level 4 engagement and to hopefully validate what the findings suggest. This is currently being collected and will be used to explain any changes that occur on these constructs. There is also the idea that perhaps the results should be controlled for by engagement as this may be a reason for any changes. There will be four more phases that data will be collected including one more in the current academic year and three across a second year following students into level 5 and level 6.

5. References

BIS. 2015. *Green Paper - Fulfilling our Potential: Teaching Excellence, Social Mobility and Student Choice*: Department for Business Innovation and Skills.

Bishop, Laura. 2016. "Another country: the trans-Atlantic alliance and the benefits of studying abroad in the USA." *Innovations in Practice* 10 (1).

Bowman, Nicholas A. 2010. "Can 1st-Year College Students Accurately Report Their Learning and Development?" *American Educational Research Journal* 47 (2).

Douglass, John, Gregg Thomson, and Chun-Mei Zhao. 2012. "The learning outcomes race: the value of self-reported gains in large research universities." In, 317-35. Springer Science & Business Media B.V.

HEFCE. April 2017. "Learning Gain." http://www.hefce.ac.uk/lt/lg/.

———. 2017. Learning gain – Pilot Projects Event. Paper presented at the Learning Gain Conference, London.

Howson, Camille B. Kandiko. 2017. "Evaluation of HEFCE's Learning Gain Pilot Projects: Year 1 Report." In, edited by Higher Education Funding Council for England.

McGrath, Cecile Hoareau, Benoit Guerin, Emma Harte, Michael Frearson, and Catriona Manville. 2015. "Learning Gain in Higher Education." In. Cambridge, UK: RAND.

Parker, Pam, Elizabeth Cleaver, and Yaz El-Hakim. 2016. "Reflections on the Teaching Excellence Framework." *Educational Developments* 16 (4).

Porter, Stephen R. 2013. "Self-Reported Learning Gains: A Theory and Test of College Student Survey Response." *Res High Educ* 54 (201–226).

Raban, Colin , and David Cairns. 2015. "Where do we go from here?" *Perspectives: Policy and Practice in Higher Education* 19 (4):107–15.

Randles, Rebecca, and Alison Cotgrave. 2017. "Measuring student learning gain: a review of transatlantic measurements of assessments in higher education." *Innovations in Practice* 11 (1):50-9.

ISSN 2398-6611 (Online)

Terry Allen Petri Nets: a novel predictive approach to in silico analysis of developmental effects of thyroid hormone metabolism in humans.

Terry Allen[1*], Richard Currie[2], Louise Dyson[3], Steve Webb[1]
[1]Dept. of Applied Mathematics, Liverpool John Moores University. [2]Syngenta UK Ltd. [3]Mathematics Institute, University of Warwick

* t.j.allen@2016.ljmu.ac.uk | http://bit.ly/webblabuk

Abstract. Thyroid hormone (TH) metabolism regulates nervous system development, and altered TH levels during critical periods of development result in adverse outcomes in the human foetus. Exogenous compounds exert thyroid effects through a variety of mechanisms such as disruption of hormone balance and result in TH metabolism dysfunction. This dysfunction can contribute to childhood neurological impairments, and understanding whether exogenous chemicals are able to exacerbate these effects has implications both for clinical practice and public health. My research focuses on *in silico* modelling of TH balance in the mother and foetus using physiologically-based pharmacokinetics (PBPK) to develop a multi-compartment model that covers key developmental stages of the human foetus when critical neurodevelopmental effects of the TH metabolic network are occurring. The current model is formulated using an extension of graph theory called Petri Nets (PN) to create a novel approach to investigating metabolic networks, thus avoiding the financial and ethical considerations associated with *in vitro*/*in vivo* techniques. My model utilises a hybrid of deterministic and stochastic methods to quantitatively model the concurrent processes involved. This approach has already shown promise in providing key input to the OECD's efforts in making better use of increased knowledge of how chemicals induce adverse effects through Adverse Outcome Pathways.

1. Introduction

Thyroid hormones (TH) are essential for the control of metabolism and nervous system development, and altered TH levels during critical periods of development result in adverse outcomes in the human foetus[1, 2]. Exogenous compounds exert thyroid effects through a variety of mechanisms such as disruption of hormone balance and result in TH metabolism dysfunction. This dysfunction can contribute to childhood neurological impairments such as mental retardation, hearing loss and brain development in humans[3], and understanding whether exogenous chemicals are able to exacerbate these effects has implications both for clinical practice and public health.

All environmental pollutants, pharmaceuticals, crop protection and industrial chemicals go through a battery of tests, many of which involve animals, to assess their potential for inducing adverse effects in humans and the environment[4]. A frequent finding is that many of these chemicals cause the induction of phase II xenobiotic metabolism, whereby these compounds are conjugated with other molecules to allow their clearance from the body. This picture becomes more complicated, however, given that Phase II metabolism is involved in the clearance of the endogenous thyroid hormones triiodothyronine (T3) and its prohormone, thyroxine (T4)[5].

2. Rationale

Life-long exposure to a vast mixture of chemicals even in low doses, which can be cumulative for persistent chemicals, and the large physiological range of thyroid hormones in humans, results in a large variation of measurements of hormone levels and enzymatic activities between individuals. Animal studies can be extremely expensive both financially and in terms of time taken to obtain data, not to mention the ethical considerations and public resistance. This, along with ethical considerations of using pregnant human test subjects makes studies of thyroid hormone metabolism in human populations very difficult. *In silico* methods, such as those pursued in my PhD, especially fully parameterised models, afford progress to be made in tackling these questions whilst avoiding the constraints.

3. Research Gap

A fully parametrised mother-foetal *in silico* model has not been established in the literature. One area in which there has been some mathematical progress is in pharmacokinetic (PK) modelling. PK modelling explores the transport of drugs through different areas of the body focussing on absorption, distribution, metabolism and excretion of the compound being examined. PK models would allow us to explore the kinetics of T3/T4 interaction throughout the body and observe how these hormones are distributed and absorbed in the different areas of interest.

Two recent PK models of T3 and T4 metabolism are from Eisenberg *et al*[6] and McLanahan *et al*[7]. Eisenberg *et al* have created a multi-compartment model that aims to link the brain and thyroid together. They model the HPT axis as a series of fast and slow compartments and use simple transport mechanisms between the HPT axis and the brain submodel to monitor T3 and T4 levels over time. Though lacking a liver compartment, which is required for our desired outcomes, this model is a good starting point for our work. McLanahan *et al* modelled the distribution of iodide, (an essential component of T3 and T4), Thyroid Stimulating Hormone, T3 and T4 throughout the body as 4 separate compartments, each with their own volume of distribution and also included liver blood and tissue compartments for each of the hormones. The work carried out by them also provides a good basis for our model and will help us parameterise any PK model we produce.

4. Biology

My research focuses on *in silico* modelling of TH balance (or *homeostasis*) in the mother and foetus using physiologically-based pharmacokinetics (PBPK) to develop a multi-compartment model representing organs that covers key developmental stages of the human foetus when critical neurodevelopmental effects of the TH metabolic network are occurring. Thyroid hormone homeostasis is maintained through a negative feedback system involving the hypothalamus, pituitary and thyroid glands (HPT axis). After being secreted by the thyroid gland in a 10:1 ratio respectively, the free concentration of T4 and T3 tend to be low because they are mostly bound to thyroxine-binding globulin, transthyretin or albumin. Rats, in comparison, do not have thyroxine-binding globulins and consequently free concentrations are higher, metabolism is faster and the thyroid system is more active than humans, making them less than ideal models for studying human thyroid hormone-dependent developmental toxicities[8]. In addition, the iodothyronine deiodinase enzymes, of which there are three types (D1, D2 & D3) are expressed at different levels in rat than in human[9]. These enzymes are essential for the biological activation and deactivation of T3 and T4. In the brain, D2 deiodinates (removes an iodine atom) T4 to the active form of the hormone, T3.

T4 and T3 can cross cell membranes, however they can also be transported across the blood-brain barrier via transport proteins[5]. After being activated by the D2 deiodinase enzyme, T3 binds to thyroid hormone receptors, which then alters gene expression and produces a biological response[10]. Most T3 is produced intracellularly from T4 by the action of D2. The D2 deiodinase is regulated by ubiquitination, which is stimulated by the presence of the T4 substrate. T4 and T3 act on the pituitary gland and hypothalamus to negatively regulate the production of thyroid stimulating hormone (TSH) and thyrotropin releasing hormone, respectively; hormones essential for the synthesis and secretion of T4 and T3 from the thyroid gland. In the liver, T3 and T4 can be metabolised to inactive forms by D1 and D3 and can also be conjugated by a number of uridine 5'-diphospho-glucuronosyltransferases (UGTs) and sulfotransferases (SULTs) to increase clearance into the bile.

5. **Model**

My model utilises a hybrid of deterministic and stochastic methods to quantitatively model the concurrent processes involved. This approach has already shown promise in providing key input to the OECD's efforts in making better use of increased knowledge of how chemicals induce adverse effects through Adverse Outcome Pathways[11]. The current model is formulated using Ordinary Differential Equations (ODEs) to describe the chemical kinetics of the reactants involved, with Michaelis-Menten terms for enzymatic reactions. A complementary approach being pursued is that of Petri Nets (PN)[12] to create a novel approach to investigating metabolic networks, thus avoiding the financial and ethical considerations associated with *in vitro* and *in vivo* techniques. PNs are parameter agnostic in that they are concerned solely with network connections, and not the values of the parameters in that network.

5.1 Mathematics - Petri Nets

PNs are directed, bipartite graphs which have well defined mathematical foundations and allow the characterisation and analysis of concurrent systems such as cell signalling and metabolic networks[12]. Graph theory states that a *graph* is an object consisting of two sets called its *vertex set* and its *edge set*. The vertex set is a finite nonempty set. The edge set may be empty, but otherwise its elements are two-element subsets of the vertex set. The theory further defines a *bipartite graph* as a graph whose vertices can be divided into two disjoint and independent sets *P* and *T* ($P \cap T$) such that every edge connects a vertex in *P* to one in *T*. A *directed* bipartite graph then, such as considered in the concept of a Petri Net, has directed edges that point *from* the vertex in a pair and points *to* the second vertex in that pair, i.e. from *P* to *T*.

In the extension of Graph theory to Petri Nets, vertices are renamed *places* and edges as *arcs*. Places can hold a finite number of marks called *tokens* to show the number of times a place appears in a given configuration of the PN. The marking, m can be considered as the configuration of tokens distributed over an entire PN. Places are linked via arcs to transitions T, which are then linked to another place, the former being termed *input places* and the latter *output places*. No arc may connect two places or two transitions. Arcs can possess arc weights, w, which serve to modify the stoichiometry of the PN to direct tokens over it. A transition is said to *fire* if it is enabled, i.e. there are sufficient tokens in all of its input places and, when the transition fires, it consumes the required input tokens, and creates tokens in its output places. This therefore changes the configuration of the PN. A transition is enabled when the number of tokens in its input places are at least equal to the arc weight going from the place to the transition and can fire at any time in a stoichiometric manner. When fired, the tokens in the input places

are moved to output places via transitions according to arc weights resulting in a new marking of the net; thus simulating the stochastic nature of the metabolic system[13].
More formally, the Petri Net, N is a *4*-tuple

N = (P,T,w,m)

where:

P = a finite set of places, T = a finite set of transitions, where P and T are disjoint, $P \cap T = 0$, w = a multi-set of arcs which assign a non-negative integer weighting to that arc, m = assigns an initial number of tokens to each place.

There are several different arc types that can be used in PNs in addition to the standard arc described above. Among them is the *read arc* which is useful in modelling enabling reactions such as enzymatic catalysis whereby the arc checks for the presence of tokens without consuming them.

In this model, the stoichiometry is governed by a Gillespie Algorithm.
The Gillespie Algorithm, also known as the Stochastic Simulation Algorithm (SSA), is a computer-oriented procedure for simulating the changes in the molecular populations of chemical species in a chemically reacting system. The algorithm requires the reactant molecules, typically solute molecules in a sea of many much smaller solvent molecules, to be dilute and well-mixed through- out the containing volume. In contrast to the traditional differential equations of chemical kinetics, which imposes not only those requirements but also the requirement that the molecular populations be very large, the SSA simulates the occurrence of individual reaction events in a way that properly reflects their inherent randomness. That randomness is often important for the relatively low molecular populations that commonly occur in cellular systems.

A discussion of the mathematical formalism behind PNs and their future outlook are discussed by Koch[14], with a non-applied background given by Murata *et al*[15]. An excellent review of PNs compared with ODEs as a mathematical modelling approach to biological systems is given by Ji *et al*[16]. The utility of PNs is that parameterisation is not a requirement; the PN is parameter agnostic, in that it works simply on how the network is wired. Where parameter values can be obtained, however, these can be included in the PN to produce a Hybrid Stochastic PN (HSPN), which has the advantage of being able to utilise some available values to model the system and can even use fuzzy logic[17].

Acknowledgements

I would like to thank the Biosciences and Biotechnology Research Council (**BBSRC**) for their Industrial Case Partnership with **Syngenta** for their funding of my entire PhD. I would also like to thanks Dr Steve Webb, Reader in Applied Mathematics for being the best DoS a PhD researcher could hope to have and for everything he has already taught me.

References

[1] G. R. Williams, "Neurodevelopmental and neurophysiological actions of thyroid hormone," *J. Neuroendocrinol.*, vol. 20, no. 6, pp. 784–794, Jun. 2008.

[2] L. Préau, J. B. Fini, G. Morvan-Dubois, and B. Demeneix, "Thyroid hormone signaling during early neurogenesis and its significance as a vulnerable window for endocrine disruption," *Biochim. Biophys. Acta - Gene Regul. Mech.*, vol. 1849, no. 2, pp. 112–121, Feb. 2015.

[3] M.-L. Hartoft-Nielsen, M. Boas, S. Bliddal, Å. K. Rasmussen, K. Main, and U. Feldt-Rasmussen, "Do Thyroid Disrupting Chemicals Influence Foetal Development during Pregnancy?," *J. Thyroid Res.*, vol. 2011, pp. 1–14, 2011.

[4] F. Maqbool, S. Mostafalou, H. Bahadar, and M. Abdollahi, "Review of endocrine disorders associated with environmental toxicants and possible involved mechanisms," *Life Sci.*, vol. 145, pp. 265–273, Jan. 2016.

[5] T. J. Visser, E. Kaptein, A. L. Gijzel, W. W. de Herder, T. Ebner, and B. Burchell, "Glucuronidation of thyroid hormone by human bilirubin and phenol UDP-glucuronyltransferase isoenzymes," *FEBS Lett.*, vol. 324, no. 3, pp. 358–360, Jun. 1993.

[6] M. Eisenberg, M. Samuels, J. J. DiStefano, J. J. D. Iii, J. J. DiStefano, and J. J. D. Iii, "Extensions, Validation, and Clinical Applications of a Feedback Control System Simulator of the Hypothalamo-Pituitary-Thyroid Axis," *Thyroid*, vol. 18, no. 10, pp. 1071–1085, Oct. 2008.

[7] E. D. McLanahan, M. E. Andersen, and J. W. Fisher, "A Biologically Based Dose-Response Model for Dietary Iodide and the Hypothalamic-Pituitary-Thyroid Axis in the Adult Rat: Evaluation of Iodide Deficiency," *Toxicol. Sci.*, vol. 102, no. 2, pp. 241–253, Oct. 2007.

[8] G. Morreale de Escobar, M. Obregon, and F. Escobar del Rey, "Role of thyroid hormone during early brain development," *Eur. J. Endocrinol.*, vol. 151, no. Suppl_3, pp. U25–U37, Nov. 2004.

[9] J. M. Bates, D. L. St. Germain, and V. A. Galton, "Expression profiles of the three iodothyronine deiodinases, D1, D2, and D3, in the developing rat," *Endocrinology*, vol. 140, no. 2, pp. 844–851, 1999.

[10] P. M. Yen, "Physiological and molecular basis of thyroid hormone action.," *Physiol. Rev.*, vol. 81, no. 3, pp. 1097–142, Jul. 2001.

[11] R. Benigni, C. L. Battistelli, C. Bossa, A. Giuliani, and O. Tcheremenskaia, "Endocrine Disruptors: Data-based survey of in vivo tests, predictive models and the Adverse Outcome Pathway," *Regul. Toxicol. Pharmacol.*, vol. 86, pp. 18–24, Jun. 2017.

[12] I. Koch, "Petri nets in systems biology," *Softw. Syst. Model.*, vol. 14, no. 2, pp. 703–710, May 2014.

[13] H. H. McAdams and A. Arkin, "Stochastic mechanisms in gene expression.," *Proc. Natl. Acad. Sci. U. S. A.*, vol. 94, no. 3, pp. 814–9, Feb. 1997.

[14] I. Koch, "Petri nets - A mathematical formalism to analyze chemical reaction networks," *Mol. Inform.*, vol. 29, no. 12, pp. 838–843, Dec. 2010.

[15] T. Murata, "Petri Nets: Properties, Analysis and Applications," *Proc. IEEE*, vol. 77, no. 4, pp. 541–580, Apr. 1982.

[16] Z. Ji, K. Yan, W. Li, H. Hu, and X. Zhu, "Mathematical and Computational Modeling in Complex Biological Systems," *Biomed Res. Int.*, vol. 2017, pp. 1–16, 2017.

[17] F. Liu, M. Heiner, and M. Yang, "Fuzzy Stochastic Petri Nets for Modeling Biological Systems with Uncertain Kinetic Parameters.," *PLoS One*, vol. 11, no. 2, p. e0149674, Feb. 2016.

ISSN 2398-6611 (Online)

Andrew Sneddon Mathematical modelling predicts the spatial distribution of metabolism in skin

A Sneddon[1*], C Murdoch[2], HE Colley[2], J Madden[3], S Smith[2], P Sharma[4], M Cronin[3], RJ Shipley[5], SD Webb[1]
[1] Applied Mathematics, LJMU, [2] Clinical Dentistry, University of Sheffield, [3] Pharmacy & Biomolecular Sciences, LJMU, [4] Molecular and Clinical Pharmacology, University of Liverpool, [5] Mechanical Engineering, UCL
[*] A.Sneddon@2013.LJMU.ac.uk

Abstract. The expression of RNA and protein for a number of phase 1 & 2 xenobiotic metabolizing enzymes has been demonstrated for both *ex vivo* human skin and *in vitro* tissue engineered human skin equivalents. The presence of these enzymes in the skin has great importance within the cosmetic and pharmaceutical industry as xenobiotic compounds delivered to the skin either topically or systemically may be metabolized to create active metabolites which are either beneficial or may cause toxicity. We have used mathematical models, parameterised by *in vitro* experimental data to inform the spatial distribution of metabolism in tissue-engineered skin samples. A coupled system of partial differential equations (PDE's) were developed to model the transport of compounds and metabolites through a geometry representative of engineered skin equivalents which include a number of the layers of the skin. Diffusion and metabolism were defined on values found in literature, specific to each layer. The model was then solved using COMSOL Multiphysics with boundary conditions which mimic a typical *in vitro* setup. The mathematical model was able to predict the spatial distributions of parent compound and metabolite within *in vitro* equivalents.

Keywords. Mathematical modelling, skin, metabolism, diffusion

1. Introduction

The skin is comprised of two primary layers; the dermis and the epidermis. The epidermis is the outermost layer of skin, which can be subdivided further into another 4 or 5 strata, depending from which area of the body the skin sample is taken from (1). The additional fifth strata; the stratum lucidum, is found in the palms and soles and is comprised of 3-5 layers of dead, flattened keratincocytes, filled with eleidin, an intermediate form of keratin (2). With the stratum corneum (SC) being the outermost layer, transport via the skin relies on the solute being able to pass through this layer. The SC is comprised of 6-20 flattened, interleaved, partially desiccated corneoecytes embedded in a lipid matrix which has an ordered, non-liquid like structure (3). The SC is the layer of the skin that has received the most attention within the literature, as it is the top most layer of the skin and the transfer of any xenobiotic compound via the skin therefore depends on both the ability and the time taken for a compound to penetrate this layer. Predictive

transdermal modelling was initially developed by Rothman in the early 1940's (4). Rothman showed that properties such as solubility of the chemical and critical influence of the vehicle needed to be considered. This was then progressed in the 1950's by Hadgraft and Somers who stated that solutes with a log octagonal-water partition coefficient between 1 and 3 had the best skin permeation (5). Extensive research has since been carried out since in an attempt to better model skin permeability for various chemicals.

One simple approach is to model the skin via a compartmental method. Compartment models consider the average concentration within a compartment for layers of the skin rather than the individual position in and around individual cells. Parameters for such models can then be derived via either approximations of physicochemical properties, or via in vitro experimentation where parameters are found by optimising the fit of the model to the data collected (6). Calculations for such models are simple, and follow the following structure; where the amount of mols of chemical in the skin, m_j, for compartment, j, which has adjacent comparements, i and k, the concentration change with respect to time for the given compartment is given as:

$$\frac{dm_j}{dt} = \left(k_{ij}c_i - k_{ji}c_j\right) - \left(k_{jk}c_j - k_{kj}c_k\right) \quad (1)$$

Compartmental models have been reviewed by Kelly (7), and expanded recently by Davies (6) who created a three-skin compartment model, where each of the skin layers were subdivided into 10 equal volume compartments to create a finite difference model. Despite the additional complexity, compartmental models are restricted in the fact that they over simplify the mechanisms of transdermal drug delivery. This is due to them not taking into consideration to complex skin geometry of the various layers of the skin, as well as not taking into consideration the various modes of mass transfer. This leads to estimation of average permeation properties from *in vitro* data, which inherently will contain sample variance.

A second approach is the so called "brick-and-mortar" model, where the bricks and mortar respectively represent the corneocytes and the lipid layers which surround them within the SC. Initial work was completed by Yotsuyanagi and Higuchi who created a two-phase model of a Hydrated SC (8), however, the model didn't consider lipid based diffusion as the corneocytes shape used was lamellar. This was then extended by Michaels in 1975, whereby the lipid-phase diffusion was then treated as being isotropic (8).

Several models have been produced, all with varying complexity with this framework. A more complete model was

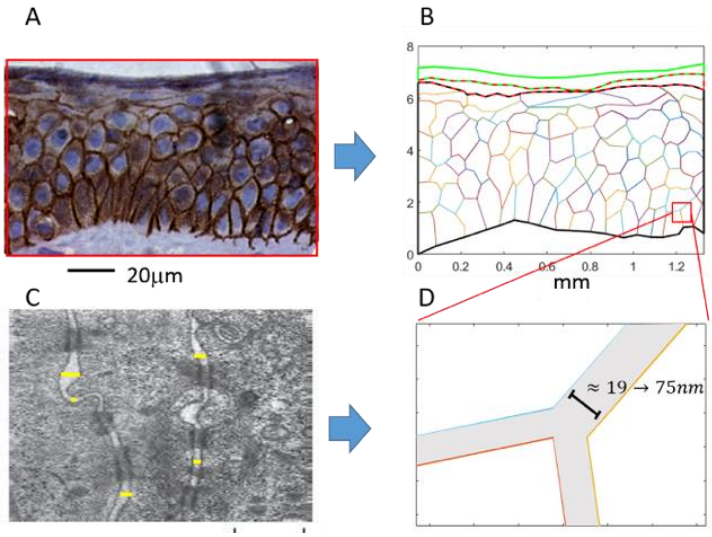

***Figure** 3 - A representation on how the geometry was created for the model*

created by Wang (3) whereby, a number of complexities were considered in order to make a more complete descriptive model of the skin physiology. An extension to this model was then published by the same author a year later with a full parameterization using experimental data (9). The improvement from this approach comes from the fact it tries to taking into account the cell and lipid matrix structure of the skin, however it doesn't taking into consideration the true, varying geometry of the skin.

2. Development of a new predictive model

Our novel approach was to take the geometry from native skin, therefore creating a realistic domain in order to predict transdermal drug delivery. Using histological images of the human skin (A), which provided the cellular arrangement for the model (B). Transmission electron microscopy was then used to obtain values for the intracellular matrix (C, D). Finally, MATLAB was used to convert the image into AutoCAD DXF format, which was then exported to COMSOL multiphysics for analysis. Figure 1 shows how the histological image was used to create a geometry.

Parameters were calculated from models within the literature and are outlined below for paracetamol (APAP) in table 1. The diffusion coefficients calculated were functions of physicochemical properties including molecular weight (MW), hydrodynamic radius and lipophilicity. A key strength of this is that it forms a predictive *in-silico* model which can be tested for any molecule whose physicochemical properties are known.

Table 1 - *The transport rates used for the model*

Layer	Author	Transport rates ($cm^2 \cdot s^{-1}$)
Strata corneum	Wang (9)	$D_{sc} = 1.3931 \cdot 10^{-11}$
Strata granulsoum	Nitsche (10)	$D_g = 8.97 \cdot 10^{-7}$
Lipid matrix	Nitsche (10)	$D_{lip} = 4.1104 \cdot 10^{-7}$
Cells	-	$D_{cells} = 3 \cdot 10^{-12}$
Transfer between cells and matrix	Crank (11)	$D_{mem} = 1.8885 \cdot 10^{-12}$
Dermis	Ramanujan (12)	$D_{derm} = 8.98 \cdot 10^{-9}$

Once the spatial distribution of the chosen xenobiotic compound was known, metabolism can be predicated with the addition of a Michaelis-Menten enzyme kinetic term, given as,

$$v = \frac{V_{max}[C]}{k_m + [C]} \qquad (2)$$

Where V_{max} is the maximum rate, k_m is the substrate concentration when the rate is half the maximum rate, and $[C]$ is the substrate concentration. Values for k_m and V_{max} were calculated from experimental data (13) and gene expression values using unconstrained multivariable minimization.

Drugs may pass into the body's systemic circulation by entering the blood via the capillaries within the dermis. Uptake can be modelling with Eq 3, given by Dancik (14) where P_{cap} is the capillary permeability estimated from the Potts-Guy permeability (P_{pg}), $P_{cap} = m \cdot P_{pg}, S$ is the capillary surface area and $Q = 22 \cdot 10^{-4} s^{-1}$ is the blood-flow limit clearance. Clearance is therefore given as,

$$K_{free} = \left[\left(P_{cap} S \right)^{-1} Q^{-1} \right]^{-1} \qquad (3)$$

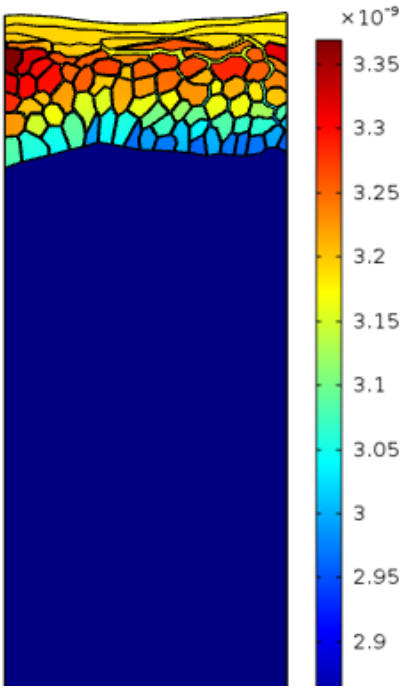

Figure 4 *– The spatial distribution of the metabolite of APAP at t=300 min, with a topical dose of* $1 \cdot 10^{-6} mol/m^3$

3. Conclusions

We were able to create a novel technique for predicting transdermal drug delivery using the geometry of native skin. This lead to time dependant solutions and predictions the spatial distribution of APAP and its metabolite *in-silico*. The model is now able to be used as a prediction tool for a wide array of compounds with transports rates being able to be predicted based on physicochemical properties. Such models have many applications across a wide range of industries as a predicative tool for many different processes. We next intend to compare predictive *in-silico* values for a number of different compounds against their *in-vivo* equivalents. We also intend to get additional geometries from native skin and compare values to other predictive methods.

4. References

1. Peck TE, Hill S. Pharmacology for Anaesthesia and Intensive CareTitle. Cambridge University Press; 2008.

2. Wilson PA, Hemmati-Brivanlou A. Induction of epidermis and inhibition of neural fate by Bmp-4. Nature. 1995 Jul;376(6538):331–3.

3. Wang T-F, Kasting GB, Nitsche JM. A Multiphase Microscopic Diffusion Model for Stratum Corneum permeability. I. Formulation, Solution, and Illustrative Results for Representative Compounds. J Pharm Sci. 2006 Mar;95(3):620–48.

4. Rothman S. The principles of percutaneous absorbsion. Clin Med. 1943;28:1305–21.

5. Hadgraft JW, Somers GF. PERCUTANEOUS ABSORPTION. J Pharm Pharmacol. 1956 Sep;8(1):625–34.

6. Davies M, Pendlington RU, Page L, Roper CS, Sanders DJ, Bourner C, et al. Determining epidermal disposition kinetics for use in an integrated nonanimal approach to skin sensitization risk assessment. Vol. 119, Toxicological Sciences. 2011. p. 308–18.

7. McCarley KD, Bunge AL. Pharmacokinetic models of dermal absorption. J Pharm Sci. 2001 Nov;90(11):1699–719.

8. Michaels AS, Chandrasekaran SK, Shaw JE. Drug permeation through human skin: Theory andinvitro experimental measurement. AIChE J. 1975 Sep;21(5):985–96.

9. Wang T-F, Kasting GB, Nitsche JM. A multiphase microscopic diffusion model for stratum corneum permeability. II. estimation of physicochemical parameters, and application to a large permeability database. J Pharm Sci. 2007 Nov;96(11):3024–51.

10. Nitsche JM, Kasting GB. A microscopic multiphase diffusion model of viable epidermis permeability. Biophys J. 2013;104(10):2307–20.

11. Crank J. The Mathematics Of Diffusion. Oxford University Press; 1975.

12. Ramanujan S, Pluen A, McKee TD, Brown EB, Boucher Y, Jain RK. Diffusion and convection in collagen gels: implications for transport in the tumor interstitium. Biophys J [Internet]. 2002;83(3):1650–60.

13. Smith S, Colley H, Sharma P, Slowik K, Sison-Young R, Sneddon A, et al. Expression and enzyme activity of Cytochrome P450 enzymes CYP3A4 and CYP3A5 in human skin and tissue engineered skin equivalents. Exp Dermatol. *In review*

14. Dancik Y, Miller MA, Jaworska J, Kasting GB. Design and performance of a spreadsheet-based model for estimating bioavailability of chemicals from dermal exposure. Adv Drug Deliv Rev. 2013;65(2):221–36.

ISSN 2398-6611 (Online)

Raul Casana Eslava Customer insights: From Fisher to Bayesian networks.

Raul V. Casaña-Eslava
Department of Applied Mathematics, 3 Byrom St. Liverpool (L3 3AF)
E-mail address: r.v.casanaeslava@ljmu.ac.uk

Abstract. The aim of this study is to segment customers into communities with similar shopping basket behaviour. This is done by finding a statistically rigorous metric for the available attributes of the model, in this case spending values by product category, which is informed by an external label representing a given indicator of relevance to the business.
A similarity metric is inferred from the posterior probability map for the external label, of which we have used loyalty. Aggregated shopping basket data is mapped into a Riemannian space using the Fisher Information metric and a Fisher Information Network (FIN) is derived using geodesic pairwise distances converted into similarity values. The Fisher metric creates a data structure that reflects the business question indicated by the class labels, by bringing closer together shopping baskets with similar outcomes of the given external label and moving apart baskets either side of classification boundaries.
Communities in this network define clusters of shopping baskets by similarity according to the metric induced by the external label. Each community is likely to have a characteristic shopping behaviour. This behaviour is characterised by a multivariate correlation model represented as Conditional Independence Map, or graphical model that reflects the statistical associations between products categories. This takes into account multiple levels of conditioning and so removes spurious associations i.e. controls for False Positives.

Keywords. Fisher Information networks, Conditional Independence maps, data structure, Euclidean embedding.

1. Introduction

This work started with the collaboration of a large UK retailer company, which shared a sample of its customer transactional data to analyse the shopping basket profiles. The main purpose of the analysis is to obtain customer insights based on customer segmentation by communities, and then obtain shopping baskets behaviours of each community. Where the communities are defined by Fisher Information Networks (FINs) [1] [2] [3], and the shopping basket behaviours are defined by Conditional Independence Maps (CI-Maps) [4].

The data consists in a sample of 30k customers based on a 3 month worth of transactional data, where customers have shopped at least 5 times. Customer transactions are categorized at product level and 5 higher hierarchical product levels: subclass, class, department, group and division. Additionally each customer contains the information of 5 external labels with multiple attributes, these labels define a discrete score of the shopper loyalty, online loyalty, life-style, life-stage and affluence. With that

information we can build a shopping basket dataset, where the observations (rows) are the customers and the features (columns) represent the aggregated transactions on each product. Instead of products we can use any other hierarchical category for decreasing the number of features.

This work analyses in detail the shopping baskets respect to the external label of loyalty, similar analysis has been carried out with the other external labels (affluence, life-style and life-stage) but the MLP obtains poor classifying performance, and consequently affects the rest of pipeline performance. Therefore we concluded the shopping baskets data only contain enough information to classify properly the loyalty labels.

Next section, 2, briefly describes the pipeline methodology, which includes the pre-processing steps and feature selection to create shopping baskets data and the algorithms to create the Fisher and Bayesian networks, section 3 shows the results with discussion. And the last section, 4, is the general conclusion.

2. Methodology

The analysis of the shopping basket is carried out by a sequence of algorithms that belong to different Machine Learning areas. The main pipeline is described as follows:

1. Data pre-processing, filtering the top 80% worth products (80/20 rule) and *log(1+X)* transformation.
2. Feature selection with CI-maps, to keep only those products associated with the external label up to second order.
3. Probability map obtained with a multilayer perceptron (MLP) classifier using distributed computing with Spark [5].
4. New metric definition based on Fisher Information, transforming the Euclidean space into a Riemannian space (distributed computing with Spark).
5. Pairwise distances manifold with All Sources Shortest Path (ASSP) algorithms. We can use Floyd-Warshall algorithm in Matlab for small datasets, or an extension of Dijkstra algorithm in Spark.
6. FIN transforming the pairwise distances into similarities, using a Gaussian kernel.
7. Community finding algorithm based on modularity optimization [6], applied over the network to select groups of similar customers in this new space.
8. Euclidean embedding of the Riemannian space to be able to apply projective methods to analyse the data with classical Multidimensional Scaling (cMDS) [7].
9. Extract the shopping profiles per community.
10. Build a Bayesian Network (BN) from a CI-Map that describes the customer behaviours of each community and models the shopping basket with a probabilistic framework.

This is complex pipeline and a detailed explanation of each point would exceed the allowed extension.

3. Main results and discussion.

In the pre-processing steps, the data is stratified by affluence labels (4 categories) in order to avoid dependences with the loyalty labels, which independence tests show both labels are dependent. The results of the different affluence subsets are similar, in this work we are going to present the analysis of the subset affluence 1.

3.1. FIN Euclidean embedding.

Following the pipeline methodology up to the FIN is obtained, we have a network based on pairwise distances with the Fisher Information metric in a Riemannian space. To visualize the structure of this network we use the cMDS algorithm to embed the FIN in a Euclidean space.

Figure 1 shows the embedded FIN using the 3 main eigenvectors, which is cigar shape distribution along the first eigenvector.

This structure reveals a lot information; the cigar shape indicates the probabilistic model is practically linear, where a logistic regression would have obtained similar results to the non-linear MLP. This effect is frequent in real noisy datasets, where linear models fit well real datasets, because of the noise and the gradual transition from one class to another. There are two main loyal distributions (labels 0 and 1) located in both extremes of the main eigenvector, where there is a progressive transition from 0 to 1. The other two labels (3 and 4) of higher loyalty present a random allocation, the reason is that its low prevalence made the MLP model ignored that observations, discriminating only the first two labels.

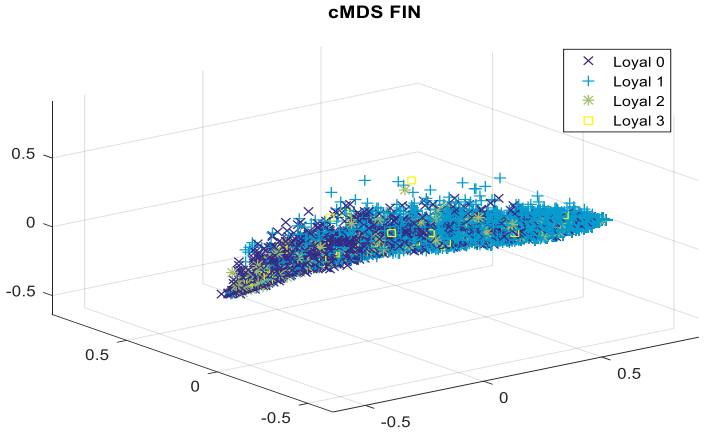

Fig. 1 cMDS of FIN with loyalty (subset AF1)

Because the embedded FIN lies practically in 1 dimension with this data, we can project all observations into the main eigenvector and analyze the labels distribution. Figure 2 shows the two main loyal distributions and the prevalence in the plot legend. Both distributions present long tails that create an intermediate region of transition where the customers do not have a clear membership.

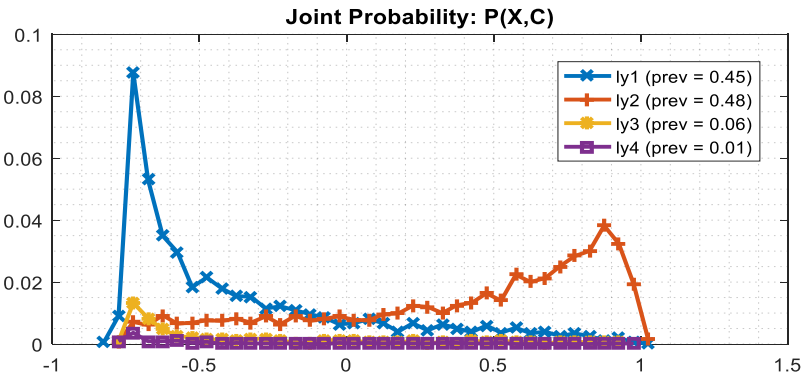

Fig. 2 Joint Probability of each loyalty class

3.2 Customer communities.

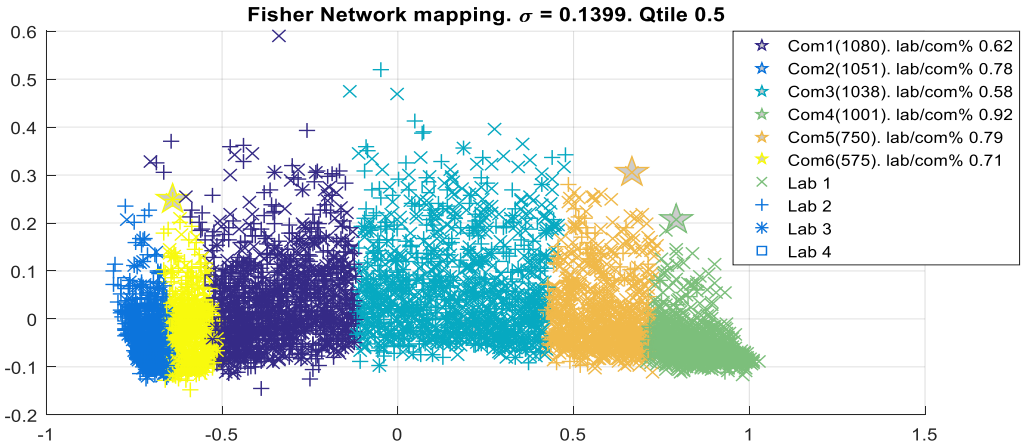

Fig. 3 Communities of the FIN with the ratio of highest loyalty label membership

Applying the community detection algorithm directly over the FIN, not the embedded FIN, we obtained 6 communities. Figure 3 shows the embedded FIN coloured by communities. Because of the linear structure, the algorithm just segmented the network into chunks because there are not real clusters or complex structures in noisy data. The communities of both extremes (com. 2 and 4) present the highest membership of a single loyalty label (78% and 92%) and they have the most marked shopping basket profile.

3.3 Bayesian networks

Figures 4 and 5 present the BN built from communities 2 and 4 which belong to the distribution extremes. The coloured class products show the most sensitive products to the shopping profiles, being the red and green ones those with less and more product worth, compared with the overall data. The class product "c10" is hub in both BNs, although each community have a different shopping basket behaviour.

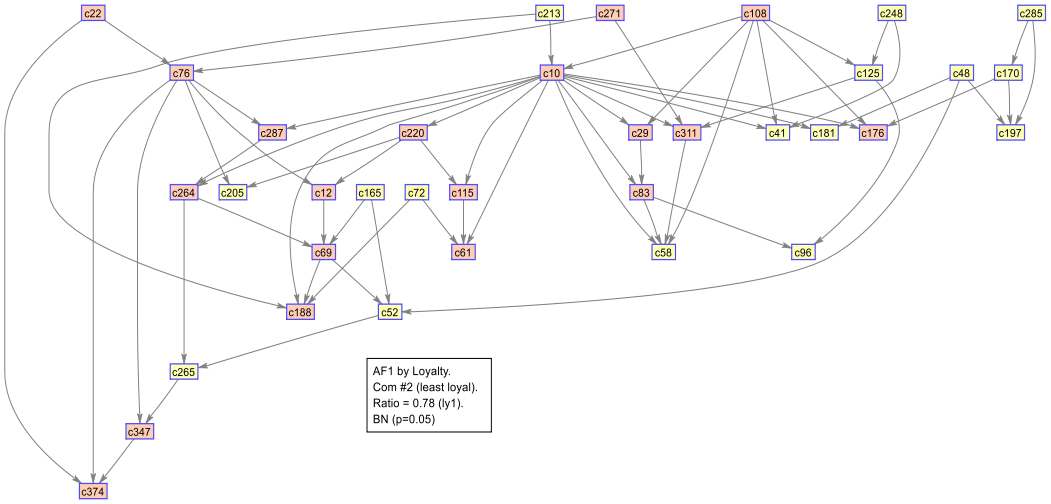

Fig. 4 BN Community #2 - least loyal (ly1)

4. Conclusion

We found that statistical models of loyalty map the data into an approximately linear space with gradual changes in the prevalence of loyalty and churn. This was found with separate models for distinct cohorts defined by the affluence label, so as to remove this attribute as a confounder for loyalty. Additionally, some communities were identified with prevalence of loyalty of 92% and churn of 78%, which is higher than the sensitivity and sensitivity of a binary classifier. The different communities are characterised by product category associations with a similar basket of products.

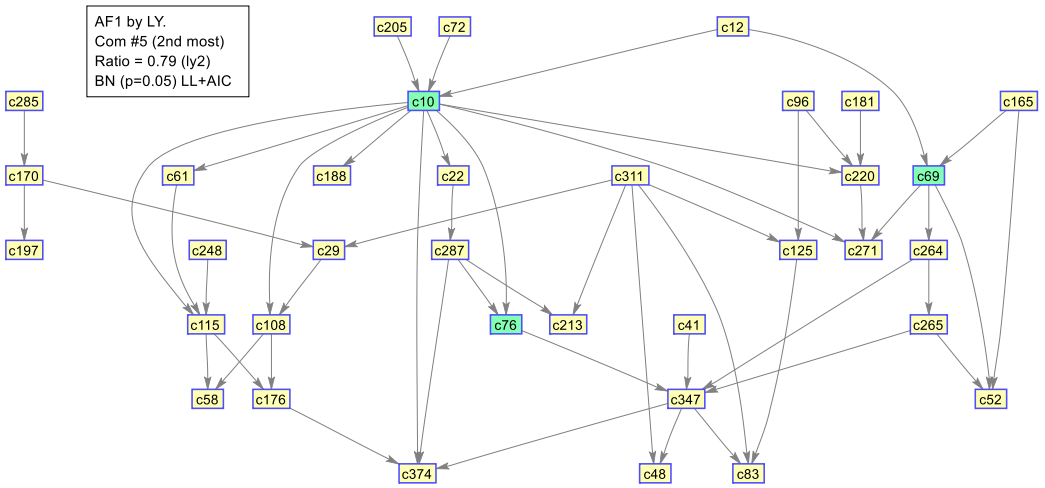

Fig. 5 BN Community #5 -2nd most loyal (ly2)

References

[1] H. Ruiz, T. A. Etchells, I. H. Jarman, J. D. Martín-Guerrero y P. J. G. Lisboa, «A principled approach to network-based classification and data representation,» *Neurocomputing*, vol. 112, pp. 79-91, 2013.

[2] H. Ruiz, I. H. Jarman, J. D. Martín-Guerrero y P. J. G. Lisboa, «The role of Fisher information in primary data space for neighbourhood mapping,» *Proceedings of the 19th European Symposium on Artificial Neural Networks, Computational Intelligence and Machine Learning*, 2011.

[3] H. Ruiz, S. Ortega-Martorell, I. H. Jarman, J. D. Martín-Guerrero y P. J. G. Lisboa, «Constructing similarity networks using the Fisher information metric.,» *Proceedings of the 20th European Symposium on Artificial Networks, Computational Intelligence and Machine Learning*, 2012.

[4] D. Bacciu, T. A. Etchells, P. J. G. Lisboa y J. Whittaker, «Efficient identification of independence networks using mutual information,» *Computational Statistics*, vol. 28, nº 2, pp. 621-646, 2013.

[5] M. Zaharia, R. S. Xin, P. Wendell, T. Das, M. Armbrust, A. Dave, X. Meng, J. Rosen, S. Venkataraman, M. J. Franklin, A. Ghodsi, J. Gonzalez, S. Shenker y I. Stoica, «Apache Spark: A Unified Engine for Big Data Processing,» *Commun. ACM*, vol. 59, nº 11, pp. 56-65, 2016.

[6] G. A. F. Seber, «Multivariate analysis of variance and covariance,» *Multivariate observations*, pp. 433-495, 1984.

[7] M. E. Newman, «Fast algorithm for detecting community structure in networks,» *Physical review E*, vol. 69, nº 6, p. 066133, 2004.

ISSN 2398-6611 (Online)

Adam Mitchinson A stochastic model of topographically influenced cell migration

AJ Mitchinson[1]*, M Pogson[2], D Conway[1], MF Murphy[3], SD Webb[1]
[1]Applied Mathematics, LJMU, [2]Quintessa Limited, [3]Pharmacy & Biomolecular Sciences, LJMU
*E-mail address: A.J.Mitchinson@2013.ljmu.ac.uk

Abstract. Cell migration is important to many physiological and pathophysiological processes, e.g. wound healing and cancer metastasis. In the absence of environmental stimuli, individual cell migration may be characterised as random motion. However, cells are known to respond to chemical and physical cues, affecting observed migratory behaviour in directed ways. For example, recent studies have shown that individual migration paths of cells alter significantly depending upon the topography of substratum travelled over – a property with significant potential for biomedical applications. Presented is a mathematical model for individual cell migration as influenced by surface topographies of substrata. The model is based on an Ornstein-Uhlenbeck process, describing the change in velocity over time of an individual particle undergoing Brownian motion. The model has been extended to account for cell responses to surface gradients. Numerical simulations produce individual cell paths with average properties comparable to that measured from experimental observations of LL24 human lung fibroblasts migrating over a flat substratum. The model is solved for three patterned substrata with significant topographical features and fit to experimental observations of LL24 human lung fibroblasts migrating over the actual substrata. The model will be useful in testing candidate substrate topographies and predicting experimental outcomes through simulation.

Keywords. Mathematical modelling, cell migration, surface topography, tissue engineering

1. Introduction

Cell migration refers to the translocation of individual or multiple biological cells (1). It plays a critical role in many physiological processes, such as morphogenesis (2) (embryonic tissue development), immune responses (1) and wound healing (1); as well as pathophysiological processes such as cancer metastasis (3) (the spreading of cancerous cells away from the original tumour site into the circulatory system and subsequently other physiological structures).
Cells are known to respond and react to various features of their surrounding microenvironment, with changes in behaviour resulting. *In vitro* studies show the migration paths of cells directionally alter when in the presence of soluble chemical gradients (chemotaxis) (4), adhesion gradients (haptotaxis) (5), mechanical gradients (durotaxis) (6) and electrical gradients (galvanotaxis) (7). *In vivo* it is thought that cells experience many of these sources of directed motion within the extracellular matrix (ECM), a

complex lattice-like structure of supporting, cross-linked and interweaving protein fibres that supports much cell migration within tissue (8).
Among the many physical cues to which cells respond *in vivo* is the varied topography presented by protein fibres within the ECM (8). *In vitro* studies show that the topography of substrata directionally affects the migration paths of cells. For example, studies focusing on migration upon micro grooved topographies have shown fibroblasts (9,10), neurons (11), endothelial (9), epithelial (12) and smooth muscle cells (9) migrate along the surface grooves in a way that is directionally consistent with the orientation of the grooves. On lattice topographies, cells have been shown to migrate preferentially along the long sides of rectangular grids (13). Micro pillars and wells have also been shown to affect the migration paths of cells (8).
Cell response to various topographies as just described has potential applications in biomedicine. Research has shown topographies to prompt stem cell differentiation (14), a tool that could potentially have significant applications in the bioengineering of tissue.
Other studies have also used topographies to help guide the growth of neurites in nerve conduits following spinal cord injury (15).

Not much is known about the underlying mechanism responsible for controlling the migratory behaviour of cells. The presented work aims to capture the major features of this biological process in a mathematical model in an attempt to elucidate some of the existing mechanisms at work during this type of cell migration.

2. Model development

A general model of this particular type of directed cell migration is currently novel in the literature. Once fit to experimental data, the model could be used for *in silico* testing of how various simulated topographies affect cell migration, without the need for *in vitro* experiments.

The Ornstein-Uhlenbeck (OU) process enables us to model the migration paths of individual cells. Originally developed to model the paths of diffusing Brownian particles, the OU process was later proposed as a general model of random cell migration (16) and extended to model chemotaxis (17) and durotaxis (18). This modelling approach allows us to view each cell as a point (representing a centroid of cell area) that moves in response to a topography without the need to consider morphology or intracellular signalling, isolating the process of migration.

As a model of cell migration, the OU process describes the time evolution of a cell's velocity using a stochastic differential equation with two components: a deterministic mean-reverting term – modelling any resistance to motion experienced by the cell, and a stochastic term – modelling any random accelerations made by the cell.

It is possible to directionally bias the OU process with the addition of a vector term indicating a direction of interest. Stokes et al,199 used a similar approach to model the directional bias observed during the chemotaxis of endothelial cells (17). An OU process with additional bias term is given by equation 1, where $\tilde{\Psi}(t)$ contains a direction vector of interest.

$$d\tilde{v}(t) = -\beta\tilde{v}(t)dt + \sqrt{\alpha}d\widetilde{W} + \widetilde{\Psi}(t)dt \quad (1)$$

Position of the cell can be found using the integration given by equation 2.

$$\tilde{x}(t) = \int_0^t \tilde{v}(t')dt' \quad (2)$$

It is possible to calculate the integration in equation 2 using exact numerical methods published by Gillespie, 1996 (19); a work in which Gillespie used the statistical properties of the OU process to derive exact updating formulas that produce an exact simulation of an OU process (shown in figure 1).

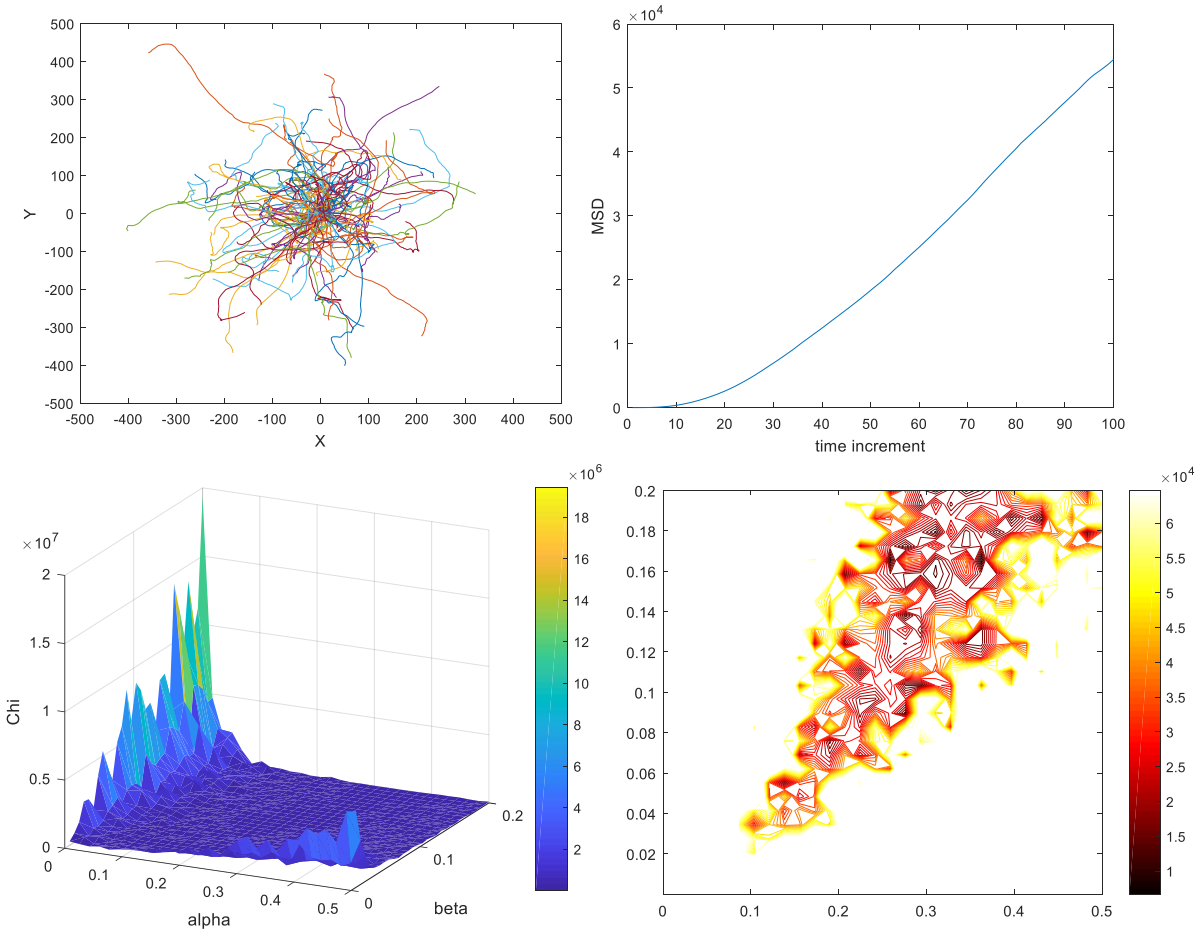

Figure 1 *– top left: 100 realisations of the OU process provide a model for individual cell migration paths; top right: mean-squared displacement (MSD) of 100 cells over time; bottom left: error surface with parameters α and β varied over ranges; bottom right: relationship between α (x-axis) and β (y-axis) at the lowest error values.*

Experimental observations in the literature (9,10,12,13) show a tendency for cells to avoid steep surface gradients. To construct a bias term for migrating cells over different topographies, a simplifying

assumption is made that cells will favour a direction orthogonal to steep surface gradients (a contour direction).

The geometry of the developed topographic bias term is shown in figure 2. Vector $\underline{\nabla \mathbf{s}}$ is the direction of steepest gradient at that specific time increment, $\underline{\mathbf{c}}$ is contour direction 1, $\underline{\mathbf{c}'}$ is contour direction 2 and $\underline{\mathbf{v}}$ is current cell velocity. The angle ϕ denotes angle between contour direction $\underline{\mathbf{c}}$ and cell velocity $\underline{\mathbf{v}}$, with $0 \leq \phi \leq \pi$.

If $0 \leq \phi < \frac{\pi}{2}$ direction $\underline{\mathbf{c}}$ is favoured, if $\frac{\pi}{2} < \phi \leq \pi$ direction $\underline{\mathbf{c}'}$ is favoured and if $\phi = \frac{\pi}{2}$ direction $\underline{\mathbf{c}}$ or $\underline{\mathbf{c}'}$ is favoured with equal probability.

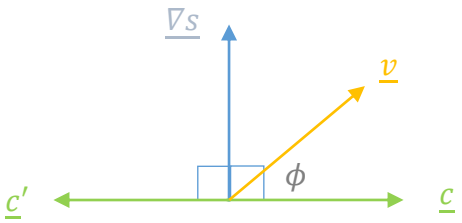

Figure 2 *– geometry of topographic bias term.*

The bias term is described by equation 3, where $\underline{\mathbf{C}}$ is the favoured contour direction dependent on angle ϕ, this term strongly weights a new cell velocity away from direction $\underline{\nabla \mathbf{s}}$ when angle $\phi = \frac{\pi}{2}$.

$$\tilde{\Psi}(t) = \kappa \underline{\boldsymbol{C}} sin|\phi| \tag{3}$$

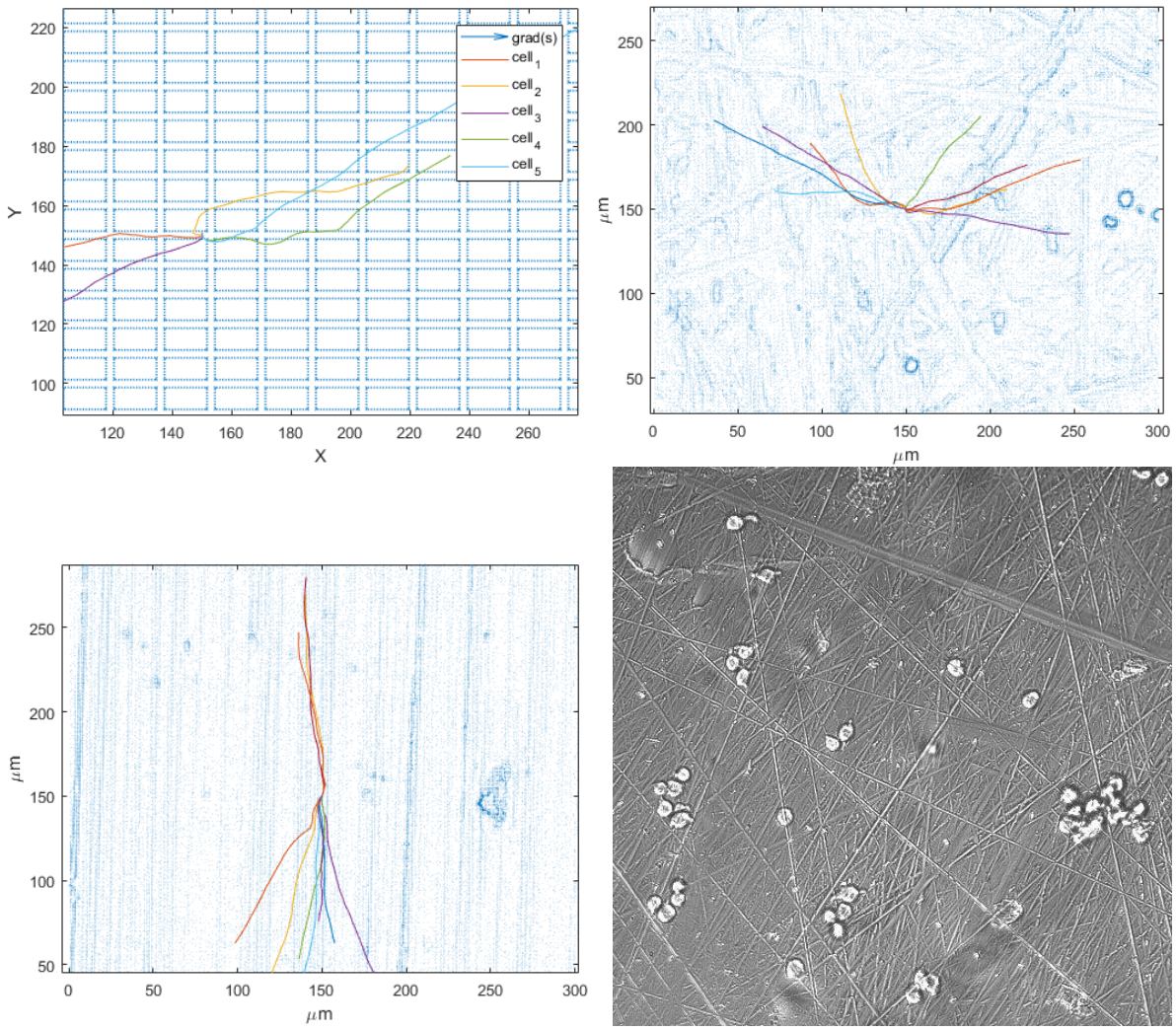

Figure 3 *– top left: simulated paths of individual cells migrating over an in silico produced lattice geometry; top right: migration over a substrate with random topographical features; bottom left: migration over a substrate with linear features; bottom right: in vitro experimental data of LL24 fibroblasts migrating over a random topography.*

To test the model and obtain more realistic simulations and predictions, the model will be parameterised using experimental *in vitro* data of LL24 (human lung fibroblast) cells migrating over different surfaces, captured as time-lapse images using a Zeiss LSM confocal microscope.

The approach was to extract the same metrics from the time-lapse images and from the simulations, obtain a measure of error (Chi) between experimental and simulated metrics and aim to minimise this error measurement using a Nelder-Mead optimisation.

Metrics of choice include mean-squared displacement, tortuosity and turn angle.

Metric extraction involved tracking of individual cell paths. Selected automated softwares were trialled, with some promising results particularly using the recently developed 'TrackMate' (20), however

ultimately results were too inconsistent for use. Cell and particle tracking appears still to be an active area of research. Instead, tracking was done manually.
Preliminary data fitting has been carried out for the flat surface, as can be seen in figure 1, with an error surface resulting from parameter value variation for α and β. The bottom right plot in figure 1 shows an interesting relationship between α and β for the smallest error values.

3. Conclusions

Surface topographies have been shown to affect cell migration in different ways, a cell behaviour that is currently the subject of exciting biomedical research. The developed model reproduces individual migration paths of cells as influenced by surface topographies, fitted to *in vitro* data of LL24 fibroblasts migrating over different surfaces. The model is capable of *in silico* simulation of cells migrating over a variety of topographies and predicting migratory behaviours over sample topographies with untested geometries. Future work will focus on using model simulations to extrapolate further understanding of this important biological process.

4. References

[1] Ananthakrishnan, R. and Ehrlicher, A., 2007. The forces behind cell movement. *International journal of biological sciences*, *3*(5), p.303.
[2] Aman, A. and Piotrowski, T., 2010. Cell migration during morphogenesis. *Developmental biology*, *341*(1), pp.20-33.
[3] Lauffenburger, D.A. and Horwitz, A.F., 1996. Cell migration: a physically integrated molecular process. *Cell*, *84*(3), pp.359-369.
[4] Zigmond, S.H. and Hirsch, J.G., 1973. Leukocyte locomotion and chemotaxis: new methods for evaluation, and demonstration of a cell-derived chemotactic factor. *Journal of Experimental Medicine*, *137*(2), pp.387-410.
[5] Carter, S.B., 1967. Haptotaxis and the mechanism of cell motility. *Nature*, *213*(5073), p.256.
[6] Lo, C.M., Wang, H.B., Dembo, M. and Wang, Y.L., 2000. Cell movement is guided by the rigidity of the substrate. *Biophysical journal*, *79*(1), pp.144-152.
[7] Zhao, M., 2009, August. Electrical fields in wound healing—an overriding signal that directs cell migration. In *Seminars in cell & developmental biology* (Vol. 20, No. 6, pp. 674-682). Academic Press.
[8] Nikkhah, M., Edalat, F., Manoucheri, S. and Khademhosseini, A., 2012. Engineering microscale topographies to control the cell–substrate interface. *Biomaterials*, *33*(21), pp.5230-5246.
[9] Biela, S.A., Su, Y., Spatz, J.P. and Kemkemer, R., 2009. Different sensitivity of human endothelial cells, smooth muscle cells and fibroblasts to topography in the nano–micro range. *Acta biomaterialia*, *5*(7), pp.2460-2466.
[10] Irving, M., Murphy, M.F., Lilley, F., French, P.W., Burton, D.R., Dixon, S. and Sharp, M.C., 2017. The use of abrasive polishing and laser processing for developing polyurethane surfaces for controlling fibroblast cell behaviour. *Materials Science and Engineering: C*, *71*, pp.690-697.
[11] Gomez, N., Chen, S. and Schmidt, C.E., 2007. Polarization of hippocampal neurons with competitive surface stimuli: contact guidance cues are preferred over chemical ligands. *Journal of The Royal Society Interface*, *4*(13), pp.223-233.
[12] Dalton, B.A., Walboomers, X.F., Dziegielewski, M., Evans, M.D., Taylor, S., Jansen, J.A. and Steele, J.G., 2001. Modulation of epithelial tissue and cell migration by microgrooves. *Journal of Biomedical Materials Research: An Official Journal of The Society for Biomaterials, The Japanese Society for Biomaterials, and The Australian Society for Biomaterials and the Korean Society for Biomaterials*, *56*(2), pp.195-207.
[13] Mai, J., Sun, C., Li, S. and Zhang, X., 2007. A microfabricated platform probing cytoskeleton dynamics using multidirectional topographical cues. *Biomedical microdevices*, *9*(4), pp.523-531.

[14] Seo, C.H., Furukawa, K., Montagne, K., Jeong, H. and Ushida, T., 2011. The effect of substrate microtopography on focal adhesion maturation and actin organization via the RhoA/ROCK pathway. *Biomaterials*, *32*(36), pp.9568-9575.
[15] Krych, A.J., Rooney, G.E., Chen, B., Schermerhorn, T.C., Ameenuddin, S., Gross, L., Moore, M.J., Currier, B.L., Spinner, R.J., Friedman, J.A. and Yaszemski, M.J., 2009. Relationship between scaffold channel diameter and number of regenerating axons in the transected rat spinal cord. *Acta biomaterialia*, *5*(7), pp.2551-2559.
[16] Dunn, G.A. and Brown, A.F., 1987. A unified approach to analysing cell motility. *J Cell Sci*, *1987*(Supplement 8), pp.81-102.
[17] Stokes, C.L., Lauffenburger, D.A. and Williams, S.K., 1991. Migration of individual microvessel endothelial cells: stochastic model and parameter measurement. *Journal of cell science*, *99*(2), pp.419-430.
[18] Stefanoni, F., Ventre, M., Mollica, F. and Netti, P.A., 2011. A numerical model for durotaxis. *Journal of theoretical biology*, *280*(1), pp.150-158.
[19] Gillespie, D.T., 1996. Exact numerical simulation of the Ornstein-Uhlenbeck process and its integral. *Physical review E*, *54*(2), p.2084.
[20] Tinevez, J.Y., Perry, N., Schindelin, J., Hoopes, G.M., Reynolds, G.D., Laplantine, E., Bednarek, S.Y., Shorte, S.L. and Eliceiri, K.W., 2017. TrackMate: An open and extensible platform for single-particle tracking. *Methods*, *115*, pp.80-90.

ISSN 2398-6611 (Online)

Tamman Kaid Development of conductive rubbers for gasket applications

Tammam Kaid, Ian Jenkinson, Ariyan Ashkanfar and James Ren
School of Engineering and Technology, Department of Mechanical Engineering and Materials, Liverpool John Moores University, 3 Byrom St., L3 3AF
E-mail address: t.kaid@2016.ljmu.ac.uk

Abstract. The work provide an overview of the process of a research project on numerical and experimental investigations of conductive materials and their applications for smart gasket. The key scientific and technical topics related to gasket materials, rubber composites, conductive materials and sensors' materials, have been reviewed including the structure of conductive materials and manufacturing process. A conductive material is developed using carbon particles as the conductive phases. Different approaches to produce the electrode materials and configuration has been evaluated and optimised. Systematic mechanical and electrical tests have been performed on the materials, and result will provide important data for modelling the materials and design optimisation.

Keywords. Conductive materials, smart gasket, rubber composites, sensors, carbon fibre particles, silicone and polymers.

1. Introduction:

Gaskets are extensively used in different types of equipment/structures in many industries, such as aerospace industries, general machinery, energy, food, etc. (Al-Ghathian et al, 2005; Mathan and Prasad 2011; Schotzko et al , 2015). A gasket is a deformable part placed in between two objects (e.g. flanges) in order to prevent leakage of any kind of the pressurized or not pressurized media (Lindvall and Minkkinen 2004; Mathan and Prasad 2011). The main materials used for making gasket is rubber and plastics. The work reported is concerned with developing conductive materials (Rubber and plastics) which can be used for smart gaskets with functions of monitoring the pressure and temperatures. Smart gaskets consisting of sensors (temperature or pressure, etc.) is increasingly being used for process control and condition monitoring (Moghaddam et al, 2014). Conductive gasket is required for different purposes (For example for EMI shielding). This is achieved by adding conductive fillers in the system. (The conductive fillers are typically metal particles or nonconductive materials like glass that are plated with a conductive metal. These gaskets are used due their functional requirements (in this case, conductivity) but they have to maintain the mechanical properties to achieve sufficient sealing.

In this work, new particle reinforced rubber composite materials with improved mechanical, thermal properties and electrical conductivity for smart gasket applications is developed. The key effects of key material and testing parameters on deformation under uniform compression and point loading is investigated. FE model with embedded sensor is simulated.

2. Experiments and results:

The experimental developments focused on the design and evaluate different mixing and curing programs. A staged manufacture process has been developed to produce particle reinforce composites with a soft matrix (Silicone rubber). The work studied a controlled curing approach to produce part with an embedment (rigid or soft one) during the rubber making process. Several approaches have been evaluated to produce the silicon rubber composites. The final process for the conductive silicone rubber and conductive polymer is illustrated in Figure 1 (a). A known quantity of resin is poured into a container, add hardener agent to the resin and mix properly. Then, degassing the mixture using a vacuum machine, after the degassing process add a certain amount of carbon fibre particles is mixed with the resin uniformly. Cast the mixture into a mould to get the desired shape. Finally, put the matrix in the oven under 50 ºC for two hours for fast curing (in case of conductive silicone rubber only). Then, release the sample from the mould and test the electrical conductivity of the composite rubber. The sample in Figure 1 (b) is a conductive silicone rubber developed using the manufacturing method. A similar mixing/blending process has been used to produce conductive plastics, a typical example is shown in figure 1 (b).

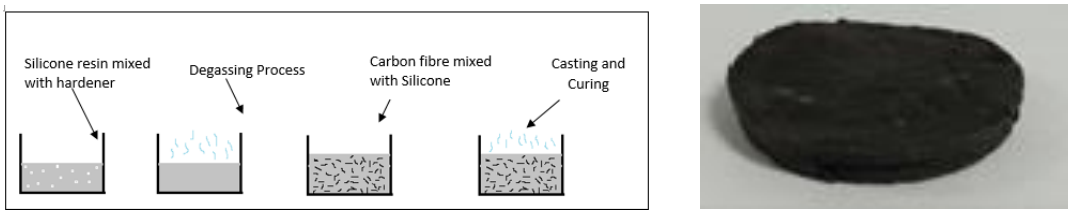

Figure 1 (a) Manufacturing method used to produce conductive silicone rubber and (b) Conductive rubber sample.

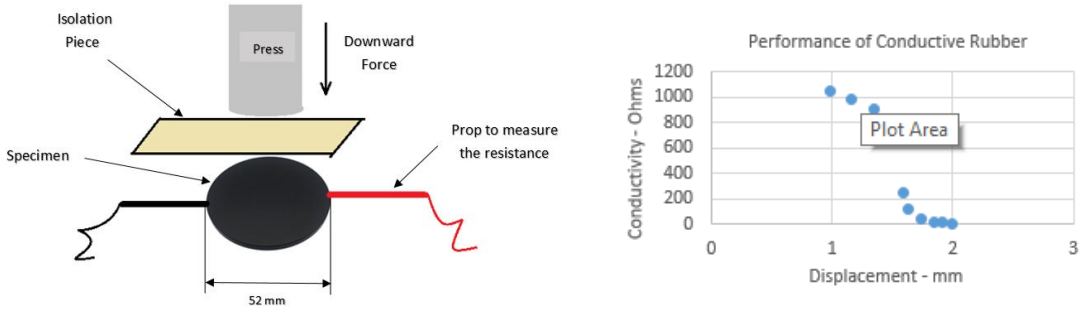

Figure 2 (a) Schematic to show the measurement of the electrical resistance under compression and (b) Compression tests and results of the electrical resistance with displacements.

Figure 3 shows FE modelling results of the gasket under compression. In the model, the conductive rubber is modelled an embedded system. The compression force is simulated by apply a uniform pressure to the surface of the gasket. Figure 3(a) shows the deformation of the gasket, while Figure 3(b) shows the deformation of the embedded sensor materials. The property of the rubber is validated against testing data. This will provide an important tool to assess the effect of gasket dimension, material properties, sensor positions etc. to optimise the design.

Figure 3. Shows FE model of compression tests and results. (a) FE model of silicone rubber gasket and (b) deformation of an embedded sensor.

3. Summary:

This work has developed a systematic approach over conductive rubber composites and its application in smart gasket for force and pressure sensing. Different manufacturing approaches to produce conductive rubber materials has been evaluated. Systematic mechanical and electrical tests have been performed on the materials, and result will provide important data for modelling the materials and design optimisation. A gasket using the conductive materials developed has been fabricated. A FE model simulating the deformation of the gasket has been developed and showed good linear force displacement curves. Future work will develop a parametric microstructure model of the carbon particle-silicone rubber composite to model the compaction and interlink of conductive particles in the gasket materials. The combination of micro and macro modelling will provide a platform for gasket design and material structure optimisation.

References:

Al-Ghathian F. M. M. and Tarawneh M. S., 2005, Friction Forces in O-ring Sealing, *American Journal of Applied Sciences* Vol**. 2 (3)**, pp.626-632.

Gosai M and , Bhavsar S.N., 2016, Experimental Study on Temperature Measurement in Turning Operation of Hardened Steel (EN36) *Procedia Technology*, Vol.**23, 311-318**

Lindvall J., and Minkkinen M., 2004, Fracture Mechanics for a Plate Heat Exchanger Gasket, Research Report, School of Mechanical Engineering, Lund University, Sweden. Mathan G., Prasad N., 2011, Studies on Gasketed Flange Joints Under Bending With Anisotropic Hill Plasticity Model for Gasket, *International Journal of Pressure Vessels and Piping* Vol. **88 (11-12)**, pp. 495-500

Schotzko T., Reuter M., Lang W., 2015, Sensor integration in rubber gaskets for structural health monitoring made by compression molding, *Polymer Testing*, Vol. **48**, 31–36.

Moghaddam A.S. and Mohammadnia S., 2014 Three dimensional finite element analysis of 4 inch smart flange on offshore pipeline, *Ocean Systems Engineering*, Vol. **4**, No. 4 (2014) 279-291.

ISSN 2398-6611 (Online)

Cong Tang Systematic Investigation of Auxetic Structures and Materials Development

Cong Tang*, Lisa Li, Glynn Rothwell and James Ren

Department of Maritime and Mechanical Engineering, Faculty of Technology and Engineering, Liverpool John Moores University, Liverpool L3 3AF

*E-mail address: C.Tang@2015.ljmu.ac.uk

Abstract. Poisson's ratio is an important material property, which is represented by the negative value of the ratio between the lateral strain and axial strain when the material is being stretched. Structure with negative Poisson's ratio (also termed auxetic material) have a wide range of potential applications in chemical engineering, sport and sensors (e.g. Piezocomposite device), etc. The general aim of this project is to develop FE models and optimization programs for simulating different types of auxetic materials and design new structures. In the work reported, FE models of two typical auxetic structures (Missing rib model and hierarchical structure) have been developed and evaluated. The results on these structures were validated against published analytical and/or experiment data. New approach has been used to develop structures with targeted Poisson's ratio (such as Poisson's ratio close to zero). A python program has been developed to automatically search for or design new structures following predefined rules and algorithms.

Keywords. Negative Poisson's ratio , FE modelling ,material development

Introduction

Poisson's ratio is an important material property, which is represented by the negative value of the ratio between the lateral strain and axial strain when the material is being stretched (Figure 1). Most materials have a positive Poisson's ratio due to shrinking in the lateral direction when being pulled For example, metals (e.g. steel, copper, aluminium) have a Poisson's ratio between 0.2-0.3; Ceramics have a Poisons' ratio range 0.1-0.2, while the Poisson's ratio for Polymers varies from 0.3 (for engineering plastics) to 0.5 for rubber (representing in-compressible, i.e. no volume change when deformed). Poisson's ratio is one of the most important material parameters, it influences the mechanical and many other functional material properties (Evans, , 1991). This is evident in the key mechanic formula when the material is under both well-defined loading conditions (compression, tension and shear) and nonstandard loading conditions (such indentation, bending etc.).

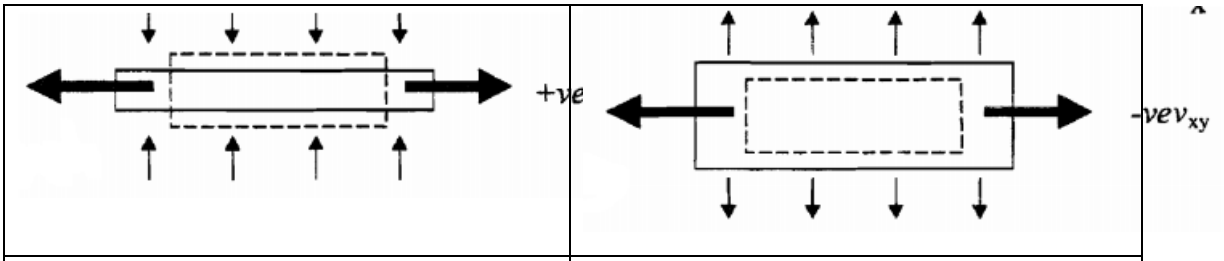

(a) Deformation of a Non-auxetic material in tension.

(b) Deformation of an auxetic material in tension.

Figure 1 *Schematics showing the different behavior of Non-auxetic and Auxetic Materials in tension.*

Method

In this study, finite element models were developed to simulate the structure and deformation of some established auxetic structures focusing on the value of the Poisson's ratio and deformation mechanisms. Experiments was also conducted on some selected samples (Figure 2 a&b) which, together with some analytical analysis, provide essential data to validate the FE model. The finite element simulation software used is abqus6.14 assisted by parametric programming using Python. Parametric Finite element simulation can significantly reduce the time and cost of materials research, in the meantime, its parametric function enables the prediction and optimization of new materials structures. . The full model is shown in Figure 2 a&b. both models consists of 3x3(axial x transverse direction) units with a dimension of 150mmx150mm. Figure 2(c&d) shows loading and boundary conditions of the two honeycomb structures. In the model and fix displacement is applied in one end, while the other side is fixed on all degree of freedom (DOFs). The Poisson's ratio is determined from the ratio of the axial and transverse strains automatically by a python code.

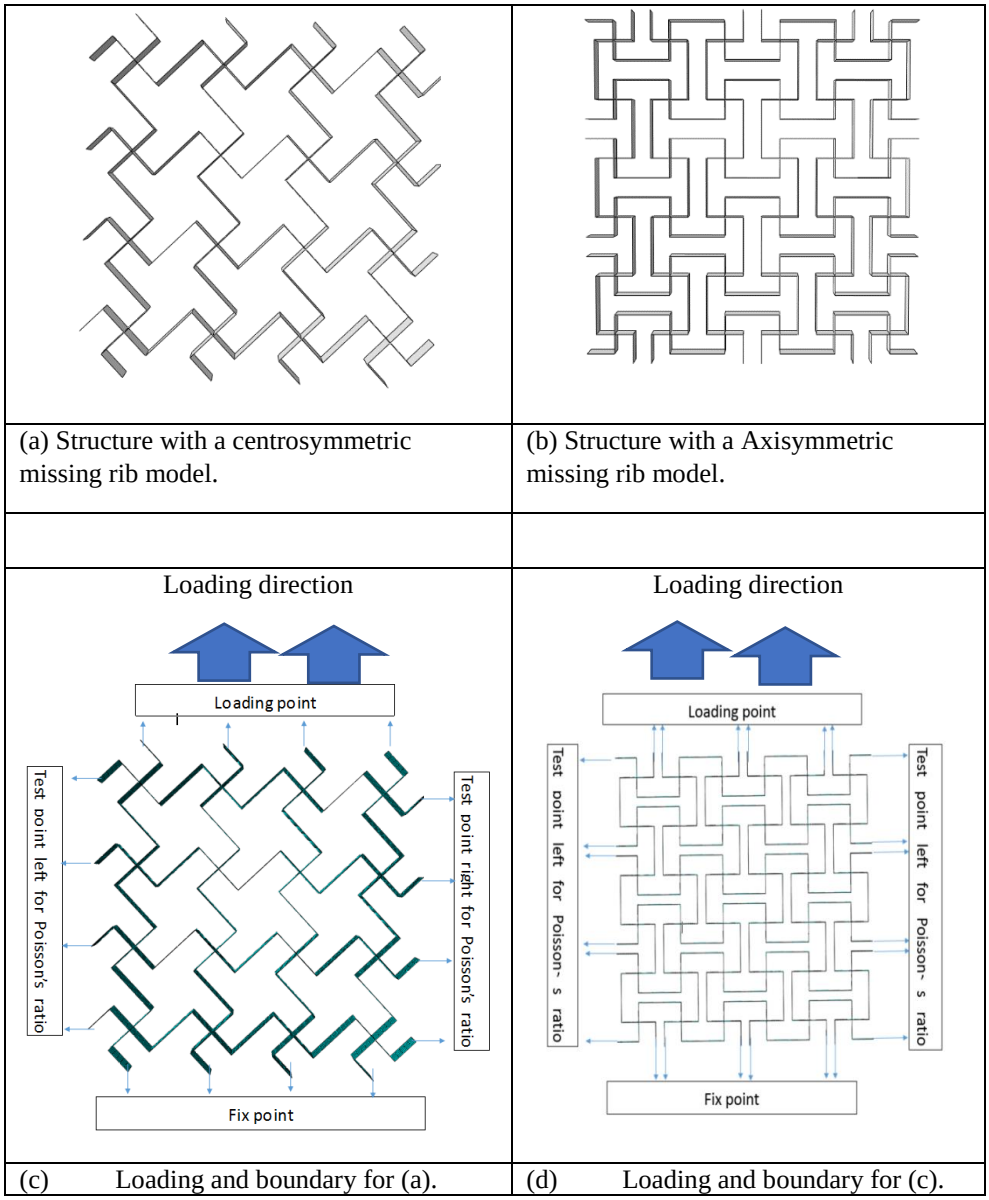

(a) Structure with a centrosymmetric missing rib model.

(b) Structure with a Axisymmetric missing rib model.

(c) Loading and boundary for (a).

(d) Loading and boundary for (c).

Figure 2 *Unit cell of Centrosymmetric missing rib and Axisymmetric missing rib model used in the FE modelling.*

Result and Analysis

Figure 3 shows the deformation (displacement) field and force-displacement of the auxetic samples in tension. The contour plot (a) is the axial displacement (U2) along the loading direction. As shown in Figures a &b, these two structures have different deformation modes but show a clear lateral expansion under tension, exhibiting auxetic behaviors. In both cases, the relationship between the force and the displacement follows a linear trend. Figure 3(c) is a comparison between the Poisson's ratio obtained from

FE modelling, analytical and a simple experiment for the Centrosymmetric missing rib structure. As shown by the bar chart, the data of Poisson's ratio are in a reasonable agreement between them. The analytical procedure was adapted from Gaspar et al (2000) to calculate the axial and transverse strain and the Poisson's ratio.

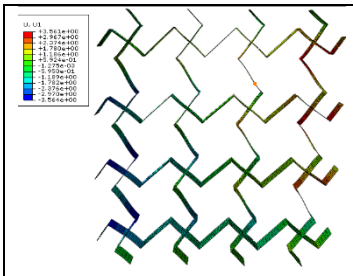

Figure 3 (a) Deformed shape of Centre symmetric model (The contour is the axial displacement U1)

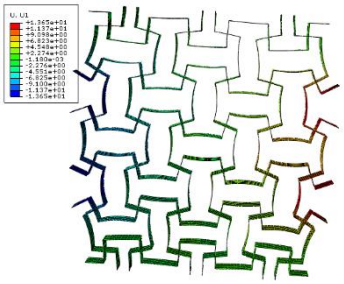

Figure 3 (b)Deformed shape of Axisymmetric model (The contour is the axial displacement U1)

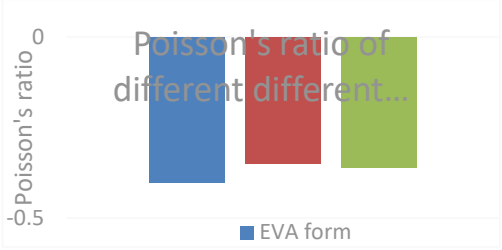

Figure 3(c) Comparison between the Poisson's ratio from FE modelling, analytical and simple experiments of the symmetric model

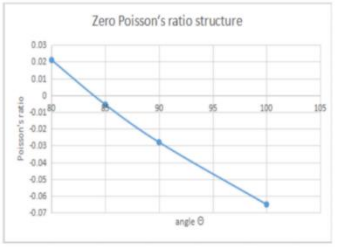

Figure 3 (d) Typical data showing the Poisson's ratio 0f mixed structures.

Based on procedure of the FE program and analysis, a python program has been developed, which is able to automatically produce FE model and calculate the Poisson's ratio. This allows the searching of structures with auxetic behaviors (or other targeted properties). The work involving looping through a wide range of combination of structures with different Poisson's ratios over different strain levels. Potential structure is stored in a database for analysis. A typical data is shown in Figure 3(d). As shown in the curve, zero Poisson's ratio structure base on hybrids of positive and negative Poisson's ratio structure can be automatically designed.

Summary

This paper reports the progress of a project on developing parametric FE models and optimization programs for simulating different types of auxetic materials and design new structures. FE models and results of two typical auxetic structures showed good agreement against published analytical and experiment data conducted on a simple model material. A python program has been developed to

automatically search for or design new structures following predefined rules and algorithms. The new approach is able to design structures with tailored Poisson's ratio (such as Poisson's ratio close to zero) based hybrid structures of different Poisson's ratios.

Reference

Evans KE (1991). Design of doubly-curved sandwich panels with honeycomb cores. *Compos. Struct,* 17: 95-111.
GASPAR, N., REN, X., SMITH, C., GRIMA, J. and EVANS, K. (2005). Novel honeycombs with auxetic behaviour. *Acta Materialia*, 53(8), pp.2439-2445.
Grima JN, Gatt R, Ravirala N, Alderson A, Evans KE (2006). Negative Poisson's ratios in cellular foam materials. *Mat. Sci. Eng*., 423: 214- 218.
Mir, M., Ali, M., Sami, J. and Ansari, U. (2014). Review of mechanics and applications of auxetic materials, Advances in Materials Science and Engineering, 1, 1-17.

ISSN 2398-6611 (Online)

Muhammad Usman A fuzzy modelling approach to standardise the prior probabilities for parent nodes of Bayesian Network (BN) model used for two-stroke engine health assessment

Muhammad Usman*, Chia-Hsun Chang, Zhuohua Qu, Zaili Yang
Liverpool Logistics Offshore and Marine Research Institute, James Parson Building, Byrom Street.
*E-mail address: M.Usman@2014.ljmu.ac.uk

Abstract: Maintenance of machinery equipment is part of necessary costs of a ship operation. With the evolution of technology, innovative models are being employed to move away from fixed interval maintenance actions towards predictive maintenance to extend the time between overhauls. A Bayesian network (BN) model has been developed as health assessment tool for a large two-stroke engine. However there was a gap in the model where prior probabilities for BN parent nodes were estimated from engine operational parameters directly through user's knowledge and experience. This study aims to address this issue by standardising the process using fuzzy modelling approach. There have been multiple inputs for each parent node of BN model hence effectiveness of the proposed approach has been demonstrated by creating a fuzzy model for scavenge air quality node. Operational inputs from engine operational data can be inserted into the fuzzy model and then output coupled with the BN which would calculate the overall health of the engine. The advantage of this user-friendly model is that it can run simulations for trending various operational parameters.
Keywords: Bayesian Network (BN), Two-stroke engine, Fuzzy Model

Introduction:

With the ever increasing commercial pressures on ship operators with shrinking margins, loss of propulsion due to machinery breakdown is just a tip of the iceberg and exhibits a significant economic loss associated with the subsequent delays and repair bills. In its 2015 annual report, the Swedish Club reported that the cost of machinery claims for the period 2012-2014 was around USD 187 million with main engine damages remain the most expensive category accounting for 37% of the total machinery claims (Swedish Club, 2015). Hence the efforts are being made from engine manufacturers and operators to enhance reliability of engine operations through better diagnostic and prognostics.

This paper further develops the work presented in Usman et al., (2017) where a Bayesian Network (BN) model was used for predictive maintenance of two stroke engines. The data from various operational parameters requires processing before it can be used as input to BN model. In previous work, operator's expert judgement was used to demonstrate the model functionality. However this work is an attempt to improve the model by introducing the fuzzy rule base approach to process the operational parameters and derive the prior probability for the BN parent nodes.

Fuzzy Control Model

Information flow through fuzzy control model as input variables go through three major transformations before coming out as results. The three stages are fuzzification, fuzzy inference and defuzzification.

Fuzzification

In the first stage, inputs are taken from variables and converted to appropriate fuzzy sets to express the uncertainties associated with the measurements (Das et al., 2014). In fuzzy modelling, membership functions are used to describe the membership of a variable to a fuzzy set. There are various functions and the simplest is the triangular membership function which has been used in this study.

Fuzzy inference

The inference process assigns one output fuzzy set to each fuzzy rule base. Then degree of truth for the activation of each rule is computed and applied to the conclusion part (then part) of the rule. Based on the degree of truth of each part of the rule *min-max* inference technique is used (Konstandinidou et al., 2006).

Defuzzification

The purpose of defuzzification is to convert each conclusion obtained by the inference engine, which is expressed in terms of fuzzy set, to a single real number (Klir & Yuan, 1995). There are various defuzzification methods in literature, e.g. weighted mean of maximum **(WMoM),** gravity centre of produced area **(COA) and centre of Maxima method**.

Fuzzy Models

There are 5 fuzzy input variables for the BN model in question. However to demonstrate the functionality, only one variable (scavenge air quality) has been described with corresponding fuzzy sets as per table below.

Table 2: Scavenge air quality

BN Parent Node	Corresponding antecedent	Details / range(s) of fuzzy sets	Desired Consequents (BN states)
Scavenge air quality	Air Pressure	1) Pressure is ACCEPTABLE as per engine makers recommendation for corresponding load 2) Pressure is LOW	Satisfactory & Unsatisfactory
	Air temperature	1) LOW (T < 42ºC) 2) ACCEPTABLE (32~52 ºC) 3) HIGH (T > 42ºC)	
	Water mist catcher performance	1) SATISFATORY 2) UNSATISFACTORY 3) POOR	

There are three antecedents or influencing factors considered to determine the quality of scavenge air going into the two-stroke engine.

Scavenge air at optimum pressure, temperature and with minimum moisture levels contribute to good combustion conditions in the two stroke engine (Griffiths, 2006). Pressure and temperature has a direct relationship hence air going into the engine at right temperature will provide sufficient mass of oxygen to facilitate complete combustion. Lower pressure and higher temperature will risk the incomplete

combustion and higher exhaust temperature (Griffiths, 2006). Pressurised scavenge air going into the scavenge space goes through scavenge air cooler, water mist catcher/separator and non-return valves/flaps before entering scavenge space.

Fuzzification of input variables

Scavenge Air Pressure

During normal operation, there is a linear relationship between the engine load and scavenge air pressure. The important factor to determine is whether the operational data i.e. scavenge air pressure is sufficient for the load engine is operating on. If the scavenge pressure is insufficient then it will impact negatively on the combustion performance and vice versa. A calculator in Microsoft Excel has been developed (appendix B) to calculate the percentage deviation (if any) from the optimum scavenge air pressure for the given load.

For the fuzzification step, two fuzzy sets have been defined i.e. 'Low' and 'Acceptable' with corresponding fuzzy membership varying from 0 to 1. Operator needs to enter the ideal scavenge air pressure against the effective power along with the current/operational scavenge air pressure. A simple graph has been developed to measure the deviation from the ideal value considering a linear relationship as shown in figure below.

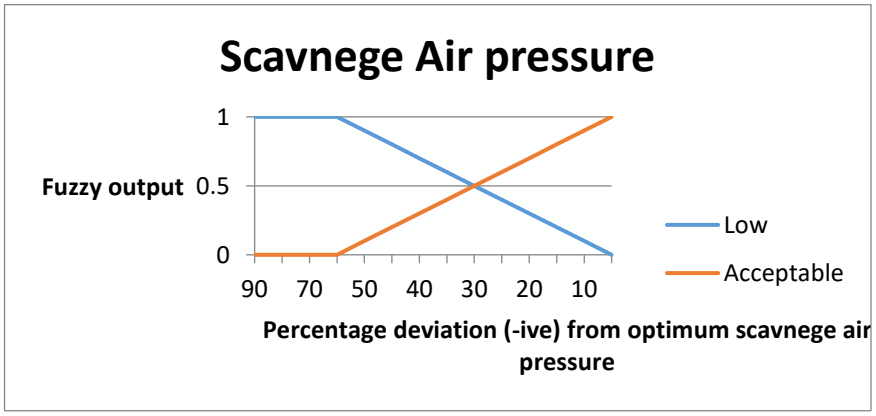

Figure 1: fuzzy membership for scavenge air pressure

The linear relationship between two variables is described as
$Pscav = mPe + b \ \in (P_{scav} \propto P_e)$

Here, P_{scav} (scavenge pressure) and P_e (effective engine power) are variables with 'm' represents slope on the graph and b is an equation constant. For simplicity, in this context, value of b has been taken as true or zero. A trend function has been used in excel to calculate the various points on the continuum.

Scavenge air temperature

Temperature is controlled by the scavenge air cooler and is kept within certain range for optimum operations. The reason for maintaining scavenge air temperature within a certain range is that too low

scavenge air temperature may cause thermal shock to cylinder components operating at relatively higher temperatures and too high temperature may cause poor combustion performance due to lack of air density and resultant higher exhaust temperatures (Wright, 2005). Density of air going into the engine will increase or decrease depending on the temperature of the air as it has an inverse relationship;

$T_{scav} \propto 1 / \rho_{scav}$

During normal operation, the amount of air is kept above the minimum required levels i.e. stoichiometric air/fuel ratio which is idealised condition of all the oxygen is consumed for combustion hence exhaust do not contain any oxygen hence other gases such as CO_2 are at maximum. The actual air/fuel ratio can be 2 to 3 times more than stoichiometric air/fuel ratio (Wright, 2005). The excess air facilitates the combustion process however its drawback is that there are increased NOx emissions (Kaltoft, 2011).

Based on FOBAS ENGINE[5] (FOBAS, 2017) data, for normal two stroke engine operation, the ideal scavenge air temperature is around 40~42^{o}C. Fuzzy scavenge air temperature will be determined based on the operational input from the engine which can determine the level of membership to a fuzzy set. For example, if the scavenge air temperature is around 46^{o}C then fuzzy scavenge air temperature will be assigned to fuzzy membership of 0.6 ‘acceptable’ and 0.4 ‘high’.

Water separator performance

Water mist catcher or water separator is fitted after the scavenge cooler and before scavenge air receiver. Its primary function is to remove water from the cooled air to avoid carry over of high moisture into scavenge space which can disrupt the lubricant film and contribute to the cold corrosion (Griffiths, 2006). It is difficult to measure directly the humidity levels for air going into the combustion chamber hence this study proposes to determine the water separation efficiency by computing the difference between the actual amounts of water condensed during operation and calculated amount as per engine maker’s guidelines.

The quantity of the water separated would depend on the load, ambient temperature and humidity in the air. The increase in difference ΔQ (tons/24 hr) would indicate poor separation efficiency and increased risk of water carry over to the scavenge space. This may also prompt the ship to investigate the reason such as scavenge drain blockage etc. It has been realised that the calculations involved may not be accurate however should provide a basis to proceed with the overall assessment of the scavenge air quality. Three fuzzy sets have been defined i.e. Satisfactory ($\Delta Q < 5$), unsatisfactory ($0 < \Delta Q < 10$, Poor (($\Delta Q > 5$).

Calculations

To demonstrate how fuzzy scavenge air quality model works, a typical engine parameters are considered and applied with fuzzy inference (If-then) rules developed in order to cover various scenarios. For scavenge air quality assessment, the fuzzy model requires 18 (if-then) rules to be developed based on 3 (Temperature) × 3 (water separation) × 2 (pressure) = 18. By inserting the typical values in BN model

[5] FOBAS ENGINE is a diagnostic tool to assess the performance of large two-stroke engines offered by Lloyds Register FOBAS. The author is the product manager responsible for development and service delivery of this subscription-based service.

based on the operational variables the conditional probability for ‘unsatisfactory’ scavenge air quality is 0.30 and ‘satisfactory’ as 0.7.

Conclusion

This model demonstrate the use of fuzzy rule base approach to compute the prior probability for Bayesian network used to determine the two-stroke engine health assessment. The work is further helped by the use of excel for easy computations. This model uses the conventional ‘min-max’ function before the defuzzification however experts believe that this does not represent the true sensitivity of the model hence next stage of the work will involve developing the fuzzy models for each BN parent node and use of evidential reasoning to improve the sensitivity of the fuzzy model.

References

ANDREWS, J.D. & MOSS, T.R. (2002) *Reliability and Risk Assessment.* Professional Engineering Publishing Limited.

Das, B., Panja, S.C., Chakrabarty R.P (2014) Fuzzy Rule-Based Decision Making to Minimize Wear Rate of Dumper Tires. Procedia Materials Science Vol 6, Page 752 – 761

FOBAS (2017) Fuel Oil Bunker Analysis & Advisory Service (FOBAS) online reporting platform [online]. Available at: https://www.fobas.com/lr_shared/jobs [Accessed: 15th December 2017]
Griffiths D. (2006) Marine Low Speed Diesel Engines. IMarEST (The Institute of Marine Engineering, Science and Technology) Publications. MEP Series: Vol 2, Part 17.
Kaltoft, J. (2011) Tier III EGR FOR LARGE 2-STROKE MAN B&W DIESEL ENGINES. Proceedings of the International Symposium on Marine Engineering (ISME) 17-21 October, 2011, Kobe, Japan.

KLIR, G.J. (1995) *Fuzzy Logic “Unearthing Its Meaning and Significance”*. IEEE Potentials. Volume: October/November 1995. Pages 10 to 15.

KONSTANDINIDOU, M; NIVOLIANITOU, Z; KIRANOUDIS, C; MARKATOS, N. (2006) *A Fuzzy Modelling Application of CREAM Methodology for Human Reliability Analysis*. Reliability Engineering & System Safety. Volume: 91. Pages 706 to 716.

Usman, M., Yang, Z., Shorten, D. (2017) Development of Bayesian Network (BN) model to estimate health factor for predictive maintenance strategy of large two-stroke marine engine. Proceedings of ‘World Congress of Condition Monitoring’, 26 June 2017, London.

WANG, J. & TRBOJEVIC, V. (2007) *Design for Safety of Marine and Offshore Systems.*IMarEST Publications.

Wright, A.A. (2005) Exhaust Emissions from Combustion Machinery. *IMarEST (Institute of Marine Engineering Science & Technology) Publications*. MEP Series: Vol 3, Part 20.

ISSN 2398-6611 (Online)

Gregory Asuelimen Advanced risk assessment in the marine Arctic seismic survey operation

Gregory Asuelimen[1*]
[1]School/Institute: Liverpool Logistics Offshore and Marine Research Institute
Liverpool John Moores University, Byrom Street. L3 3AF. UK
[*]G.Asuelimen@2014.ljmu.ac.uk

Abstract Arctic environments generally are characterised as remote regions of the earth with harsh climates and difficult-to-work environment. Global warming playing an important role in the Arctic region has its effects and discrepancies. Thus, its effects has positioned the Arctic region as a commercially available and an attractive area of development, giving way to an increased oil and gas exploration, fishing, tourism and research activities. Conversely, the rate of discrepancies in global warming has added a major factor to the uncertainty in the Arctic region given way to increased risks. Vessel operation in this region is usually a complex one with high repercussions. In a bid to manage and reduce the high risk of uncertainty in marine seismic survey operation, a review of some of the notable Qualitative and Quantitative risk management techniques has been carried out. Formal Safety Assessment as adopted by IMO was selected in this paper in order to systematically reduce the operational hazards in marine arctic seismic surveying since the safety of marine operations against marine hazards has traditionally relied on the rules of the International Maritime Organization. In conclusion, controlling the risk of uncertainty depends on the most cost effective method derived from the formal safety assessment.

Keywords Advance risk management, seismic survey, Formal Safety Assessment, Marine Safety, Arctic region, Cost Benefit Analysis.

1. Introduction

The Arctic environment is generally characterised as remote regions of the earth with harsh and, difficult-to-work environment. Regardless of the challenging and hostile nature of the Arctic waters, shipping sector and others (such as oil and gas, tourism and fishery and research sectors) are relentless on exploring this region because of the vast reserves of natural resources including Hydrocarbons.

The first step in most offshore oil and gas exploration is pinpointing the location of resources (Shell International, 2014); this is often done using a seismic survey vessel. A seismic vessel is a dedicated and sophisticated vessel, which navigate about water bodies letting off explosives and gathering the reverberated results of explosion through attached hydrophones. The gathering of seismic data has been carried out in the various Arctic regions for over 50 years (NPC, 2015). The earliest marine seismic data gathering included a 2D seismic profiles (refraction and reflection) using both land acquisition equipment for winter periods, and a towed marine streamer in summer periods.

Ever since the improvement in seismic data gathering methodologies and 3D technology in 1980s, there has been a great innovation in data acquisition, including time lapsed or 4D seismic. The improved technologies have been known as one of the most notable development for reducing and controlling risk and thus, improving drilling and production success in the Exploration and Production (E&P) industry. With the exclusion of the orthodox 2D offshore Arctic Exploration and Development Technology, quite a lot of these improved seismic methodologies and technologies have not been suitable for use in the Arctic. The main reasons been that there is a higher risk prospect in the arctic region, and the lack of development of technology to suit the Arctic operations, considering the overall cost of E&P of hydrocarbons offshore in the Arctic (NPC, 2015).

The development of safe and economic oil and gas facilities offshore in the Arctic is considered to be more technically challenging than in any other environment chiefly because effective strategies have yet to be developed (Ronald, 2016). In general, the main challenges in carrying out a seismic survey operation in the Arctic according to Cowling, 2011, Critchlow, 2014, Gourvenec and White, 2010) include:

- The remoteness of the region resulting in a very late rescue response in the event of mishap,
- Geological complexity such as the presence of ice, icebergs etc.
- Limitations in navigation technology resulting to poor radio-navigation infrastructure,
- Poorly mapped areas,
- High cost of investment,
- High ecological impact of an accident etc. and
- Inexperience and uncertainty

Even with the higher operational risk viewpoint in the arctic region, only a limited number of advanced risk assessment models have been developed to lower risk and improve safety, according to result from web of science and google scholar 2018. In order to lower risk/ threats, and improve safety, it is imperative to first identify possible initiating hazardous events leading to a full-blown accident or reveal the causes of accidents/ incidents, which have happened in the past.

With the increasing shipping activities in the Arctic, there is a strong likelihood that the increased traffic might cause more accidents (Henry Fountain, 2017, CBC news, 2015). The most significant risk factors faced by mariners in the Arctic include drifting ice and extremely low temperature (Floris Goerlandt et al., 2017). Although it is perceived that accidents are rare in the Arctic, however, this could be as a result of lack of documented incident/ accident data (Wilfried H et al., 2015). The lack of proper record of accident data does not negate the need to cultivate advanced risk management model chiefly because accidents in this region often result in high consequences. G. Zhang and V. Thai (2016) in their risk assessment study concluded that most shipping accidents rarely happens but when it happens, it comes with high consequences.

The aforementioned risks and overall cost of reducing seismic operation risk in the Arctic are two of the major factors to be considered in carrying out a risk management and control in the Arctic waters.

1.1 Objective of the PhD research

The effective risk management in Marine Arctic Seismic Survey Operation has given way to the objective of this research, the objectives are:

1. Identify all hazards in Marine Arctic Seismic Survey Operation
2. Analyse and Estimate the risks
3. Identify possible risk control options to reduce the most significant hazards
4. Check if selected reduction measure is cost effective using a Cost Benefit Analysis
5. Apply the most cost effective risk reduction measure for an informed decision-making process

2. Identification of Hazards

2.1. Preparatory step

Before initiating any risk management process, the definition of the problem at hand is attempted with respect to the system, goal, and operation (Asuelimen, 2018). The purpose of this preparatory step is to gain access to the problem carefully with respect to the regulations under review; this in return, will assist in determining the extent and depth of the FSA application (Asuelimen, 2018)

This preparatory step is given to all FSA and Polar Code applications. This is essential because a misguided definition on a system such as vessel operation, often lead to insufficient recommendations, which in turn may take out major risk categories from the system being assessed. This preparatory step helps to simplify the goal of the assessment.

2.2. Hazard Identification

To identify a hazard, it is important to understand what constitutes a hazard and what does not. Artic hazards, which includes weather and other natural condition in themselves, do not cause harm to the environment or to anyone. However, operating in such environment becomes hazardous when humans and vessels come in contact with it, and until then it remains a potential hazard.

For many managers, the identification of hazards may well be the most difficult part of the risk assessment process (Eugene Tucker, 2015). Hazard Identification (HAZID) is a systematic method of identifying hazards and their corresponding events that could give way to a significant consequence to personnel, environment and/ or property. The key focus in HAZID phase is to ensure that the process is pragmatic and not confined only to hazards that have materialized in the past (IMO, 2012).

For a complex system and scarce historic data, it is not practical to rely on system level data and observations (Anders Jensen and Terje Aven, 2018). The traditional methods of hazard identification which include literature review, expert judgement, brainstorming sessions can be modified to develop risk assessment techniques such as event trees, fault trees, HAZOPS, swift analysis, checklist procedures et cetera. However, the main problem in the application of the traditional techniques is the lack of linearity in complex systems. For example in Fault Tree or Event tree, it is presumed that if a sequence of events happens, a specific outcome will result. This method is more predictive in nature hence not pragmatic in real scenario, as complex system with uncertainty do not allow such predictive modelling. Accidents happen in an unexpected manner.

A more suited Nonlinear technique in identifying hazards in complex system is the functional resonance analysis method (FRAM) introduced by E. Hollnagel, 2012. The new, nonlinear technique has it setback such as time consumption and its difficulty in developing a network reflecting a complex system. With the FRAM method, it is not possible to support the quantification of probabilities of successes or non-successes (Slater D, 2016). Hence, the FRAM method is difficult to carry out, requiring so much skill and competence. This has left the traditional methods more practical. Expert judgement, literature review and brain storming sessions help to strengthen the weakness of the traditional method of identifying hazards. Expert Judgement methodology for simplicity is divided into three stages:

1) Choosing the experts
2) Elicitation
3) Aggregation.

The elicitation stage refers to the process of proposing opinions or expert judgements through different means. This is typically supplied through interviews and/or questionnaires. The aggregation phase is the means of taking the average or converging of the different expert opinions offered in the study (Endrina, Rasero, & Konovessis, 2018)

3. Risk Analysis

The purpose of Risk Analysis is to give proper attention on high-risk areas and focus on factors, which affect the level of risk (IMO 2002). Owing to the complexity and the dynamic nature of Arctic hazards, different aspects of investigation, analysing the safety concerns and/ or riskiness of Arctic hazards have to be taken into account, as the consequences of such unpredictable hazards are normally far reaching. Hence, risk analysis in this stage requires an advanced screening or risk ranking processes on the significant basic hazard events, to support the achievement of a desirable outcome.

The traditional ways of carrying out risk analysis and investigation include the assessment of the likelihood (L) of accident occurring and the consequences (S) of such accident. This traditional method of risk analysis considering only L and C does not offer robust information on the variety of the performances of a risk analysis process, nor can it fully demonstrate the level of safety, risk and intermediary states.

Therefore, a variety of states of a top event (undesirable outcome) in a risk analysis need to be identified separately. A variety of advanced risk analysis techniques have been introduced by Academic Bodies (AB), and used by the Maritime industries. The variety of risk analysis techniques includes ALARP, Failure Mode Effects and (Criticality) Analysis (FMEA and FMECA), Bayesian Network (BN), Fault Tree Analysis (FTA), Event Tree Analysis (ETA), Preliminary Hazard Analysis (PHA), Cause-Consequence Analysis (CCA) and Human Reliability Analysis (HRA) all of which employ either qualitative or quantitative techniques (Bai & Jin, 2016, HSE, 2000, Sutton, 2015, Alyami et al., 2014).

These aforementioned techniques and much more have been advanced in different industrial settings, often in response to real-world system problems. The concerned risk analyst or safety officer needs to choose the right approach for the system. The selection method can be problematic given the different risk analysis techniques and the various specific methods involved. According to Alyami et al., 2014, there is no single precise approach for a specific activity or system features, but some approaches are more exact and suitable than others, and a decision framework is helpful in the selection process.

4. Risk control options

To investigate risk control options, the high risk areas from the risk analysis stage needs to be selected for risk control (Wang and Ruxton, 1998), (Wang and Pillay, 2003). This is later followed by identifying the risk reduction measures otherwise known as RCOs. The drive of RCOs is to present effective and practical options having the following stages:

I. Targeting areas having high risks.
II. Identifying possible risk control measures.

5. Cost Benefit Analysis

The Cost Benefit Analysis (CBA) phase is the process of selecting the most cost effective way of reducing the high risk areas. If the method selected from the RCO phase outweighs the benefit of risk reduction, then, the CBA is negated. A perfect example is choosing to spend 3,000,000 Pounds on building a car with indestructible material to reduce road accident. The Cost Benefit Analyst will rather choose to spend 5,000 Pounds on traffic lights to reduce road accident than the 3,000,000 Pounds option, as it outweighs the agreed cost of human life which according to the offshore industry is assumed to be £2,000,000 contained in Annex D of the first revision of NORSOK standard Z-013 (Skjong et al., 2007)

6. Decision-making/ Conclusion

The stake-holders decide the most practical method of reducing the identified operational hazards. The selected method will truly addresses the most cost effective way to improve safety, taking assessment back from step 1 to step 4. In conclusion, this research has shown a proactive, systematic, transparent and cost effective way to effectively manage high risk and uncertainty in the marine Arctic seismic survey operation. The findings from this paper can be adopted by safety engineer to address high risk in other maritime risk research.

References:

Anders Jensen and Terje Aven, A new definition of complexity in a risk analysis setting, Reliability Engineering & System Safety Volume 171, March 2018, Pages 169-173

Alyami, H., Paul, L., Zaili, Y., Ramin, R., Stephen, B. & Jin, W. 2014. An advanced risk analysis approach for container port safety evaluation. Maritime Policy & Management, 41 (7), 634-650

Alyami, H., Yang, Z., Ramin, R., Bonsall, S. and Wang, J. 2016. Advanced uncertainty modelling for container port risk analysis. Accident Analysis & Prevention, http://dx.doi.org/10.1016/j.aap.2016.08.007

Asuelimen Gregory, Blanco Davis, Zaili Yang, Ben Matellini, Formal Safety Assessment of A Marine Seismic Survey Vessel Incorporating Fault Tree Analysis, Journal of Marine Engineering and Application, 2018. Under Review.

Bai, Y., & Jin, W.-L. (2016). Chapter 1 - Introduction. In Marine Structural Design (Second Edition) (pp. 3-18). Oxford: Butterworth-Heinemann

CBC News, Arctic ship traffic grows, accident toll spikes: report, 2015. http://www.cbc.ca/news/canada/north/arctic-ship-traffic-grows-accident-toll-spikes-report-1.3017079

Cowling, J. (2011) Arctic oil exploration: Potential riches and problems. Available at: http://www.bbc.co.uk/news/business-14728856 (Accessed: 12 April 2016).

Critchlow, A. (2014) Arctic drilling is inevitable: If we don't find oil in the ice, then Russia will. Available at: http://www.telegraph.co.uk/finance/newsbysector/energy/11080635/Arctic-drilling-is-inevitable-if-we-dont-find-oil-in-the-ice-then-Russia-will.html (Accessed: 12 April 2018)

Endrina, N., Rasero, J. C., & Konovessis, D. (2018). Risk analysis for RoPax vessels: A case of study for the Strait of Gibraltar. Ocean Engineering, 151, 141-151. doi:https://doi.org/10.1016/j.oceaneng.2018.01.038

Eugene Tucker, Chapter 6 – Risk Assessment, Business Continuity from Preparedness to Recovery. A Standards Based Approach, 2015, Pages 91–106. Available online 23 January 2015

Floris Goerlandt, Habtamnesh Goite, Osiris A. Valdez Banda, Anders Höglund, Paula Ahonen-Rainio, Mikko Lensu, An analysis of wintertime navigational accidents in the Northern Baltic Sea. Safety Science, 2017, pages 66-84

Gourvenec, S. and White, D (2011) Frontiers in Offshore Geotechnics, 2 edition. London, UK: Taylor and Francis Group.

G. Zhang, V.V. Thai, Expert elicitation and Bayesian network modeling for shipping accidents: a literature review. Saf. Sci., 87 (2016), pp. 53-62.

Henry Fountain, With More Ships in the Arctic, Fears of Disaster Rise, New York Times, 2017. https://www.nytimes.com/2017/07/23/climate/ships-in-the-arctic.html

HSE. 2000. Health and Safety Executive. Review of hazard identification techniques.Health and Safety Executive. [online]. available:http://www.hse.gov.uk/research/hsl_pdf/2005/hsl058.pdf (accessed 25 April 2018)

IMO (2002). Guidelines for Formal Safety Assessment (FSA) for use in the imo rule-making process

IMO. (2012). Revised Guidelines for Formal Safety Assessment (FSA) for Use in the IMO Rule-making Process. IMO, London. Retrieved from London

NPC, Arctic Potential: Realizing the Promise of U.S. Arctic Oil and Gas Resources (www.npc.org)

Ronald O'Rourke, "Changes in the Arctic: Background and issues for Congress" Congressional Research Service, 2016 (https://www.fas.org/sgp/crs/misc/R41153.pdf)

Skjong, R., Vanem, E., & Endresen, Ø. (2007). Design, Operation and Regulation for Safety. Risk Evaluation Criteria. 3. Retrieved from http://www.transport-research.info/sites/default/files/project/documents/20130130_135847_22756_SAFEDOR-D-04.05.02-2005-10-21-DNV-RiskEvaluationCriteria-rev-3.pdf

Shell International, Geophysical imaging, Shell International Exploration and Production B.V, page 8 the Netherlands. https://www.shell.com/energy-and-innovation/overcoming-technology-challenges/finding-oil-and gas/_jcr_content/par/textimage.stream/1444725407967/f916a9f8105fef5080cee8e860dcfb6e17497306f03bd15593 5b69e187e4be36/geophysical-imaging-brochure-2014.pdf. Viewed 30th April 2018

Skjong, R., Vanem, E., & Endresen, Ø. (2007). Design, Operation and Regulation for Safety. Risk Evaluation Criteria. 3. Retrieved from http://www.transport-research.info/sites/default/files/project/documents/20130130_135847_22756_SAFEDOR-D-04.05.02-2005-10-21-DNV-RiskEvaluationCriteria-rev-3.pdf

SUTTON, I. 2015. Chapter 5 - Hazard Identification, In Process Risk and Reliability Management (Second Edition), Gulf Professional Publishing, Oxford, 193-271

Wang, J., & Ruxton, T. (1998). A Design-for-safety Methodology for Large Engineering Systems. Journal of Engineering Design, 9(2), 159-170. doi:10.1080/095448298261606

Wang, J., & Pillay, A. (2003). Technology and Safety of Marine System. UK: Elsevier Ocean Engineering Series

Wilfried Harberli, Colin Whiteman, John F Shroder, Snow and ice-related hazards, risk, and disasters, 2015, Elsevier. ISBN: 978-0-12-394849-6

E. Hollnagel, FRAM, the functional resonance analysis method, Modelling complex socio-technical systems, Ashgate, UK, Surrey (2012)

Slater D, Ale BJM. Systems analysis, from failure to success: Cambrensis working paper, 2016.

Ref:

Anders Jensen and Terje Aven, A new definition of complexity in a risk analysis setting, Reliability Engineering & System Safety Volume 171, March 2018, Pages 169-173

CA Ericson, Hazard analysis techniques for system safety, John Wiley & Sons, Hoboken, New Jersey (2005)

Google Scholar

……..for 16, 17 ref above, go to https://www.sciencedirect.com/science/article/pii/S0951832017304635

ISSN 2398-6611 (Online)

Igor Deplano Multiple Heterogeneous Knapsack Problem with realistic container loading constraints

Igor Deplano, Trung Thanh Nguyen
Department of Maritime and Mechanical Engineering James Parson Building, Byrom Street, Liverpool, L3 3AF
igor.deplano@gmail.com; T.T.Nguyen@ljmu.ac.uk

Abstract:

This paper discuss the scalability issues of a mixed-integer linear model that solves Multi-Heterogeneous Knapsack Problem giving priority to smaller bins and considering the following constraints: non overlapping, boundaries and positioning (both constrained and free), rotations (around z axis), orthogonal displacement, weight limit, stability, weight distribution in a pyramidal region and load bearing considering items arbitrary centre of mass. We study the trade-off in adding more constraints to make the problem more realistic and the complexity of finding a solution.

Keywords. Linear programming, Multi-heterogeneous knapsack problem, Container loading problem, Physical Internet, Packing

1. Introduction

The aim of this paper is to discuss the scalability issues of a Mixed Integer linear Programming Model (MIP) for the Multi-Heterogeneous Knapsack Problem (MHKP) considering the Container Loading Problem (CLP) constraints including stability, weight limits, weight distribution and load bearing constraints [1] and giving filling priority to smaller bins. We want to extend the state of the art considering items with arbitrary centre of mass (CoM) and restricting the acceptable bins' global centre of mass in a pyramidal region. This model can be used as a base model for further research on heuristics for both the Knapsack packing and Bin packing problems. We study the impact of the CLP constraints in the complexity of the solution space. The pyramidal region choice is a trade-off between the need of having a packing solution and achieving the desirable conditions for keeping safe the container handling operations such as lifting and truck transport. We exploit the work made so far in the Physical Internet initiative [2,3,4] by using their containers dimensions as proxy for dealing with real world instances. It is important to underline that even if the problem instances arise from the Physical Internet Containers, the problem can be adapted to any common container or box types just by restricting the bins to standard dimensions, e.g. 20' and 40' for ISO-standard containers.

2. Model summary

The model objective and constraints can be summarized as following:

Minimise wasted space giving priority to smaller bins (1)

Subject to:

each item must be assigned to at most one bin (2)

assigned items can rotate orthogonally along the vertical axis (3)

assigned items must be positioned on a grid (4)

assigned items must be placed inside bins limits (5)

assigned items must not overlap (6)

assigned items have to be placed on the ground or one or more items, they can't float in middle air (7)

the sum of the items weight assigned to a bin must be lower or equal than the bin's supported weight limit (8)

the global centre of mass of every bin must fall inside a pyramidal region (9)

for each assigned item, the stacked weight over it must be lower than its load bearing limit (10)

We consider three submodels called V0, V1, V2, each including a subset of the constraints. The submodel V0 contains constraints (2) - (8). The submodel V1 includes constraints (2) - (9). The submodel V2 includes constraints (2) - (10). Given *n* the number of items and *m* the number of bins, the models complexities are shown in Table 1.

Table 1: models complexities

	constraints	variables
V0	$n^2m^2-nm^2-n^2m+2nm+25n^2+3m-15n$	$9n^2+nm+m+9n$
V1	$n^2m^2-nm^2-n^2m+11nm+25n^2+8m-7n$	$9n^2+4nm+m+12n$
V2	$n^2m^2-nm^2-n^2m+11nm+31n^2+8m-12n$	$10n^2+4nm+m+12n$

3. Experiments and discussion

In most of the researches in the literature, given a fixed dimension for the bin, items dimensions are generated randomly. This procedure, although widely used could lead to results that are difficult to compare with the characteristics of real world scenarios. A dataset would be ideal if useful for both academic and industry field. Thus, we built our test instances picking randomly containers and items from

the types defined in the full theoretical set of Physical Internet containers. The set consists in 24 types of bins and 440 types of items [3].
All the instances follow the same item distribution. The set of available type of items is ordered by increasing volume in such a way that every instance is made of 70% of items after the median (higher volume), and 30% before (lower volume).
The aim of this experiments is to test the impact of the constraints on the difficulty of finding a solution. Each experiment terminates with a final script that validate the solution found. We tested the three models listed in Section 2. All versions have been implemented in OPL and solved using IBM CPLEX 12.7. The machine used to perform the experiments was an Intel Core i7-4790 CPU @ 3.60GHz, 16GB RAM, with Windows 7 Enterprise 64-bit.

Table 2: 10 item 1 bin, average values over 1000 random instances, time in milli-seconds

feature	V0	V1	V2	dataset
Available items	10	10	10	10
Packed items	9.813	9.817	9.386	-
average weight	23.312	23.01	24.5	22.657
average objective	0.5316	0.5328	0.5407	-
Average solving time	330.16	432.86	7019.56	-

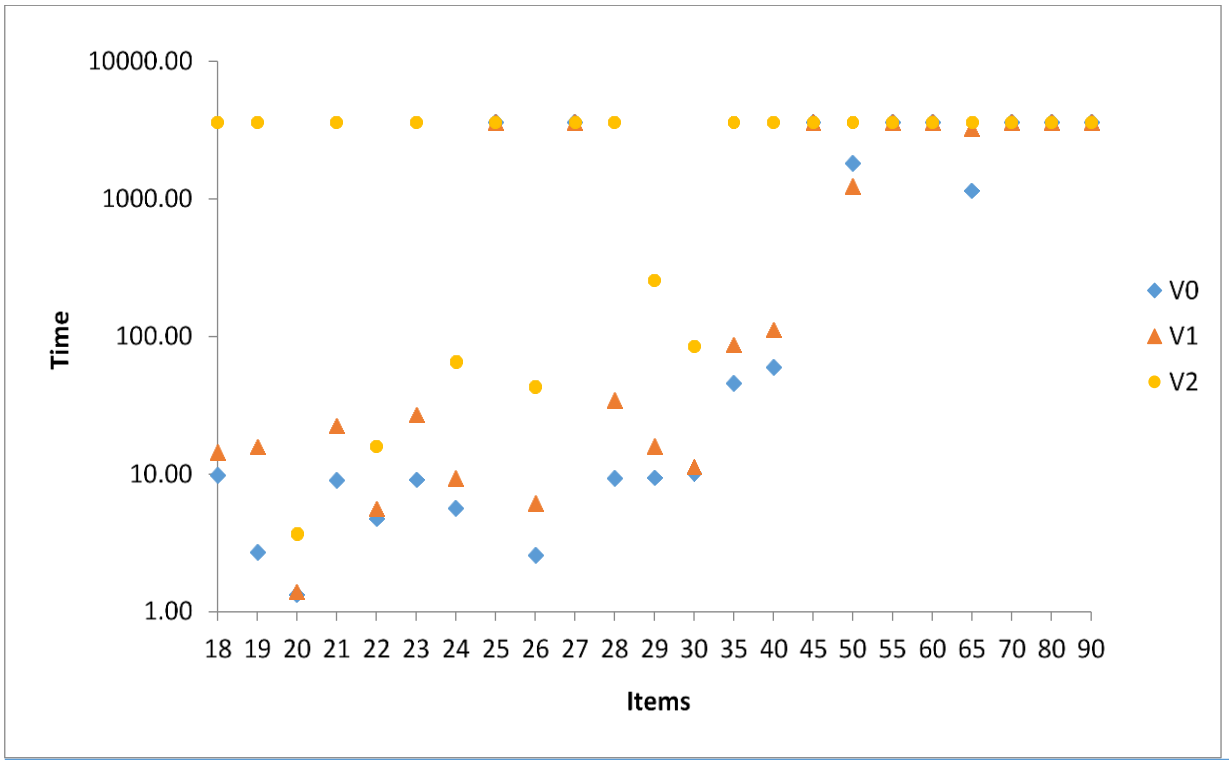

Figure 1: Time to achieve a solution for experiments using 1 bin, from 18 to 90 items. Time in logarithmic scale. One hour is the time limit for solving the problem.

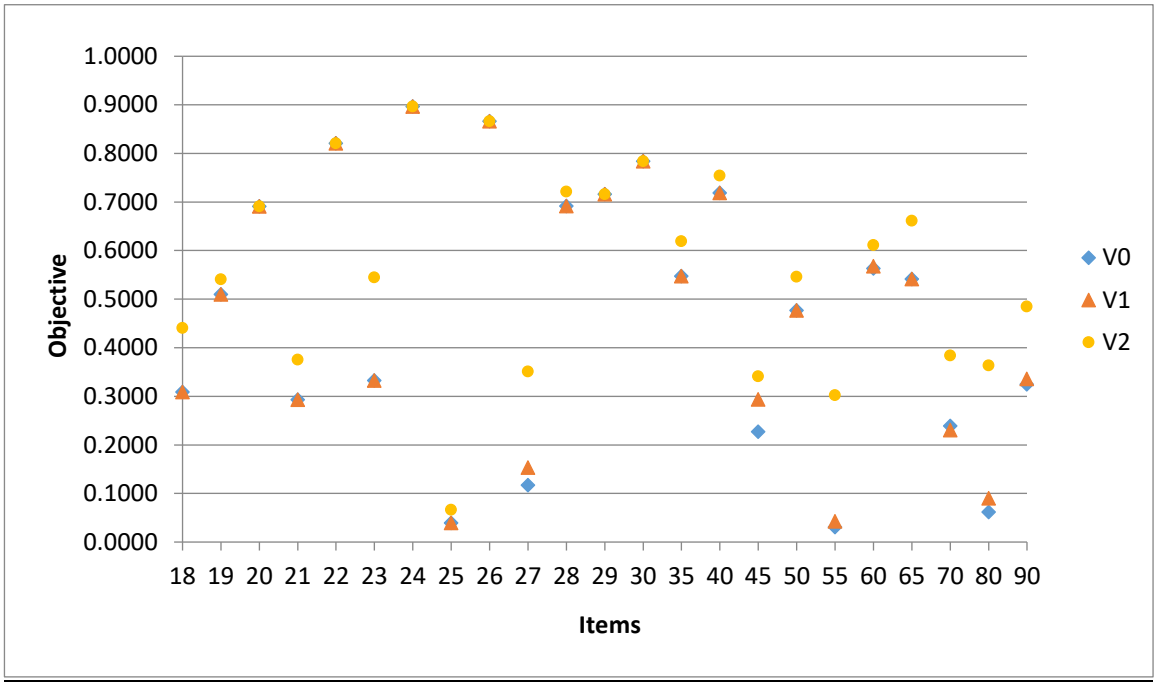

Figure 2: Objective value of the experiments using 1 bin, from 18 to 90 items.

As reported by many authors, the complexity of the problem depends obviously on the number of items, the number of bins and their dimensions. The first two can be explained by looking at how the number of variables and the number of constraints grow according to the number of items and bins, as shown in Table 1. The item/bin dimensions involved affect the number of feasible positions in the solution space. Thus, considering large spaces increases the difficulty. A possible way to reduce this complexity is using the Arcflow formulation [5,6].

In the first group of experiments we focus on packing 10 random items in the smallest bin, with dimensions 120 × 120 × 120. In Table 2 we report the average features values of the solutions found for all the 1000 instances solved with V0, V1 and V2. The dataset column represents the features of the dataset. The average objective value is the result of minimizing the wasted space (1), solving time measures the time from starting the pre-solving phase to the solution or the time limit.

V0 is not affected directly by the weight but it packs less items than V1 because it chooses items with bigger volume than V1. The degradation of the objective between V0 and V1 is 0.12% and the time to achieve a solution increases by about 30%. V2, instead, is about 15 times more complex to solve than V1. V2 chooses items with higher load bearing limit which will have also higher volume. We hypothesize that the complexity is due to the combination of the following factors: higher volume items imply a higher centre of mass along the vertical axis and this brings a lower feasible solution space. Similarly, the higher is the items volume the higher will be the probability of having asymmetric centre of masses. Those factors combined with the restricted base will force the solver to explore more nodes before finding a solution.

The second group of experiments has been made for testing the behaviour of the model using only one bin. We solved from 18 items to 90 items, each experiment had a time limit of 60 minutes. In Figure 1 we show the time for achieving a solution and in Figure 2 the relative objective value for V0, V1 and V2. In almost every case, V2 final objective is about 100% worse than V1. In some instances, for example the one with 70 items, we can see that V1 obtains a better objective than V0 in the time limit, this can be due to a different choice in the nodes to explore.

4. Conclusions

This mixed integer linear programming model can provide good quality solutions, in some cases the mathematically proved global optimum, only in small instances. We studied the trade-off in adding more constraint to make the problem more realistic and the complexity of finding a solution. The experiments showed that, even with very small instances, the computational time for finding the optimal solution considering the load bearing constraint was up to 16.2 times longer than without considering it. Further research is necessary to design new algorithms to deal with large scale instances in reasonable computational time and memory.

References

[1] Bortfeldt, A. and Wäscher, G. (2013). Constraints in container loading–a state-of-the-art review. European Journal of Operational Research, 229(1):1–20.

[2] Montreuil, B. (2011). Toward a physical internet: meeting the global logistics sustainability grand challenge. Logistics Research, 3(2-3):71–87.

[3] Sallez, Y., Pan, S., Montreuil, B., Berger, T., and Ballot, E. (2016). On the activeness of intelligent physical internet containers. Computers in Industry, 81:96–104.

[4] Landschützer, C., Ehrentraut, F., and Jodin, D. (2015). Containers for the physical internet: requirements and engineering design related to fmcg logistics. Logistics Research, 8(1):1–22.

[5] Brandao, F. (2012). *Solving Bin Packing Related Problems Using an Arc Flow Formulation*. PhD thesis, Universidade do Porto.

[6] de Carvalho, J. M. V. (1999). Exact solution of bin-packing problems using column generation and branch-and-bound. *Annals OR*, 86:629–659.

ISSN 2398-6611 (Online)

Cameron Kelly Investigation into the uses of Life Cycle Analysis (LCA) as an alternative method of selecting tidal power schemes

Name of author(s)
Cameron Kelly, LOOM Research institute, Liverpool John Moores University, Liverpool L3 3AF, UK
E-mail address: C.kelly1@2012.ljmu.ac.uk

Abstract. Tidal power generation is a renewable source of energy, however this does not automatically guarantee that it is an environmentally-friendly method of producing power. In an attempt to ascertain the true environmental effects of tidal power generation, this investigation outlines the key stages of a project which has set out discover the direct impact that a Tidal Stream Generator (TSG) has on the environment. To achieve this, a comprehensive Life Cycle Analysis (LCA) will be conducted in order to determine the impact of a TSG from "cradle to grave". This will produce a holistic assessment of the costs associated with this renewable energy source.

While a project may seem environmentally friendly does not mean that it will be economically viable. Similarly, economic impact will be a major factor in company's decision to invest in a project or not. In order to account for this in the proposed study, a Cost Benefit Analysis (CBA) will also be undertaken using data generated from a Technical Feasibility Study (TFS), which is conducted to identify the position of the TSG in a hypothetical location.

By combining the results of TFS and CBA, the author intends to create an innovative methodology which can help support decision-making within an emerging renewable energy industry that will be at the forefront of producing reliable, renewable and sustainable power for generations to come.

Keywords. Tidal power, Life Cycle Analysis, Technical Feasibility Study, Cost Benefit Analysis Feasibility study,

Introduction

Tidal power is the generation of power from the global shift in sea levels caused by the interaction between the gravitational forces of the Earth, Moon and Sun. Typically two tidal periods occur every 24 hours and 50 minutes, which is the time it takes for the Moon to realign overhead at the same point on the Earth. This is due to the rotation of the moon around the Earth being in the same direction as the rotation of the Earth.

Currently it is accepted that there are four major methods for extracting tidal energy: Tidal barrages, Tidal lagoons, Dynamic tidal power and Tidal stream generators (1). The focus of this report is on Tidal Stream Generators (TSG) which are also known as Tidal Stream Convertors. They consist of devices that are positioned directly in flowing tidal stream and come in a variety of different styles. These vary from the traditional 'bladed' tidal turbine to the more unfamiliar orientations, such as: tidal kites and oscillating hydrofoil concepts.

TSG technology is currently still in its infancy as a source of renewable energy. New devices are being developing and tested, as companies compete with each other to develop their own technology as it is scaled to commercial levels. In a world looking to reduce its environmental impact and tackle climate change the appeal of a renewable, predictable source of power is clear to see. But why should that be the limit, This report outlines the key analysis packages for site selection for tidal power schemes in an environmentally-friendly way. This is done through the combination of LCA and a CBA, and then combining them within an overall feasibility study to understand the effects of site selection of a turbine.

Technical Feasibility Study

A Technical Feasibility Study sets out to assess a sites ability to produce power. In order to achieve this, initially the site has to be compared to the specification of the proposed turbine to determine if it conforms to the local/national requirements (planning/nautical/Health & Safety). Typically at this stage the water depth, site access and ability to connect to the local power grid are assessed. Any problems encountered at this stage of the feasibility study will, most likely, put a hold on development.
Once it is clear that a turbine can be positioned at the site, the next stage is to determine the power available using Equation 1. In order to account for varying tidal conditions the power produced can be calculated over a lunar month providing a realistic assessment of the potential available output power. To do this, water velocity data for the lunar month has to be obtained via a computer simulation or from onsite data measurements. Equation 1 demonstrates the power, P, calculation of tidal turbine (2), where, ρ is the density of seawater (kg/m^3), A is the swept area of the turbine blades (m^2), V is the velocity of water flowing through the turbines (m/s), and CP is the turbine power coefficient. The power, P, is generated in Watts.

$$P = \frac{\rho A V^3}{2} C_P$$

CBA

As mentioned at the outset, one of the major factors a company must take in to account when choosing to invest in a project is the financial viability or Return On Investment (ROI), of the scheme of which the agreed ‘strike price’ for energy produced is a major factor. The current strike price for tidal power is fixed at £305 per MWh until 2019. Using the power data generated by the feasibility study it is possible to calculate how much the device will earn over its lifetime, by extrapolating the power generated during the lunar period. The lifetime earnings can then be offset against the costs associated with the project, including installation, maintenance (including ‘down time’) and, also, decommissioning in order to calculate the lifetime profits and the ROI.
ROI is, almost without exception, the most important indicator for investors in determining the value of the scheme and whether or not it should receive investment.

LCA

Life Cycle Analysis, also known as Life Cycle Assessment, is a method of holistically examining a product or system with respect to a functional unit. It was first used by the Coca-Cola company in 1969 when they commissioned the Midwest Research Institute to quantify the emissions and resource requirements for different beverage container materials for their soft drinks. Unfortunately, this report was unpublished (3),

however it established the concept of LCA which, in turn, lead to the modern regulations developed by the International Organization for Standardization (ISO) in ISO 14040 and ISO 14044.

Methodology

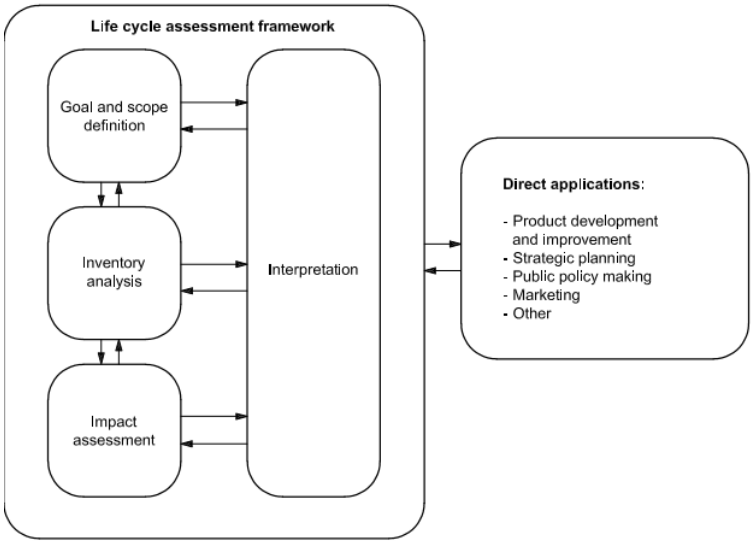

Figure 1: Key stages of conducting a LCA (4)

The framework set out by ISO 14040 outlines the four key phases for conducting a LCA which can be seen in Figure 1. The four key areas are further defined in ISO 14044 as;

- Goal and Scope: details the extent of the investigation conducted by outlining the product/system being investigated and defining the boundary conditions of the assessment and the functional units that will be used.
- Inventory Analysis: outlines all of the parts and processes in the system being investigated, providing data on inputs to the process such as material and energy and the outputs such as emissions and waste.
- Impact Assessment: this collates all the information from the inventory analysis in to the relevant impact categories specified in the Goal and Scope.
- Interpretation: defines how the results are reported, ensuring that the process is fair and the method conforms to the regulations set out in ISO 14040 and the results meet the criteria set out in the Scope.

Impact categories

There are a number of varying impact categories that make up the functional unit for an LCA investigation. The goal of the functional unit is to create a base unit for comparison against other studies. The key

functional unit for this particular report will be Global Warming Potential (GWP). There are a number of different gases that contribute to GWP. In order to collate all the different emissions carbon dioxide equivalents are calculated for each of the gases that contribute to the GWP using conversion values. This allows for the gases to be collated in to the functional unit of kg/CO^2eq which is used in the Kyoto Protocol (5).

Combination

To bring together the above three work packages (TFS, LCA & CBA) into a developed methodology it is important to understand the effects that each has on the other because the data generated in each methodology will feed between them and inform results. The following Table 1 shows some of the impact that site selection can have on each of the main work packages.

Table 1: The effects of site selection on the key methodologies

Methodology	Impact of site selection
Technical Feasibility Study	• Outlines characteristics of selected sites – factors that affect the amount of power available at each of the locations • Confirms if the site meets the specifications of the turbine • Determines the distances from the location from the Grid connection and the distance travelled by the maintenance craft
LCA	• Location of the site effects the travel distance which will result in changes in the environmental impact of the turbine with regards to laying of the connection cable and the amount of fuel used to reach the site.
CBA	• Changes in the power available effect the profitability of the scheme • Changes in distance from maintenance ports and gird connection result in changes in the quantity's of material used resulting in a change in the cost of the project

The functional unit of the final analysis will be, £/kgCO^2eq. This quantitative outcome will be generated by combining the data from the CBA and LCA. This value can be used to compare a number of locations within a specified site allowing a user to identify a preferred site with respect to the environment and the financial aspect. In order to be industry friendly, the methodology will incorporate user defined cut-off options that allow users to identify and eliminate sites that don't meet specified characteristics. One such example for this requirement is a minimum ROI; because companies will only invest if a minimum ROI is achieved. In this case only results from sites that could meet this value will be displayed. Once a site is selected, it will be possible to interrogate the methodology to determine more information about the individual components that comprise the product, thereby allowing a greater in-depth look into any sites chosen.

Conclusion

By combining these three methodologies into one combined assessment the intention is to create, a decision making tool to assess the environmental and financial impact of site selecting tidal turbines. These considerations mean that the very core of the process is built on the understanding of the environmental impact and strives to reduce the environmental footprint of a what is a highly attractive renewable energy resource.

References

[1]. *Tidal energy extraction: renewable, sustainable and predictable.* **Nicholls-Lee, R.F. Turnock,.** s.l. : Science Reviews Ltd, Spring 2008, Science Progress , Vol. 91. ISSN: 0036-8504.
[2]. *Overview of Tidal Power Technology.* **Sleiti, A. K.** 2015, Energy Sources, Part B, Planning and Policy.
[3]. **Guinée, Jeroenb, et al.** *Life Cycle Assessment: Past, Present and Future†.* s.l. : ACS, 2011. pp. 90-96.
[4]. **International Organization for Standardization.** *Environmental management — Life cycle assessment — Principles and framework.* s.l. : International Organization for Standardization, 2006. p. 8. ISO 14040.
[5]. **Climate Change 1995.** *e Science of Climate Change: Summary for Policymakers and Technical Summary of the Working Group I.* 1995. p. page 22.
[6]. **The Treasury.** *Investing in Britain's future.* HM Treasury. London : s.n., 2013. ISBN 9780101866927.
[7]. **International Organization for Standardization.** *Environmental management -- Life cycle assessment -- Requirements and guidelines.* 2006. ISO 14044.
[8]. *Alternatives to the Global Warming Potential for Comparing Climate Impacts of Emissions of Greenhouse Gases.* **Keith P. Shine, Jan S. Fuglestvedt, Kinfe Hailemariam, Nicola Stuber.** 3, s.l. : Springer, Febuary 2005, Climatic Change, Vol. 68, pp. 281-302.

ISSN 2398-6611 (Online)

Lei Wang Research on risk management methods for healthcare supply chain in hospital setting

Name of author: Lei Wang
School of Engineering, Technology and Maritime Operations,
Address: Room1.21, James Parsons Building, Liverpool Logistics Offshore and Marine Research Institute (LOOM), Byrom street, Liverpool, L3 3AF
Email: L.Wang@2015.ljmu.ac.uk

1. Introduction

Research has revealed that the healthcare cost has soared to unprecedented levels threatening the sustainability of hospitals and the healthcare system in general. Therefore, healthcare institutes and hospitals have been forced to adopting new models of operations where uncertainties are not only managed clinically but also by the hospital as an organization in a bid to ensure efficiency within the hospital operations (Bourlakis, 2011). In particular, similar to other industries, the healthcare sector (see figure 1) generally consists of four main components: producers, purchasers, providers, and payers (Burns, 2008).

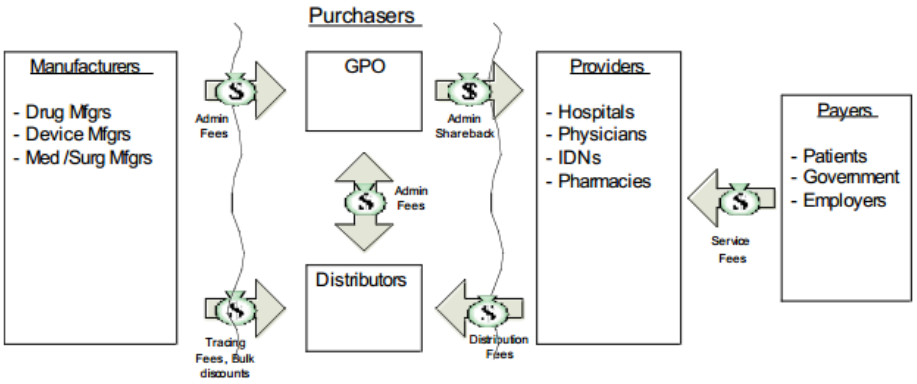

Figure 1: Health care value chain *(source adapted from ROi, Mercy case study and Burns, 2008)*

The philosophy of supply chain management (SCM) is founded on the management of all activities from upstream to the downstream process, which including identification of the customer demand, solving problems of functional division that occur within and between each parties, storage, distribution, redistribution, procurement as well as information management (Pinna *et al.*, 2015). Healthcare supply chain management (HSCM) is different from the traditional SCM in other industries as it handles a diversity of items in widely varying quantities in response to the larger number of diagnosis types and procedures. In spite of many researchers assert that implement SCM would reduce organizational costs, reduce cycle time and lead to higher performance without compromising quality of services.

Unlike the commercial industries, the risks arising from the healthcare industry's internal system and the surrounding environment may cause the serious consequence, even the patients' death. Concerning the increasing emphasis on risk management in the uncertain healthcare supply chain environment, there is an urgent demand for practical decision support tools that support supply chain risk management in hospital setting. However, the topic is still infancy and only a few numbers of systematic academic studies on this topic can be found over the last decades. Nevertheless, literature review reveals that the current healthcare systems' SCRM model are not capable of meeting challenges faced by hospitals. The risks and uncertainties in healthcare supply chain network have not yet been fully explored. In addition, to the best of our knowledge no research has been published to develop a thorough and sound risk management framework for evaluating integrated SCRM performance across the whole chains in public healthcare sector, especially in respect of medicine perspective. Meanwhile, no studies have examined the efficiency of currently implemented supply chain risk mitigation strategies in the public healthcare organizations. In light of this, this thesis aims to propose an integrated risk management framework that takes explicit account of multiple types of risk factors in aiding decision-making as well as compares and ranks the current implemented alternative risk mitigation strategies using fuzzy set theory and multiple criteria decision analysis methods.

2. Research Methodology

In pursuit of meeting the requirements of the research objectives, this thesis conducts the empirical studies from both China and UK healthcare industries and borrows three steps of risk management procedure as the main method, which includes risk identification, assessment and risk mitigation strategies identification as well as evaluation. In order to ensure the analysis is systematic and inclusive, various types of risk factors are identified through a related systematic literature review and are validated through a set of questionnaire survey and Email & face-to-face discussion. Risk assessment is conducted through two stages of questionnaire surveys and evaluated through Fuzzy Analytic Hierarchy Process (AHP) and Interpretive Structural Modelling (ISM). AHP was initially devised by Saaty (1977) as a powerful and flexible decision making method for the complex criteria structure in different level. In principal, it aims to facilitate the decision maker to decompose the complex problems into a series of smaller sub-problems and enable to making several pair-wise comparisons, assign priority weights to each elements in different levels. The Fuzzy AHP method extends the classic AHP method by combining the concepts of fuzzy set theory as the conventional AHP fails to reflect human thinking style. Interpretive Structural Modelling (hereinafter, "ISM") is a qualitative and interpretive method which supports decision-making process to identify the structure of complex relations of elements by analyzing two elements pair-wisely (Pfohl *et al.*, 2011). The structural mapping of ISM model provides decision makers with the solutions for complex issues by highlighting the interconnections of elements in a graphical manner. Thereafter, risk mitigation strategies are identified through conducted empirical studies *(i.e. documentation review, direct observation and semi-structural interview)* and evaluated through Fuzzy Technique for Order Preference by Similarity to Ideal Solution (TOPSIS). It is based on the suggestion that the selected option should be closer to the positive ideal exposition and far from the negative ideal exposition when addressing complex issues. The most preferred alternatives should have the shortest distance from the positive ideal solution and the longest distance from the negative ideal solution (Hwang and Yoon 1981).

3. Findings

The identified 34 risk factors are classified into three main categories: internal to the hospital *(i.e. process and control risks),* external to the hospital but internal to the supply chain network *(i.e. supply and demand risks)* and external to the supply chain network *(i.e. environmental risks)*. Among these, the risks within the external to the hospital but internal to the supply chain network have the most significant impact on hospital's operation. More specially, "shortage of drugs, unavailability of drugs on the market" and "counterfeiting risks", have the most significant impact among the 34 risk factors. On the other hand, the risk factors such as "Poor IT system, lack of data standardization", "lack of visibility concerning placement and availability of stock" have both strong driving and dependence power, which would strongly influence some other risks. To mitigate these risks, the currently implemented strategies, such as "implementing outsourcing strategy", "implementing E-Procurement strategy" and "implementing single sourcing strategy" are identified through the empirical studies. After collecting the Fuzzy TOPSIS survey, the result indicates that "developing advanced information technology & system" and "Implementing E-procurement strategy" are the most important effective in strengthening both robustness and resilience in the hospital supply chain network.

3.1 Research Implications

This is the first study which had developed a comprehensive risk management framework in healthcare SC that effectively integrates supply chain risk identification, risk assessment as well as mitigation strategy identification and evaluation. The novelty of the developed framework lies in the factor that a systematic and practical decision making tools are proposed supporting hospital managers making strategic decisions on healthcare SCRM. This is different from the existing SCRM literature that only focus on one piece of area, either the assessment of supply chain risks or the evaluation of risk mitigation strategies. Therefore, this thesis is the first attempt to fill the research gap. Furthermore, compared with several studies using secondary data, this thesis uses empirical data to conduct the identification and evaluation of risk mitigation strategies, it enables the results more close to the reality situation in healthcare setting.

3.2 Practical Implications

The profile of risk sources, the priority weighting and inter-relationship among these risks, the ranking of mitigation strategies provide a guideline for hospital managers to anticipate and proactively deal with potential risks. This thesis uses UK and China healthcare industries as the cases to apply the framework, the finding also can be applied in other countries and regions. Moreover, fuzzy set theory is applied to support decision makers to deal with uncertainty caused elements and unknown data in the decision-making process promptly.

4. Research Limitations

Whilst the research makes valuable contributions to the academic, as well as the practitioner spheres, however, no research is believed to be through without discussing its limitations. The limitations of this research are discussed below. Firstly, in this study, the risk factors have been retrieved only from ten research articles and one official interim report due to the limited research focused on healthcare supply chain risk management so far. Secondly, the confidential nature of healthcare industry when conducting the empirical studies highlights the difficulty of gathering primary and secondary data. Thus, the sample selection is limited to some certain professional role, so that most participants involved in this research are either have abundant knowledge in academic or with rich practical experience and hold a position at or above the manager level in practitioner fields. Therefore, a further limitation of the research is reflected

in the size of the sample. Thirdly, the proposed integrated model is highly depends on the knowledge, experience and attitude of respondents that might leading to the subjective bias

Keywords: Supply chain risk management, healthcare, MCDM method, ISM, Fuzzy AHP, TOPSIS

5. References:

[1] Bourlakis, M., Clear, F., and Patten, L., 2011, Understanding the UK hospital supply chain in an Era of patient choice, *Journal of Marketing Management.* **27**. pp. 401- 423

[2] Burns, L.R., and Lee, J.A, 2008, Hospital purchasing alliances: utilization, services, and performance, *Health Care Management Review*. **33**, pp.203-215

[3] Hwang, C.L., and Yoon, K. 1981, *Multiple Attributes Decision Making Methods and Applications*. Berlin: Springer.

[4] Pfohl, H.C., Gallus, P. and Thomas, D., 2011. Interpretive structural modeling of supply chain risks. *International Journal of Physical Distribution & Logistics Management*, **41,** pp.839-859.

[5] Pinna, R., Carrus, P.P., and Marras, F., 2015, Emerging trends in healthcare supply chain management- An Italian experience. *Applications of Contemporary Management Approaches in Supply Chain. INTECH.*

[6] Saaty, T.L., 1977. Decision making with the analytic hierarchy process. *International journal of services sciences*, **1.** pp.83-98.

ISSN 2398-6611 (Online)

Zhisen Yang Research developments of game theory in transportation: Current situation and Future direction

ZHISEN YANG
Liverpool Logistics Offshore and Marine (LOOM) Research Institute
Liverpool John Moores University
Z.Yang1@2015.ljmu.ac.uk

Abstract. The last thirty years witnessed the increasing applications of game theory in transportation. In order to figure out the true research values in terms of both reach and affect significance of such applications, it is of vital importance to understand the development trends of this research field. In this paper, an extensive review of the applications of game theory in transportation is conducted. 112 papers from 60 journals and conferences from 1983 to 2017 are collected to form the database, with regard to different criteria including, names and geographic locations of authors, the involved disciplines, the main topics and the discussed transportation modes. The evolution in these aspects indicates research of game theory in transportation focuses more on road transportation, and is being fast expanded from North America to Asia, from profit optimization to route selection, from engineering subjects to engineering-centered multi-disciplinary research fields.
Key words: Review, Game theory, Transportation

1. Introduction

Game theory, a mathematical tool to study the conflicts and cooperation between rational decision-makers, has becoming a popular and powerful methodology over the decades. Although originating from economics and mathematics, it has offered insights for scholars in many branches of disciplines (Myerson, 1991), such as economics (Rabin, 1993), computer science (Bouzya & Cazenaveb, 2001) and psychology (Henrich, et al., 2006). One reason for the popularity of game theory is that its associated quantitative models and hypothetical examples can help researchers understand real competitive situations better even if the defined situations are unrealistically simplified (Myerson, 1991).

In the past decades, transportation infrastructures are built at an unprecedented rate, which on one hand contributes to economic prosperity, but on the other hand poses many problems to modern society, including but not limited to congested transportation networks, vehicle collisions, transportation mode selection, infrastructure security and profit/cost optimization in transportation networks (Díaz-Parra, et al., 2014). It is not difficult to find that many transportation related issues, involving multiple stakeholders, are essentially of conflict and cooperation characteristics, which can be well modelled by the game theory. The applications of game theory in transportation attract attention of many scholars, forming a connected pool of research with abundant topics, multi-disciplinary knowledge, various transportation modes and novel methodologies. Sorting how such research was developed in this academic field can help scholars better understand the current situation and future directions of game theory in transportation...

This study carefully analyzed over 100 papers from Web of Science relating to the applications of game theory in transportation published in various journals from 1983 to 2017. Based on this database, the trends of geographic locations and disciplines of authors, main topics and involved transportation modes are analyzed and described. The results indicate research of game theory in transportation is global and multi-disciplinary.

2. Data

In order to collect relevant papers, ‘game theory’ and ‘transportation’ are used as two key words when searching in Web of Science, resulting in over 300 articles. Further, the papers that do not set transportation issues as main research target are excluded, mainly referred to papers about transportation in logistics. Book chapters, papers written in other languages and lack of basic information are also excluded. Meanwhile, articles focused on wireless transportation such as information transmission and telecommunication are excluded as this study only consider physical transportation.
Finally, in this study, 112 papers are systematically reviewed from 60 academic journals and 13 conference proceedings from 1983 to 2017, covering multiple disciplines including computer science, economics, engineering, mathematics, management and transportation. At the same time, the database comprises different transportation modes, including road, rail, air and water transportation.
After the database is established, the collected papers are categorized against different criteria, including geographic locations of authors, disciplines of authors, main topics and involved transportation modes. Each criteria is an important component of a paper and can be easily obtained through carefully reading. Understanding the evolution of papers in these aspects is useful to clarify the trends, which is an indispensable step in our study. If one article has more than one author the information of all involved authors is used. In addition, the paper allows for two or three main topics from one paper. It is mainly due to the fact that one topic is sometimes unable to exclusively present the objective and true content of the paper effectively. Examining these papers against the criteria will help identify the current trends and future directions of the use of game theory in transportation.

3. Research developments of game theory in transportation

3.1 General analysis
To start our research, the 112 published papers are first classified into several groups by time: ‘Before 2000’, ‘2000-2005’, ‘2006-2011’ and ‘2012-2017’. The number of papers and involved journals are listed in Table I. Conference papers are divided into two categories: ‘IEEE conferences’ and ‘other conferences’, because a considerable part of conference papers collected in this study come from IEEE conferences.
The number of papers and involved journals every five years is experiencing an upward trend. Before 2000, only 4 relevant papers were published. However, when it came to ‘2012-2017’, the most recent period, 56 articles were published, occupying 50% in the database. If the period was extended to recent decade, 95 papers (84.8%) were included. This observation shows the increasing awareness of the importance of game theory research in transportation, which may be due to the increasing number of transportation issues brought by growing transportation demand.

Table 1. Number of papers and journals from 1983-2017

	Before 2000	**2000-2005**	**2006-2011**	**2012-2017**
Number of papers	4	13	39	56
Number of journals	4	8	26	34

After the analysis of the papers relating to the congested transportation network, vehicle collisions, transportation mode selection, or infrastructure security and profit/cost optimization, it reveals that the core of these transportation issues are in nature optimization and decision-making problems. In addition, the availability of different types of data and the appearance of powerful computational software makes mathematical methodology more applicable to researchers. These factors may count for the increasing importance of game theory in transportation.

3.2 Trend in geographic location of authors

To understand the change of research geographical areas, locations of authors are investigated. In this study, the number of publications is used to represent the contribution of a country or region. If one researcher published more than one paper in a year, the location of this author will be counted multiple times equal to his publications. For the papers of multiple authors, all of the authors' locations will count. The country or region contributing to the most publications was the core geographical area of that time. Table II lists the spatial distributions of authors.

Table 2. The number of papers by geographic locations over time

	Before 2000	**2000-2005**	**2006-2011**	**2012-2017**
Number of countries	2	8	22	22
Number of papers	4	13	39	56
Asia	0	5	15	26
Africa	0	0	0	0
America (North)	3	5	11	16
America (South)	0	0	2	1
Europe	1	4	18	21
Oceania	0	0	0	2

This research field was first initiated by North American researchers. Although limited publications were recorded before 2000, it was still obvious to find North American scholars dominated at that time. Since entered 21st century, Asian and European scholars gradually became productive. The European research team experienced a burst of publications from 4 during 2000-2005 to 18 during 2006-2011, and maintain a stable productivity till now. The number of Asian scholars increased rapidly from 5 (2000-2005) through 15 (2006-2011), and to 26 (2012-2017), which makes the region ranked the top around the world currently in terms of the quantity of the publications.

3.3Trend in disciplines of research

Many transportation issues occurred because of growing transportation demand in recent years, requiring solutions from different subjects. Therefore, scholars having different research backgrounds are attracted to conduct relevant studies. In this paper, the affiliations of authors are used to represent the involved disciplines, and the findings are listed in Figure III.

First, only some authors from engineering, management and social science began to apply game theory into the transportation field. Since 2000, mathematics and natural science became two emerging disciplines, following engineering and social science. In the past decade, more researchers from advanced fields of computer & technology and transportation & logistics stepped into this area and made increasing contributions.

Engineering has always been the core discipline of this research field over the past thirty years. The scope of engineering expanded significantly from 2 subjects (before 2000) to 12 subjects now. Meanwhile, it contributes to 47 papers, occupying 42% of total number of papers.

In general, the broader areas, long history and large amount of authors involved make engineering the biggest contributor in the use of game theory in transportation. There is sufficient evidence during this review study that engineering subject will remain its leading position for a certain time. Transportation & logistic, as well as computer & technology may be two potential forces in the future because of their expansion rate on subject areas and gradually increased researchers.

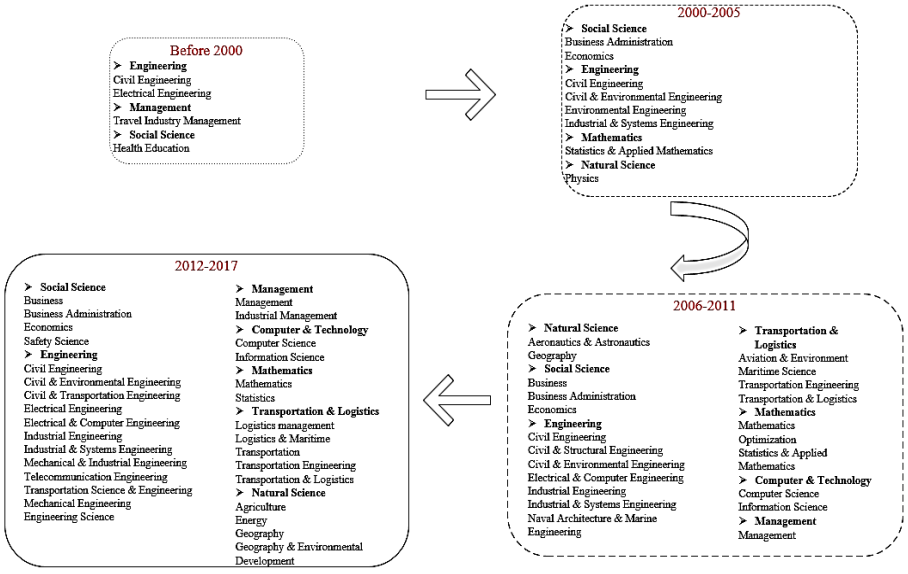

Figure 1. Trends of disciplines

4. Conclusion

Research of game theory in transportation attracted increasing interests over the past thirty years. The decision-making and optimization functions of game theory can help solve many transportation issues, such as congested transportation network, vehicle collisions and transportation mode selection. To understand its current situation and future directions, an extensive review of 112 papers are collected from 60 journals and conferences study is conducted in this study. The following research findings are obtained.

Among the geographic locations of the researchers, Asia, North America and Europe were proved the most productive areas. America has a leading position. In recent years, the relevant publications in China grow fast, showing a trend of developing itself to be another hotspot in this research field.

The amount of disciplines involved in this study increased significantly, not only prompting the prosperity in research topics, but also reflecting a multi-disciplinary research nature. Engineering has

always been the core discipline because of its broader areas, long history and large amount of publications. Meanwhile, researchers from different disciplines explored many topics, stimulating the expansion of the range of research topics.

References

Adler, N., 2001. Competition in a deregulated air transportation market. European Journal of Operational Research, 129(2), pp. 337-345.

Andrea Lodi, E. M. N. E. S.-M. T. B., 2016. Design and Control of Public-Service Contracts and an application to public transportation systems. Management Science, 62(4), pp. 1165-1187.

Bell, M. G. H., 2006. Mixed Route Strategies for the Risk-Averse Shipment of Hazardous Materials. Networks and Spatial Economics, 6(3), pp. 253-265.

Bouzya, B. & Cazenaveb, T., 2001. Computer Go: An AI oriented survey. Artificial Intelligence, 132(1), pp. 39-103.

Cardinal, J., Labbe, M. & Langerman, S., 2009. Pricing geometric transportation network. International journal of Computational Geometry, 19(6), pp. 507-520.

Díaz-Parra, O., Ruiz-Vanoye, J. A. & Loranca, B. B., 2014. A Survey of Transportation Problems. Journal of Applied Mathematics, 2014(2014), pp. 1-17.

GIANLUCA CRIPPA, C. J. A. P., 2009. Optimum and equilibrium in a transportation problem with queue penalization effect. Advances in Calculus of Variations, 2(3), pp. 207-246.

Henrich, J. (. J. et al., 2006. Costly punishment across human societies. Science, 312(5781), pp. 1767-1770.

Jean Cardinal, M. L. S. L. B. P., 2009. Pricing Geometric Transportation Networks. International Journal of Computational Geometry & Applications, 19(6), pp. 507-520.

ISSN 2398-6611 (Online)

Khaled Mohamed Al-Badani Investigating the Effect of Welding Parameters on the Manufacturing Procedures of Thermocouple Tubes

Khaled Al-Badani, James Ren, Lisa Li and David Allanson
Department of Maritime and Mechanical Engineering, Faculty of Engineering, Liverpool John Moores University

E-mail address: K.A.Mohamed@2015.ljmu.ac.uk

Abstract. Stainless steel tube welding is an important manufacturing process with many applications. This paper investigates various selection of parameters in welding thin stainless tubes used as sheath for thermocouple sensors. For sheathed thermocouple, the end of the tubes sheath is normally closed through welding. The quality of the weld is critical to the integrity and response of the thermocouples. The geometry of the welding pool has numerous quality properties, such as the overall width, height, roundness, toughness and hardness, which needs to be properly controlled. In this work, controlled welding tests and analysis has been conducted on stainless tubes of different sizes, the quality of the weld, micro hardness and surface roughness is investigated and the key factors controlling the welding process is established.

Keywords. Welding, Tube closure, hardness, surface roughness

1. Introduction

Sheathed thermocouples are widely used in many industries for temperature measurement and process control. A thermocouple is assembled by spot welding two dissimilar wires together (Figure 1). There are three main types of thermocouples: bare wire, insulated and grounded insulated. Bare wire thermocouples are in a simple form with the wire directly jointed together and used in temperature measurement. In an insulated thermocouple, the welded tip and wires are embedded with an insulation (normally MgO) covered by a sheath of protective material (normally stainless steels). Figure 1 illustrates the structure of two types of sheathed thermocouples. In a ungrounded junction, the thermocouple junction is insulated from sheath and ground; For a grounded structure, thermocouple junction is an integral part of the sheath. The closure of the sheath directly influences the response time and protection of the sensors. The joint of the thermocouple wires are normally welded by Capacitor Discharge (CD); while the stainless tube is normally welded by Tungsten inert gas (TIG) Welding (TIG) welding process [1-2].

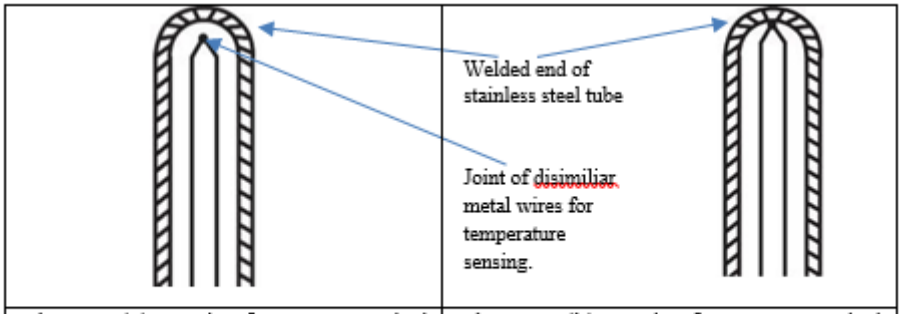

Figure 1(a) End of a ungrounded Sheathed thermocouple

Figure 1(b) End of a ungrounded Sheathed thermocouple

The quality of the weld of the stainless tube is critical to the integrity and response of the thermocouples. The welding of the stainless tube is a complex process due to the material composition (i.e. multiple alloying elements) and properties of stainless steels. The composition needs to be balanced to maintain the corrosion resistance [3-4]. Coefficient of thermal expansion of stainless steel is high compared to carbon steels, so it is prone to distortion and stress inducement if the proper welding procedure is not followed. In addition, stainless steel is a reactive metal that quickly forms an oxide layer on the surface and strength of the weld area become weak. Therefore, welding of stainless steel is difficult. For thermocouples, the shape of the sheath end needs to be properly controlled, as it directly influences the response time of the temperature measurements. An improve the understanding of the effect of welding parameters on the material factors such as hardness, microstructure and surface roughness is very important. In this work, controlled welding tests and analysis has been conducted on stainless tubes of different sizes, the geometry of the welding pool such as the overall width, height, roundness was established. Some key material characteristics crucial to the quality of the weldment including microhardness and surface finish is investigated and the key factors controlling the welding process is established.

2. Testing Conditions

Figure 2(a) setup of the welding tests.

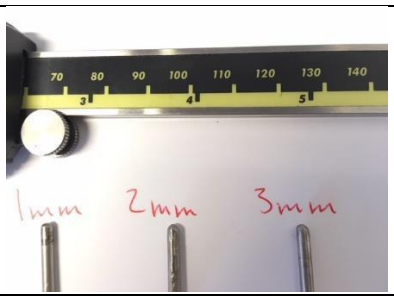

Figure 2(b) Welded end of stainless steel tubes.

Figure 2 shows the welding setup (a) and some welded samples (b). The welding apparatus is able to control the height and position of the TIG through newly designed frame. The TIG welding torch is fixed with the height adjustable block unit. A tungsten electrode is used and Argon gas is flow through the torch; TIG Welding machine with a Rectifier (made by FRONIUS) covers a current range 10-180 A and voltage up to 230V, depending on the current setting has been selected. Ar gas is supplied to the welding torch with a particular flowrate, so that an inert atmosphere formed and stable arc created for welding. A fan is placed behind the welding apparatus to draw air from the workpiece prior to the weld discharge, to prevent oxidation during and after the solidification phase. Figure 2(b) shows some typical welded tips of different tube diameters. A Brukker GTK surface texture system was used to measure Surface Roughness of the welded tip for all specimens. These readings will help determine the change in the surface condition, including potential oxidation. A design of experiments (DOE) has been used to produce samples under different parameters including Electrode Workpiece distance (mm), Argon Gas Flowrate (l/min), Voltage (V) and Current (A).

3. Results and Analysis

As a key dimensional characteristics of the welded tip, width of the welded samples were measured to calculate the overall tip size. This average value (over at least 5 readings) was then plotted against the applied welding current for various welded heights as shown in Figure 3. It can be clearly seen that the weld tip width increases almost linearly with the increase of the welding current. The micro hardness test was performed to measure the hardness values for the welded stainless steel tube ends within the cross section. The hardness distribution will help demonstrate the changes in the mechanical properties of the welded zone. Figure 5 shows the hardness values within the weld zone taken from the top centre of the welded tip and towards the base material, for different samples performed with different welding speed and welding current. Figure 4A shows the data for welding height of 2mm, while Figure 4B shows the data for a 3mm welding height. From both graphs, it can be clear that the micro hardness value reaches its maximum value, in the range between 40 to 80HV, near the welding zone. This value keeps on decreasing as the measurement is recorded towards the base material zone. It can be noticed from the welded samples achieved by a welding height of 2mm and various welding current, that the micro hardness values keeps on decreasing rapidly from a distance of 2mm and onwards. However, for the welded samples achieved with a welded height of 3mm, the hardness reaches that of the base stainless steel after 5 mm distance mark.

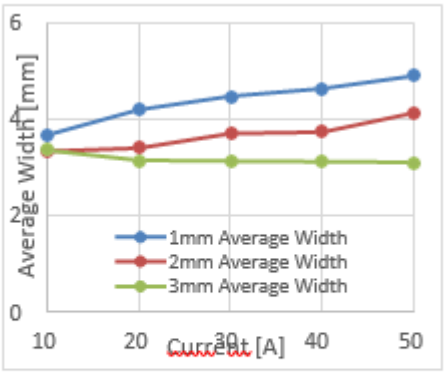

Figure 3-Welding Width of the samples with different welding Height and welding current conditions.

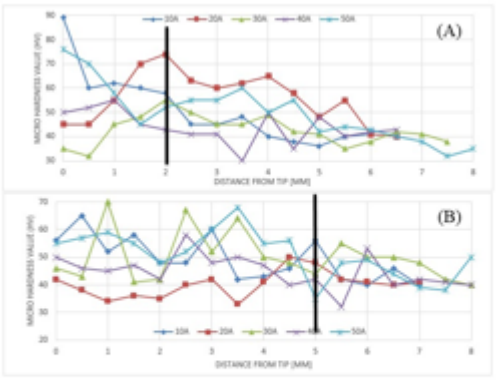

Figure 4 Micro Hardness Value from the center of the weld zone towards the base material for welding done with various welding currents and welding height of (A) 2mm and (B) 3mm rapidly.

Figure 5 illustrate two 3D scan of the welded zone of the welded tips cross sections for the samples prepared using different welding height and current. Straightaway, it can be noticed that samples produced by welding height of 1mm, suffered burning due to close distance of the welding operation. It can also be understood from the images that there is no specific changes that could be noticed from the weld specimen. Though, the cross section of the 3D weld zone scan demonstrate a clear effect of the welding parameters changes, i.e. welding current and height. Also the referenced scans produced by the Bukker GTK surface texture system highlights the welding penetration changes with the adjustment of the welding height and current settings. This is apparent from the welding depth, which increased with the welding current and decreased with the welding height. The test also revealed that that, for a particular value of welding current, welding depth found decreases as the welding speed increases. All these observations are important for optimise the welding regimes to avoid surface defects[5].

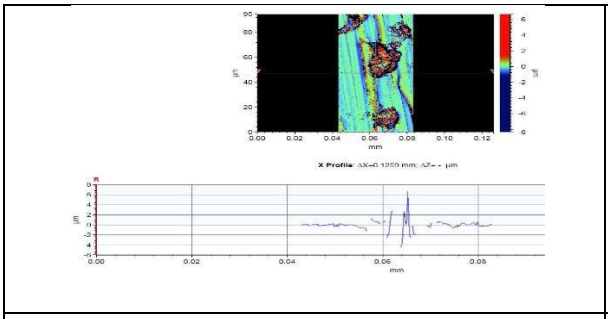

Figure 5(a) Average Surface Roughness scan recording for a welding height of 1mm and welding current of 30A. Burned samples detected

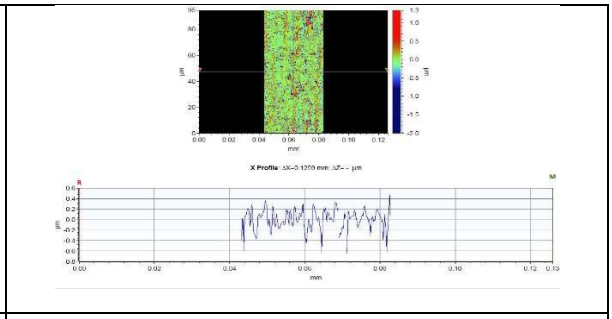

Figure 5(b) Average Surface Roughness scan recording for a height of 2mm and welding current of 3A.

4. Summary

Stainless steel tube welding is an important process in manufacturing sheathed thermocouples. The

dimension of the joints and quality of the weld is critical to the response of the thermocouples. In this work, controlled TIG welding tests and analysis has been conducted on stainless tubes of different sizes, the quality of the weld, microhardness and surface is investigated and the key factors controlling the welding process is established. A design of experiments (DOE) has been used to produce samples with different parameters including Electrode Workpiece distance (mm), Argon Gas Flowrate (l/min), Voltage (V) and Current (A). The geometry of the welding pool was quantified by measuring the overall width, height, roundness. Detailed materials properties such as microhardness, surface roughness is studied. The results show that a uniform tip can be produced of a good repeatability with the development of the automated welding frame. The width of tip depends heavily on the welding height and current; The micro hardness values of the welding zone decrease as the distance from the centre of the weld increases due to the change of in the microstructure associated with the thermal process. Surface roughness of tube is found to changes with the distance from the welding zone, which highlight the influence of the thermal process or potential phase changes. Microstructure burns was also observed in some welding conditions, which will damage the corrosion resistance of the material. Future work will combine the experimental results with modelling and detailed materials characterisation to development a welding map for guiding the optimisation of the welding process.

References:

[1] Loto R., 2017, Study of the corrosion behaviour of s32101 duplex and 410 martensitic stainless steel for application in oil refinery distillation systems. *Journal of Materials Research and Technology*, 6(3), 203-212.

[2] Raveendra, A., & Kumar, B. R.(2013). Experimental study on Pulsed and NonPulsed Current TIG Welding of Stainless Steel sheet (SS304). International Journal of Innovative Research in Science, Engineering and Technology, 2(6), 5-15.

[3] Li, D., Lu, S., Dong, W., Li, D., & Li, Y. (2012). Study of the law between the weld pool shape variations with the welding parameters under two TIG processes. Journal of Materials Processing Technology, 212(1), 128-136.

[4] Brytan Z., Niagaj J., Reiman Ł., 2016, Corrosion studies using potentiodynamic and EIS electrochemical techniques of welded lean duplex stainless steel UNS S82441, *Applied Surface Science*, 388 A, 160-167.

[5] Hsieh C. and Wu W., 2012, Overview of intermetallic sigma phase precipitation in stainless steels. ISRN Metallurgy, 1, 1-16.